Development of Electrochemical Detection for Capillary Electrophoresis

by

JianYun Wen

A Thesis

Submitted to the Faculty of Graduate Studies and Research

In Partial Fulfillment of the Requirements for the Degree

of Doctor of Philosophy

In

Chemistry

Department of Chemistry

University of Saskatchewan

January 1998

DEVELOPMENT OF ELECTROCHEMICAL DETECTION FOR CAPILLARY ELECTROPHORESES

JIANYUN WEN

1998

Copyright

THIS THESIS IS DEDICATED TO:

MY SON, WILLIAM YANG,

AND

THE MEMORY MY LATE MOTHER, MINGQIU CAI.

ABSTRACT

The main goal of this work was to develop a reliable and sensitive electrochemical (EC) detection for analytes separated by capillary electrophoresis (CE). To achieve this goal, a series of potential waveforms, such as constant-voltage, two-step pulsed-voltage, combinations of two-step pulsed-voltages, and triangular-voltage, were examined. To enhance S/N, selection of analytical data from potential waveform was evaluated, experimental conditions were optimized, and analytical data were treated by a series of signal analysis techniques. In this work, metal ions were chosen as test analytes.

As the first step in this study, CE experimental parameters were examined. Although this was not the main purpose of this work, it was important for proper evaluation of the EC detection approaches. The parameters optimized included the choice of electrolyte, the concentration and pH of the electrolyte, capillary size and conditioning, and alignment of the capillary with the electrode. The results showed that capillaries ($\leq$ 50 μm ID) aligned with the electrode within 20 $\pm$ 5 μm offered the best compromise in minimizing the influence of high-separation voltage on EC detection and maximizing S/N. Studies of electrolytes showed that α-Hydroxyisobutyric acid (HIBA), in the range of 8 to 12 mmol/L with pH 4.4 to 5.0, offered reproducible and selective separation of the test metal ions.

Since it is necessary to understand the electrode/analyte response to optimize EC detection, electrochemical behavior of the electrolyte and analytes and the factors affecting the behavior were studied by on-line cyclic voltammetry (CV). The parameters investigated included adsorption of organic electrolytes, deposition of metal ions, and H^+

and O_2 reactions. The results showed that on-line CV was an effective tool for optimization of CE/EC conditions. From these studies it was found that the adsorption of organic components of the electrolytes on Au and Pt electrodes reduced background noise by decreasing the double layer capacitance and by inhibiting O_2 reduction, that some metals deposited on the electrode to cause changes in the electrode surface and that these surface changes affected background reactions such that baseline shifts and distort peaks were obtained.

The first EC approach studied in CE was pulsed amperometric detection (PAD) with the potential frequency of 5 to 8 Hz at both Au and Pt 25 μm disk electrodes. To optimize PAD detection, pulse duration and applied potential were examined for both cathodic deposition and anodic stripping analysis. Under the optimal conditions detection limits for metal ions were in the range of 2.0×10^{-7} to 2.0×10^{-5} mol/L, and the response factors were constant to within ± 5% over the range of 50 μmol/L to 1000 μmol/L. A comparison of PAD for spiked and real snow samples with atomic absorption spectrometry showed good agreement.

To improve PAD detectability in CE, a number of experimental parameters were evaluated. These parameters included sample stacking, potential waveform shape and frequency, and special signal treatments, such as the use of a lock-in amplifier or digital Fourier analysis. In the study of sample stacking, stacking conditions that could enhance sensitivity and keep response factor within 5% were determined. The results showed that when samples were prepared at electrolyte concentrations about 7 to 8 times less than that used for the electrophoretic separations, sensitivity improved by 10 times without loss of

linearity ($< \pm 5\%$) over 1.0 μmol/L to 100.0 μmol/L. The use of a multiple-step pulse waveform to provide multiple adsorption/desorption of the analyte gave a maximum signal-to-noise ratio (S/N) enhancement up to 10 fold. Signal analysis techniques that improve S/N via discriminating between symmetrical and unsymmetrical signals (harmonic analysis and phase-sensitive detection) gave improvement in S/N of 4 to 6. Although significant improvements in baseline stability were observed due to rejection of symmetrical background signals, the overall performance in limits of S/N was not as good as that for the conceptually simple multiple-step waveform approach. Other approaches such as the use of high pulse frequencies (100 to 200 Hz), digital filters, and average smoothing also enhanced S/N 2 to 5 times.

The next EC technique investigated was a fast-scan voltammetric detection over sweep rates of 20 to 1,000 V/s at Au disk electrodes (25 and 10 μm); some studies were also done with 25 μm Pt disk electrodes. The waveform applied to the electrode consisted of a preconcentration period (55 to 330 ms) followed by cyclic voltammetry (2 to 100 ms) with both CV current and CV charge from the integration of CV current versus time as the analytical signal. The results showed that maximum response was obtained at sweep rates of 100 to 200 V/s; sweep rates of > 400 V/s caused peak tailing due to trapping of the analyte at the electrode. With this CV detection approach, co-migrating analytes could be identified and quantified. Response factors for metal ions over the range 1.0×10^{-7} to 1.0×10^{-5} mol/L were $\leq 5\%$, and detection limits were in the range of 5×10^{-9} mol/L to 4×10^{-8} mol/L, which are one to two orders of magnitude better than results obtained previously with pulsed amperometric detection.

ACKNOWLEDGMENTS

I would like to thank my supervisor Professor R. M. Cassidy for his guidance during this work, for helping me in developing the skills to analyze and solve the problems, for his efforts in teaching me how to write scientific reports, and for giving me many opportunities to learn. I would also like to thank my co-research supervisor, Professor A. Baranski for his guidance during this work, for his efforts in teaching me in electrochemistry and for his computer programs. Thanks also to the members of my supervisory committee professors, J. W. Quail and J. O. K. Boison for their help and useful comments. I wish to thank the Department of Chemistry, University of Saskatchewan for giving me the opportunity to broaden my knowledge. My deep gratitude to my good friend Mrs. Louise Grassmann and my son, William Yang for their support and encouragement throughout this work. Thanks also to my labmates for their help. The financial support of University of Saskatchewan, the Natural Sciences and Engineering Research Council of Canada, and Waters Corporation is gratefully acknowledged. The financial support of University of Saskatchewan, the Natural Sciences and Engineering Research Council of Canada, and Waters Corporation is gratefully acknowledged.

Table of Contents

List of Tables

Table Page

List of Figures

List of Symbols and Abbreviations

A	surface area of an electrode
AC	alternative current
AD	analog-digital
C	coulombs; concentration
CE	capillary electrophoresis
CME	chemically modified electrode
CV	cyclic voltammetry or cyclic voltammogram
CVD	constant voltage amperometric detection
D	diffusion efficiency
EC	electrochemical
EOF	electroosmotic flow
F	faraday constant
FTIR	fourier transform infrared
h	hour
HIBA	α-Hydroxyisobutyric acid
ID (i.d.)	internal diameter
LC	liquid chromatography
$_M^{n+}$	metal ions
min	minute
μ_{eo}	electroosmotic mobility
μ_{ep}	electrophoretic mobility
μm	micrometer
PZC	potential of zero charge
PAD	pulsed voltage amperometric detection
RSD	relative standard deviation
R_S	solution resistance
SCE	saturated KCl Calomel reference electrode
S/N	signal-to-noise ratio
UV	ultraviolet
v.s.	versus

1. INTRODUCTION

1.1. Capillary Electrophoresis (CE)

1.1.1. Historical Background

Capillary electrophoresis (CE) is the descendant of numerous electrophoresis and chromatography techniques, and the history of its development can be traced back over more than one century. Pioneering studies on electrophoresis were made in 1897 by Picton and Linder[1] and Kohlrausch,[2] who developed a theory of ionic migration, which established the basis of all electrophoretic principles. In 1900, Hardy[3,4] discovered the characteristic mobilities of many biological molecules by observing globulin movement in "U" tubes, and this discovery greatly stimulated the interest in electrophoretic work. Tiselius is the first one to apply electrophoresis as an analytical tool for protein separation in 1930s.[5] Primary theories of electrophoresis and electroosmosis were developed by Smoluchowski[6], Schwerin,[7] and Keedall and Crittenden[8] in 1910s to 1920s. In 1965, Hjerten[9] provided the earliest demonstration of the use of high electric-field strength in 3 mm diameter (i. d.) tubes for free-solution electrophoretic studies. Virtanen[10] described the advantages of using small-diameter columns in electrophoresis in 1974. In 1979, Mikkers et al[11] performed zone electrophoresis in polymer capillaries. For most of the early applications, electrophoretic separations were performed with capillaries of $\geq$ 100

μm i.d., and the separation efficiency was often limited by Joule heat. Modern CE theory based on narrow capillaries (≤100 μm i.d.) started to develop in the 1980s, and the most widely accepted initial demonstration of the power of modern CE was made by Jorgenson and Lukacs,[12-14] who described dispersion theory and electroosmosis in small capillaries (<100 μm). Since then, CE has offered rapid and efficient separations for small amounts of analytes.[15,16] This microseparation technique shows great promise in the separation of biomolecules, and organic and inorganic molecules.[17-19] Although CE is a powerful separation technique, some limitations exist, the major of which is the lack of sensitive detection modes available due to the extremely small sample zone and column dimensions of capillaries. Hence, improvement in detection area is essential for the development of CE techniques.

1.1.2. Fundamental Aspects Of CE Separation

1.1.2.1. Electrical Double Layer

Ion migration in CE depends on the composition of separation medium and functional groups present on the capillary wall. When the inner wall of a capillary comes into contact with an electrolyte solution, an electrical double layer forms at the surface-liquid interface. The structure of the double layer and variation of the potential across the electrical double layer is shown in Figure 1.1. The surface charge is generated on the capillary due to dissociation of silanol groups in fused-silica capillaries and this charge is negative at most pH conditions (>2). In the immediate vicinity of a capillary wall

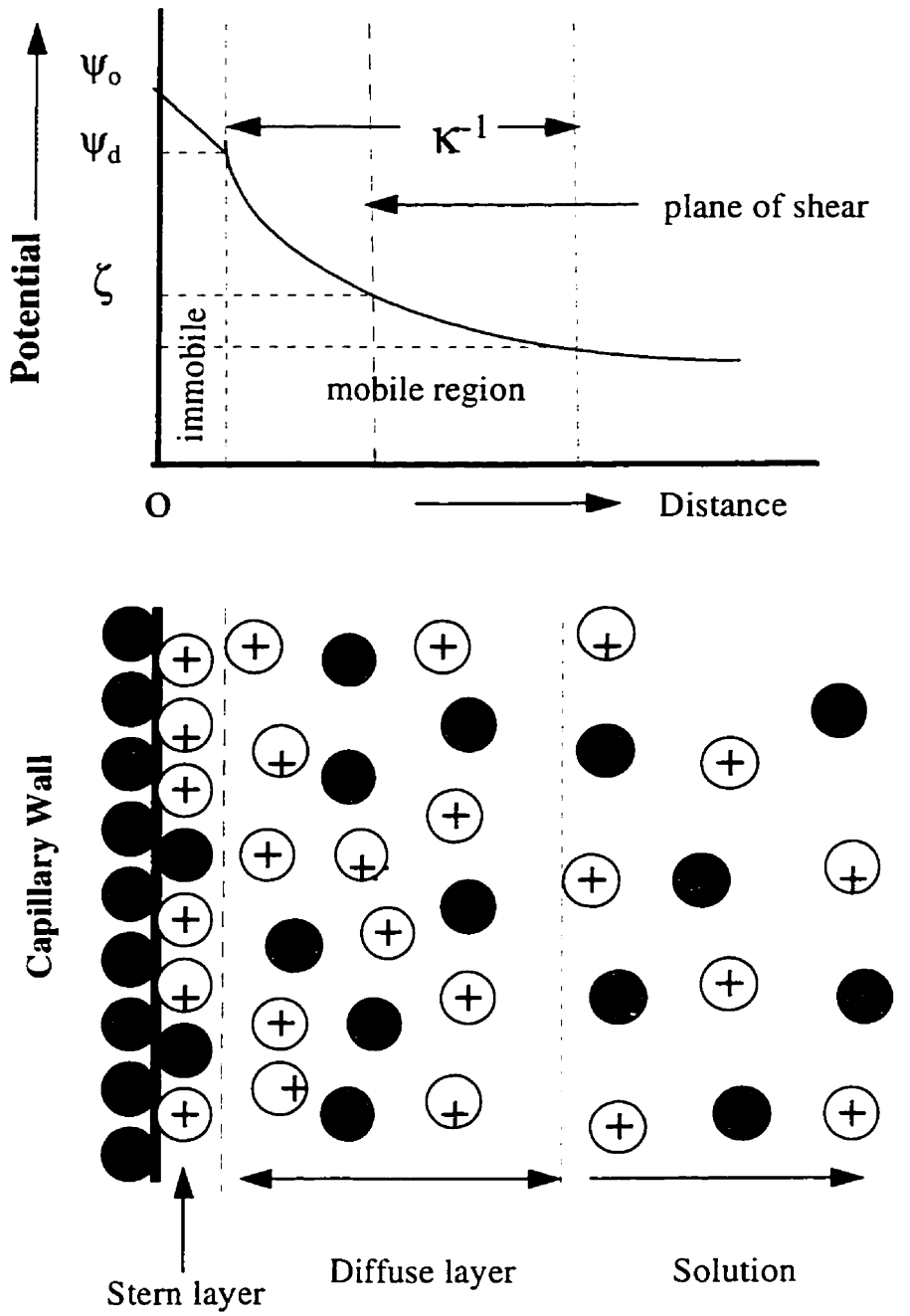

Figure 1.1 Representation of an double layer. ζ and κ^{-1} are the zeta potential and the thickness of the double layer, respectively.

carrying negative charges, oriented dipoles of water molecules and solvated cations are attracted near the capillary wall to form an immobile layer that is termed Stern layer (see figure 1.1). Other counterions are held less tightly in the diffuse layer and can move by thermal motion. Due to the spatial distribution of ions, an electric potential established at the silica-solution interface. The value of this electric potential decreases linearly in the stern layer and exponentially in the diffuse layer (see figure 1.1). At the surface of shear between the charged surface and the electrolyte solution, the electric potential is called the zeta (ζ) potential. Since not all of the negative charges on the wall are counterbalanced by positive species in the immediate vicinity of the wall, ζ-potential is often a negative value at the inner surface of the capillary,[20] and the magnitude of this value is proportional to the surface charge density (σ^*) and the thickness (κ^{-1}) of the double layer. The formation and structure of the double layer on the capillary is important because some aspects of a CE separation depend on the nature of this layer.

1.1.2.2. Electroosmosis and Electrophoresis

Two important phenomena exist in CE: electroosmosis and electrophoresis. Electroosmosis is the bulk flow of liquid due to the effect of the electric field on positive counterions adjacent to the negatively charged capillary wall. At a certain distance from the capillary wall the positive ions becomes mobile (see figure 1.1), and when an electric field is applied, this layer of positive ions migrates towards the negative electrode (cathode), resulting in a bulk flow of liquid (via viscous forces). This flow is termed

electroosmotic flow (EOF). The mobility (μ_{eo}) of electroosmotic flow can be expressed by the Helmoholtz- Smoluchowski equation:[21]

$$\mu_{eo} = -\varepsilon \zeta / (4\pi\eta) = \sigma^* \kappa^{-1} / \eta \qquad (1.1)$$

where ε is the dielectric constant (Fm^{-1}) in solution, ζ is the zeta potential (V), η is the viscosity (Poise) in solution, σ^* is the surface charge density (Cm^{-2}), and κ^{-1} is the thickness (m) of the electrical double layer. This thickness of the double layer depends on the ion concentration (C_i) in solution. Since the EOF velocity is related to properties of the double layer, the concentration and pH in the electrolyte, and the electric field strength, changes of these parameters should be useful for selectivity control in EOF.

In the presence of an electric field, charged particles move to the anode or cathode, and this movement is termed electrophoretic migration. The electrophoretic mobility of an ion (μ_{ion}) is related to the charge ($Z_i e$) of the ion and the translation friction coefficient ($6\pi\eta r_i$), shown by the following equation,[22]

$$\mu_{ion} = (10^7 Z_i e)/(6\pi\eta r_i) \qquad (1.2)$$

Where $Z_i e$, η are the same as before; and r_i is the radius of the charged particle. The changes in the effective charge on an ion and the viscosity in the buffer should be useful to adjust the electrophoretic mobility of the ion. In most pH conditions (> 2), EOF is

cathodal, and thus, cations move in the same direction as the EOF; anions move in the opposite direction to the EOF. The mobility of ions in an applied field is shown in Figure 1.2. The apparent mobility of an ion is the algebraic sum of electroosmotic and electrophoretic mobility.

The electrical double layer, electroosmotic flow and electrophoretic mobility are basic factors in CE, and the proper control of these effects will improve the CE separation. Other factors, such as, Joule heat, zone dispersion are also important in understanding and controlling the performance of CE separation.

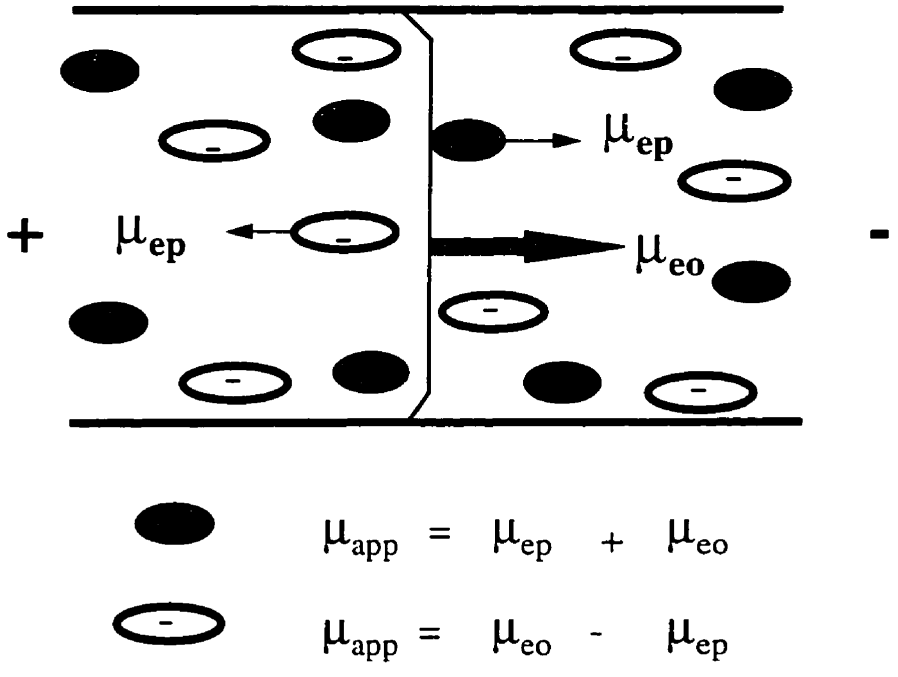

Figure 1.2 Mobility of ions in an applied field.

1.1.3. Electrochemical Detection Methods in CE

The common detection methods in CE are based on spectroscopy, but all of these have limitations. Absorption UV-Vis detection is limited by the short pathlength of the detection cells in small-diameter capillaries, and by the fact that a variety of compounds lack chromophores at useful wavelengths or have small absorption efficiency. Z-shaped UV detectors can increase pathlength, which enhances the detection sensitivity, however, the improvements are limited. Indirect UV detection is a universal mode of detection, but improvements in detection limits are required. Fluorescence detection is the most sensitive mode presently available in CE,[23,24] however, many samples of interest require pre- or post- column derivatization due to lack of inherent fluorescence. Mass spectrometry is potentially sensitive and provides structural information of the sample. However, the high cost of this instrument limits its widespread use. Electrochemical (EC) detection with microelectrodes (μm-electrodes) has been shown to be one of the most sensitive detection techniques even at extremely small sample volumes (μL to nL).[25] Other advantages for EC detection at μm-electrodes include fast response, negligible ohmic effect, and suitability for single-cell analysis. Therefore, these electrochemical detection techniques at μm-electrodes are potentially useful in CE.

In the present study of EC detection, metal ions were chosen as classic test analytes because a number of metal ions are electroactive at the accessible potential range of aqueous system, possess fast electrode responses at solid electrodes, and are

easily handled. In addition, separation and detection of trace metal ions in microseparation has growing practical significance because of its great environmental and biomedical concern. The analysis of trace metal elements helps in establishing modes and strategies to control and remove metal pollutants, in understanding the role that trace metals play in the structure and function of biological systems, and in developing new drugs, catalysts and other products.

The choice of electrode is an important factor in EC detection. The electrode must have an accessible potential range suitable for the given purpose, and it also should give sensitive electrode response for the analyte of interest. The most commonly used μm-electrodes include Hg film, carbon, and noble metal electrodes (such as Au and Pt). Of these, mercury film electrodes have the widest cathodic potential, however, these electrodes need to be renewed for reproducible electrode response, and they suffer from the anodic dissolution of Hg at potentials greater than 0.4 V Versus (Vs) SCE.[26] Compared to the other type of electrodes mentioned here, Pt electrodes have a narrower cathodic potential range due to the low overpotential of H^+ evolution, but this does not seriously limit their application. Both, Au and Pt μm-electrodes offer fast responses for some electroactive species owing to the formation of surface oxides (Au-O, Pt-O) at these electrodes; reduce activation barrier for the oxidation of aliphatic compounds because unsaturated surface d-orbitals (Au and Pt) can adsorb and stabilize free-radical intermediate oxidation products. Therefore, Au and Pt electrodes were chosen as working electrodes in most of this work.

1.2. History of Electrochemical Detection in CE

The first analytical application of electrochemistry was made in 1801 by Gruikshank,[27] who electrolyzed a solution of copper and silver qualitatively. Since then, various theories in determining the rate of electrode reactions and in describing the potential-current relationship were developed.[28-30] One successful step toward the potential-controlled EC technique was made by Heyrovsky,[31,32] who developed a DC voltammetric theory at a dropping mercury μm-electrode in 1922, and interpreted the current-potential characteristics exhibited by the dropping mercury electrode. This development marked a significant advance in EC methodology and paved the way to novel detection modes in electroanalytical chemistry. For this contribution, he was received the Nobel prize in 1959. For successful EC detection in separation systems it is critical to meet simultaneously the requirements for both separation and detection. The first on-column EC detection for microcolumn liquid chromatography (LC) was described by Manz and Simon in 1983,[33] where an 1 μm i.d. ion-selective electrode was inserted into the end of a 25 μm i.d. LC column for the potentiometric detection of K^+. A similar experimental device was used by Jorgenson's group in 1984 for amperometric,[34] differential pulsed,[35] and scanning voltammetric[36] detection of ascorbic acid, catechol, and 4-methylcatechol in LC. Other applications of EC-LC for inorganic,[37] organic,[38,39] biomoclecules[40,41] and small molecules[42] have been discussed in literature.

The application of the EC detection in CE is not straightforward. First, the size and geometry of the detector cell must meet the requirements of sample volumes in the

range of several nL to 10 nL; secondly, the method of measurement must minimize the influence of high separation voltages on the detection system; thirdly, signal handling techniques should reflect correctly and precisely the characteristics of flowing analytes. μm-electrodes can be used with extremely small sample volumes without loss of sensitivity, and modern computer technology offers sampling rates fast enough to match the change in concentration of the analyte in flowing systems. However, reducing the effects of the high voltage is more complicated.

1.2.1. End-Column EC Detection

One approach used to reduce the interference from the high separation voltage is by introducing a grounded fracture close to the end of the capillary where detection is performed. This method is termed off-column EC detection. The first off-column EC detection device was introduced by Wallingford and Ewing[43] who used a porous glass coupler to decouple the electrode from the separation potential, and a typical diagram of off-column electrochemical detection is shown in Figure 1.3 A. The fracture was located before the end of the capillary and covered with the porous glass coupler (D), which allows ion movement to the ground electrode but not bulk flow. As a result, the separation voltage drops across the fracture, and analytes are pumped into the detection capillary by electroosmotic flow. Besides the porous glass coupler, porous graphite,[44] Nafion,[45] and Pd metal[46] tubes were also used to decouple the high separation voltage.

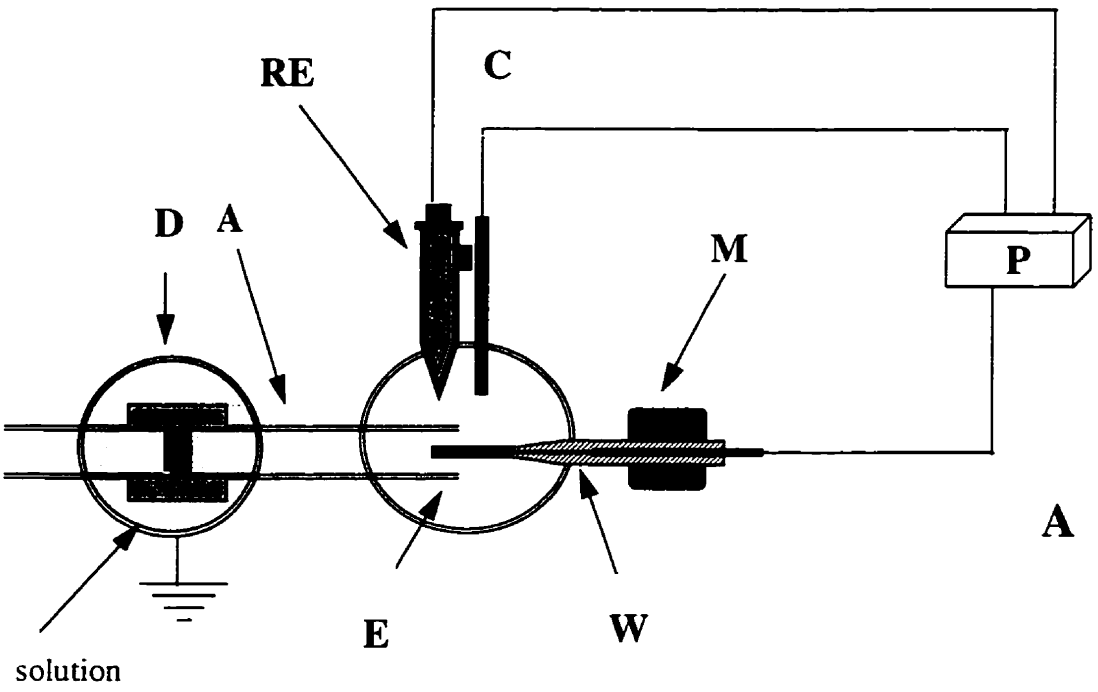

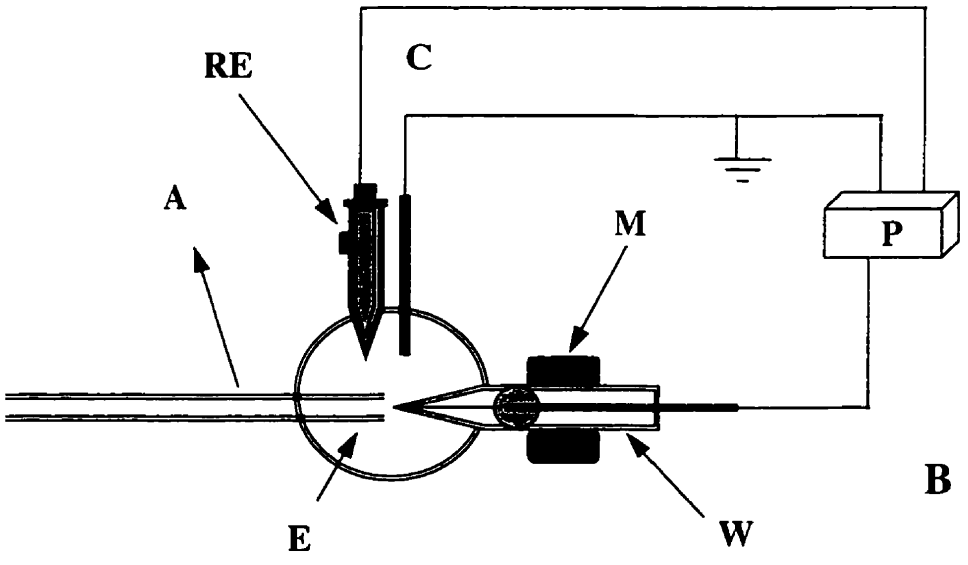

Figure 1.3 Diagrams of off-column (A) and end-column (B) electrochemical detection: (A) capillary; (C) counter electrode; (E) electrolyte reservoir; (D) decoupler; (M) micropositioner; (P) potentiostat; (RE) reference electrode; (W) working electrode.

Of these materials, Nafion and Pd metal tubes possess high mechanical strength, but the latter is restricted in application to several types of electrolytes. Although off-column EC can minimize the interference of high separation voltage, a major drawback of these systems is the difficulty associated with making the porous joint. This limitation has hold back the widespread application of this mode in CE, although some reports of its use exist from literature.[47-49]

An alternative setup, in which the working electrode is placed outside of the end of the separation capillary, has been reported in CE.[50] This technique is termed end-column EC detection, and requires no porous joint. Still, a concern in end-column EC detection is the influence of the high separation voltage. Fortunately, for small sized capillaries this is not significant because of a rapid decay of the electric field strength at the end of these capillaries.[51,52] A typical end-column EC detection diagram is shown in Figure 1.3 B, where the alignment of the working electrode with the capillary is usually adjusted with a three-dimension micropositioner. Although there is no need to isolate the EC detector from the high separation voltage at small capillaries, the analytical and background signal is still affected by the residual electric field at the end of capillary. Such an effect depends on the placement of the electrode and internal diameter of the capillary. Therefore, it is worthwhile to examine these experimental conditions to minimize the effect of high separation voltage on EC detection although background noise from high separation voltage has been studied in few papers.[52]

1.2.2. Constant-Voltage Amperometric Detection

Several electrochemical approaches that have been investigated in CE are amperometry, conductimetry, voltammetry and potentionmetry. Of these, amperometric techniques have been most commonly used because they are simpler to implement experimentally and provide good sensitivity. Amperometric detection includes two modes: constant-voltage and pulsed-voltage detection. Constant-voltage amperometric detection (CVD) at solid electrodes is the simplest detection approach for electroactive compounds, and has been used for the determination of parathion,[53,54] catechol and catecholamines,[40] dopamine,[55] and chlorophenol[56] in LC and flowing injection. However, inconsistent electrode response[43,57] is often caused by fouling of the electrode, and distortion peaks[58,59] were reported for the direct reductive detection of protein and carbohydrates at solid electrodes due to sample matrices and/or reaction products of the analytes. Electrode contamination also occurred at Au and Pt electrodes for CVD analysis of metal cations.[60] The use of Hg liquid-film electrodes can provide some improvements in reproducibility,[61,62] but the utility of this approach is limited by the stability of the Hg films deposited onto a gold substrate.[62] Although the problems associated with electrode fouling are less serious in flowing systems where the working electrode is continuously washed with the electrolyte and exposed to the sample zone for only short period, reproducible analysis still requires improved electrode stability. Solid electrodes are most effectively cleaned by mechanical polishing; this process, however, is tedious and

requires dismantling of the detector. Continuous mechanical cleaning in flowing liquids by using blades moving against the electrode or adding particles of an abrasive material to the liquid[63] is onerous and unsuitable for use with CE separation. In another approach,[64,65] the working electrode (Pt) was regularly lifted from the solution, heated to a red glow by passing electrical current through the electrode, and re-immersed in the solution. Obviously this method is rather awkward and gives poor reproducibility in the response due to the change in the electrode surface.

Other approaches that can be used to extend the range of constant-voltage detection involve the use of indirect amperometric detection and chemically modified electrodes (CMEs). Indirect amperometric detection is feasible for metal ions, and but it is usually not recommended due to its poor sensitivity, and some unexpected problems when an electrophore is added into the electrolytes.[66] The use of CMEs may offer some specific advantages, such as, acceleration of electron-transfer reactions, and permselective transport and preferential accumulation of analytes at the electrode surface. Although some CMEs provide consistent electrode responses combined with very low detection limits for certain applications,[67-71] their use is limited by practical problems, such as slow response, low capacity and low mechanical strength of thin films.[72-74] Additionally, some CMEs consisting of special coated films can not last very long and need recoating with new layers to keep a sensitive and reproducible electrode response. Consequently, the growth of CMEs is restricted by these limitations.

1.2.3. Pulsed-Voltage Amperometric Detection

Pulsed amperometric detection (PAD) is a detection scheme based on a multi-step potential waveform which achieves detection of the analytes, and cleaning and reactivation of the electrode surface. Electrochemical cleaning and activation by cycling of the electrode potential between positive and negative values was first reported in the 1960s.[75] The most commonly used pulsed-potential waveforms include bi- and tri-step shapes. Pulsed voltage prevents large concentrations of electrogenerated species from accumulating at the solid electrode, and maintains electrode activity by alternating oxidation and reduction potentials. Such a cleaning strategy has been applied to the electrochemical detection of many organic and inorganic substances: good detection limits and long-term stabilities of PAD detection have been claimed for amino acids,[76,77] aminoglycosides,[78] carbamates,[79] alkanolamines,[80] starch,[81] inorganic and organic sulfur-containing compounds,[82,83] and carbohydrates[84-87] at Pt and Au electrodes. Most of these applications were used in flow injection or LC.[76-96] PAD techniques have recently been applied in CE[97-99] and such applications are increasing. For metal ions, results reported for flow-injection systems for Fe and Cu[90] suggest that pulsed voltage methods may be required, and this conclusion was also suggested by studies in CE systems.[62] Although PAD has been applied for a number of species, detailed and systematic study is lack in CE, especially for metal ions. To optimize PAD analysis, the experimental parameters, such as pulse waveform, the electrode potential, and selection of analytical data, need to be examined for improved EC performance because these parameters affected the analytical and background signal.

1.2.4. Voltammetric Detection

Voltammetric detection by electrochemical stripping has always been regarded as one of the most sensitive electrochemical techniques. Combined with a typical preconcentration time of 5 to 10 min, detection limits are down to 10^{-9} to 10^{-11} mol/L.[100-104] However, most early applications were applied to bulk solutions and limited to slow scan rates[101-106] (less than 10 V/s) to avoid broadening of stripping peaks, which could result in poor discrimination of the analytes; these procedures usually involved the use of a hanging mercury drop or a mercury-film electrode.[107-109] Slow scan voltammetry can not be used to monitor narrow analyte peaks in flowing solutions. The use of high-frequency potential waveform with μm-electrodes can eliminate this limitation. Fast scan voltammetric detection was first introduced into LC and flow injection system in the 1980s.[35] and its detection potential in LC for electroactive compounds has been examined by several groups.[110-112] When these studies were presented, there were no reported investigation of scanning voltammetric detection in CE. Application of fast voltammetric detection in CE is a new area. Potential advantages of fast scanning voltammetric detection in CE include peak purity evaluation; characterization of electrochemical behavior of the background electrolyte and the analyte; resolution of co-migrating analytes; use of a preadsorption voltage in the waveform to permit analyte preconcentration; and selection of optimum voltage ranges for integration of the anodic and/or cathodic currents in the cyclic voltammograms. Therefore, the fast scanning voltammetry is worth to be explored in CE. For fast CV detection, experimental parameters, such as sweep rate, electrode potential, and preconcentration time, affect the electrode response and need to be optimized.

1.3. Principle of Electrochemical Detection

1.3.1. Electrochemical Process

Electrochemical detection is often accomplished by monitoring the electron transfer during the reduction/oxidation process of the analyte shown as follows:

$$O + ne^- \rightleftharpoons R \qquad (1.3)$$

where O and R are the oxidized and reduced forms, respectively, of the redox couple. Current that originates from oxidation or reduction reaction is called faradaic current. The driving force of the reaction is determined by the potential difference across the electrode/solution interface as described by the Nernst equation.

$$E_e = E_o + R_gT/nF \ ln \ (a_o/a_R) \qquad (1.4)$$

where the activities of O and R are denoted by a_o and a_R, respectively; E_o is the standard potential for the redox reaction; R_g is the universal gas constant (8.314 JK^{-1} mol^{-1}); T is temperature in Kelvin; n is number of electrons transferred in the reaction; and F is Faraday constant (96,487 Coulombs). In a practical EC-CE system, the oxidation and reduction potentials of an analyte are affected by the electrode, the electrolyte and other species existing at the electrode, and the electric field from the high separation voltage. Therefore, the detector potential should be chosen according to its practical reaction potentials, which can be obtained by an on-line end-column cyclic voltammetry.

In an electrochemical solution, an electrical double layer forms at the electrode /solution interface, and the electric double layer resembles an ordinary capacitor. The total capacitance (C) of the double layer is a combination of the capacitance of the compact layer (C_H) and the diffuse layer (C_D) in series, thus the total capacitance is given as follows,

$$1/C = 1/C_H + 1/C_D \qquad (1.5)$$

In general, the electrical capacitance at the solid/solution interface is $\sim 10^{-5}$ Fcm^{-2}.[113] The charge of the double layer results in a non-faradaic charging (capacitant) current, which is often a considerable component of the background currents. The adsorption or desorption of electroactive and electroinactive species lead to another type of non-faradaic current; in these instances, no chemical reaction occurs, and consequently electrons are not completely transferred across the electrode-solution interface. During electrochemical detection, the total current which flows through the electrochemical cell is the sum of the faradaic and non-faradaic currents.

1.3.2. Practical Consideration

The composition and structures of an electrical double layer at an electrode surface are important because electron-transfer reaction often takes place in the layer. In practical electrochemical system of interest, the property of the electrical double layer (the electrode surface) may be changed by the presence of organic compounds and deposition

of metals. Such changes will influence the electrochemical process at the electrode. Therefore, the effects of these factors on the electrode process should be concerned, especially on H^+ and O_2 reduction, because they are common electrochemical reactions and may be major contributors to background current and noise in aqueous system.

1.3.2.1. Adsorption of Organic Compounds

For the CE separation of metal ions, organic compounds are often chosen as electrolytes, and thus the adsorption of the electrolytes needs to be considered. It is well known that organic molecules can adsorb on Au and Pt electrodes, and the characteristics of these adsorptions are a result of competing interactions of the molecules with two phases, the electrode surface and the solution. According to the nature of adsorption forces, the adsorption at electrodes in real situations can be classified in four different types: purely electrostatic adsorption,[114,115] specific ionic adsorption,[116] unchanged species adsorption,[117] and chemisorption.[118] The adsorption of some organic molecules on Pt and Au electrodes and the role of adsorbed species have been investigated by various techniques, such as cyclic voltammetry,[119,120] FTIR spectroscopy,[121] potentionstatic charge displacement,[122] scanning tunneling microscopy,[123,124] UV/Visible reflectance spectroelectrochemistry,[125] in-site infrared and surface-enhanced Raman spectroscopy,[126] chronocoulometry,[127] and radiotracer techniques.[128,129] The results from the above studies illustrate that surface reconstruction of the electrode occurs in the presence of organic species, and this reconstruction affects the electrochemical reactions at the electrode.[119-129] It has been reported that some adsorption can accelerate

or inhibit the electrochemical reactions at the electrode and/or cause a shift in the potential of zero charge (PZC).[130,131] For example, Bromic ions (Br^-) adsorbed at a Pt electrode increased the reaction rate of hydrogen evolution, but these ions adsorbed at Pb or Ga inhibited hydrogen evolution.[132] The results for cyclic voltammetric studies show that the adsorption of acridine and quinoline derivatives inhibited oxygen reduction.[100] The inhibitation of electrode processes caused by the adsorption of electroinactive substances arises from the occupation of catalytic sites by these molecules.[133] From a practical perspective, the adsorption of organic molecules may play an important role in EC detection, and thus should be considered.

1.3.2.2. Deposition of Metals

During the detection of metal ions, metals from the reduction step may deposit on the electrode surface, and consequently affect the electrochemical reactions of analytes and other species existing on the electrode surface because the deposition of metals can cover the electrode surface and function as a second type of electrode. The studies from cyclic voltammetry showed that deposition of Zn and Tl on Au and Pt surfaces suppressed hydrogen evolution.[134,135] Results reported for scanning tunneling microscopy studies have revealed that Cu, Pb and Ag deposited on Au[136,137] and Pt[138,139] electrodes partially or completely inhibit oxygen reduction. It has been reported[140,141] that the reduction of H_2O_2 is inhibited on Cu and Ag, on which O_2 gains only two electrons to form H_2O_2. Therefore, deposition of metal layers at the electrode surface is important because metals

have different electrochemical properties from Au or Pt electrode and their deposition could change electrochemical reactions on the electrode. Although the positive potential in PAD and fast CV voltammetric detection may be able to prevent the deposition of some metals, a comprehensive examination for the deposition of metals and its effect on the electrode response is desirable for the detection of metal ions.

1.3.3. Analytical Signal

Potential-controlled EC detection involves the measurement of current at controlled potential, which can be constant, a continuous pulse and triangular shaped potential, or one or more combinations of these. The electrode response are often displayed in the form of current (or charge) versus time, which is termed electropherograms, and/or in the form of current versus potential, which is termed voltammogram. Cycling of the electrode potential between positive and negative values is a common detection mode at solid electrodes, and typical simple bipolar and triangular potential waveforms and their corresponding responses are shown in Figure 1.4. For a bipolar potential waveform (Figure 1.4A), the current response is often time-domain signal (Figure 1.4B). The negative potential is for reduction reaction and the corresponding cathodic current decays to a steady state (faradaic current) in several milliseconds[143]; the positive potential is for oxidation reaction and the corresponding anodic current decays to zero. The initial high current observed in Figure 1.4 B is from the charging current and it decays in several microseconds.[142] For a triangular potential waveform (Figure 1.4C),

the current response can be time-domain (Figure 1.4D) and potential-domain (Figure 1.4E) signals. The oxidation reaction occurs at the forward sweep and generates anodic current; the reduction reaction generates cathodic current at the backward sweep. Both cathodic and anodic currents can be used as analytical signals, and it is possible to select the data points over a certain period upon one potential step as the analytical signal. Since the electrode response depends on experimental parameters, such as the value and duration of the applied potential, and waveform shape and frequency, thus optimization of these parameters is useful for maximum S/N. Processing the current and presenting some modified signal as a function of either time or potential can often offer some S/N advantages over the original current signal. Common modifications are to use "background"-subtraction, signal averaging, and integration of current versus time. In addition, since faradaic, charging and adsorption currents have different distribution in fundamental and higher harmonic response, the use of Fourier transformation may be able to differentiate signal from noise to improve S/N.

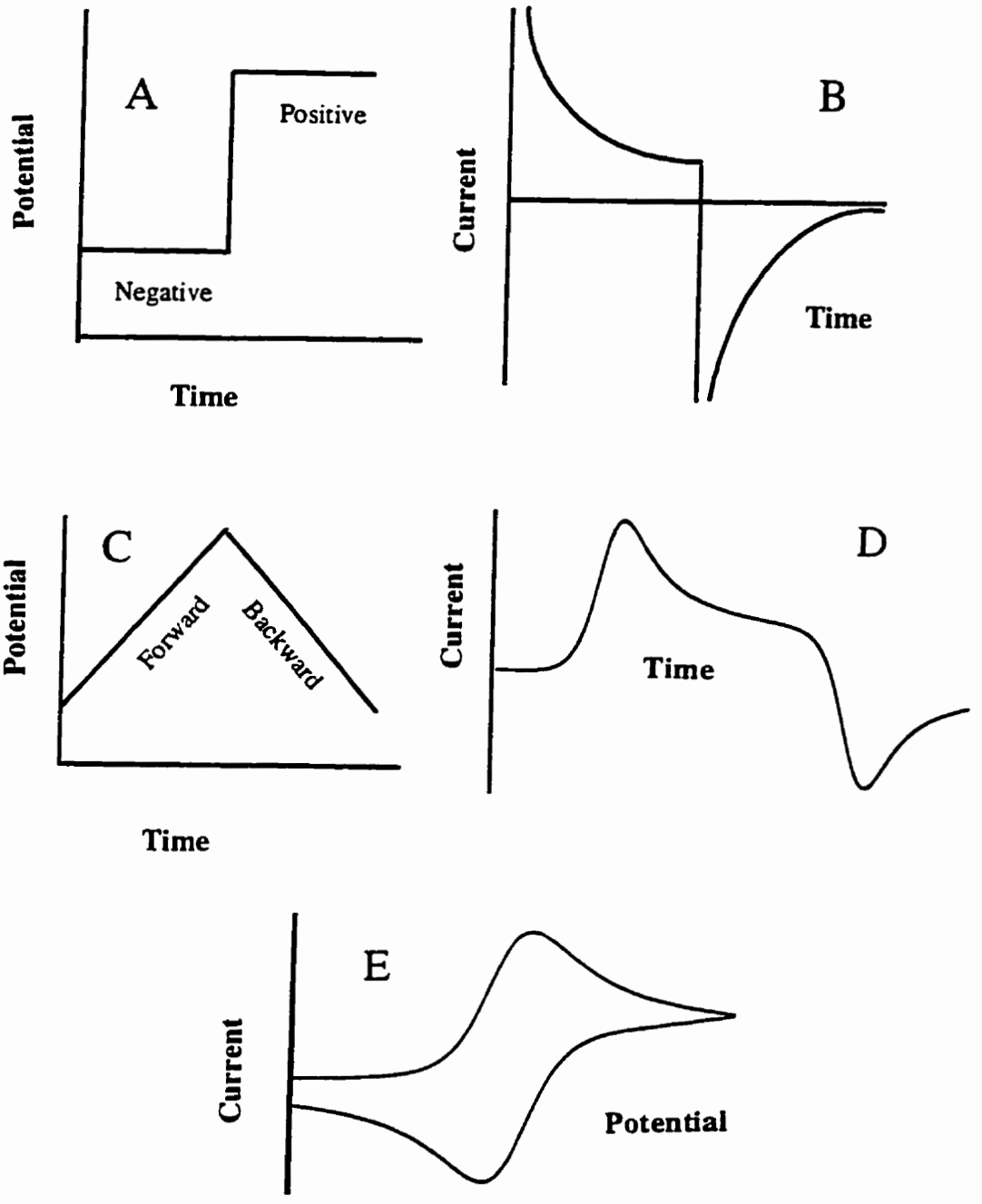

Figure 1.4 Variation of voltage and current with bipolar and triangular potential waveforms. A and B, applied pulse-potential waveform and corresponding current-time response; C, D and E, applied triangular-potential waveform, corresponding current-time, and current-potential signals.

1.4. Scope of Present Research

As the first step in this, a number of the CE experimental conditions were optimized. Although these studies were not the main goal of this thesis, they were important because optimum conditions were required for a proper evaluation of EC detection in CE. These experimental conditions included the concentration and pH in the electrolyte required for separation of the analytes, capillary size and conditioning, alignment of the electrode with the capillary, and separation voltage. The ultimate goal for these studies was to achieve high-separation efficiency, reproducible EOF, and a complete separation for the test metal ions to permit a proper focus on EC investigation.

To understand electrode response, required to optimize EC detection, electrochemical behavior of the electrolyte and analytes, and the factors affecting these behavior were examined by on-line CV at both Au and Pt electrodes. Such studies can provide information on the reaction potential region, and the relative kinetics and reversibility of the analytes. The processes of adsorption of organic electrolytes and deposition of metal ions, and their effects on the analytical and background signal, and H^+ and O_2 reductions, were examined because these factors may change the electrode surface and thus the electrode response.

The first EC approach studied in CE was PAD at both Au and Pt 25 μm disk electrodes. To optimize PAD detection, pulse duration, and the applied oxidation and reduction potentials were evaluated in terms of analytical and background signals for both cathodic and anodic detection. To evaluate the performance of the detection system, PAD

was used for the analysis of spiked and real samples, and compared with atomic adsorption spectrometry. The reproducibility and linearity of PAD detection were examined by repetitive injection and calibration curves.

To further improve S/N, a number of experimental approaches were examined. These parameters included sample stacking, potential waveform shape, data selection, and signal analysis techniques. Stacking conditions were evaluated to obtain lower detection limits via sample preconcentration without loss of either separation efficiency or reproducible electrode response. A variety of multistep and fast-frequency potential waveforms were evaluated to optimize S/N. Another alternative approach is to monitor the first and second harmonic responses by means of Fourier transformation. Since capacitance current is more symmetric than faradaic current, the second harmonic Fourier transformation is expected to improve S/N via reducing the capacitance current, which is major component of the background current.

The second EC approach investigated was a fast-scan voltammetric detection. In this study, CV current and CV charge from integration of current versus time were used as analytical signals. To optimize the fast CV detection, the experimental parameters that affected the electrode response were examined, and these parameters included sweep rate over 25 to 1,000 V/s, 25 and 10 μm Au electrodes, CV potential, preconcentration. Co-migrating analytes were identified and quantified by two metal ions with sufficient different electrochemical behavior to evaluate the extra resolve power of the fast CV detection in CE.

2. EXPERIMENTAL SECTION

2.1. CE Separation

2.1.1. CE Apparatus and Procedures

Polyimide coated fused silica capillaries, 25 μm ID × 350 μm OD, were obtained from Polymicro Technology Inc. (Phoenix, AZ); typical lengths were of 55 to 65 cm. Before use, new capillaries were washed with H_2O for 0.5 h, then with 0.1 mol/L HCl for 1 h, and finally with the operating electrolyte to obtain reproducible EOF. Between separations, the capillary was rinsed with the separation electrolyte for about 5 min. This process was done by a syringe sucking these solutions through the capillary at a linear flow rate 5 to 10 mm/min. The capillaries were cut with a cleaving tool from Supelco (Bellefonte, PA) and a clean cut is needed to avoid sample adhesion during injection. For capillary storage, a flow of the electrolyte was maintained by placing the two ends of capillaries in electrolyte with a height differential of approximately 10 cm; 0.8 mL polyethylene vials (Cole-Parmer Instrument Co., Niles, IL) were used as containers for the carrier electrolyte and for the standards and samples. The electrolytes were remade every two to three months and were replaced daily in the separation reservoir to avoid chemical and pH changes. All CE solutions were filtered through a 0.2-μm Nylon-66 membrane

syringe filter (Cole-Parmer Instrument, Chicago, IL). The anodic end of the high-voltage (0 to 30 kV) power supply (Spellman, High Voltage Electronics Corp. Plainview, NY) was placed in a Plexiglas box equipped with a safety interlock switch on the access door. Platinum wires were used as the electrodes. Co-electroosmotic mode (electroosmosis and electrophoresis have the same direction) was used for the separation of metal ions. One end of the capillary for sample injection was connected with the anode of the power supply, and the other end for the EC detection served as the ground.

2.1.2. Sampling Injection

Metal ion stock solutions (~ 0.01 mol/L), were diluted to the desired concentration with the operating electrolyte prior to injection. Two modes of sample introduction were used: hydrodynamic and electrokinetic injection. The hydrodynamic injection introduces samples into fused-silica capillaries by placing one end of the capillary in a sample vial positioned at a certain height (10 cm) over the other end of capillary; and electrokinetic injection introduces samples into the capillary by employing 5 kV potential over 10 s at the anodic side. Under these sampling conditions for Tl^+ (5.0×10^{-5} mol/L) for hydrodynamic injection, the volume introduced into the end of the capillary was calculated[20] to be approximately 1.7×10^{-3} μL; and for electrokinetic injection, the amount of sample injected[20] was 1.8×10^{-13} mol which was equal to the analyte in 3.7×10^{-3} μL of the sample solution, and the sample volume injected into capillary was evaluated by electroosmotic flow to be approximately 6.2×10^{-4} μL.

2.2. Electrochemical System

2.2.1. EC Apparatus

The three-electrode electrochemical system consisted of a saturated KCl calomel reference electrode (Fisher Scientific Co., Ottawa, ON), a Pt wire (0.5 mm^2) counter electrode, and 10 or 25 μm Au or Pt home-made disk working electrodes. The counter electrode served as the ground for the separation voltage. The end-capillary EC detection was used. The alignment and distance between the working electrode and the end of the separation capillary was adjusted with a XYZ micropositioner (± 1 μm) (Kinger, Garden City, NY). The detection cell and home-made potentionstat were placed in a Faraday cage to minimize environmental noise. The schematic diagram of CE unit with electrochemical detection is shown in Figure 2.1.

The electrochemical system was controlled with a pentium/16 MB RAM IBM personal computer equipped with a PCL-818 high performance data acquisition card (B & C Microsystem Inc. Sunnyvale, CA). Computer programs for constant-voltage and pulsed amperometric and for on-line cyclic voltammetric detection were used to control the application of the potential to the electrode, the collection and display of the data.

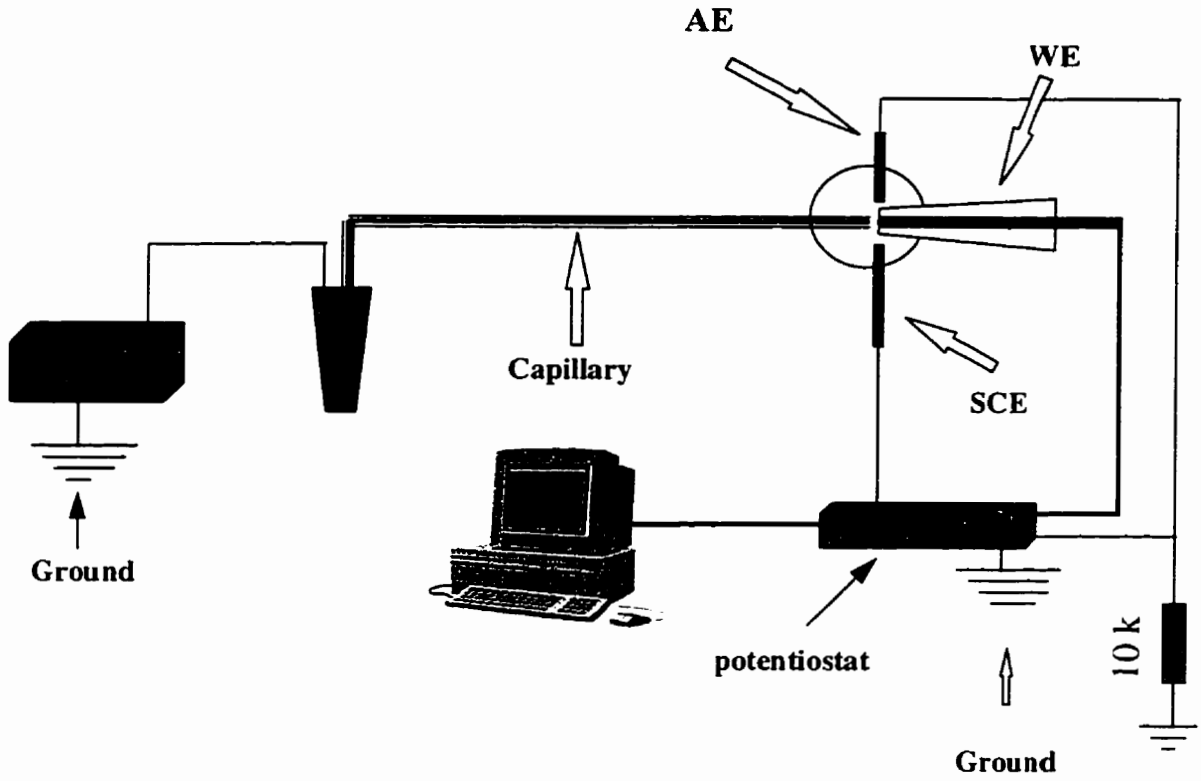

Figure 2.1 Schematic diagram of CE separation with an end-column EC detection. (HV), high-voltage supply; (WE), working electrode; (SCE), saturated KCl calomel reference electrode; (AE), Pt auxiliary electrode. This is a schematic diagram for the potentiostat shown in Figure 2.3.

The electric circuit diagram of the potentiostat for constant and pulsed voltage amperometric detection is shown in Figure 2.2 and for fast CV detection in Figure 2.3, where all resistors had an error ±1%. The circuit in Figure 2.2 is basically composed of a summing inverting amplifier (No.1) and a differential amplifying circuit with a gain of 100 (Nos. 2,3, and 4). A high-impedance amplifying circuit (No. 5 and 6) was placed in the reference-electrode input circuit to ensure that the current flowing through the capillary did not pass through the reference electrode. Several capacitances were placed in the output circuit and the working electrode input circuit as low-pass filters to minimize electronic noise. The voltage produced by the signal current was amplified via Nos 2, 3 and 4 operational amplifiers and sent to the AD converter with the minimum step size corresponding to 0.0015 pA. The data obtained were monitored in real time on the computer screen. The amplifiers were LF353N wide-bandwidth dual-JFET operational amplifier obtained from Electronics (Toronto, Canada). The potentionstat in Figure 2.3 was built with 4 FET operational amplifier (TL074, National semiconductor Corp.) and was designed to operate together with a high speed data acquisition card (PCL-818), which provided four digital output channels, two digital-to-analog converters (ADCs), and an analog-to-digital converter (DAC). Three input voltage lines E_{in1}, E_{in2}, E_{in3} are shown in the diagram. The E_{in1} is used to accept the excitation waveform generated by the first DAC on the computer card, and this converter has a fixed reference voltage; the E_{in2} is used for positive feedback IR compensation, and it accepts the output from the second DAC; the E_{in3} is used to adjust offset of the input voltage.

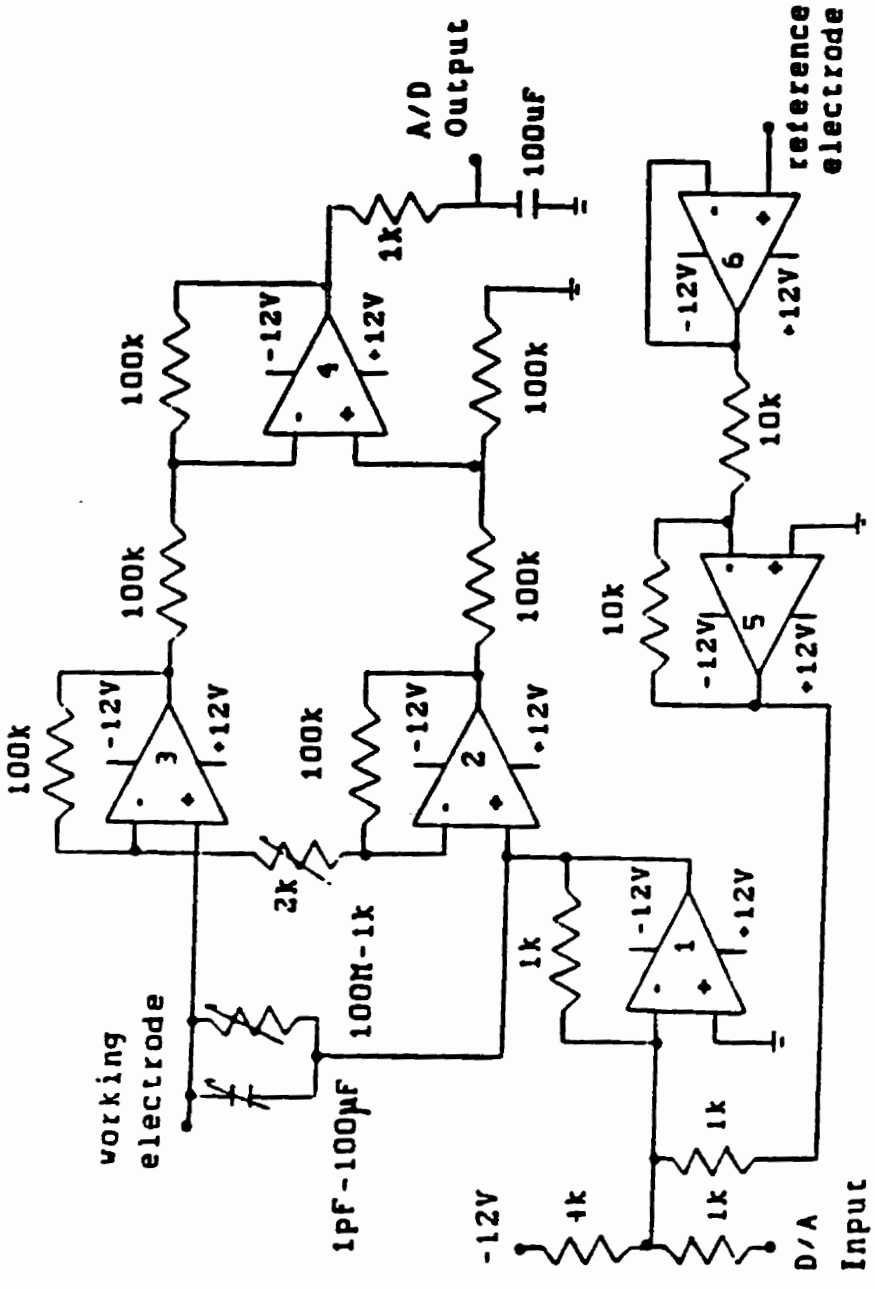

Figure 2.2 Electric circuit diagram for amperometric detection. This is the schematic for the potentiostat used for amperometric detection.

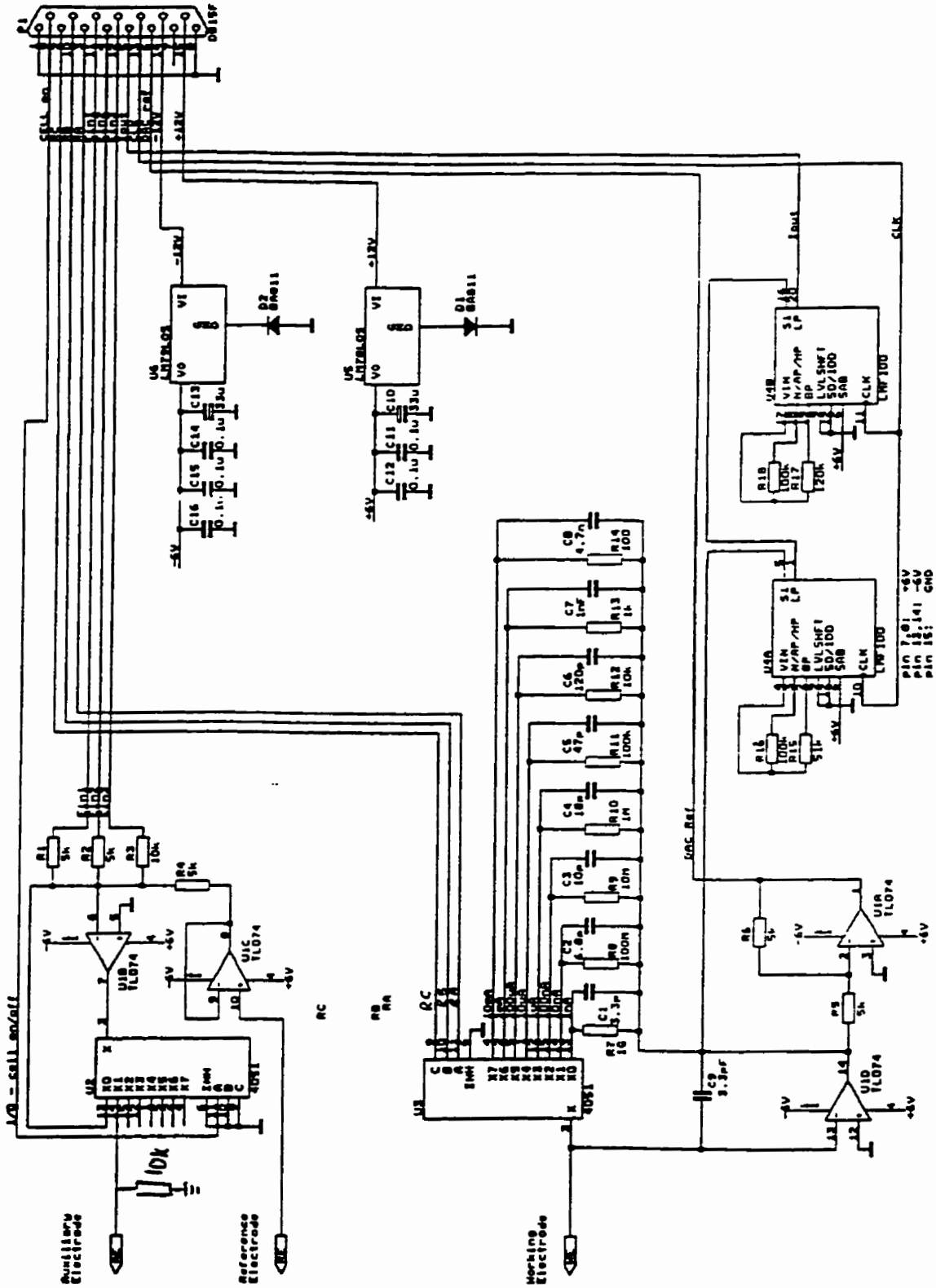

Figure 2.3 Electric circuit diagram for fast-scan voltammetric detection

The sensitivity of the output current can be changed from 0.01 A/V to 10^{-9} A/V by changing the feedback resistor of the current follower, which is selected by means of an eight-channel analog multiplexer (4051, National Semiconductor) controlled by the computer. The output of the current follower is inverted by an U1A TL074 amplifier to provide positive feedback IR compensation and used as a reference voltage for the second DAC, which acts as a current divider, and the thus the fraction of current used in positive feedback can be digitally controlled. Details in regard to the electric diagram was described elsewhere.[145]

2.2.2. Fabrication of μm-electrodes

A diagram of the microelectrode is shown in Figure 2.4. Au and Pt μm-electrodes (10 and 25 μm) from gold (99.99%) and platinum (99.9%) wires obtained from Goodfellow (Cambridge, England), were made by sealing a piece of wire (about 10 mm in length) into the tip of a soft-glass tube with a Bunsen burner. New μm-electrodes were polished with carborundum abrasive paper and 0.3 μm alumina powder. The other end of wire was connected to a copper lead by a piece of solder. Hg film μm-electrodes were made by electrochemically depositing a Hg film (~ 2-5 μm thick) on a 25 μm Au or Pt electrode. The plating was carried out in an aqueous solution of 1 M $Hg_2(ClO_4)_2$ and 1 M $HClO_4$, with an excess of elemental mercury, under constant-current conditions. A detailed procedure was described elsewhere.[62]

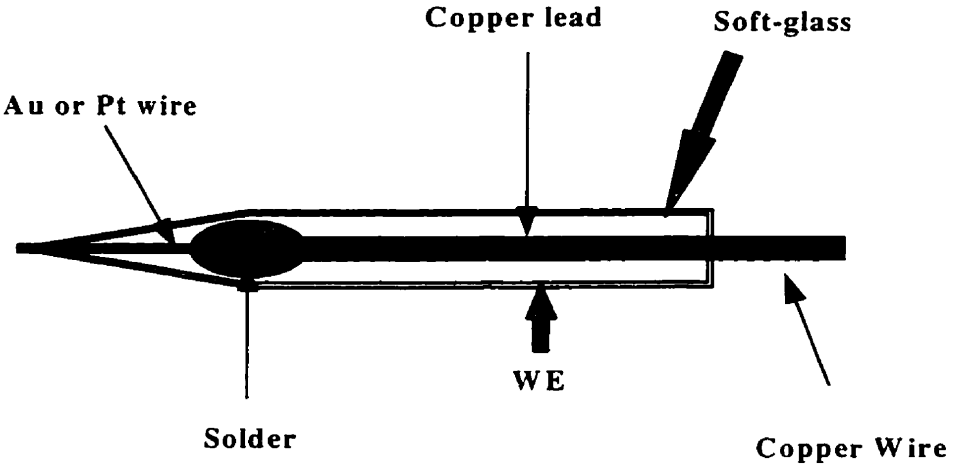

Figure 2.4 Diagram of working electrode.

2.2.3. Electrochemical Methods and Procedures

2.2.3.1. Cyclic Voltammetric Studies

For the CV studies, a triangular potential waveform was imposed on an electrode and the current response was observed. Prior to the CV sweep, each metal ion was reduced at an initial potential which had a value in the range of -700 to -1200 mV, depending on the standard potentials of metal ions for a certain time (t_p). The electrode potential was then scanned linearly from the initial potential (E_1) to a positive vertex potential (E_2) in a forward direction and then back to E_1. The selection of the CV potential range depended on the nature of the analyte. The voltammogram was recorded at ~ 4,000 data points per second (each point was an average of 10-17 A/D conversions). Several voltammograms ($\geq$ 15) were obtained while a narrow analyte peak passed by the

working electrode. In the voltammogram, reduction currents were recorded as positive signals, and oxidation currents as negative signals.

2.2.3.2. Pulsed Amperometric Detection

Pulses for amperometric detection were either bipolar with a frequency of 5 to 1000 Hz, or consisted of a combination of several square pulses with different frequencies. For most PAD studies, the potential for the reduction of analytes was -1200 to -700 mV, and for the oxidation of analytes, 100 to 200 mV. For PAD with frequencies from 5 to 8 Hz, the analytical signal monitored was the average current measured over the last 24, 48, or 72 ms of the reduction pulse for cathodic detection, and over the first 48 or 72 ms of the oxidative step for anodic detection. For PAD with frequencies of more than 8 Hz, the signal was selected by four different methods: the average current measured over whole reduction pulse for cathodic detection; the average current over whole oxidation pulse for anodic detection; the total anodic and cathodic currents; and the average cathodic and anodic current over one pulse.

2.2.3.3. Fast Scan Voltammetric Detection

For fast scan voltammetric detection, the potential waveform used was similar to that for cyclic voltammetric studies. Two types of signals were used for the analytical response. One was the maximum peak current in the voltammogram, referred to as the CV current. The second was the current integrated vs time over the CV, with units of

Coulombs; this response would be referred to as the CV charge. The current was integrated between the initial potential (E_1) and the vertex potential (E_2), and in the electropherogram was plotted as $[Q_{(t)} - Q_o]$, where $Q_{(t)}$ is the CV charge for one scan, and Q_o is the average CV charge for the background electrolyte obtained during the first 7-10 scans in the CE separation. Since CV charge gave better S/N, this is the response used for most of the data discussed in the fast scan voltammetric studies. For all of the above experiments, oxygen was not removed unless otherwise indicated.

2.3. Sample Preparation

Melted snow samples from campus were filtered through a 0.45-micron Nylon-66 membrane filters from Cole-Palmer (Cole-Palmer Company, Chicago, IL), and stored in acid cleaned polyethylene bottles; sample pH was adjusted with acetic or nitric acid to 4.8.

2.4. Chemicals

2.4.1. Inorganic & Organic Chemicals

All chemicals were of analytical grade and were used without further purification. The solutions were prepared from double-distilled deionized water (Corning, Mega-Pure system, MP-6A & D2, Corning, NY), and were stored in the dark. Chemicals for the electrolyte, creatinine was purchased from Sigma (Sigma, St. Louis, MO); α-hydroxyisobutyric acid (HIBA) was from Aldrich (98% Aldrich, Milwaukee, WI); succinic acid was from AnalaR (The British Drug Houses Ltd.); Lactic acid, L-tartaric acid and

malonic acid were from Aldrich (98% Aldrich, Milwaukee, WI); Acetic acid, HCl, H_2SO_4 and NaOH were from BDH (BDH, Toronto), and Phosphoric acid was from Baker (Baker Chemical Co., Phillipsburg, NJ). Chemicals for neutral marker test, catechol was from Aldrich (98% Aldrich, Milwaukee, WI); 1.4-benzoquinone and 1.4-dithiabenzene were from Eastman Kodak Company (Rochester, NY).

2.4.2. Metal Ions

All chemicals were of analytical grade and were used without further purification. Stock solutions of metal ions (0.01 mol/L) were prepared in deionized water, and samples were diluted to the desired concentration before use. Reagent grade metal salts used were: thallium(I) nitrate, chromium(III) acetate, mercury(II) chloride, iron(III) nitrate, and nickel (II) nitrate purchased from Fisher (Fisher Scientific Co. Fair Lawn, NJ); lead (II) nitrate from (Anachemia, Montreal); cadmium(II) nitrate and zinc(II) nitrate from (Merck & Co. Inc. Rahway, NJ, USA); silver(I) acetate from (BDH, Toronto); cobalt(II) acetate from (General Chemical Division, Allied Chemical & Dye Corp., NY); iron(II) sulfate from (J. T. Baker Chemical Co. Phillipsburg, NJ), and copper(II) acetate from (BDH, Toronto).

2.5. Principles

2.5.1. Signal Analysis Techniques

The following is a brief overview of the principles involved in the data treatments used in these studies. More detailed discussions of these principles can be found elsewhere.[100] When a small ac potential

$$E_{AC}(t) = \Delta E \cos(\omega t) \qquad (2.1)$$

is applied to a working electrode, the resulting current can be expressed as,

$$I_{AC}(t) = \Delta I_1 \cos(\omega t + \varphi_1) + \Delta I_2 \cos(2\omega t + \varphi_2) + \Delta I_3 \cos(3\omega t + \varphi_3) + \ldots \qquad (2.2)$$

where ΔI is the magnitude of the ac current, ω is the angular frequency of the applied potential waveform ($\omega = 2\pi f$, f is the frequency of the applied potential waveform), φ is the phase shift of the ac current with respect to the applied potential, and the subscripts refer to a particular harmonic of the current response. The most important in eq. (2.2) is the first term (called the fundamental response of the electrode) which describes the current at the same frequency as the applied potential. The magnitude, ΔI_1, and the phase shift, φ_1, depend on the electrode impedance:

$$\Delta I_1 = \frac{\Delta E}{|Z|} \qquad (2.3)$$

$$\varphi_1 = \text{atan}\,[Z_{rel}/Z_{img}) \qquad (2.4)$$

where Z_{rel} and Z_{img} are real and imaginary components of the electrode impedance and $|Z| = \sqrt{Z_{rel}^2 + Z_{img}^2}$ is the module of the electrode impedance. Mathematically, the ac current

can be represented as a vector whose magnitude is described by ΔI_1, and the orientation by φ_1. In the absence of faradaic processes, the real part of the impedance is equal to the solution resistance, and the imaginary part depends on the double layer capacitance of the electrode (C_{dl}) and the frequency:

$$Z_{img} = -\frac{1}{C_{dl}\omega} \qquad (2.5)$$

Theoretically, the phase shift for the background current can be between 0 and –90 deg, depending on the frequency and size of the electrode and the conductivity of the supporting electrolyte. If the flow of current is limited by the solution resistance ($Z_{rel} >> |Z_{img}|$) the phase angle is close to 0 deg. Such a situation is obviously undesirable for voltammetric detection, hence under most experimental condition the phase shift should be between about –30 and –90 deg. When a faradaic process takes place both the magnitude of the current and the phase shift increase. The latter effect allows implementation of

phase sensitive detection. In this case the monitored quantity (ΔI_p) is a projection of the current vector on an axis which was rotated by φ_p with respect to the original X axis:

$$\Delta I_p = \Delta I_1 \cos(\varphi_1 + \varphi_p) \qquad (2.6)$$

As long as the analyte is absent, φ_1 is equal to the phase shift of the background current (φ_b) hence, if φ_b is set to $90° - \varphi_p$ the ΔI_p is equal to zero. However, when the analyte appears near the electrode the φ_1 changes and a non-zero value of ΔI_p is observed.

Additional terms in eq. (2.2) describe higher harmonics generated by the electrode process. In general, higher harmonics are generated by non-linear systems (i.e. systems which do not produce response proportional to the magnitude of the excitation). In the absence of faradaic processes, the electrode/solution interface can be treated as a near-linear system. However, in the case of reduction or oxidation the relation between current and potential is described by an exponential function; thus, it is non-linear and generates higher harmonics. The even harmonics are characteristic of unsymmetrical periodic signals. Consequently, a strong second harmonic generation can be expected for the deposition and stripping of metals ions, since in this case the current-time dependencies for the reduction and the oxidation processes are significantly different. The higher harmonic response can be easily obtained by means of Fourier analysis. It is expected that this method of data processing can provide a significant improvement in the signal to background ratio. In addition to the above data treatment processes, standard Fourier-transform filters, moving-average smoothing, and polynomial smoothing were also examined to improve S/N.

2.5.2. Digital Signal Process

The operation for moving average smoothing can be mathematically represented as,

$$Y_{s(i)} = \Sigma\, Y_{(i+j)} / (2m+1) \qquad (2.7)$$
$$j = -m \text{ to } m$$

Here, $Y_{s(i)}$ is the value of the smoothed data points, $Y_{(i+j)}$ is the original value, 2m+1 is the size of the window. The operation for polynomial average smoothing is given as follows,

$$Y_{s(i)} = \Sigma\, C_i Y_{(i+j)} / (NORM) \qquad (2.8)$$

here, $Y_{s(i)}$ is the value of the smoothed data points, $Y_{(i+j)}$ is the original value, C_i the tabulated value for a given window size (2m+1), NORM is a normalizing factor. The values of C_i and NORM can be obtained from the reference paper.[144] The rectangular low-pass function in digital filtering can be presented in the form

$$H_{(f)} = \begin{cases} 1, & \text{when } |f| \le f_O \\ 0, & \text{when } |f| > f_O \end{cases} \qquad (2.9)$$

$H_{(f)}$ is the shape of the filter function, f_O is the cutoff frequency. Exponential low pass filtering sets the frequency beyond which little or no signal information is present while leaves those corresponding to signal component changed according to following form:

$$H_{(f)} = \begin{cases} 1 - \log(f/f_O), & \text{when } |f| \le f_O \\ 0, & \text{when } |f| > f_O \end{cases} \qquad (2.10)$$

$H_{(f)}$ is the shape of the filter function.

2.6. Calculations

The number of theoretical plates, N, was calculated from equation,

$$N = 5.54\ (t_{mig} / W_{1/2})^2, \qquad (2.11)$$

where t_{mig} corresponds to the migration time of the analyte in seconds, and $W_{1/2}$ is the width of the peak at half its maximum height. For the end-column electrochemical detection, electroosmotic mobilities (μ_{eo}) were calculated from the migration time (t_{eo}) of the neutral marker in seconds,

$$\mu_{eo} = L^2 / (V^* t_{eo}) \qquad (2.12)$$

where L is capillary length in cm, V is the separation voltage in Volts. Apparent mobility (μ_{mig}) was calculated from the migration time (t_{mig}) of the analyte in seconds,

$$\mu_{mig} = L^2 / (V^* t_{mig}) \qquad (2.13)$$

Electrophoretic mobility (μ_{ep}) was calculated from:

$$\mu_{ep} = \mu_{mig} - \mu_{eo} \qquad (2.14)$$

The sensitivity (S) was obtained from:

$$S = (I-m) / C \qquad (2.15)$$

Where I is the electrode response of the analyte, C is the concentration of the analyte, and m is the y-axis intercept obtained from the analysis of least-square regression by using the original response-concentration data.

RESULTS AND DISCUSSIONS

3. CE EXPERIMENTAL PROCEDURES

The research in this section is not main goal for this thesis. However, it is important in studies of electrochemical detection to achieve a complete separation and reproducible migration times, and it also is necessary to minimize the influence of high separation voltage on the EC detection. For these purposes, some CE experimental parameters were examined initially. These parameters included choice of electrolyte. the concentration and pH in the electrolyte, capillary conditioning, alignment of capillary with the electrode, and methods used to measure EOF.

3.1. Choice and Role of Electrolyte for CE Separation of Metal Ions

Separation of analytes in CE is based on differences in their electrophoretic mobilities in the electrophoretic media. Since the ionic conductivities of some cations, such as Co^{2+}, Ni^{2+}, Cu^{2+} and Zn^{2+}, are similar, their mobilities are too close in many instances to expect selective separation based only on the migration behavior of free cations. To achieve a separation of these metal ions it is necessary to alter their mobilities. Usually, this can be achieved by adding a weak complexing agent in the electrolyte. The

interaction between the metal ion M and complexing agent L^- can be described by the following equations,

$$M^{n+} + L^- \Leftrightarrow ML^{(n-1)+} \quad (3.1)$$

$$M^{n+} + 2L^- \Leftrightarrow ML_2^{(n-2)+} \quad (3.2)$$

The apparent electrophoretic mobility (μ_{app}) of the metal ion is then a combination of the mobility of the free metal ion and its complexes:

$$\mu_{app} = \alpha\mu_m + \beta\mu_{mL} + \gamma\mu_{mL2.....} + \mu_{eo} \quad (3.3)$$

where α, β, γ are the mole fractions of each species in the capillary, and μ_m, μ_{mL}, μ_{mL2} are the mobilities of the free ion, and 1:1 and 1:2 metal complexes, respectively. The complexes, being larger and possessing a less positive charge, usually migrate more slowly than the fully dissociated ion, consequently leading to a smaller μ_{app}. Since the stability constants for metal complexes, even from the same period or group of the periodic table, vary in a broad range, adjusting μ_{app} by addition of a complexing agent into the electrophoretic buffer is a possible method for a successful CE separation. This auxiliary separation mode has provided a good separation for a number of cations.[145-160] The complexing agents used for metal ions from literatures include crown ethers;[145-147] 8-hydroxyquinoline-5-sulphonic acid;[148] glycolic, succinic and citric acid;[149,150] cyanide;[151,152] 4-(2-pyridylazo) resorcinol;[153,154] ethylene diaminetetraacetic acid (EDTA);[155-157] and α-hydroxyisobutyric acid (HIBA).[158-161]

HIBA is a weak acid ($pK_a = 4.70$) that can form complexes with a wide variety of metal ions. It has been used as a complexing agent for lanthanides,[162] and later was used to resolve metal ions in the form of HIBA complexes in CE.[163] The role of HIBA for selectivity control has been reported for the separation of metal ions in CE for direct and indirect UV detection in several papers.[159-161] Creatinine, a weak base ($pK_b = 4.83$), has been used as a UV-adsorbing co-ion for indirect UV detection,[49] and combined with HIBA, it makes a good buffer that can prevent the pH change at the electrode. Since this electrolyte system can provide good resolution of the test metal ions of interest in this work it was selected as one of major electrolytes for further investigation. The pH in the electrolyte was adjusted by using acetic acid because strong acids, such as hydrochloric or sulfuric acid, led to higher background noise. The effect of HIBA on the CE separation of metal ions is shown in Figure 3.1. Figure 3.1 A is the electropherogram obtained without HIBA for Tl^+, Co^{2+} Ni^{2+}, Zn^{2+}, Cd^{2+}, and Pb^{2+}. This figure shows only four peaks because Ni^{2+}, Co^{2+} and Zn^{2+} co-migrated. The result when 0.010 mol/L HIBA was added is shown in Figure 3.1 B. This figure shows that with HIBA all these metal ions were resolved. The overall migration time of the metal ions decreased in order (from longest to shortest): $Pb^{2+} > Cd^{2+} > Zn^{2+} > Ni^{2+} > Co^{2+} > Tl^+$. Obviously, the overall mobilities of the metal ions depend on their apparent radii and charges in the electrolyte.

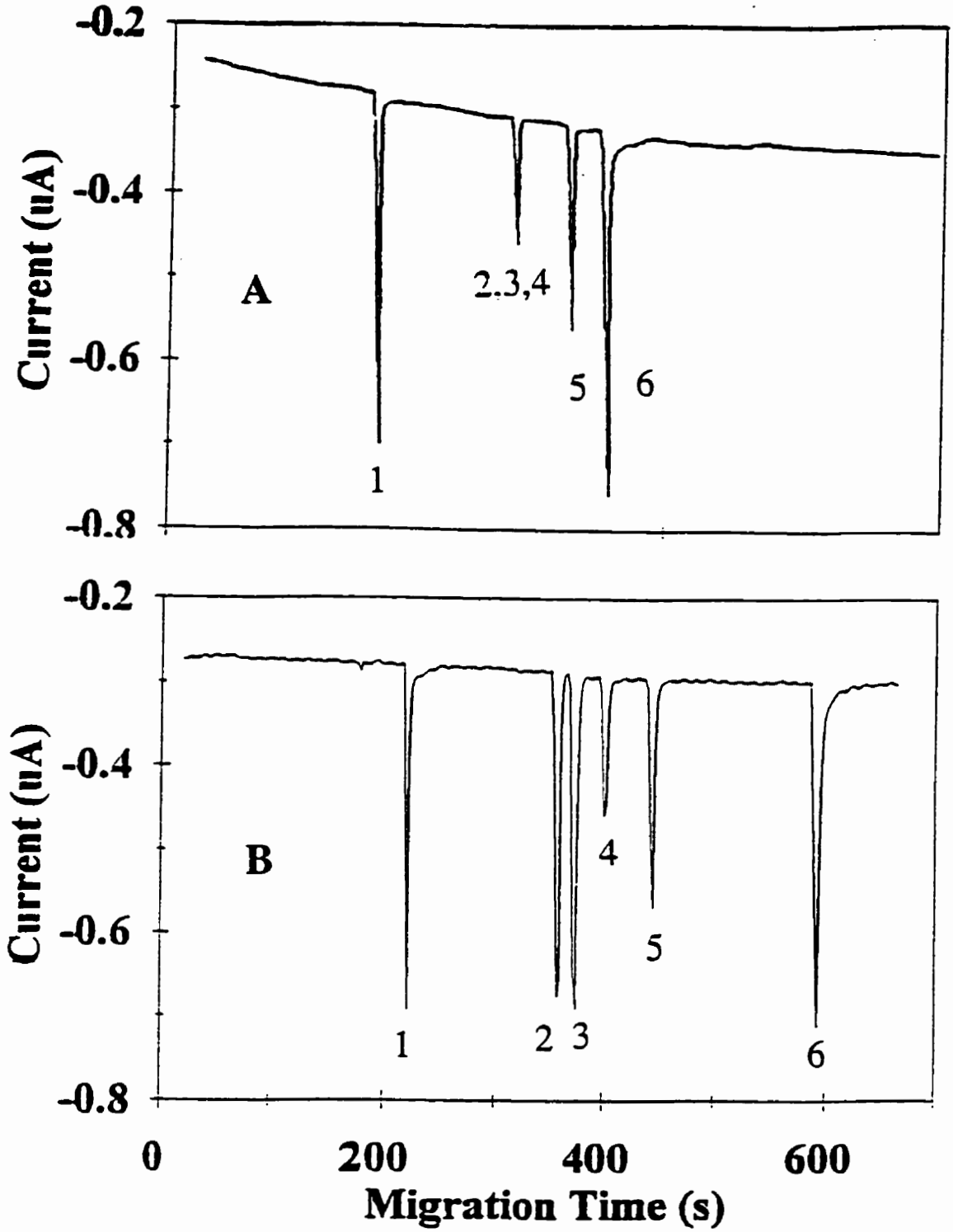

Figure 3.1 Separation of a mixture containing Tl^{+}, Co^{2+}, Ni^{2+}, Zn^{2+} Cd^{2+}, and Pb^{2+} detected at a 25 μm Au electrode. Experimental conditions: pulsed amperometric detection; -1100 mV for 96 ms and 200 mV for 96 ms with data collected over the first 48 ms; electrolyte; 0.030 mol/L creatinine without HIBA (A) and with 0.010 mol/L HIBA (B), pH was adjusted by acetic acid to 4.8; electromigration injection with 5 kV potential for 10 s; separation voltage, 20 kV over a 25 μm i.d. × 60 cm capillary; analyte concentration, 10.0 μmol/L; peak identification: (1), Tl(I); (2), Co(II); (3), Ni(II); (4), Zn(II); (5), Cd(II); (6), Pb(II).

3.2. Capillary Conditioning

Conditioning of a new capillary has a significant effect on the separation of metal ions. The changes observed in the migration time for repetitive injection of a neutral marker (catechol) in a new capillary without any rinsing step prior to use is shown in Figure 3.2 A. These results show that the migration time decreased steadily, corresponding to an increase in electroosmotic velocity. Several methods[62,161,164] have been reported to treat a new capillary for reproducible EOF. Of these methods, the following procedure[164] was found to be appropriate for the separation of metal ions: the capillary was rinsed with deionized water for 30 min, then with 0.1 mol/L HCl for 60 min, and then with the electrophoretic buffer for 60 min. The electroosmotic velocity obtained in a conditioned capillary is shown in Figure 3.2 B where a reproducible migration time (<5%) is observed. Other procedures, consisting of various amounts of water, NaOH and methanol, gave irreproducible EOF and poor peak shapes, probably due to interaction between the metal ions and the negatively charged surface silanol groups at the capillary wall.

3.3. Measurement of Electroosmotic Mobility

Electroosmosis is one of the most troublesome aspects of capillary electrophoresis. Therefore, a precise characterization of the electroosmotic flow is highly desirable not

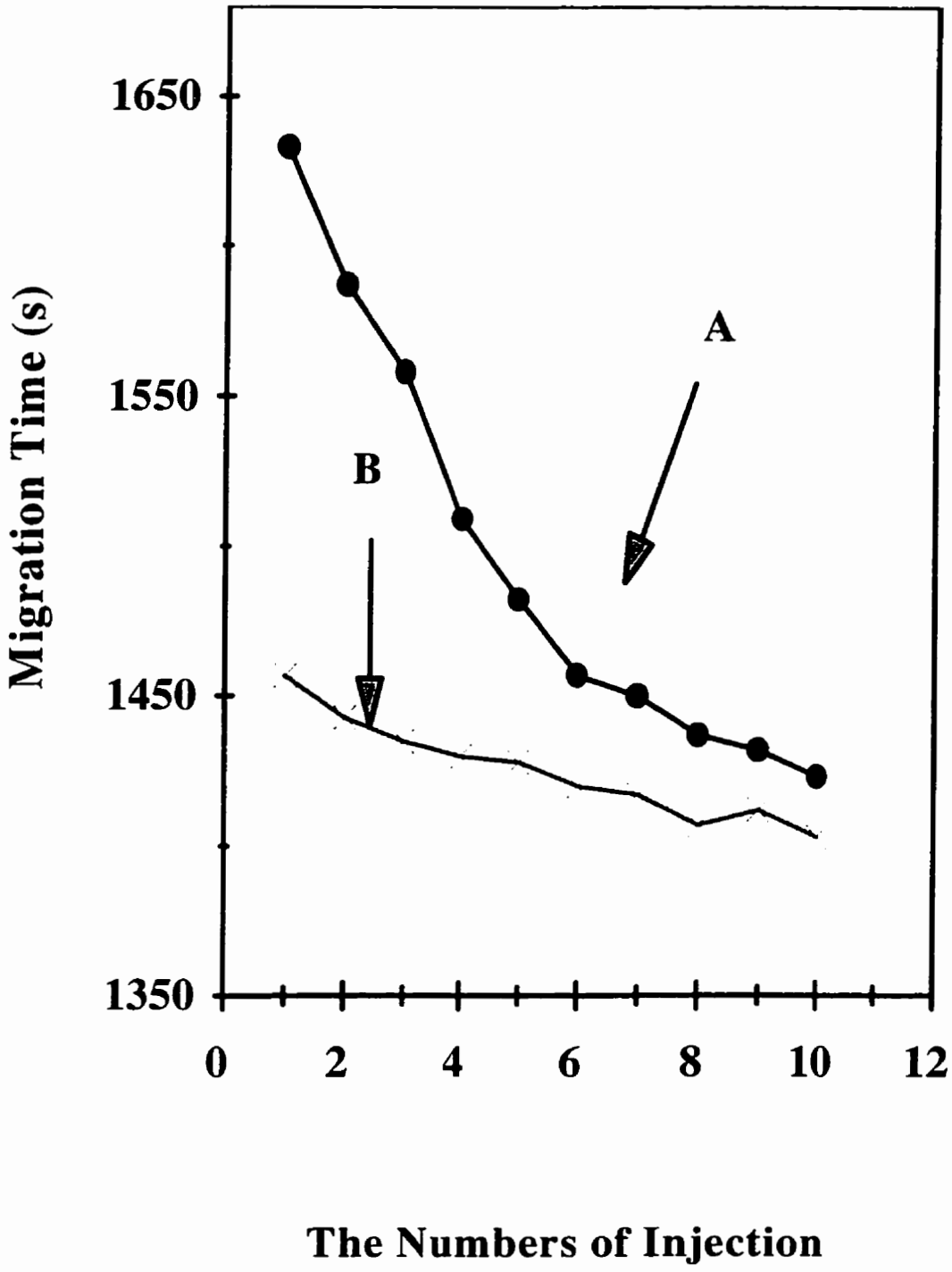

Figure 3.2 Migration time of a neutral marker (catechol) over repeated injections at an unconditioned (A) and conditioned (B) capillary. Experimental conditions: EC detection at 700 mV with a 25 μm Au electrode; separation voltage, 20 kV over a capillary with 59.6 cm in length; neutral marker, catechol, 5.0×10^{-4} mol/L; other conditions as for Figure 3.1.

only for understanding CE results but also for optimizing CE analysis. The methods that have been reported to monitor EOF include measuring the change in weight in one buffer reservoir[165,166], the change in the migration time of neutral compounds,[167-171] or monitoring the change in electrophoresis current[172] or in conductivity[173] when water or an electrolyte with different concentration from the electrophoretic electrolyte is introduced into a capillary.

3.3.1. Neutral Markers

The most common approach to measure μ_{eo} is to use a neutral marker.[167-171] A neutral marker chosen for monitoring EOF must obviously show negligible interaction with the capillary, and be readily detected; the latter property is often difficult to achieve in EC detection. The neutral compounds, catechol (E_o = + 0.7 V), 1,4-benzoquinone (E_o = -0.54 V), and 1.4-dithiabenzene(E_o = + 0.69 V) were examined as EOF markers. 1,4-Benzoquinone and 1.4-dithiabenzene did not give signals, and catechol, which responded at a potential of > 700 mV, gave a weak signal and was accompanied by high background current and noise, probably because of the oxidation of HIBA and/or the Au electrode. However, a noticeable signal was obtained for catechol at a concentration of more than 1.0×10^{-4} mol/L, and thus provided a feasible method to measure EOF in spite of its poor sensitivity at the pH of 4.4 to 4.8 required for the CE separation of metal ions.

3.3.2. Monitoring of Current Changes

Another method to measure EOF is to monitor the change in conductivity or electrophoretic current when an electrolyte with a different concentration from the carrying electrolyte is introduced[173,174] into the capillary via EOF. For this purpose, a 10.0 kΩ resistor was inserted between the counter electrode and ground. A chart recorder was connected directly across the resistor, and the current through the resistor was monitored when the carrier electrolyte concentration (C) was replaced by diluted (C_1) electrolyte (C_1 = 1/2 C). The result showed that the current fell continuously until the entire capillary became filled with the diluted electrolyte. The electroosmotic mobility was calculated from the capillary length (L) divided by the time (t) required for complete filling of the capillary tube ($\mu_{eos} = L/t$). Compared to the result using a neutral marker (catechol), the EOF mobility obtained by the current-monitoring had a difference of approximately ±10%, due to noise which made it difficult to measure the change in current and/or due to the change in EOF caused by the conductivity different in sample zone and the running electrolyte.

In aqueous systems, EC detection can have significant background currents from H^+ evolution, O_2 reduction, adsorption of electrolytes, and charging currents. These currents are expected to change when a small sample of water or diluted electrolyte migrates past the electrode. Since water is neutral, monitoring the change in background current by introducing a small sample of water might offer a feasible way to measure EOF velocity. Thus, this method was examined by monitoring the electrode response, and a

negative peak, mainly from the reduction of H^+ and electrolyte adsorption, was obtained. This method gave an EOF value ±5% different from that obtained with catechol, and this difference might be caused by the difference of conductivity in water region and the electrolyte region and by the factor that water is not an absolutely neutral compound. However, under certain conditions, the signal disappeared after more than 5 to 6 measurements, likely due to the changes at the electrode surface (it was noted in the experiments that small bubbles formed at the electrode surface). This problem can be eliminated by mechanically cleaning the electrode surface, but this was inconvenient. The above three approaches can be used to measure EOF, however, the signals from catechol (1.0×10^{-3} mol/L) and water were mainly used for the measurements of EOF in this work due to their simplicity and precision.

3.4. Alignment of Capillary with Working Electrode

In an end-capillary electrochemical detection, alignment of the μm-electrode with the capillary is important since it affects analytical and background signals, and shifts the applied EC potential. To evaluate these effects, the electrode was adjusted in increments from 0 to 80 μm from the end of the capillary by a three-dimension micropositioner. When the distance was < 20 μm, both background current and noise began to increase significantly. The effect of alignment on the electrode potential was examined via shifts in O_2 reduction observed by fast cyclic voltammetry at the end of the capillary. Results under separation voltages of 20 and 25 kV are shown in Figure 3.3. Obviously, the closer the capillary was to the working electrode, the more the electrode potential was shifted.

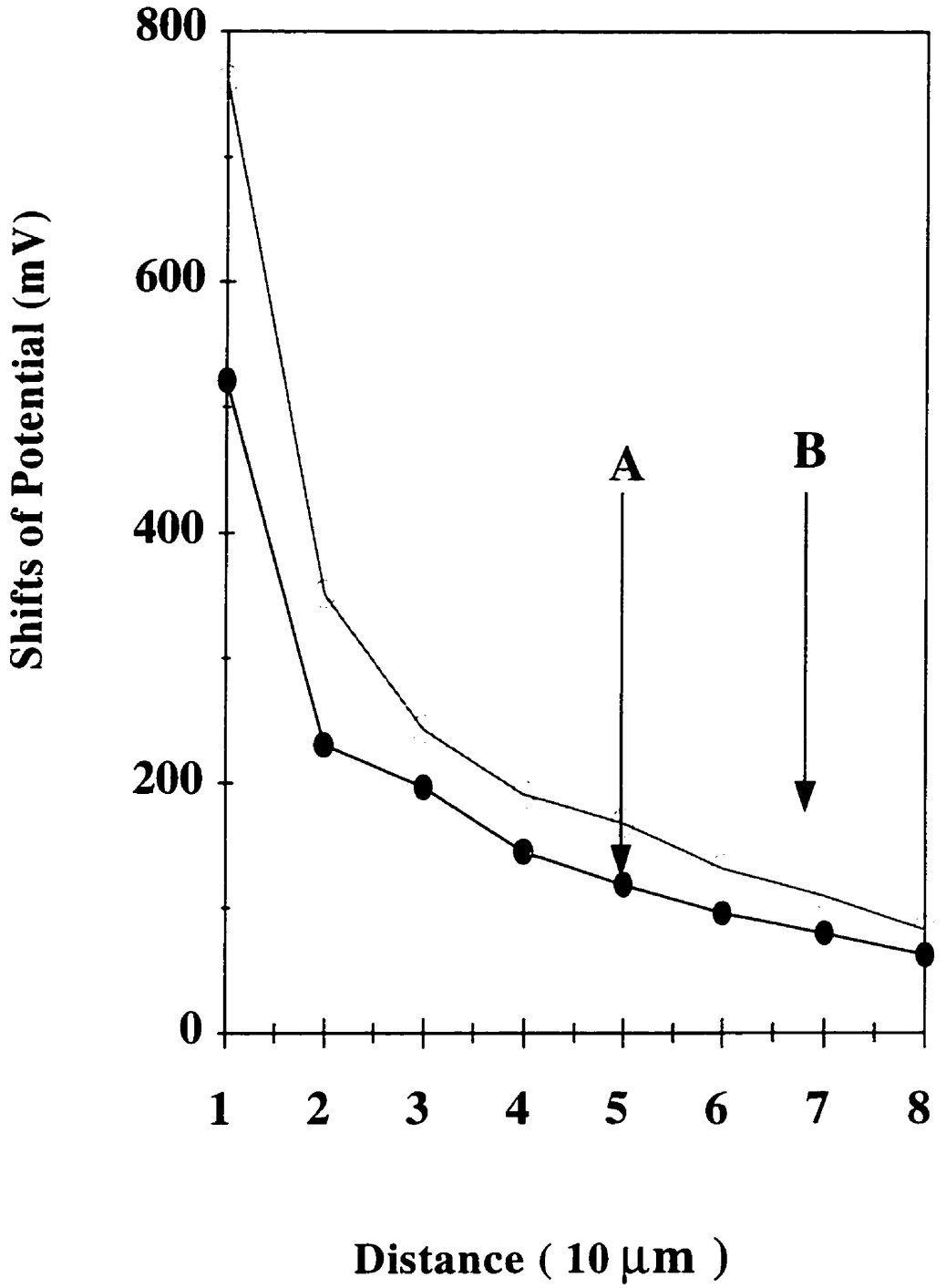

Figure 3.3 Effect of the distance between a 25 μm Au electrode and the capillary end on the reaction potential for O_2 under 20 (A) and 25 kV (B) separation voltage. Experimental condition: on-line fast CV detection at 20 V/s; CV potentials, -1000 to 1000 mV; analyte, O_2 dissolved in the electrolyte; other conditions as for Figure 3.2.

There was a significant rise in the electrode potential when the electrode was brought < 20 μm from the end of the capillary. When the distance between the end of the capillary and the electrode was more than 40 μm, the analytical signals of the analytes decreased due to dilution. Thus the distance was adjusted to ~20 ± 5 μm to maximize S/N, to reduce peak broadening, and to maintain small potential shifts.

The effect of separation voltage on applied potential was also examined. The results obtained at 25 μm Pt, Au and Hg-film electrodes are shown in Figure 3.4. It is observed in this figure that the electrode potential shifted with the separation voltage, and such shifts increased significantly for both Au and Pt electrodes when the separation voltage was > 20 kV. The potential change at Pt electrodes is similar to that at the Au electrode, but, Hg-film electrodes gave a different behavior. Theoretically, the effect of the applied electric field at the same size electrodes should be identical as the result observed in Figure 3.4 at the Au and Pt electrodes indicates. The different behavior of Hg-film electrodes was due to the difference in the size and shape of the Hg-film electrode from 25 μm electrodes. For most of the studies, 20 kV was chosen to attain fast and efficient separation, and to control shifts of EC potential within 200 mV. For a wide range of experimental conditions the shift in electrode potential observed on application of a 20 kV separation voltage was in the range of ~ 150 mV, and week-to-week variation of applied potential was ≤ 50 mV.

Since electric fields will decay faster at the end of a smaller i.d. capillary, the use of small i.d. capillaries should improve EC detection performance in CE. Although the effect

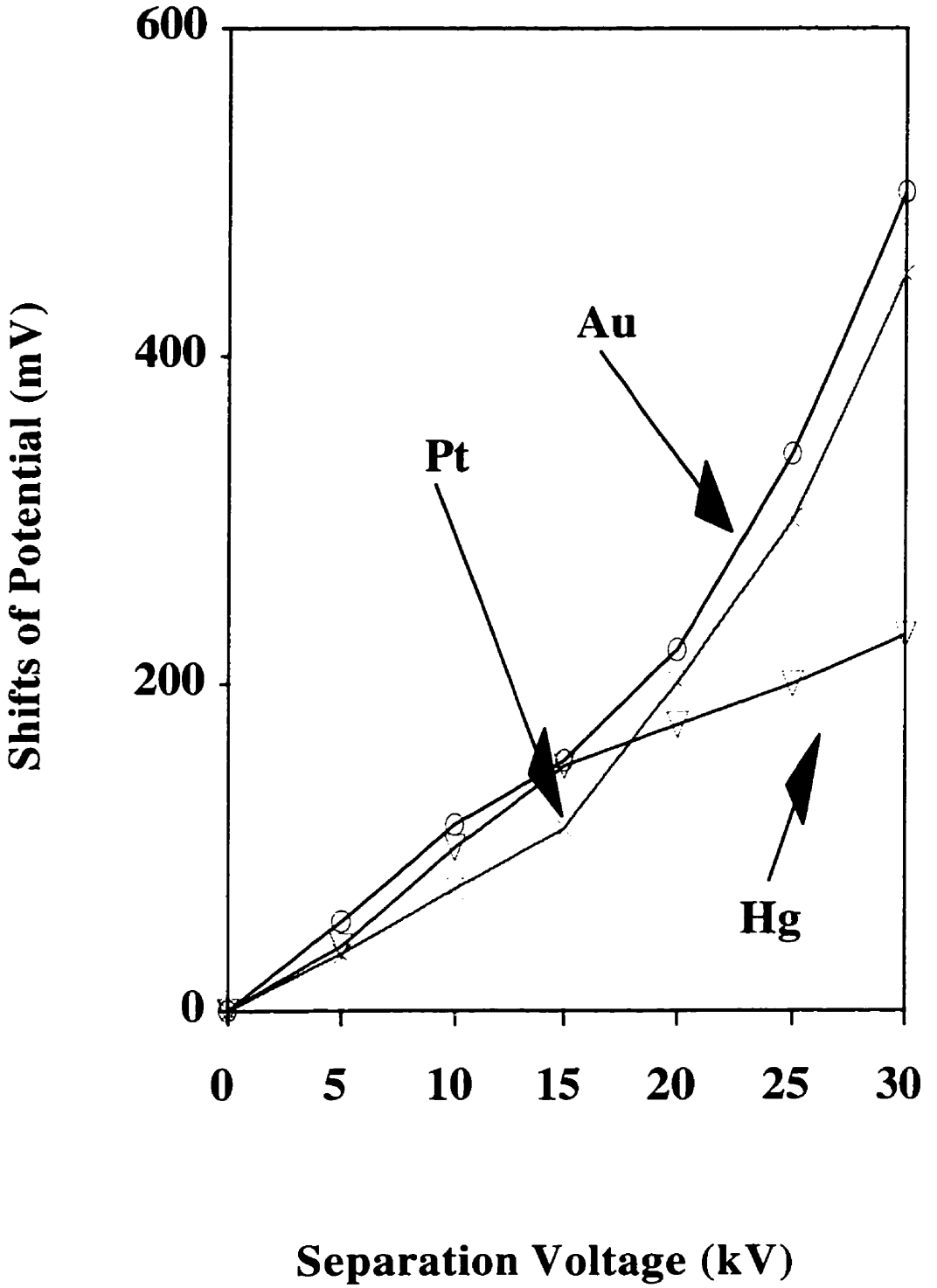

Figure 3.4 Effect of high separation voltage on O_2 reduction potential at a 25 μm Au, Pt and Hg electrodes; the distance between the capillary and the working electrode was adjusted to ~ 20 μm; other experimental conditions as for Figure 3.3.

of such an electric field has been estimated to be unimportant for very small capillaries ($\leq$ 25 μm),[50,52] it is of interest to determine its effect on the EC detection in this system. Thus, the effects of the electric field on the electrode response was examined with a 25 μm Au electrode adjusted to ± 20 μm of the end of 10, 25, 50, 75 μm ID capillaries. The shifts of the electrode potential of O_2 reaction are shown in Figure 3.5. Compared to those for small capillaries ($\leq$ 25 μm), shifts of the electrode potential for capillaries ($\geq$ 50 μm) were > 2 times greater. The internal diameter of the capillary also affects the background noise. When the capillary was $\geq$ 50 μm, the background noise began to increase appreciably, and the peak-to-peak noise was > 4 fold compared to that for 25 μm capillaries. These results suggest that capillaries $\leq$ 25 μm should be chosen for metal ion separation to minimize the background noise and shifts of the electrode potential caused by the electric field from the high separation voltage.

3.5. Optimization of CE Separation of Metal ions

CE electrolyte parameters also need to be optimized for high separation efficiency and resolution of the metal ions. Common approaches used to improve the resolution include: adjusting pH[174,175] or concentration of the electrolyte,[176] adding simple organic solvents,[177,178] and altering the walls of the capillary.[13,49,179] Of these approaches, adjusting pH and the concentration of the electrolyte are the most common methods used to optimize CE separations. Although the effect of pH and HIBA for metal

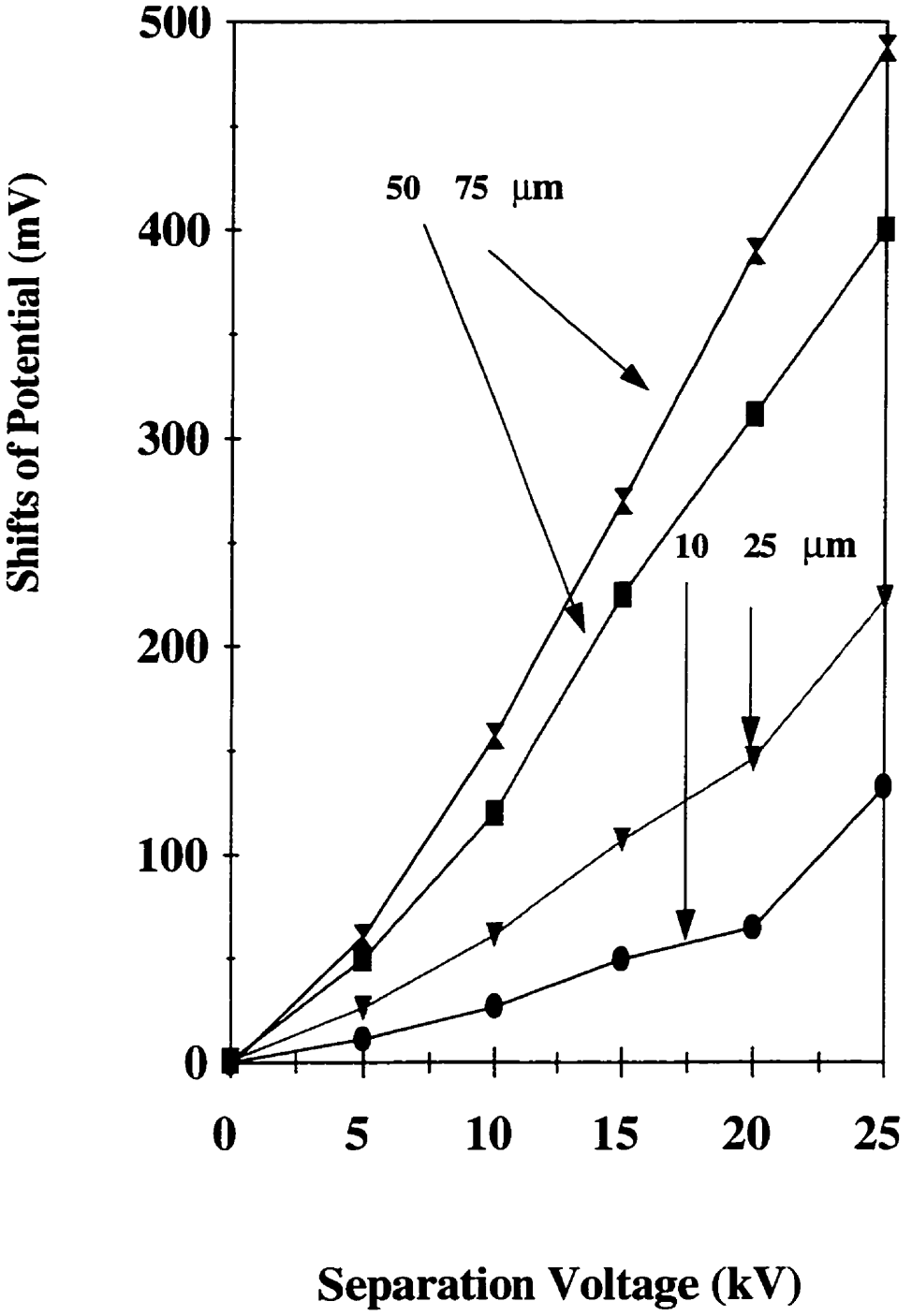

Figure 3.4 Effect of the electric field on the EC reaction potential using a 10, 25, 50, 75 µm capillary, respectively. Experimental conditions: fast on-line CV at a 25 µm Au electrode; the working electrode was adjusted within ~ 20 µm to the capillary; analyte, O_2; other experimental conditions as for Figure 3.3.

ion separations has been reported,[158] most of the metal ions studied were different from those which I was interested in. Therefore, it was desirable to examine these CE parameters.

The effect of pH on the CE separation was evaluated at pH's ranging from 3.5 to 6.0 for metal ions over 1.0×10^{-5} to 1.0×10^{-4} mol/L. Lower pH values give insufficient metal complexation. pHs of > 6 were not used because these pH values could lead to the formation and precipitation of metal hydroxides, and also lead to a rapid increase in electroosmotic mobility. The influence of pH on the migration time of Tl^{+}, Cd^{2+}, Zn^{2+}, Ni^{2+}, Co^{2+} and Pb^{2+} is shown in Figure 3.6. These results show that an increase in the pH resulted in a decrease in the migration times for these metal ions. It is also observed in Figure 3.6 that the migration order was also altered by the pH: at pH < 4.5, Cd^{2+} moved faster than Zn^{2+}; at pH > 4.5, Zn^{2+} moved faster. The decreases in migration times are mainly due to an increase of EOF because EOF is a function of negatively charged silanol groups on the inner wall of the capillary, which increases with pH. The change in electrophoretic mobility of the ions with pH is shown in Figure 3.7. It is observed in Figure 3.7 that the electrophoretic mobilities of the metal ions began to decrease significantly above pH 5, presumably due to the onset of complexation with HIBA. This complexation would then decrease the effective charge on the metal ions to produce lower electrophoretic mobilities. Resolution of these metal ions was achieved at a pH range of 4.4 to 5.5. Lower pHs led to high background current and noise due to H^{+} evolution.

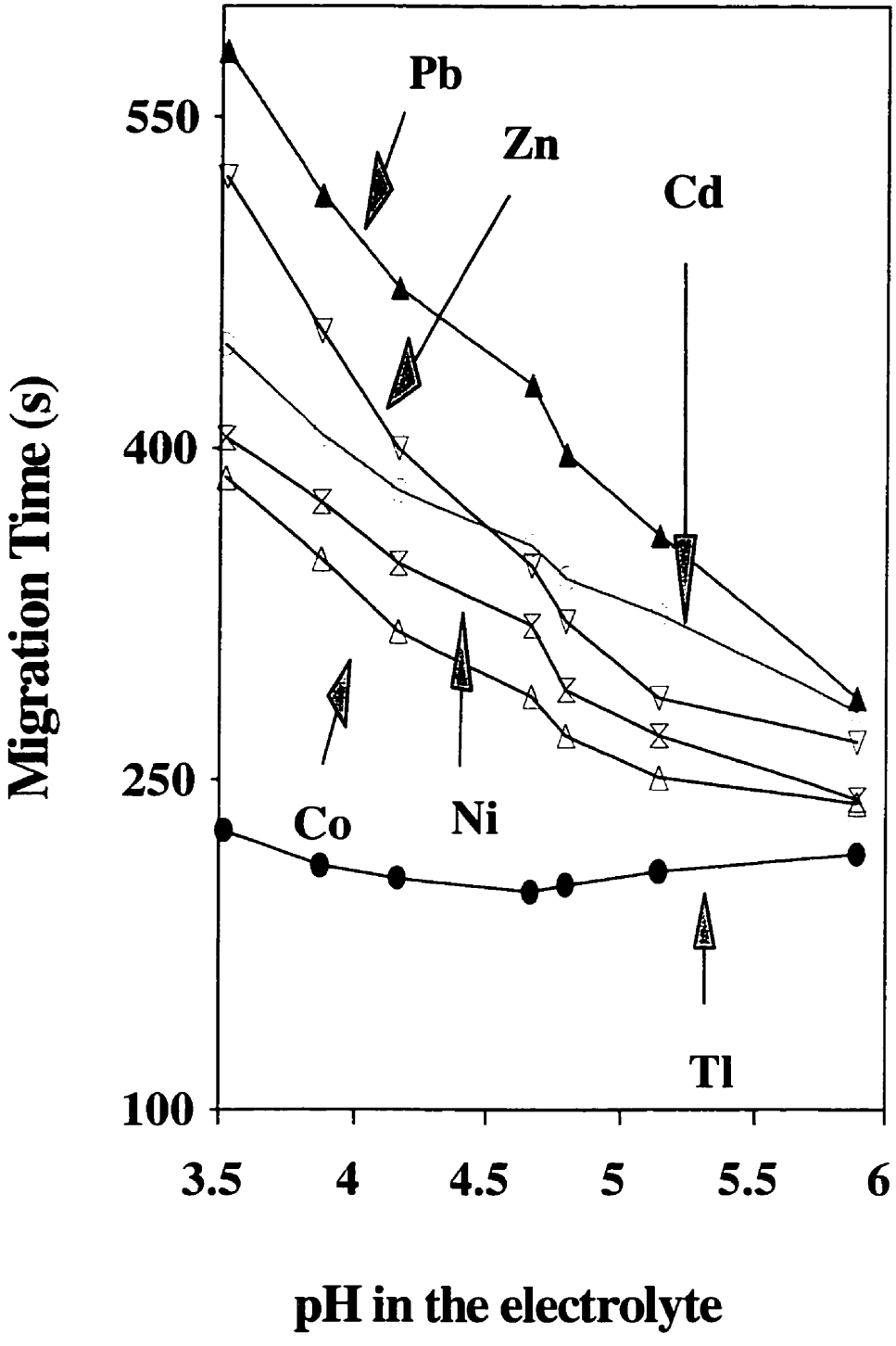

Figure 3.6 Effect of the pH on the migration times of metal ions. Experimental conditions: PAD detection; -1100 mV for 96 ms and 200 mV for 96 ms with data collected over the first 48 ms; electrolyte, 0.008 mol/L HIBA with 0.03 mol/L creatinine; the pH was adjusted with acetic acid to pH (3.5 to 6.0). analytes, 5 X 10^{-5} mol/L; other conditions as for Figure 3.1.

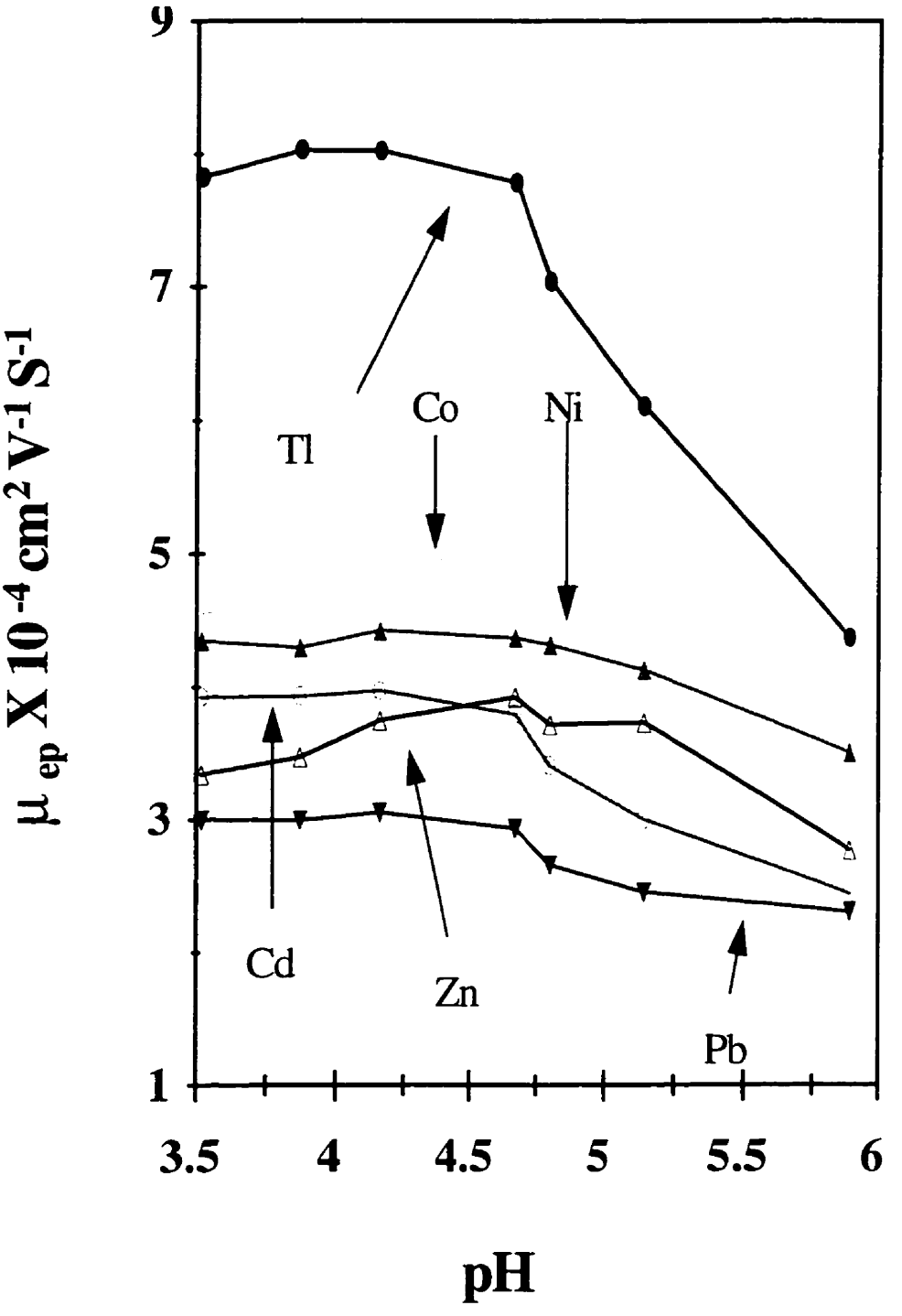

Figure 3.7 Effect of the pH on the electrophoretic mobility of metal ions. Experimental condition: 0.008 mol/L HIBA, 0.030 mol/L creatinine; analytes, 5 X 10^{-5} mol/L; other conditions as for Figure 3.6.

The effect of the concentration of the electrolyte on the separation of metal ions was examined in HIBA over a concentration range of 0 to 24 mmol/L combined with 0.04 mol/L creatinine, with the pH adjusted to 4.58 to 4.60. The effect of the concentration of HIBA on the separation Tl^{+}, Co^{2+}, Ni^{2+}, Cd^{2+}, Zn^{2+}, and Pb^{2+} is shown in Figure 3.8 & 3.9, which shows that the migration rates increased and the electrophoretic mobilities of all analytes decreased with the concentration of HIBA. Two factors controlled the increase in migration time: the first one is the decrease of EOF due to the decrease of double layer thickness (κ^{-1}); the second factor is the decrease of electrophoretic mobilities that resulted from the increase of complex formation. It is also observed in Figure 3.8 that Co^{2+} and Ni^{2+} comigrated when the HIBA concentration was < 4.34 mM, and that Cd^{2+} and Zn^{2+} comigrated when the HIBA concentration was >16 mM. When the concentration of HIBA increased from 6 mmol/L to 24 mmol/L, the electrophoretic current increased from 15.4 to 23.6 μA, and higher concentrations in the electrolyte would result in higher electrophoretic currents. Since high electrophoretic currents lead to Joule heat that deteriorates the separation performance, the optimal concentration of HIBA for the CE separation of these metal ions should be limited to the range of 6 to 16 mM. Under these experimental conditions, separation efficiencies varied from 50 000 to 400 000 theoretical plates for a separation voltage of 20 kV. The lower efficiencies observed for some of the metal ions might be related to slow rates of ligand exchange.

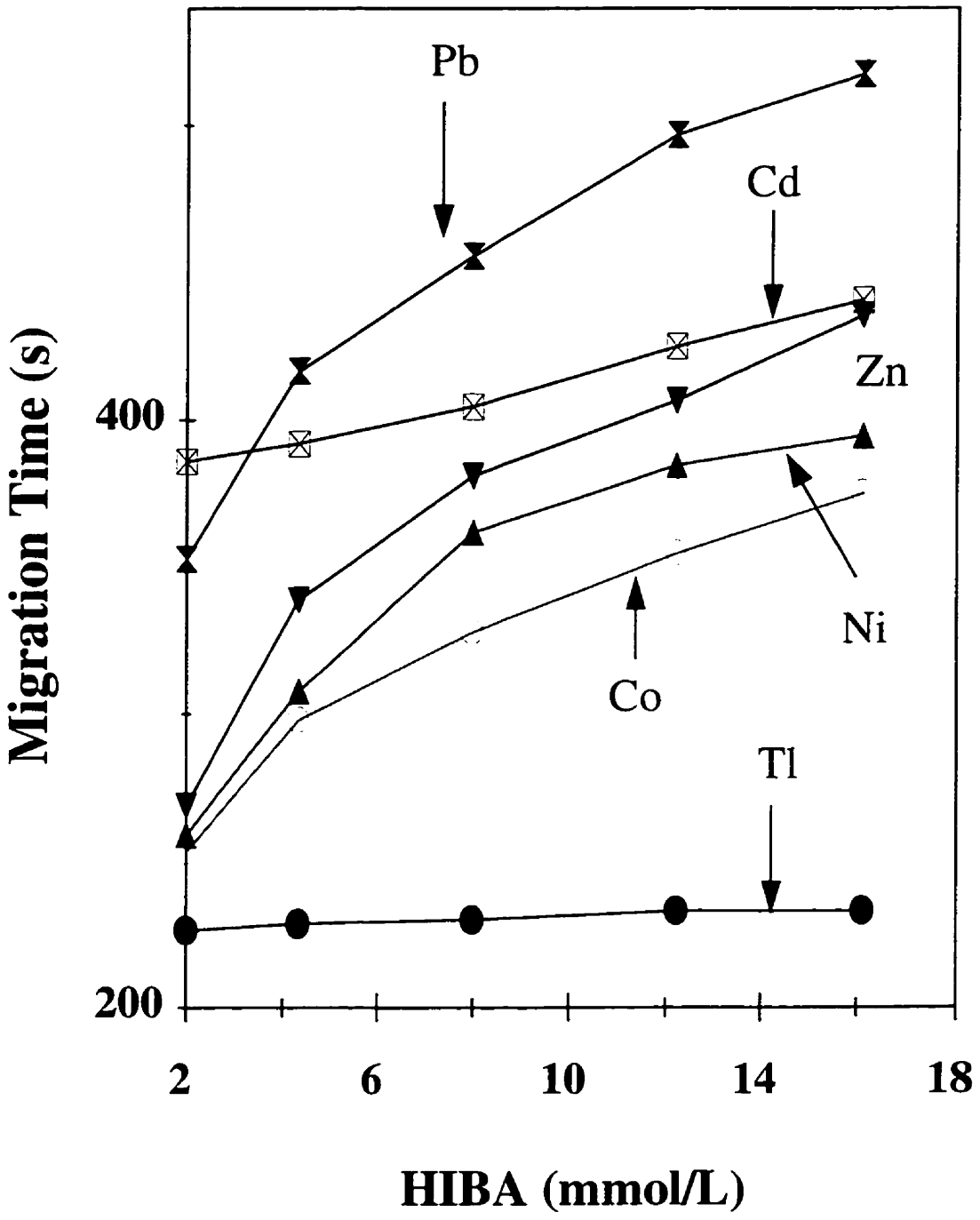

Figure 3.8 Effect of the concentration of HIBA on the migration time. The electrolytes were 30 mmol/L creatinine with HIBA, the pH was adjusted with acetic acid to 4.8; analytes, 5 X 10^{-5} mol/L; other conditions as for Figure 3.6.

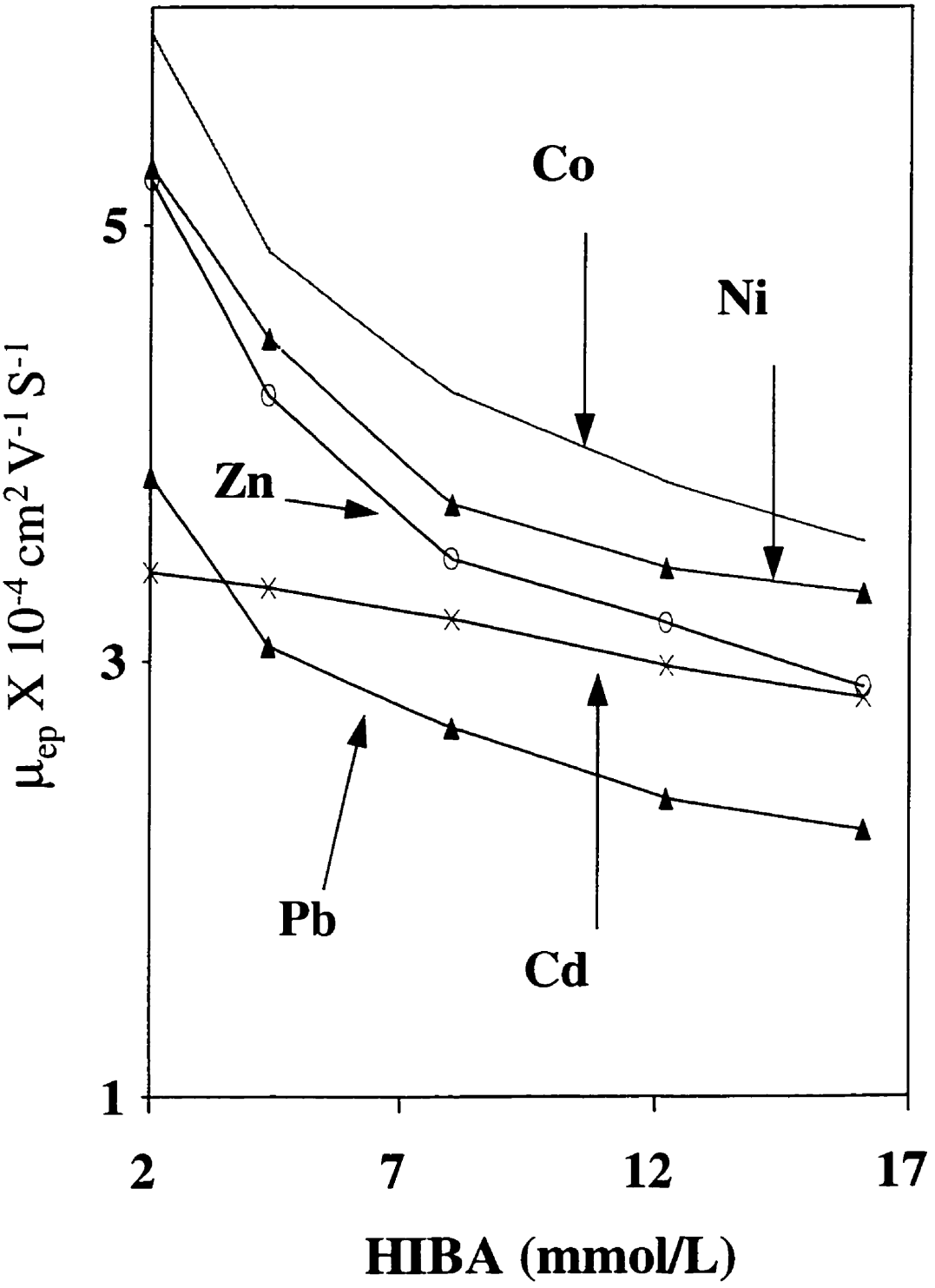

Figure 3.9 Electrophoretic mobility as a function of the concentration of HIBA; conditions as for Figure 3.8.

The other complexing agents evaluated were: lactic acid (pKa = 3.08), L-tartaric acid (pK_a = 2.98, 4.34), malonic acid (pK_a = 2.83, 5.69) and succinic acid (pK_a = 4.16, 5.61) over a concentration range of 4 to 20 mmol/L. Succinic acid in the range of 8 to 12 mmol/l at the pH (4.4 to 4.8) was found to give a complete separation for a mixture of the test metal ions, and a typical electropherogram for Tl^{+}, Co^{2+}, Ni^{2+}, Zn^{2+}, Cd^{2+}, Cu^{2+} and Pb^{2+} is shown in Figure 3.10. The electrolytes consisted of 8 mmol/L succinic acid combined with 40 mmol/L creatinine at a pH of 4.8. Comparing the electropherogram with those obtained in HIBA, the separation of metal ions in succinic acid was in a narrower time span. However, lactic, malonic and tartaric acid with pH's in the range of 4.3 to 4.7 could not resolve all the test metal ions. In conclusion, succinic acid (8 to 12 mmol/L) at pH (4.4 to 4.8) could also be chosen for separation of metal ions in CE.

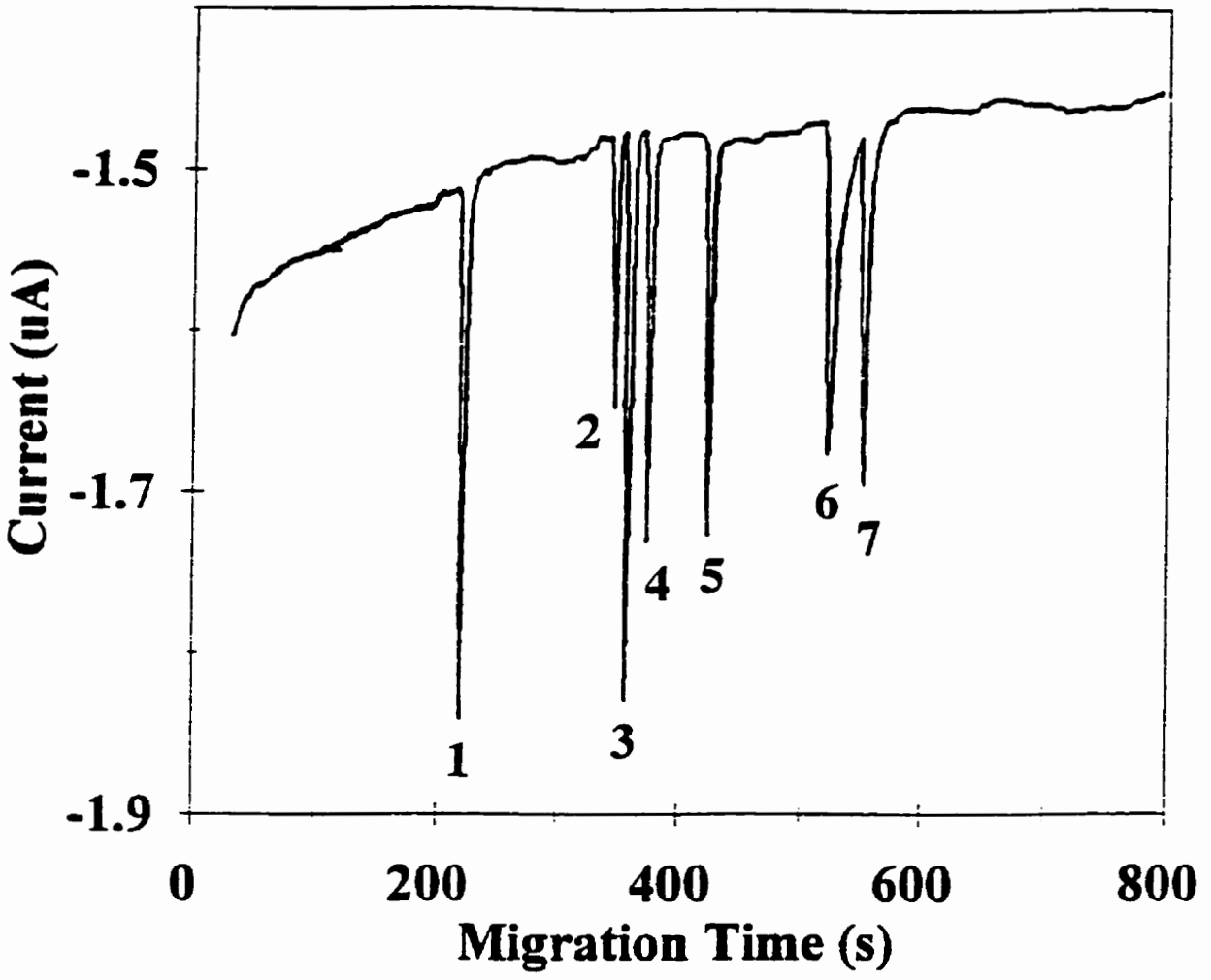

Figure 3.10 Separation of a mixture containing Tl^{+}, Co^{2+}, Ni^{2+}, Cd^{2+}, Zn^{2+}, Pb^{2+} and Cu^{2+} at a 25 μm Au electrode. Experimental conditions: electrolyte; 0.040 mol/L creatinine with 0.008 mol/L succinic acid, pH was adjusted with acetic acid to 4.8; analyte concentration, 10.0 μmol/L; peak identification: (1), Tl(I); (2), Co(II); (3), Ni(II); (4), Zn(II); (5), Cd(II); (6), Cu(II); (7) Pb(II); other conditions as for Figure 3.1.

4. ON-LINE CYCLIC VOLTAMMETRIC STUDIES

4.1. Introduction

In electrochemical detection, the electrode response usually originates from the electrochemical reaction of the analyte at the electrode. Since the electrode response depends on the hydrodynamics and electrokinetics of the analyte's electrochemical reaction, it is essential to understand these characteristics to optimize EC detection. Electrochemical behavior of metal ions is related to many factors: nature and concentration of the analyte and electrolyte; the electrode material and crystallographic orientation; the electrode potential; formation of oxide layers during the oxidation process; adsorption of anions; decomposition of metal complexes; deposition of metals; and interactions between analyte/analyte and analyte/electrode. Undoubtedly, electrochemical reaction processes at the electrode are intricate, and thus several factors need to be considered to optimize the electrode response for analytical applications.

Cyclic voltammetry (CV), where current is measured as a function of a linearly varying applied potential, is a common electrochemical approach used to study electron-transfer and chemical reactions at the electrode/solution interface. Since analyte behavior under CE conditions was of interest, an on-line CV system was used to study the

electrochemistry of the analyte and background electrolyte at both Au and Pt electrodes. The factors affecting the electrochemical behavior of metal ions, such as the applied EC potential, H^+ and O_2 reactions, the adsorption of the organic electrolyte, and the deposition of metals, were evaluated.

4.2. On-line CVs of Electrolytes

The cyclic voltammogram (CV) obtained at a 25 μm Au electrode in 8 mmol/L HIBA and 30 mmol/L creatinine saturated with air is showed in Figure 4.1 (A). The results in Figure 4.1A show that a peak appeared at -180 mV, which implies the existence of an electrochemical reaction at the electrode. Originally, the peak was predicted to be caused by O_2 reduction because it appeared at the region for O_2 reduction. To confirm this, the CVs of the electrolyte was examined via degassing. At first, N_2 gas was passed through the electrolyte solutions at the two ends of the capillary for 20 min to remove O_2. The result was surprising because the voltammogram of the electrolyte was the same as that before degassing. The N_2 was suspected to contain some O_2, and thus Ar (99.9%) was used for degassing. However use of Ar also caused little change in the voltammogram. These results suggested that the peak at -180 mV was not from O_2 reduction. It is known that some organic compounds adsorb on Au and Pt surfaces,[119-129] and this process leads to adsorption and desorption currents in the CVs. Thus the peak at -180 mV might be from adsorption of HIBA or creatinine at the electrode. Similar CV behavior to that

shown in Figure 1.1A, with slight shifts in shape and position of the adsorption peak, was also observed with succinic acid and creatinine, and an acetic acid buffer. To help confirm that these peaks resulted from the adsorption of organic compounds at the electrode, cyclic voltammograms were recorded in phosphate, perchlorate and nitrate electrolytes (20-60 mM, pH = 3.2 ~ 4.7). These electrolytes are expected to exhibit less adsorption on the electrode, and adsorption has been shown to be particularly weak for perchlorate electrolytes. In all these cases O_2 reduction was observed, and a typical result for phosphate is shown in Figure 4.2, where the peak occurred in 200 mV was from O_2 reduction, and this response was easily removed via degassing. Therefore, the peak observed in Figure 4.1A is most likely from the adsorption of HIBA or creatinine. These results suggest that organic molecules in the electrolyte decreased the rate of O_2 reduction, possibly due to their adsorption at active sites of the electrode or via other changes in the O_2 reduction process. This conclusion is also supported by the results reported in the literature for acridine and quinoline derivatives.[49]

During these CV studies it was found that the use of high vertex potentials was always accompanied by high background current and noise. A typical result for the background CVs obtained at a high vertex potential (700 mV) is shown in Figure 4.1 B. Compared to Figure 4.1A a new peak was observed at ~ 100 mV and the organic adsorption peak appeared to shift to a more negative potential (~ -300 mV).

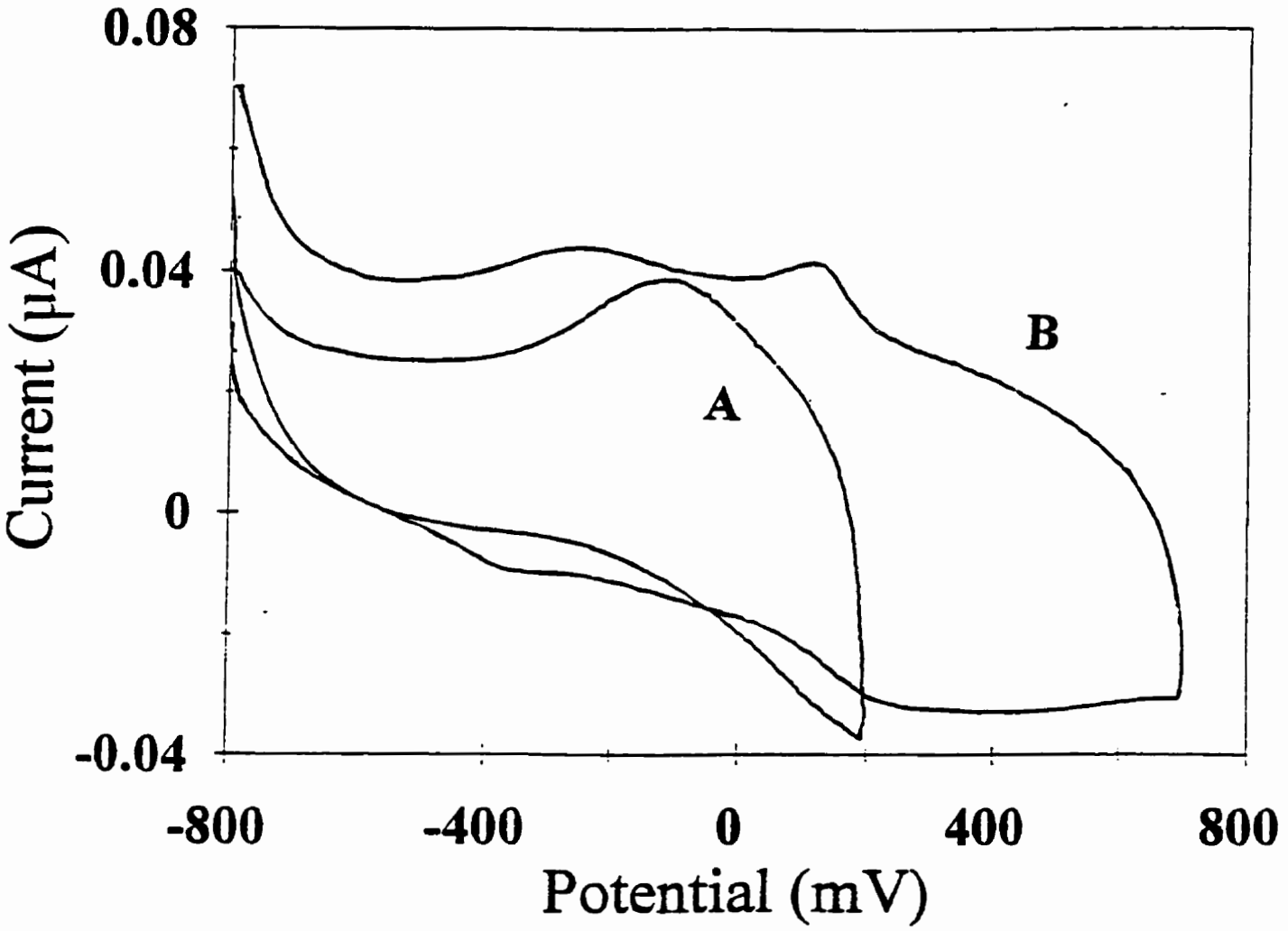

Figure 4.1 On-line cyclic voltammograms with a 25 μm Au electrode for HIBA/ creatinine electrolytes. Experimental conditions: cathodic current is considered as positive current; on-line CV detection; applied potentials, -800 mV for 55 ms and then scanned to 200 mV (A) or 700 mV (B) at 20 V/s; electrolyte, 0.030 mol/L creatinine and 0.008 mol/L HIBA at pH 4.8; separation voltage, 20 kV over 25 μm × 60 cm capillary.

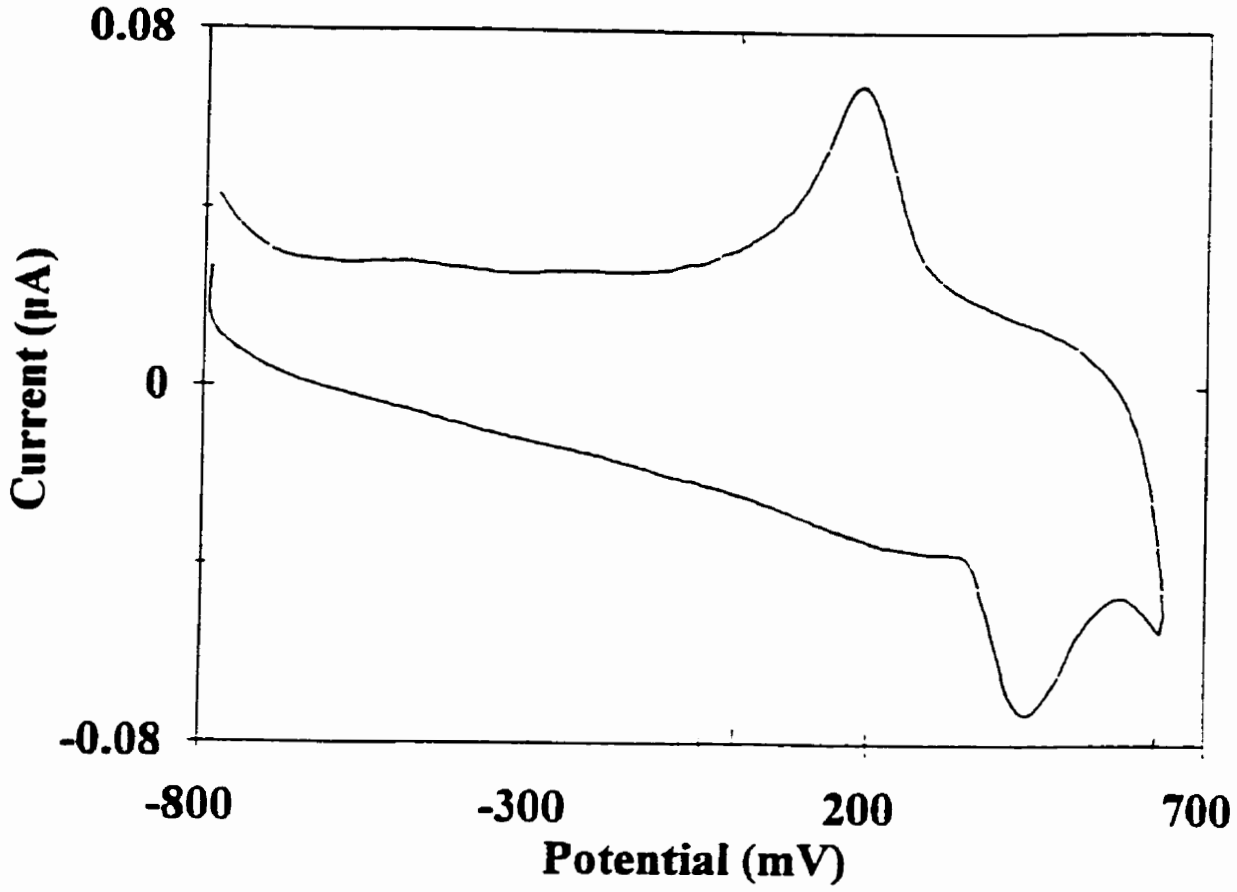

Figure 4.2 On-line cyclic voltammograms with a 25 μm Au electrode for phosphoric acid (1.0×10^{-2} mol/L) electrolytes. Experimental conditions: cathodic current is considered as positive current; on-line CV detection; applied potentials, -800 mV for 55 ms and then scanned to 700 mV at 20 V/s; other conditions as for Figure 4.1.

When this solution was degassed (N_2 or Ar) the only significant change in the CVs was the elimination of this peak at 100 mV as shown in Figure 4.3. CVs obtained with a high vertex potential (Figure 4.1 B) showed a larger capacitance current relative to lower vertex potential conditions (Figure 4.1 A), possibly caused by a decrease in the thickness of the double layer since the capacitance (charging) current is related to the double layer thickness according to the following relationship,

$$i_c = E/R_s\, e^{-t/R_sC_d}, \qquad (4.1)$$

where E is the electrode potential (V), R_s is the resistance (Ω) in solution, t is time (s). C_d is the total capacitance of the electrode/solution interface and its magnitude is reversibly proportional to the thickness of the electric double layer (κ^{-1}). It is known from the above equation that thin double layers will lead to a large charging current. The fact that the double layer was thinner suggested that the organic adsorption layer might have been stripped off the electrode at the high vertex potential, which would lead to re-appearance of O_2 reduction, an increase in the capacitance currents, and thus, higher background noise. The peak-to-peak noise obtained over repeated injection at vertex potentials of 700 mV and 200 mV, respectively is shown in Figure 4.4. The results show that the peak-to-peak noise obtained with the higher vertex potential was almost 2-times higher. Similar behavior has been described by Chen's group who studied the mechanism of metal

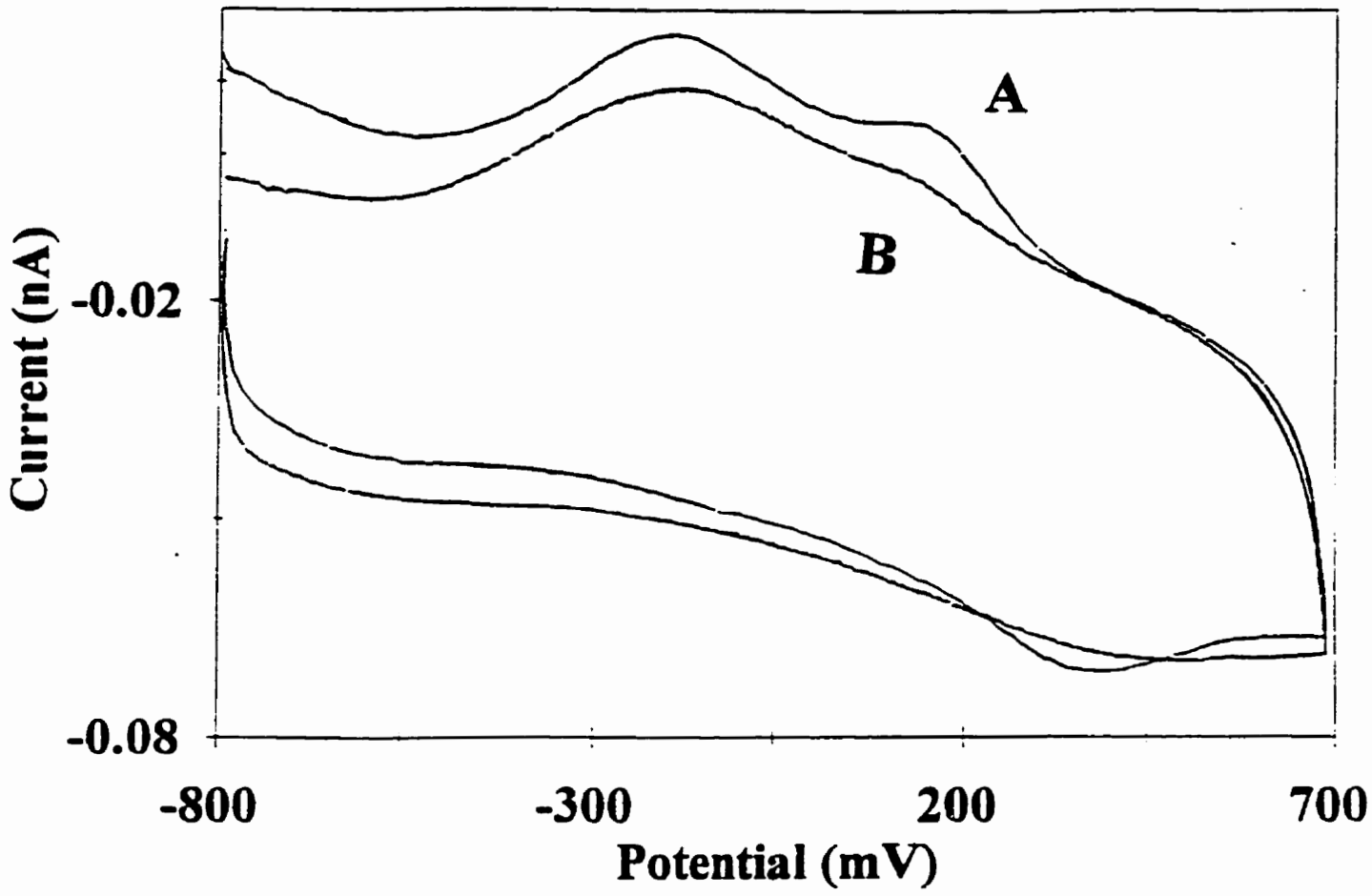

Figure 4.3 On-line cyclic voltammogram at a 25 μm Au electrode for HIBA/ creatinine electrolyte before (A) and after (B) degassing. Experimental conditions: on-line CV detection; applied potentials, -800 mV for 55 ms and then scanned to 700 mV at 20 V/s; electrolytes, 0.035 mol/L creatinine and 0.008 mol/L HIBA at pH 4.88; N_2 degassing for 10 min; other conditions as for Figure 4.1.

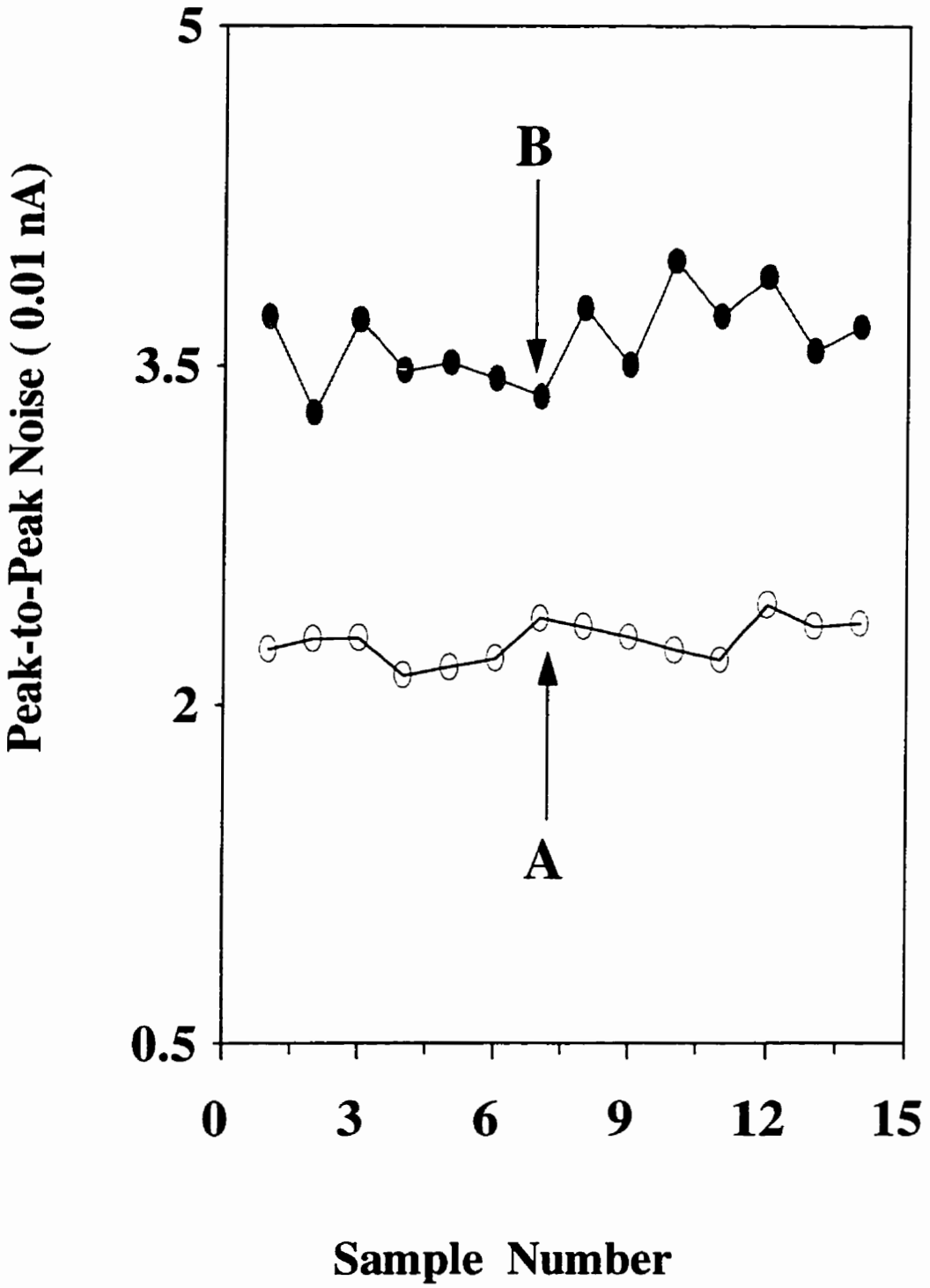

Figure 4.4 Effect of the CV vertex potential on the peak-to-peak noise. Experimental condition: on-line CV detection; applied potentials, -800 mV for 55 ms and then scanned to 200 mV (A) or 700 mV (B), other conditions as for Figure 4.1.

deposition at Au electrodes in perchlorate solutions.[180] Another factor responsible for the high background noise might be the formation of oxides (AuOH or AuO) on the Au surface resulting in pitting and roughening of the surface, which may lead to the higher noise observed when potentials of more than + 650 mV were used at some stages in the applied waveform.[181]

Background CV studies were also performed at different potentials with Pt electrodes in electrolytes consisting of 8 mmol/L HIBA with 30 mmol/L creatinine, and 10 mmol/L succinic acid with 30 mmol/L creatinine. A typical CV obtained with a Pt electrode is shown Figure 4.5. The peak shape is similar to that shown above for Au electrodes, with slight shift in the organic peak potential (- 180 mV). Thus, these and the above CV studies illustrate that the organic electrolytes adsorbed at Au and Pt electrode surfaces led to smaller background currents and baseline noise by decreasing the capacitance current and inhibiting O_2 reduction. These studies also suggest that these organic molecules can be desorbed at higher positive potentials, which allows high capacitance current and O_2 reduction to occur. Thus to minimize noise in EC detection, high positive potentials should be avoided. Consequently, the inhibition of oxygen reduction by adsorbed organic electrolytes offers important advantages and makes it possible to perform electrochemical detection without degassing.

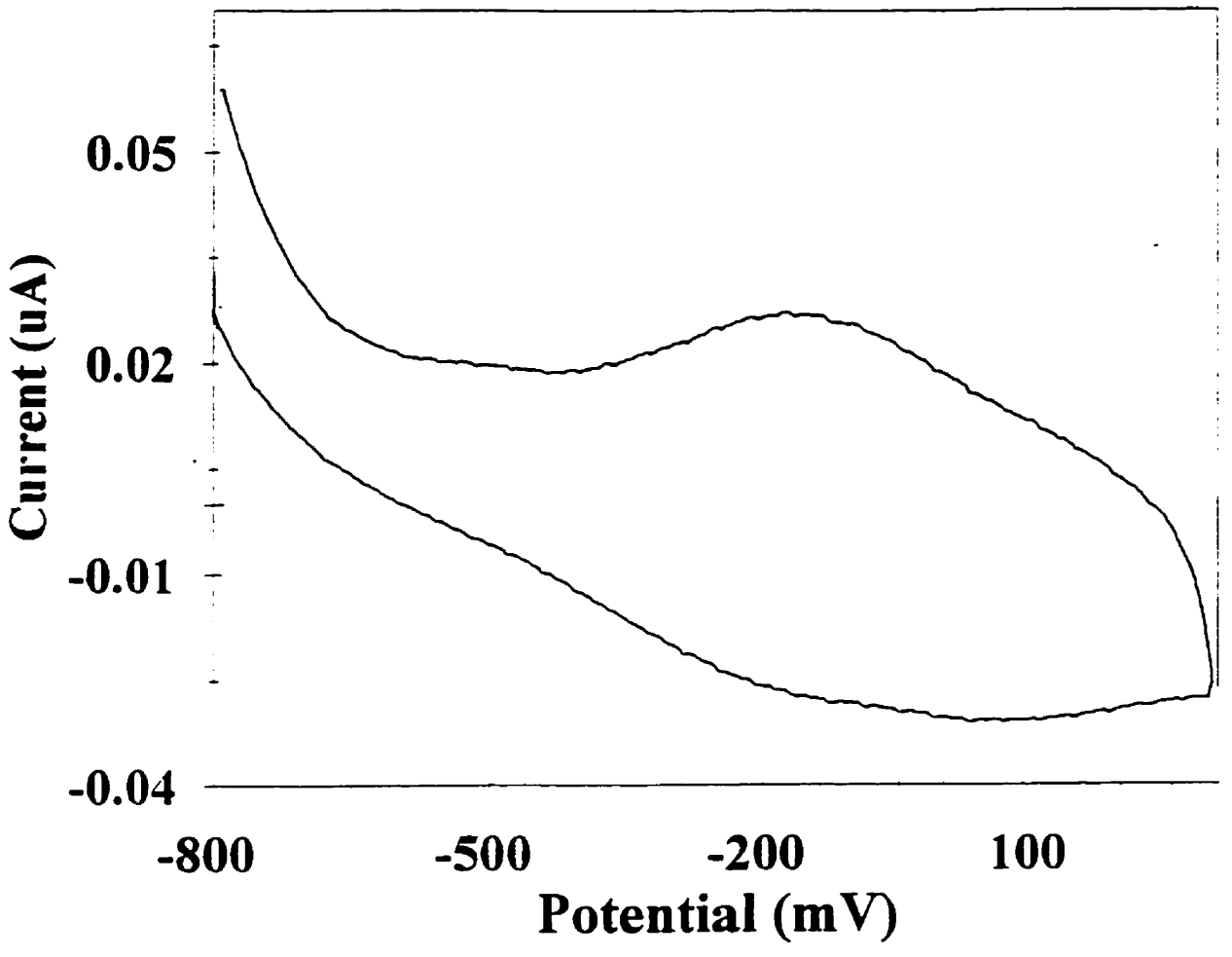

Figure 4.5 On-line cyclic voltammograms with a 25 μm Pt electrode for HIBA/creatinine electrolytes. Experimental conditions: cathodic current is considered as positive current; on-line CV detection; applied potentials, -800 mV for 55 ms and then scanned to 300 mV at 20 V/s; other conditions as for Figure 4.1.

4.3. On-line CVs of Metal Ions

In the early parts of these studies, deformed peaks, negative peaks and irreproducible responses were observed under certain conditions in EC detection of metal ions. Appearance of these problems depended on the analytes present in a mixture and on the analytes injected previously, which implied that electrode behavior might have been changed by the analytes. These changes in electrode behavior could be caused by reagent adsorption, deposition of metals, and H^+ or O_2 reactions. To help understand the factors affecting electrode response, on-line CVs for Tl^+, Zn^{2+}, Cd^{2+}, Ni^{2+}, Co^{2+}, Cu^{2+}, and Ag^+ were analyzed under a variety of CE experimental conditions.

As shown in Figure 4.1, there is a large residual current, mainly from capacitance charging current, and this current makes it difficult to observe the CVs of the analytes. To minimize this problem, the first 5 to 10 CVs of the background electrolyte were averaged and then subtracted from CVs collected at all other parts of the CE separation. CVs of all analytes were also examined without background subtraction to determine if there were any changes in the background current (faradaic or capacitance). Experimental results at a Au electrode showed that Tl^+, Zn^{2+}, Cd^{2+}, Ni^{2+}, and Co^{2+} gave normal CVs with no appreciable change in background current. A typical set of on-line CVs with background subtraction is shown for Tl^+ in Figure 4.6. Each of the CVs in Figure 4.6 was recorded at a different point on the Tl^+ CE peak (~ 150 ms intervals). These results show that the on-line CV system gave good CV signals even for low concentrations (2 μmol/L to 3 μmol/L). This sensitivity was ≥ 100 fold larger relative to that obtained with off-line CV

analysis, which was done in bulk solution with background-subtraction. This improvement appears to be related to a stable background signal in the CE separation process in which ion movement transfers the analyte ions from the injected sample solution into the homogeneous background electrolyte. The results of CV studies on the test metal ions are discussed below according to their kinetic behavior.

Fast Kinetics Thallium forms +1 and +3 oxidation states, but the most stable oxidation state in aqueous solution is Tl^+. The standard potential for a Tl/Tl^+ electrode vs. SCE is:[182]

$$Tl^+ + e^- \rightarrow Tl \qquad E^o = -0.580\ V \qquad (4.2)$$

Since the potential for Tl^+/Tl^{3+} electrode is 1.25 V, Tl^+ usually presents a one electron transfer EC reaction in solution. Figure 4.6 shows that the oxidation/reduction of thallium in the range of -250 mV to -290 mV vs. SCE; the current in the forward sweep is larger than that in backward sweep because of the preconcentration of Tl^+ during the 55 ms period prior to each CV sweep and metal ions moving away from the electrode during the reduction step. The reduction potential of Tl^+ is shifted from the value (~ - 876 mV vs. SCE) expected from the Nernst equation [$E = E_o + (RT/nF)\ \ln(Tl^+)$] due to the effects of the electrical field from the separation voltage (20 kV), underpotential deposition of Tl^+, and complexation by HIBA.[183,184] The difference between the cathodic and anodic peak potentials was ~ 50 mV. This small difference in peak potentials, combined with the CV peak shape, implied that the electrochemical reaction for Tl^+ was relatively fast and reversible.

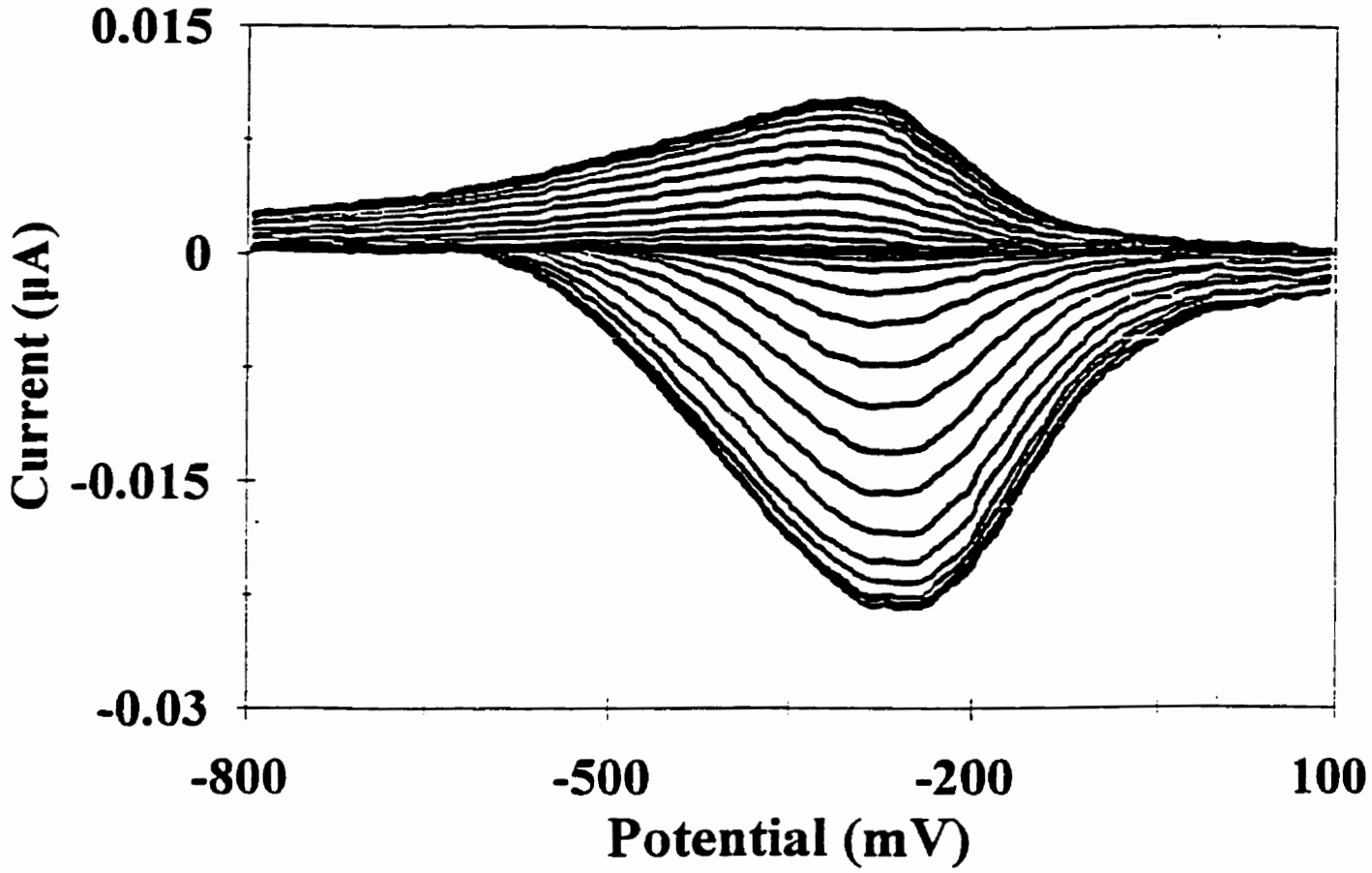

Figure 4.6 On-line cyclic voltammograms across a Tl^+ peak with a 25 µm Au electrode. Experimental conditions: on-line CV detection; applied potentials, -800 mV for 55 ms and then scanned to 100 mV and then back to -800 mV at 20 V/s; analyte concentration, 50 µmol/L; 10 cm hydrodynamic injection for 10 s; other conditions as for Figure 4.1; anodic currents are negative.

From the results obtained for Pb^{2+}, it also appears to be fast and reversible. Pb has two oxidation states (+ 2 and + 4), and the important oxidation state is +2.[185]

$$Pb^{2+} + 2e^- \rightarrow Pb \qquad E^o = -0.3703\ V\ (vs.\ SCE) \qquad (4.3)$$

The CVs for Pb obtained are shown in Figure 4.7 where the anodic and cathodic peaks appeared at -180 and -240 mV, respectively.

Intermediate Kinetics Zn usually forms the divalent ion as follows,

$$Zn^{2+} + 2e^- \rightarrow Zn \qquad E^o = -\ 1.007\ V\ (vs.\ SCE) \qquad (4.4)$$

It is observed in the CVs of Zn^{2+}, shown in Figure 4.8, that its oxidation/reduction peaks centered at -650 and -800 mV respectively; the difference (- 150 mV) in the peak potentials indicates that Zn has a quasi-reversible EC behavior at the Au electrode. Some negative current in the CVs of Zn^{2+} were observed at potentials of less than -900 mV; this is caused by H^+ evolution and would be discussed in the next section.

Slow-Kinetics For Cd^{2+}, the only stable oxidation state in aqueous solutions is +2. The Cd/Cd^{2+} half reaction is,

$$Cd^{2+} + 2e^- \rightarrow Cd \qquad E^o = -0.6465\ V\ (vs\ SCE) \qquad (4.5)$$

The oxidation and reduction peaks for Cd^{2+} are separated by ~ 500 mV as shown in Figure 4.9; the reduction peak occurred at -400 mV and the oxidation peak at 100 mV.

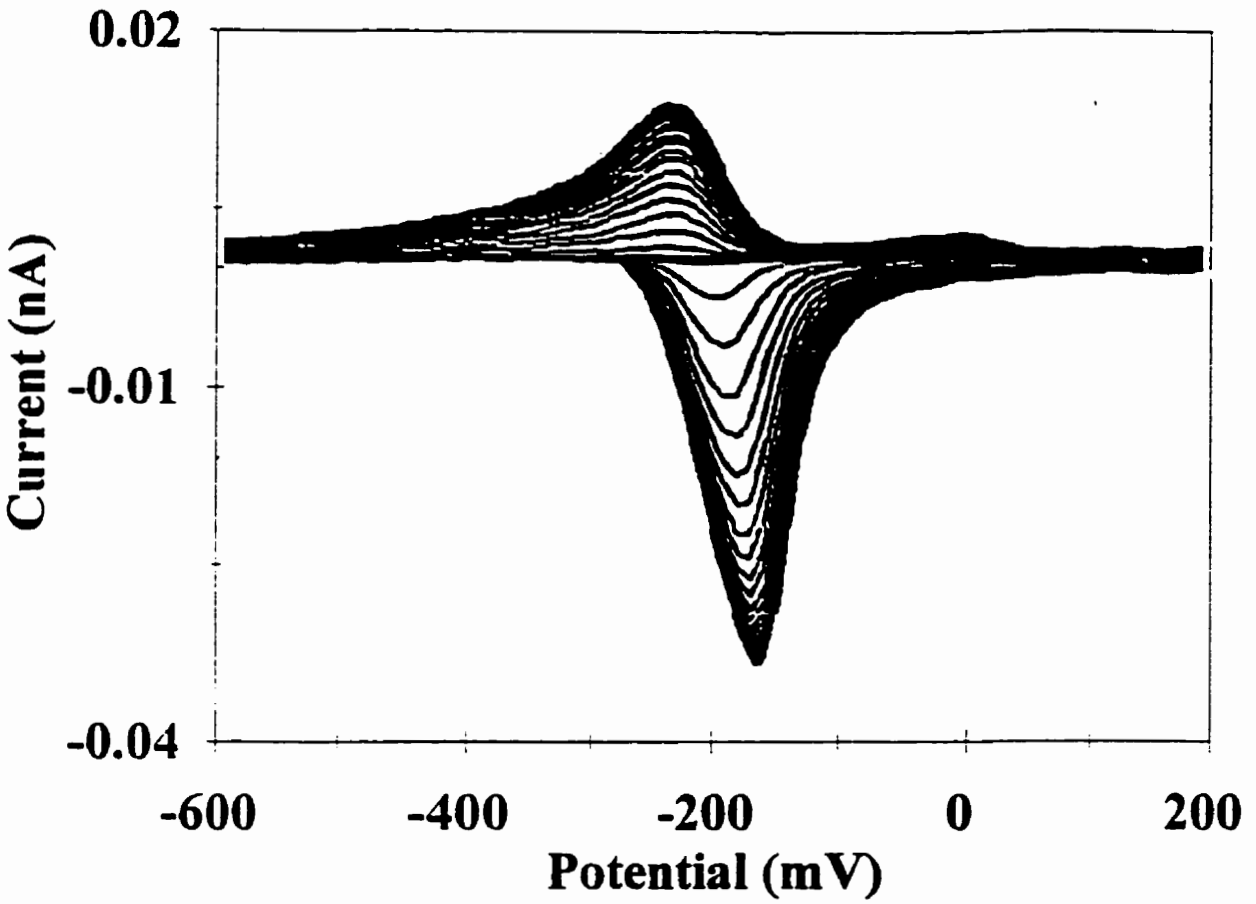

Figure 4.7 On-line cyclic voltammograms across a Pb^{2+} peak with a 25 μm Au electrode. Experimental conditions: on-line CV detection; applied potentials, -600 mV for 55 ms and then scanned to 200 mV at 20 V/s; analyte concentration, 50 μmol/L; 5 kV electromigration injection for 10 s; other conditions as for Figure 4.1.

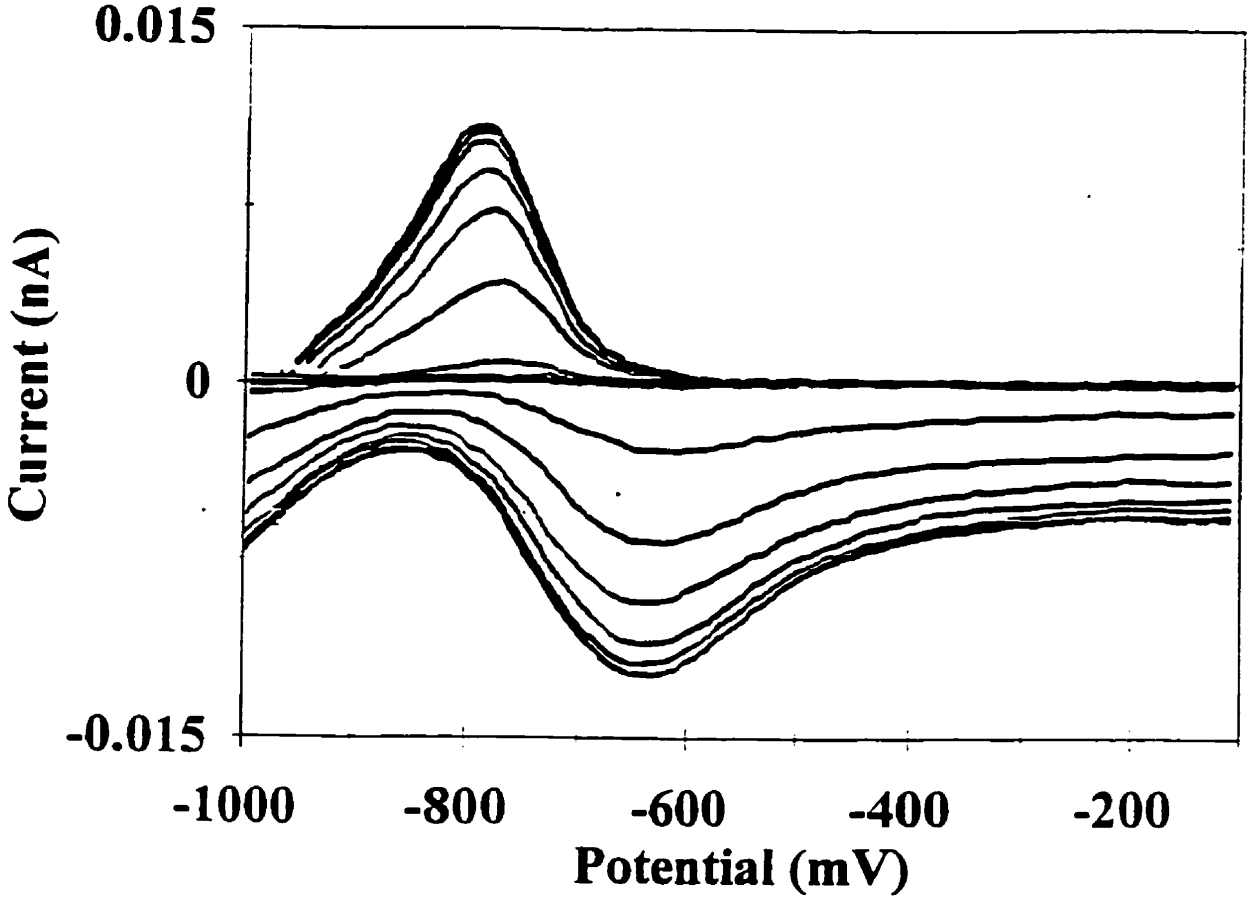

Figure 4.8 On-line cyclic voltammograms across a Zn^{2+} peak with a 25 μm Au electrode. Experimental conditions: on-line CV detection; applied potentials, -1000 mV for 55 ms and then scanned to -100 mV at 20 V/s; analyte concentration, 50 μmol/L; 5 kV electrokinetic injection for 10 s; other conditions as for Figure 4.1.

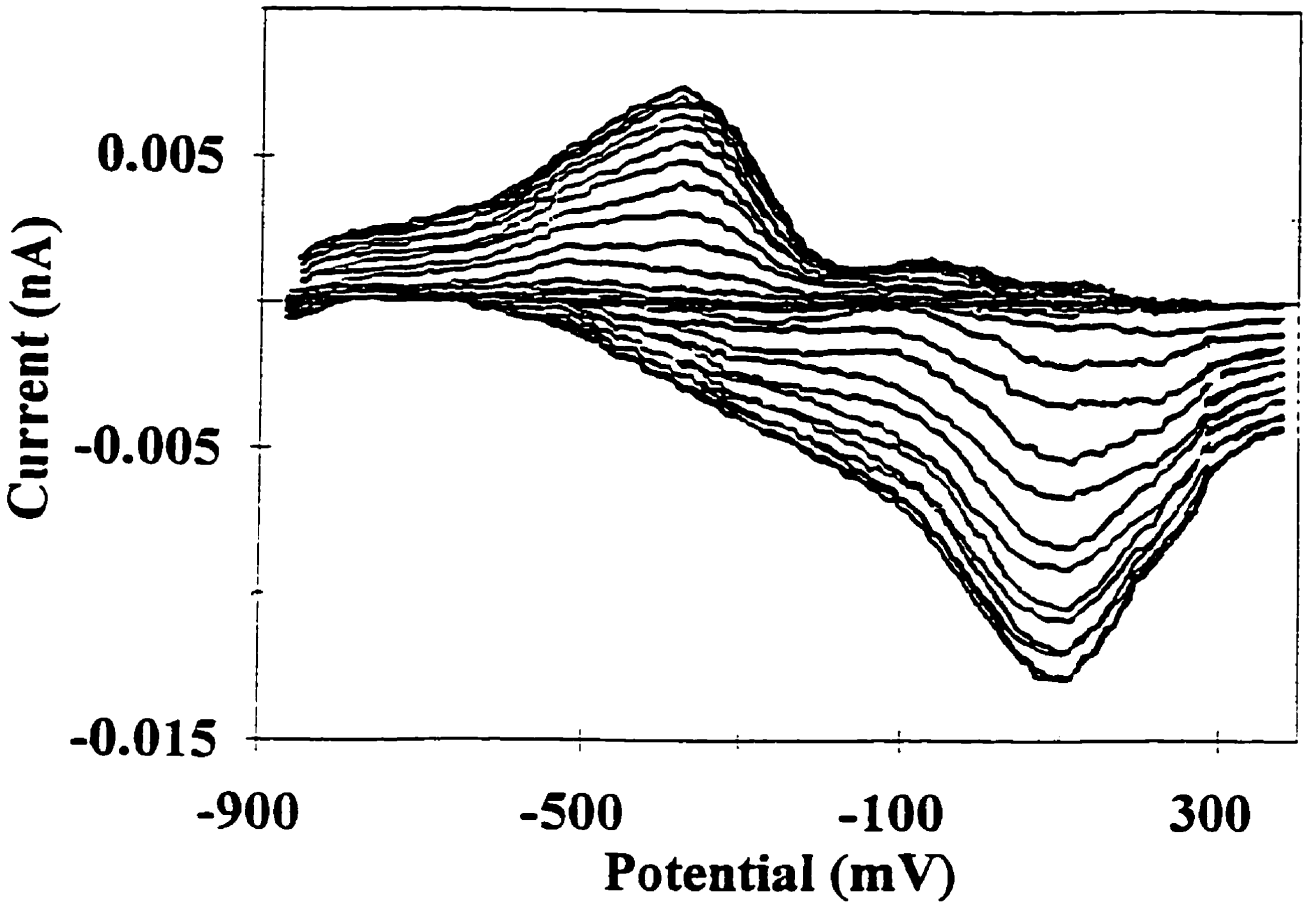

Figure 4.9 On-line cyclic voltammograms across a Cd^{2+} peak with a 25 μm Au electrode. Experimental conditions: on-line CV detection; applied potentials, -900 mV for 55 ms and then scanned to 400 mV at 20 V/s; analyte concentration, 50 μmol/L; 5 kV electrokinetic injection for 10 s; other conditions as for Figure 4.1.

This separation of the cathodic and anodic peak was caused by slow kinetics of the electron transfer, and thus the reaction for Cd can be considered to be irreversible at the Au electrode.

Ni and Co are two adjacent transition metal elements and have similar standard potentials. The Ni/Ni^{2+} and Co/Co^{2+} reactions are shown as follows,

$$Ni^{2+} + 2e^- \rightarrow Ni \qquad E^o = -0.472\ V\ (vs.\ SCE) \qquad (4.6)$$

$$Co^{2+} + 2e^- \rightarrow Co \qquad E^o = -0.521\ V\ (vs.\ SCE) \qquad (4.7)$$

However, these two metal ions were actually reduced at much more negative potentials (≤ -900 mV) in aqueous solution due to slow kinetics of the electron transfer. The CVs for Ni^{2+} are shown in Figure 4.10 where the cathodic and anodic peaks were farther separated than those for Tl^+, Pb^{2+}, and Zn^{2+} The oxidation reaction started at -200 mV and continued until the vertex potential (100 mV) on the forward sweep; on the backward sweep, the reduction reaction started at -700 mV and a rapid increase of positive current was observed at the potential of < -900 mV due to hydrogen evolution. The cathodic and anodic peaks for Co^{2+} were also well separated as shown in Figure 4.11, with the oxidation peak appearing at -300 mV, and its reduction adsorption starting at -700 mV. Hydrogen evolution caused the rapid increase of the current at potentials more negative than -900 mV. These studies show that Ni^{2+} and Co^{2+} need more negative reduction potentials than their standard potentials, and their EC reaction are more irreversible than Zn^{2+}. The irreversibility of the Ni and Co stripping reaction has also been described by other researchers.[185,196]

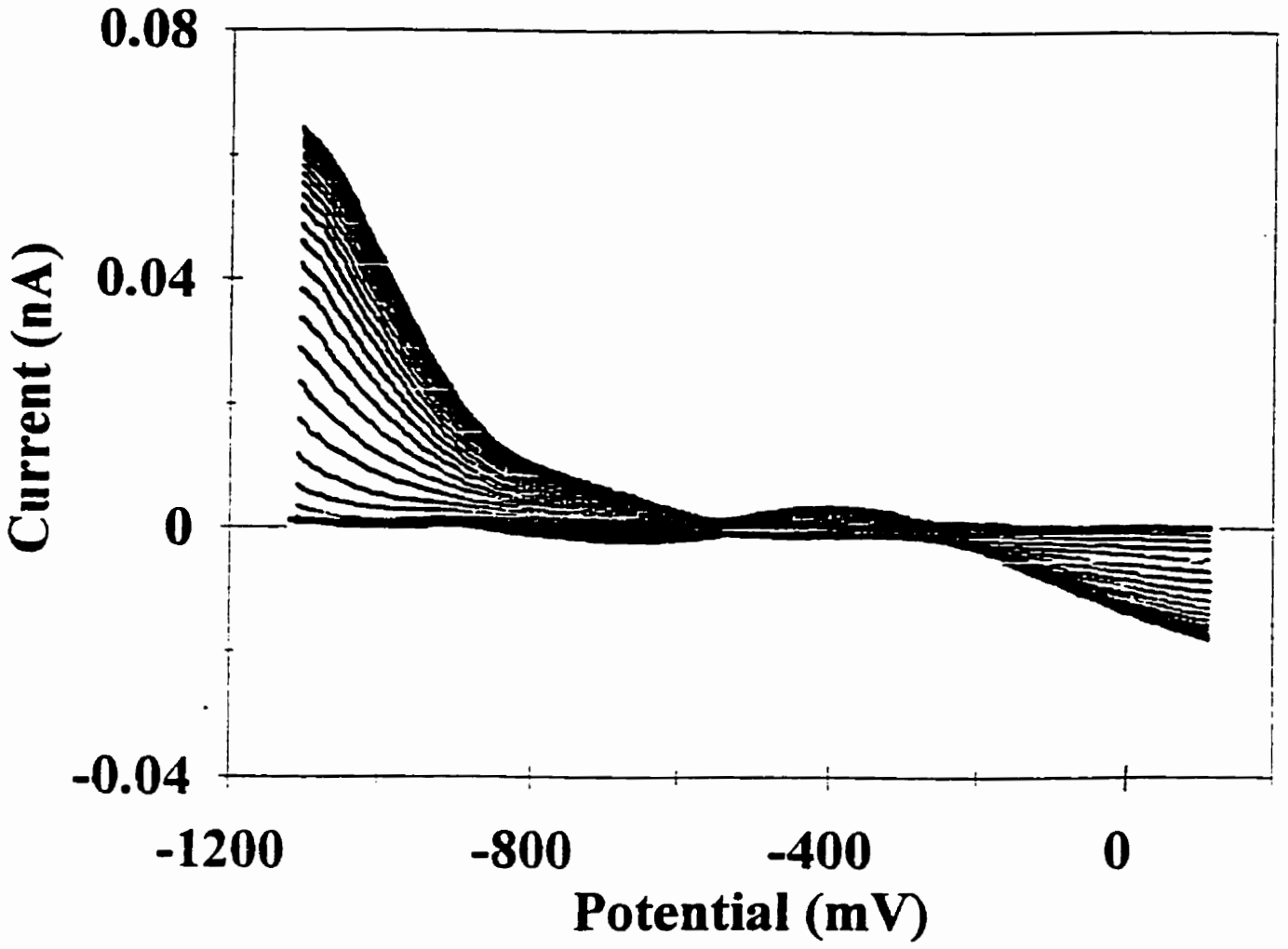

Figure 4.10 On-line cyclic voltammograms across a Ni^{2+} peak with a 25 μm Au electrode. Experimental conditions: on-line CV detection; applied potentials, -1100 mV for 55 ms and then scanned to 100 mV at 20 V/s; analyte concentration, 50 μmol/L; 5 kV electromigration injection for 10 s; other conditions as for Figure 4.1.

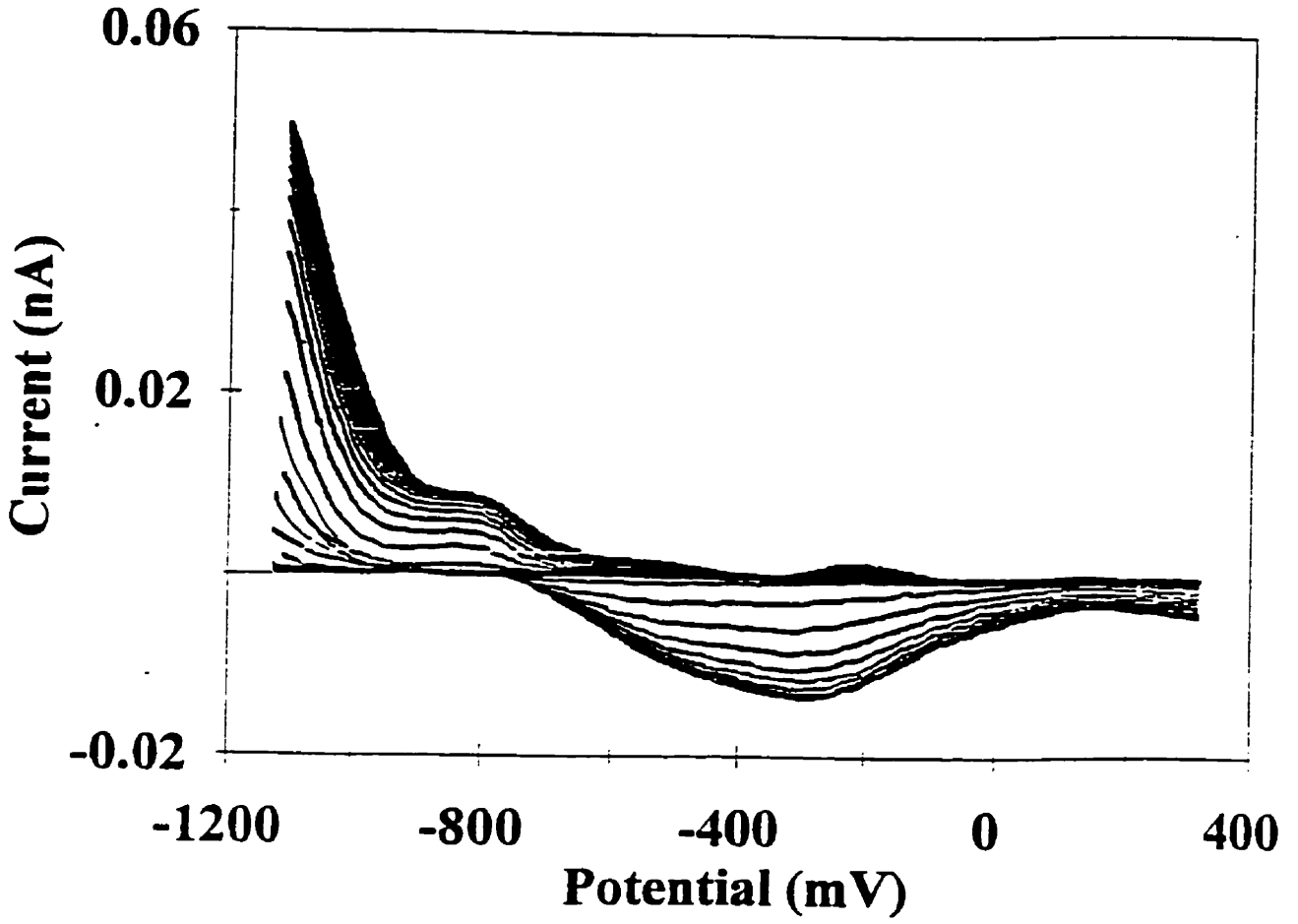

Figure 4.11 On-line cyclic voltammograms across a Co^{2+} peak with a 25 μm Au electrode. Experimental conditions: applied potentials, -1100 mV for 55 ms and then scanned to 300 mV at 20 V/s; on-line CV detection; analyte concentration, 50 μmol/L; 5 kV electromigration injection for 10 s; other conditions as for Figure 4.1.

Copper forms compounds in two oxidation states, +1 and +2, and their electron-transfer reactions are represented as follows,

$Cu^{2+} + 2e^- \rightarrow Cu$ $\quad E^o = 0.096\ V\ (vs.\ SCE)$ (4.8)

$Cu^{+} + e^- \rightarrow Cu$ $\quad E^o = 0.276\ V\ (vs.\ SCE)$ (4.9)

In the absence of species that can stabilize [Cu^+], Cu is often oxidized into Cu^{2+}. Ag usually shows a +1 oxidation state because Ag^{2+} is a very strong oxidizing reagent, and is not stable in aqueous system. The Ag/Ag^+ electrochemical reaction is.

$Ag^{+} + e^- \rightarrow Ag$ $\quad E^o = 0.5551\ V\ (vs.\ SCE)$ (4.10)

The CVs of both Cu^{2+} and Ag^+ gave two sets of peaks, and the result for Cu^{2+} is shown in Figure 4.12. At first sight these two sets of peaks seem to represent two different electron transfer processes. However, it was observed in the CVs of Cu^{2+} that the current collected in presence of the metal ion was smaller than the current collected in absence of the metal ion, indicating that the background current decreased when metal ion was reduced at the electrode. Ag^+ gave the results similar to Cu^{2+}. Thus, for Cu^{2+} and Ag^+, it was the changes in background current instead of electrochemical reaction that led to the two sets of peaks in their voltammograms. Therefore, the CVs of Ag^+ and Cu^{2+} did not really show evidence for the electrochemical reaction of Cu^{2+} and Ag^+.

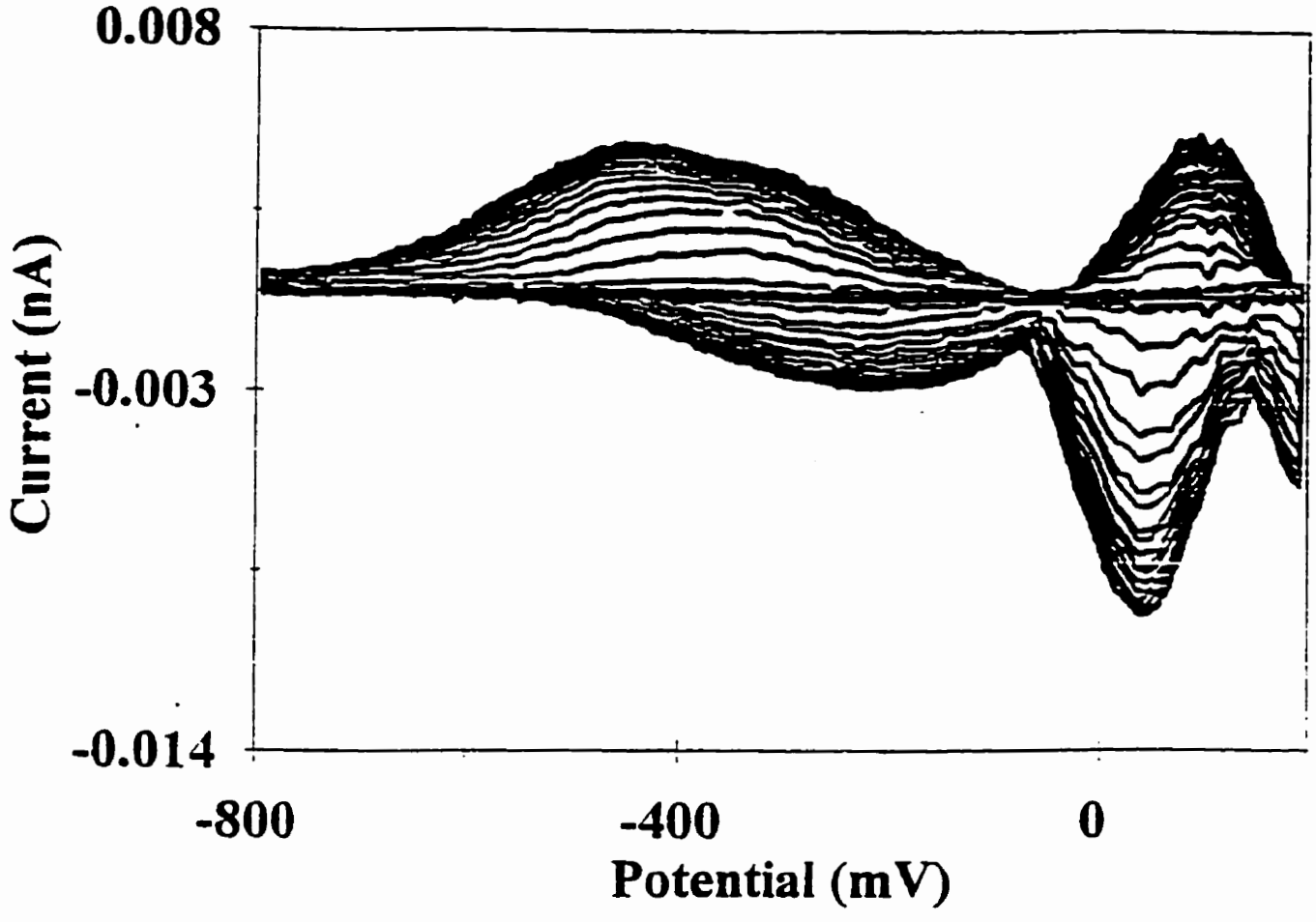

Figure 4.12 On-line cyclic voltammograms across a Cu^{2+} peak with a 25 μm Au electrode. Experimental conditions: on-line CV detection; applied potentials, -800 mV for 55 ms and then scanned to 200 mV at 20 V/s; analyte concentration, 50 μmol/L; 5 kV electromigration injection for 10 s; other conditions as for Figure 4.1.

CVs of the analytes on newly polished Pt electrodes were similar to those obtained at newly polished Au electrodes with the following differences: for Tl^{+}, Pb^{2+} and Cd^{2+}, the cathodic and anodic peaks shifted toward more negative potentials; and for Zn^{2+}, the cathodic peak moved to a more negative potential (-900 mV) and the anodic peak to a more positive (-475 mV). These changes were likely due to the difference in the adsorption energy of the analytes at Au and Pt surfaces.[133] Comparison with those (Figure 4.6 to 4.11) obtained in HIBA and creatinine, the CVs of metal ions obtained in succinic acid and creatinine gave similar shape with slight shifts of peak potentials. For example, the oxidation and reduction peaks of Tl^{+}, Pb^{2+} and Co^{2+} in succinic acid and creatinine, shifted toward a more positive potential at Au or Pt electrodes; for Cd^{2+}, shifted toward a more negative potential region. These shifts were caused by the difference in the complex formation constants and in the adsorption of anions at the electrode.

The use of high vertex potentials not only changed the CVs of the electrolyte but also affected the shape and peak potentials in the CVs of metal ions. The result for Tl^{+} when the CV vertex potential is changed from 400 to 700 mV is shown in Figure 4.13. Compared to Figure 4.6, it can be observed in Figure 4.13 that the oxidation and reduction peaks shifted positively to - 50 and -150 mV, respectively and the voltammogram was noisy. These changes might be caused by changes in the electrode surface because CV studies of the electrolyte showed that organic species adsorbed at the electrode could be stripped off when the CV potential was 700 mV (see section 4.2).

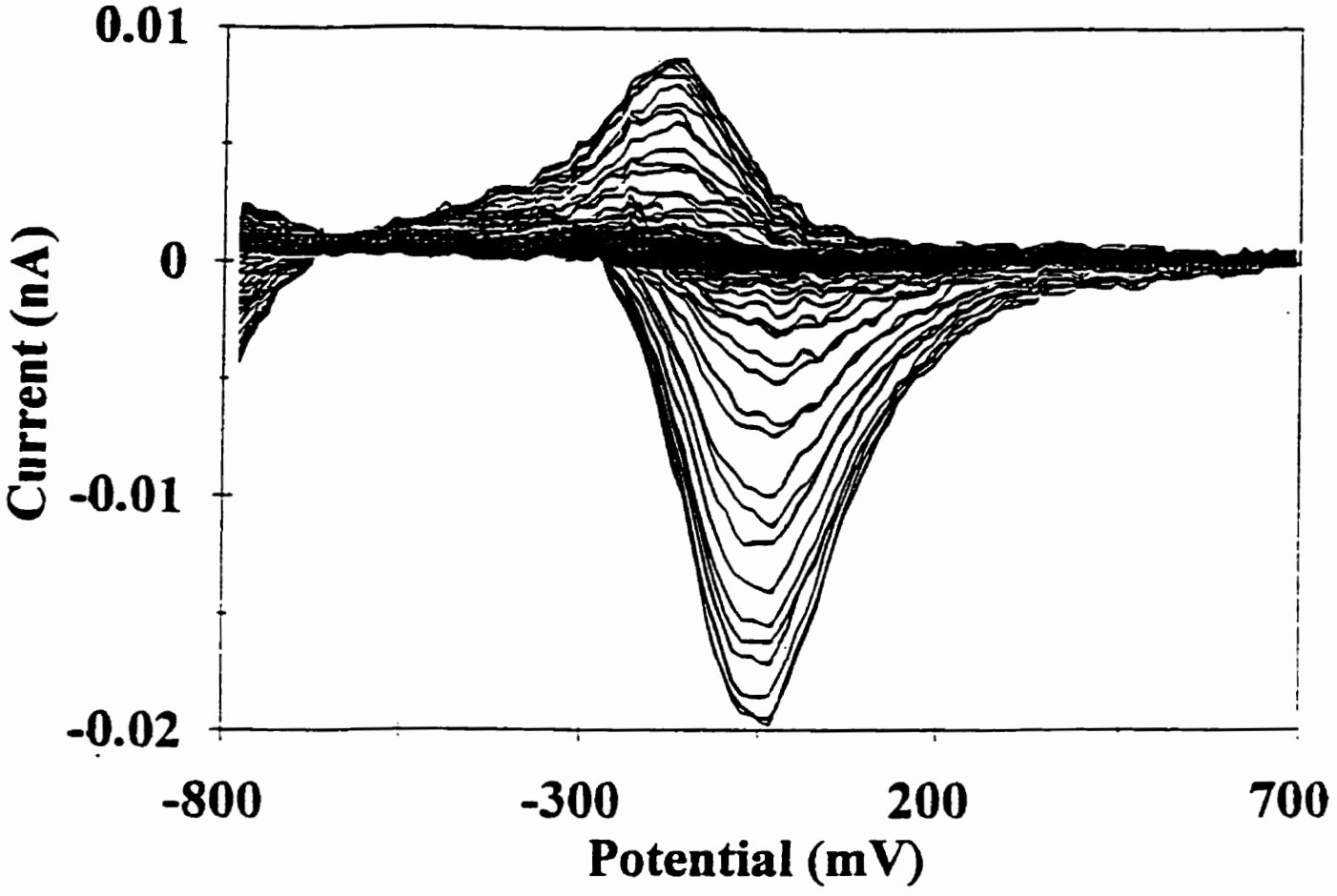

Figure 4.13 On-line cyclic voltammograms across a Tl^+ peak with a 25 µm Au electrode. Experimental conditions: on-line CV detection; applied potentials, -800 mV for 55 ms and then scanned to 700 mV at 20 V/s; analyte concentration, 50 µmol/L; 5 kV electrokinetic injection for 10 s; other conditions as for Figure 4.1.

In addition, the electrode surface might be oxidized at the high positive potential, thus contributing to a high background noise. The same increase in noise was also observed in succinic acid and creatinine, and in an acetate buffer when a high vertex potential was applied. Consequently, high oxidation potentials (> 400 mV) were usually not chosen for EC detection.

4.4. Stability of Au and Pt Electrodes

Reproducible electrode response is important for analytical applications. Analyte interaction with Au and Pt surfaces might affect electrode response, and to examine this possibility analytical and background signals were examined over repeated injections of analyte (up to 10 times). A typical result obtained for repeated injection of Tl^+ (5×10^{-5} mol/L) is shown in Figure 4.14. No change was observed in Figure 4.14 for either the background signal or analyte responses. Similarly, no change was observed in the background signal when Co^{2+}, Ni^{2+}, Zn^{2+}, or Cd^{2+} were injected, nor in the peak shapes/responses for the other analytes present in the sample (Tl^+, Co^{2+}, Ni^{2+}, Zn^{2+}, and Cd^{2+}). These results illustrated that repetitive reduction/oxidation of these metal ions on Au electrodes did not induce significant changes in the electrode surfaces.

However, the electrode behavior after detection of Pb was different from the above metal ions. Although no change was observed in the background CVs over repeated injection for Pb^{2+}, changes were observed the CVs of Pb^{2+} and some other analytes. For example, the CVs from a Cd^{2+} peak, after repeated sampling with Pb^{2+}, is shown in Figure 4.15. Compared to the result in Figure 4.9, a new peak occurred at ~ -100 mV in Figure 4.15 and the peak potential shifted considerably. Some other metal

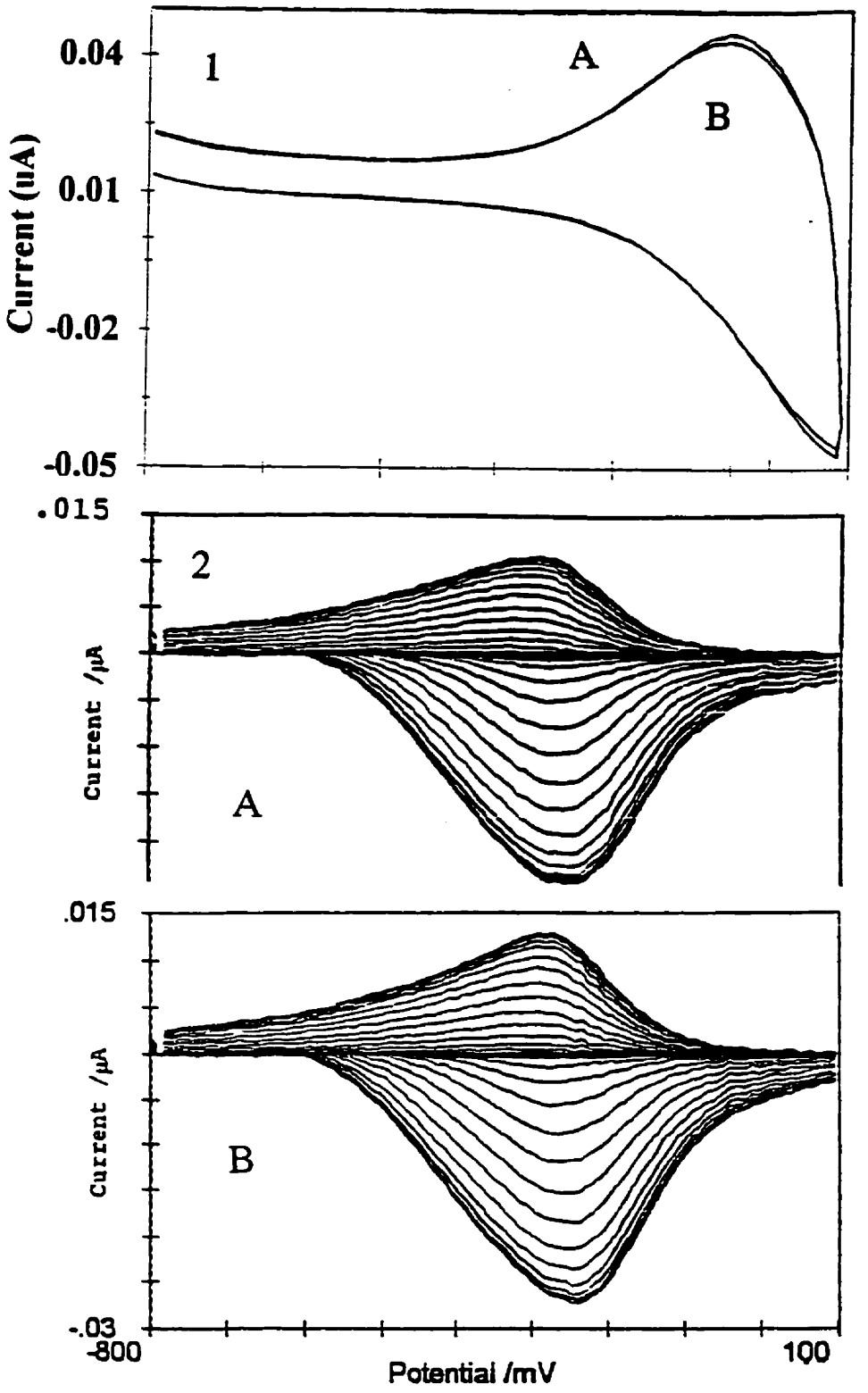

Figure 4.14 On-line background voltammograms (1) and Tl^+ voltammograms (2) in HIBA/ creatinine electrolytes with a 25 µm Au electrode before (A) and after (B) detecting Tl^+ (up to 10 times). Experimental conditions: cathodic current is considered as positive current; applied potentials, -800 mV for 55 ms and then scanned to 100 mV at 20 V/s; Tl^+, 50 µmol/L; other conditions as for Figure 4.13.

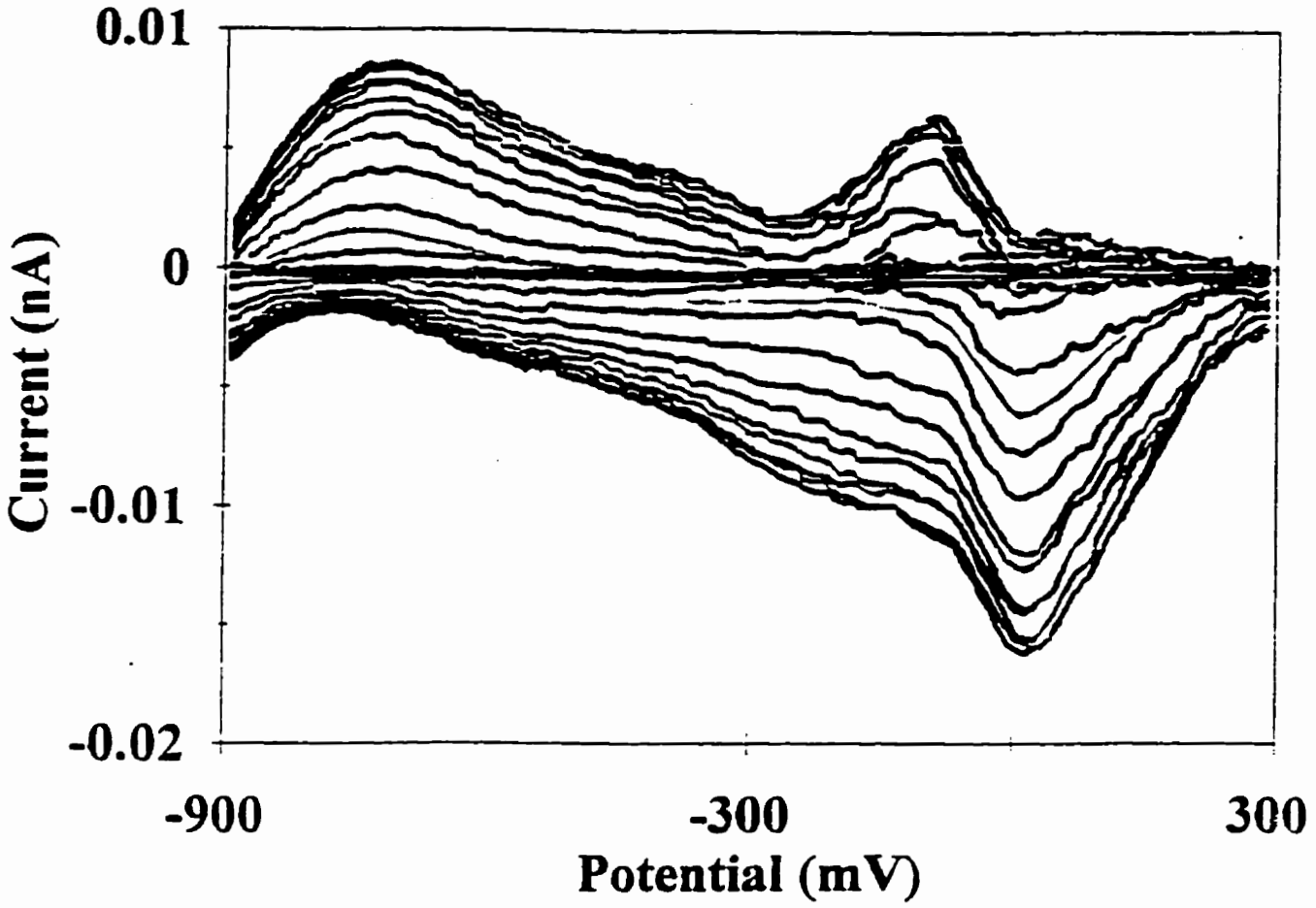

Figure 4.15 Effect of injection of Pb^{2+} samples on subsequent cyclic voltammograms across Cd^{2+} peaks at a 25 μm Au electrode. Experimental conditions: on-line CV detection; applied potentials, -900 mV for 55 ms and then scanned to 300 mV at 20 V/s; analyte concentration, 50 μmol/L; electromigration injection at 5.0 kV for 10 s; after the electrode was used to detect five Pb^{2+} samples., other conditions as for Figure 4.7.

ions (Tl^+, Zn^{2+}) also showed changes in their CVs, such as shifts in peak potential and changes in peak shape after the electrode was used to detect Pb^{2+}. Pt electrodes gave results similar to those at Au electrodes. The change in the electrode response due to Pb detection was prevented when the CV vertex potential was adjusted to 400 mV, likely because of more complete stripping of Pb from both Au and Pt electrodes. Literature results from X-ray scattering have revealed that Au electrodes are substantially roughened after deposition and stripping of Pb possibly due to formation of a Pb-Au surface alloy.[187] It has also been reported that O_2 reduction on Pt/Pb_{ads} could be enhanced by Pb_{ads},[188] which may lead to Pb peak tailing or baseline shifts. Consequently it appears that the effects of Pb^{2+} may be related to a combination of changes in electrode properties and incomplete stripping of Pb. Therefore, for EC detection when Pb^{2+} is present, a vertex potential of ~ 400 mV should be chosen for detection of the Pb^{2+} peak, but this will be at the cost of higher background currents and noise (see above section 4.2).

The detection of Cu^{2+} and Ag^+ had even stronger effects on the reproducibility of the response of Au and Pt electrodes. Noise increased following detection of the peaks of these metal ions, and a decrease in background current could be observed after Cu^{2+} or Ag^+ deposited on the electrode. The CVs are shown in Figure 4.16 when a 25 μm Au electrode was placed in HIBA/creatinine electrolyte with and without Cu^{2+} (2.0×10^{-5} mol/L). Comparison of these two CVs show that the current at ~ 300 mV in the presence of Cu^{2+} (injecting concentration of 2×10^{-5} mol/L), was smaller than that in the absence of Cu^{2+} due to the decrease in the background current when Cu^{2+} deposited on the electrode.

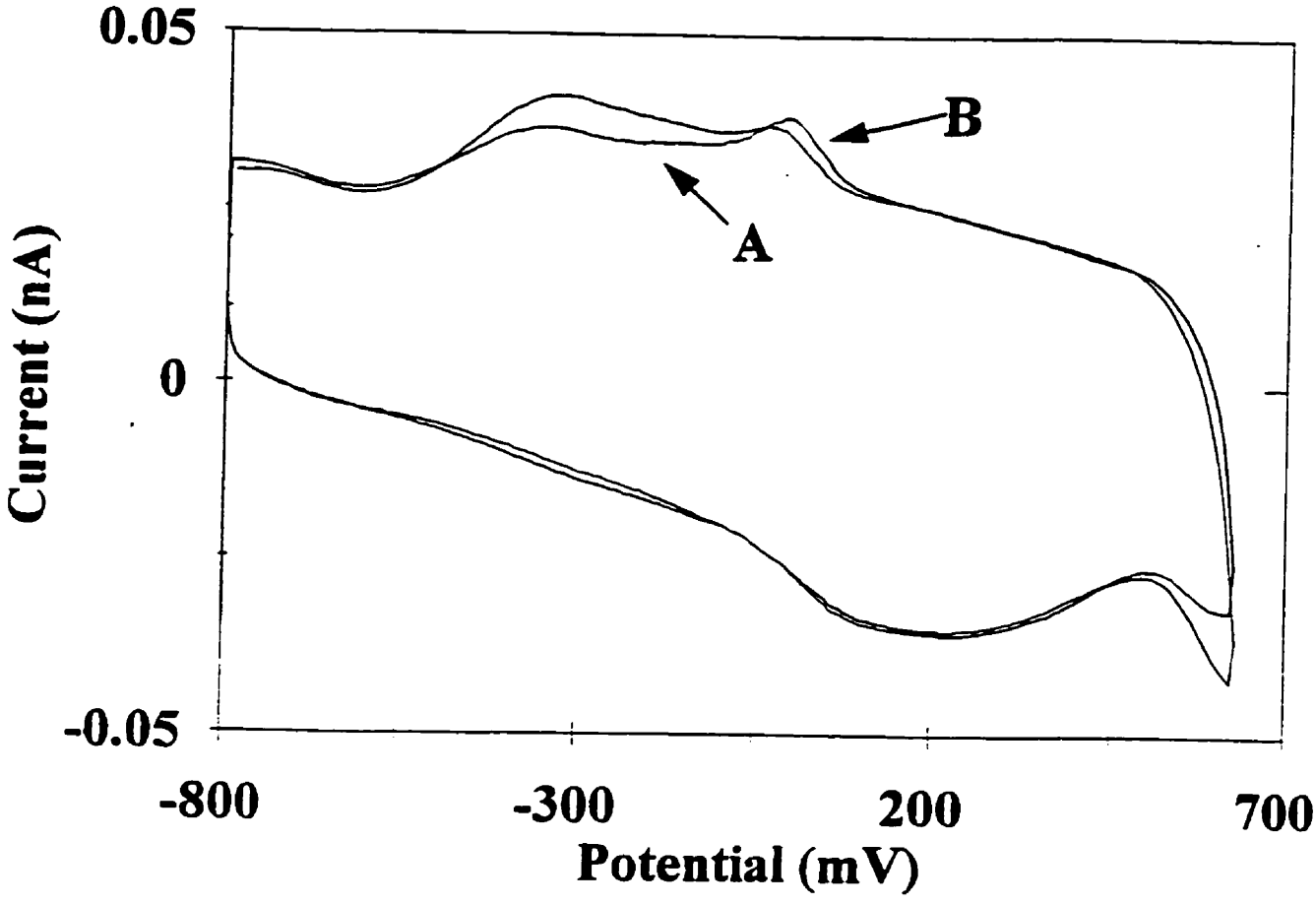

Figure 4.16 Voltammograms at a 25 μm Au electrode for HIBA/creatinine electrolytes with (A) and without (B) Cu^{2+}. Experimental condition: applied potentials, -800 mV for 55 ms and then scanned to 700 mV at 20 V/s; Cu^{2+}, 20 μmol/L; 0.008 mol/L HIBA with 0.030 mol/L creatinine, pH 4.8.

Literature results reported for scanning tunneling microscopy studies[189] have suggested that deposition of Cu^{2+} at Au and Pt surfaces induces changes in the electrode surface. It was also reported[139,190] that deposition of copper at a Au surface could completely block active sites of a Au surface to inhibit some reactions (such as O_2) due to the replacement of catalytic sites by electroinactive Cu or CuO. To determine if adsorption of organics could be a factor in the responses observed for Cu^{2+}, CVs of Cu^{2+} were examined in phosphate and nitrate buffers. In these inorganic electrolytes, the analytical signal was 4-5 times as large as the background current when 1.0×10^{-4} mol/L Cu^{2+} was added. These results and the above results suggested that decreases in the background currents were caused by organic compounds. Similar results were also observed at Pt electrodes. How the organic compound caused a decrease in background current and an increase in background noise is not known with certainty. But it would probably be due to the coadsorption of organic compounds and complexes of metal-organics. The decrease in the background current often led to negative peaks for Cu^{2+} and Ag^{+} detection when the concentration of these analytes was $\leq 2.0 \times 10^{-5}$ mol/L; and small & broadening peaks for higher concentrations. A high vertex potential (> 400 mV) could not prevent the changes in background current observed during the EC detection of Cu^{2+} or Ag^{+} because the adsorbed organics and metal layers would form at the backward sweep even though they could be stripped of the electrode at the forward sweep as indicated in the CV studies of electrolytes (see Figure 4.1). Therefore, the sensitivities for Cu^{2+} and Ag^{+} were poor in the HIBA/creatinine or succinic acid/creatinine electrolyte. The use of inorganic electrolytes can improve the detection of Cu^{2+} and Ag^{+}.

4.5. H_2 Evolution

The above CV studies help explain some problems associated with peak shape and changes in the electrode response, but for Ni^{2+} and Co^{2+}, which did not show any evidence for altering electrode response, shifted baselines and distorted peaks were still observed under certain conditions. A factor that might cause this behavior is a change in the electrode response for H^+ evolution; the rate of this reaction depends on the activation energy of H^+ reduction on the electrode,[191] which is a function of the electrode materials and their structures. Hydrogen has a high-overpotential (or no adsorption) on Au, Hg, Pb, Tl, Cd, Zn surfaces; and a low-overpotential on Ni, Co, Pt surfaces.[192] For the pH values in the electrolyte (4.4 to 4.8), H^+ evolution starts to occur at a potential $\leq$ - 700 mV. For Tl^+, Pb^{2+}, Cd^{2+}, Cu^{2+} and Ag^+ detection, the applied potential required for detection could be adjusted to avoid H^+ evolution, but for Zn^{2+}, Ni^{2+}, and Co^{2+} a potential of $\leq$ -900 mV is needed. As a result, the change in the current from H^+ reduction was often observed (see section 4.3) in the voltammograms of Zn^{2+}, Ni^{2+}, and Co^{2+} due to deposition of these analytes. A decreased current was observed in the voltammogram of Zn^{2+} and an increase in voltammograms of Ni^{2+}, and Co^{2+}. These changes are consistent with the shift in H^+ overvoltage caused by these metals (see above). A change in H^+ reduction at Pt electrodes was observed in the CVs for most of the test metal ions due to differences in the activation energy between Pt surfaces and the other metal layers. Therefore, metal-ion peaks can contain responses both from the reactions of metal ions and H^+, and in some instances this caused baseline to shift. This problem can be avoided if the detection response is taken only during the anodic portion of a voltage pulse. This is

not a limitation because this mode of data analysis usually gives maximum S/N (discussed in section 4.3). One possible cause of H^+ reduction is the change of the pH close to the electrode. To help reduce these effects, a moderately-high concentration of creatinine (30 to 50 mmol/L) was added into the electrolyte to prevent this change.

4.6. Effect Of Electrolyte On Electrochemical Detection in CE

The composition of the background electrolyte is expected to have some effect on the analyte signal, and this was studied briefly for the HIBA/creatinine system used in this work. Different amounts of HIBA and creatinine were added to the electrolyte, the pH was adjusted with acetic acid to a final value of 4.8, and the effect of the ratio of these two components on the analytical signal was examined. Typical results for Tl^+ was shown in Table 1, and other metal ions gave results similar to Tl^+. The results show that low concentrations of these components resulted in unstable baselines and low analytical signals, possibly due to poor buffering capacity, which would make the system susceptible to pH changes at the surface of the electrode (see above). Larger concentrations of these components resulted in more stable signals, but larger concentrations of HIBA reduced analyte response, possibly as a result of large complexation of the metal ion, which would cause peak broadening as a result of slow exchange between different metal complexes. Therefore, the optimal concentration of HIBA for CE and EC systems was 0.008 to 0.01 mol/L and creatinine was 0.03 to 0.05 mol/L.

4.7. Conclusion

On-line CV studies of the analyte and electrolyte components gave useful information for understanding the nature of the electrochemical reactions of the analytes, which is required to optimize EC detection. Compared to Pt, Au electrodes provided better reproducibility, likely due to a weaker interaction between the electrode/analyte and electrode/electrolyte. Therefore, Au μm-electrodes were chosen for most of the analytical studies reported in chapters 5, 6 and 7.

Table 1. Effect of electrolyte composition on detector performance for Tl(I). Experimental conditions: separation voltage, 20 kV over 25 μm × 60 cm capillary; 25 μm Au disk electrode; pulse voltage, -850 mV for 72 ms and 100 mV for 96 ms; analyte, Tl(I) at 100 μmol/L; electromigration injection with 5 kV for 10 s.

Electrolyte	Peak Current (nA)	Baseline
5 to 8 mmol/L HIBA 20 mmol/L creatinine	1.0 to 1.5	unstable
20 mmol/L HIBA 20 to 30 mmol/L creatinine	0.4 to 0.5	stable
10 mmol/L HIBA 40 to 50 mmol/L creatinine	3.0 to 2.5	stable

5. PULSED AMPEROMETRIC DETECTION IN CE

5.1. Constant-Voltage and Pulsed Amperometric Detection

Although constant-voltage amperometric detection (CVD) can offer a reproducible electrode response for metal ions at Hg or Hg-film electrodes,[193] detection at solid electrodes is expected to alter the electrode response because analytes may deposit onto the electrode. To evaluate the change under controlled conditions detector response was monitored as a function of time when a freshly polished electrode was placed in metal ion solutions having concentrations of 10, 100, and 500 μmol/L. All of the test metal ions had an effect on electrode response, and typical CVD results are shown for Pb^{2+} in Figure 5.1 (CVD curves A, B and C). The CVD response changed as the analyte deposited onto the electrode, and as expected this change was the greatest for solutions having the largest concentration of analyte; the response for the 500 μmol/L solution of Pb^{2+} changed 25% in the first 200 s. Similar studies with other test metal ions showed that for Tl^{+}, Co^{2+}, Cd^{2+}, Cu^{2+} and Ag^{+} an increase in response with time was observed, for Ni^{2+} a decrease, and for Zn^{2+} only a small change (~2%). The CVD detection was also evaluated under CE conditions with both Pt and Au electrodes. Distorted peaks (broadening, tailing, and baseline shifts) were often observed for CVD detection of metal ions. Typical results for Tl^{+}, Cd^{2+}, and Pb^{2+} is shown in Figure 5.2, which shows that the background current shifted after each peak.

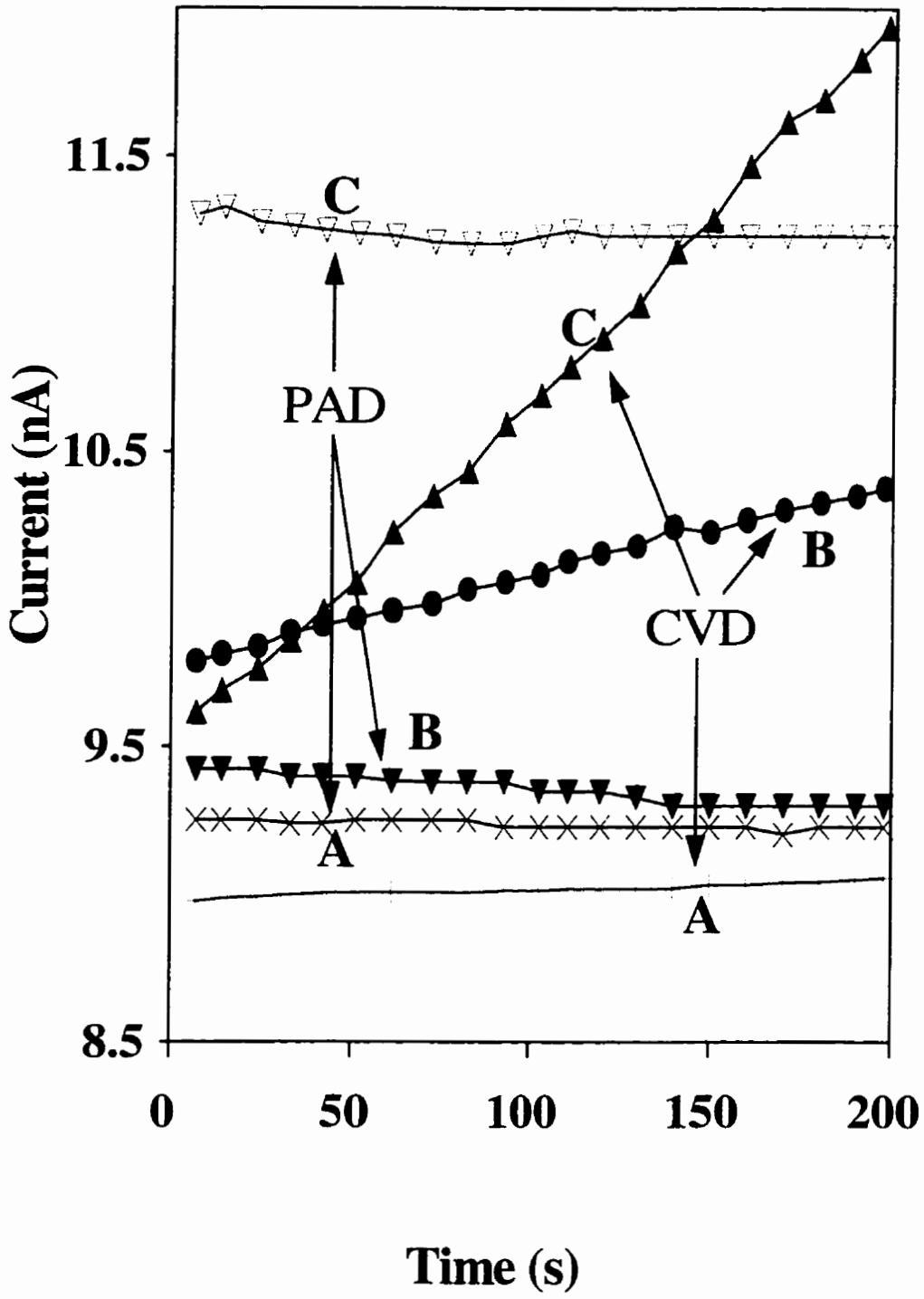

Figure 5.1 Current-time response for Pb^{2+} at a 25 μm Au electrode in CE. Constant voltage detection (CVD curves), -850 mV vs SCE; pulsed-voltage detection (PAD curves), -850 mV vs SCE for 72 ms (data collected over last 24 ms) and 100 mV for 96 ms; electrolyte, 0.03 mol/L creatinine, 0,008 mol/L HIBA, pH 4.76; analyte concentration, A, B, C, 10, 100, 500 μmol/L, respectively.

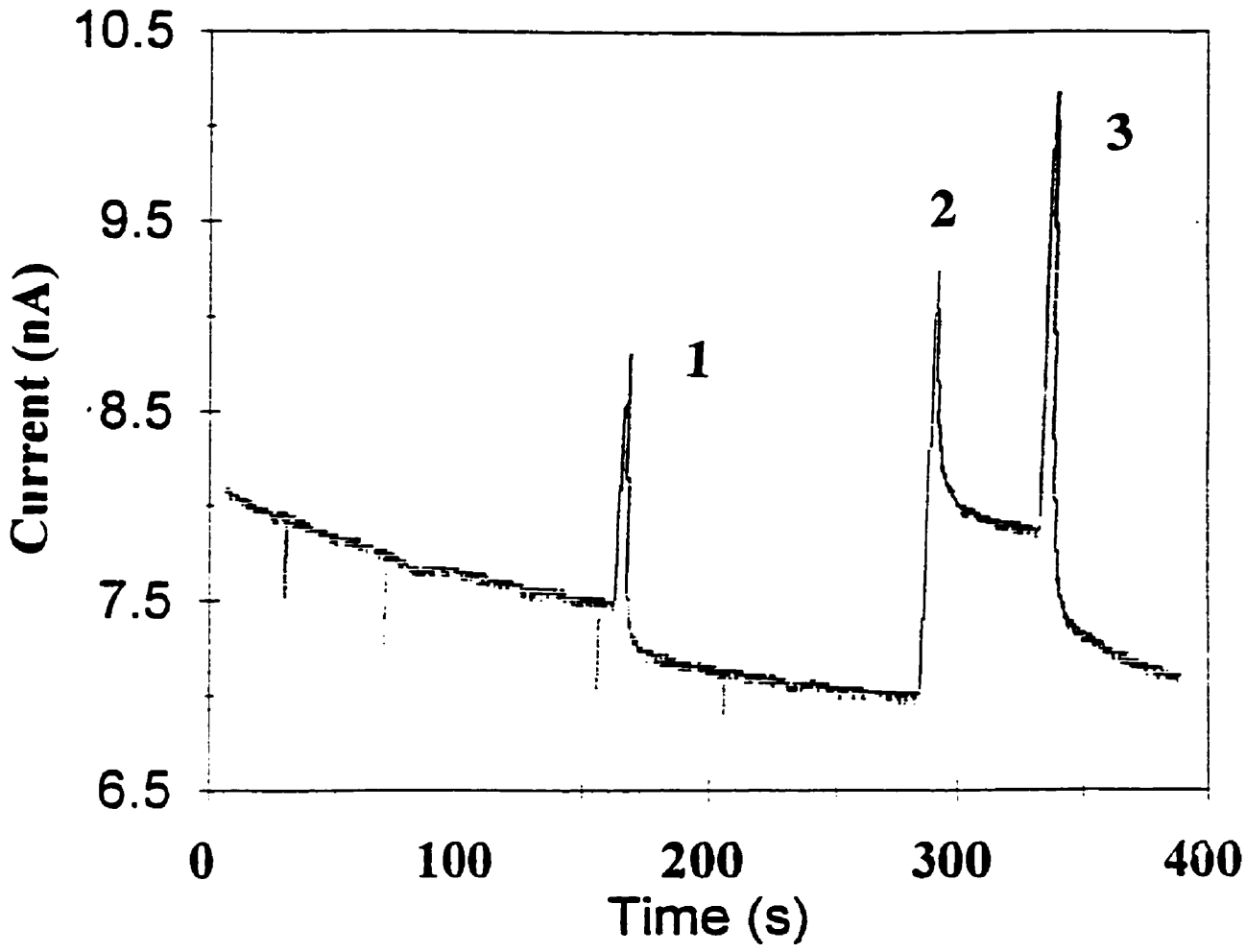

Figure 5.2 Electropherogram of metal ions with constant voltage detection at a 25 μm Au electrode. Experimental conditions: applied potential -800 mV; electrolyte, 0.03 mol/L creatinine with 0.008 mol/L HIBA, pH 4.8; analyte concentration, 200 μmol/L; sample injection, 5 kV electromigration for 10 s; separation voltage, 20 kV over 25 μm i.d. × 60 cm capillary; peak identification: (1), Tl^{+}; (2), Cd^{2+}; (3), Pb^{2+}.

The electrode responses of metal ions under CE conditions were also examined for replicate sample injections, and the result for Tl^+ is shown in Figure 5.3. It is shown in Figure 5.3 that the electrode response gradually increased for subsequent injections, and the relative standard deviation (RSD) of the electrode response (for 25 injections) was > 15%. Similar results were observed for Co^{2+}, Ni^{2+}, Zn^{2+}, Cd^{2+}, Pb^{2+}, Cu^{2+}, Ag^+ and Hg^{2+} with RSD in the range of 8.04% and 20%. These changes in the electrode response and the baseline were probably caused by the deposition of metal ions on the electrode. These results indicate that detection under constant voltage conditions is not a viable analytical approach because the metals deposited in the electrode alter the electrode surface, which can enhance or reduce the electrode response of metal ions and other compounds.

An alternative approach that can avoid the above problems is the use of multistep potential waveforms. The use of a simple square-wave waveform offers the possibility of cleaning the electrode with an oxidative step and using both reduction (cathodic) and oxidation (anodic) currents for detection. Use of cathodic detection was evaluated initially for data collected over the last 24 ms of the reduction step. For pulsed amperometric detection (PAD), the detector response as a function of time when a freshly polished Au electrode was placed in Pb^{2+} solutions (10, 100, and 500 µmol/L), varied less than 0.6% within the first 200 s (see PAD results in Figure 5.1). Similar results were obtained for Tl^+, Co^{2+}, Ni^{2+}, Zn^{2+} and Cd^{2+}. For all of the test metal ions, the average current with PAD detection varied by < 1% within the first 200 s for concentrations up to 1000 µmol/L. Use of the anodic current, where data was collected in the first ~ 48 ms of the oxidation step, also showed an average current within ± 1% for the test metal ions.

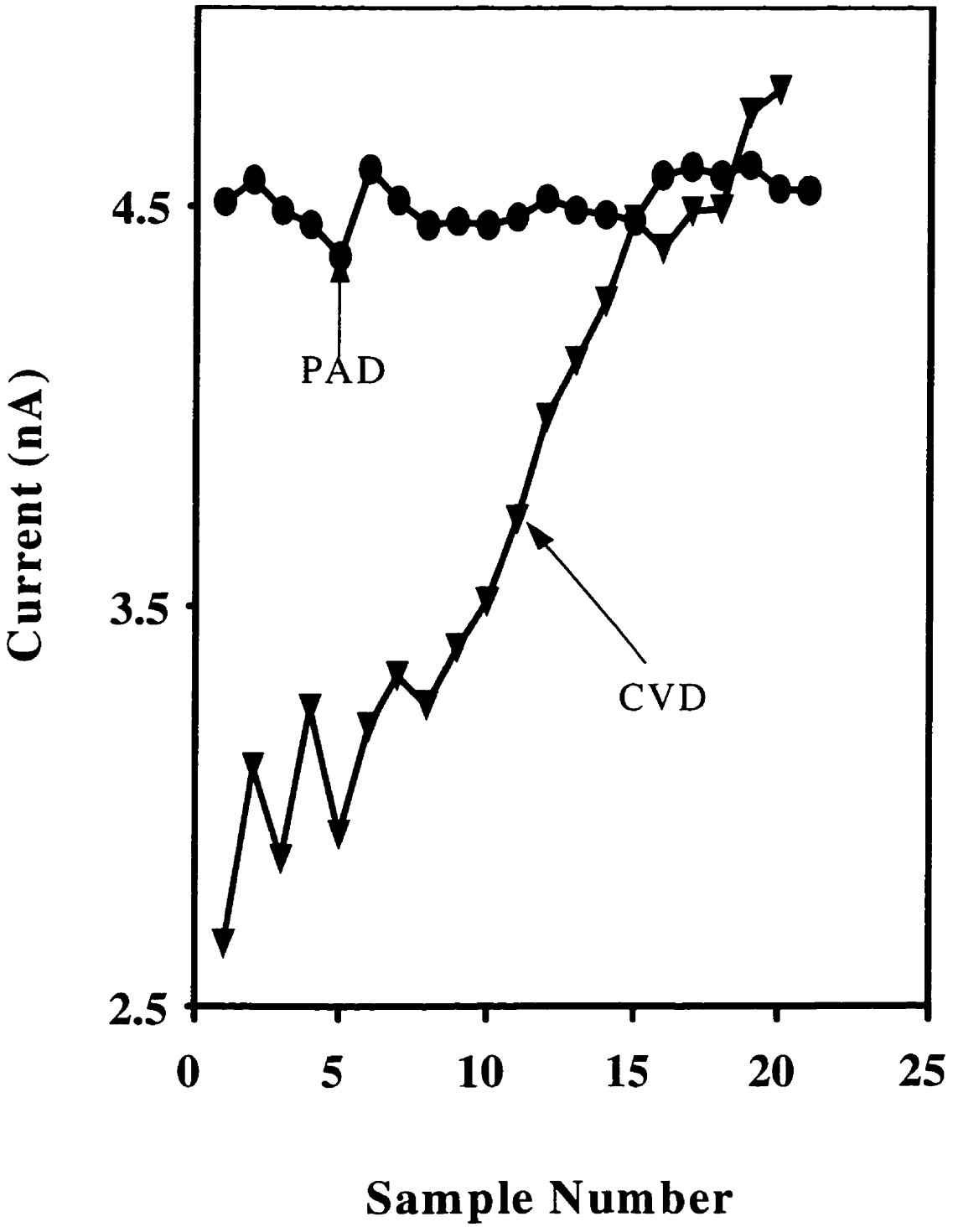

Figure 5.3 Electrode response (Peak Height) for repetitive injection at a 25 μm Au electrode with CVD and PAD detections. Experimental conditions: electrode potential for constant-voltage, -850 mV; for pulsed-voltage, -850 mV for 66 ms with data collected over last 24 ms, 200 mV for 132 ms; analyte concentration Tl^+, 100 μmol/L; other conditions as for Figure 5.2.

For Cu^{2+} and Ag^{+}, with concentration less than 50 μmol/L, the change in average current was within 2%; but this change increased rapidly when the metal ion concentration was more than 50 μmol/L. Under CE conditions, PAD electrode responses were also examined for repeated injection (up to 20 times) for metal ions in the range of 1.0×10^{-5} to 1.0×10^{-3} mol/L, and a typical PAD result for Tl^{+} (100 μmol/L) is shown in Figure 5.3. The excellent RSD value of 2.7% for PAD is clearly much smaller than that for the CVD results also shown in Figure 5.3. Consistent electrode response (RSD < 5%) was also obtained for PAD detection of Co^{2+}, Ni^{2+}, Zn^{2+}, Cd^{2+} and Pb^{2+}. These results indicated that PAD detection should provide reproducible electrode response for most of the test metal ions in CE since an oxidation step can strip accumulated metals from the electrode surface. Consequently this approach was examined in more detail.

5.2. Waveform and Current' Time Response

The pulse waveform chosen for initial studies was a simple bipolar pulse, shown in Figure 5.4, in which the negative potential was used to reduce metal ions, and positive potential was used to clean the electrode. Since it was important to know the current's time response curve upon application of a step voltage, the electrode response was monitored for the application of both positive and negative pulses. Figure 5.5 shows the response obtained with the test analyte Tl^{+} at a Au electrode when a bipolar pulse was applied; similar behavior was observed with Pt electrodes. The first part of Figure 5.5 corresponds to current changes upon application of a -850 mV pulse. A significant

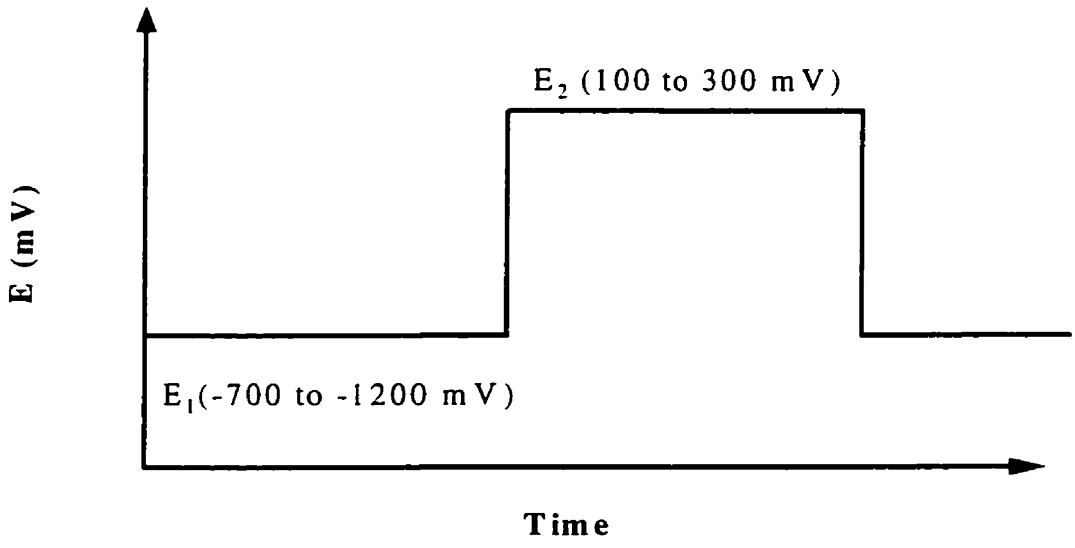

Figure 5.4 A simple bipolar potential waveform

contribution to the initial high current is the charging current, which should decay within several microseconds for a 25 μm disk electrode.[142] The decay of the faradaic response to an approximately steady-state condition took less than 1 ms, which agrees with that expected for the theoretical response of μm-electrodes.[143] The data in Figure 5.5 suggest that it may be possible to use the currents after 1 ms for analytical response, which is termed cathodic detection in this report. When the voltage was changed to + 200 mV at 16 ms, the current observed was anodic, and can be attributed to the stripping of the analyte deposited during the reductive part of the pulse. It can be seen that this current took longer (~ 10 ms) to decay, and the shape of this curve was a function of the amount of metal ion deposited and the nature of the metal ion. For detection with anodic signals, integration over the first 10 ms of the oxidative step was normally required for optimal detection; slightly longer times were required for higher concentrations of metal ions.

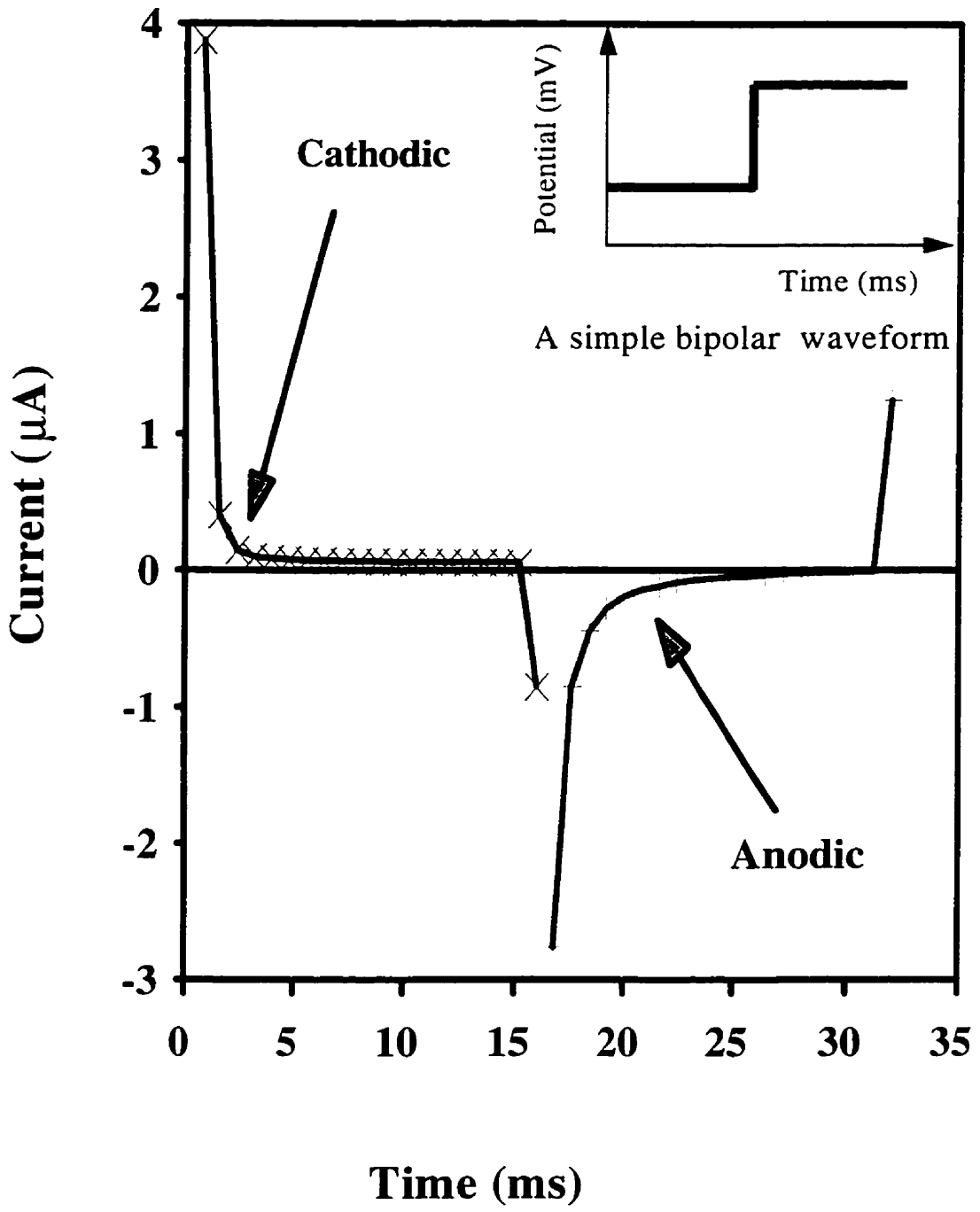

Figure 5.5 Response for Tl^+ at 25 μm Au electrode. Experimental conditions: electrode potential, -850 mV from 0 to 16 ms (data collected over 0.8 ms intervals) and then changed to 200 mV at 16 ms; electrolyte, 0.035 mol/L creatinine, 0.008 mol/L HIBA with pH 4.8; analyte concentration, 100 μmol/L.

5.3. Optimization of Pulse Parameters

5.3.1. Cathodic Detection

Signals obtained with PAD will depend on pulse duration and voltages applied during the pulse. Consequently the effect of these parameters was examined. The test metal ion used initially for these studies was Tl^+ at a concentration of 100 µmol/L. The effect of the oxidation potential (cleaning) on signal was examined in the +500 mV to -500 mV range. When the cleaning potential at Au was larger than 300 mV, the background current and noise increased quickly, possibly as a result of the increase in capacitance current, oxidation of the Au µm-electrode, and/or hydrogen and O_2 reductions (see section 4.1). This increase in background current and noise resulted in the relative standard deviations of electrode response increasing to above the 5% level; degradation of reproducibility was also observed at Pt electrodes with cleaning potentials above 300 mV. When the cleaning potential was less than -300 mV the standard deviations also increased above 5% because not all of the deposited analyte was being removed during the cleaning step.

The influence of reduction voltage was also evaluated in terms of the analytical and background signal. During cathodic detection, background signals and reproducibilities were relatively constant until the reduction voltage was less than -700 mV, and at the potential more negative than -1000 mV baseline noise increased rapidly. Cyclic voltammetric studies indicated that changes observed in the signal below this potential were primarily due to H^+ reduction (see section 4.1). The reduction potential has an effect on the current, and the response observed for Tl^+ is shown in Figure 5.6. As expected,

the analyte signal increased to a plateau as the voltage was adjusted to values above that required for the diffusion-limited current (-400 to -700 mV for Au electrode; -350 to -700 mV for Pt electrode in Figure 5.6). Below -700 mV a decrease in analyte signal was observed, and this decrease was likely a result of change in the background current caused by H^+ reduction because deposition of the analyte during the detection pulse can affect the kinetics of hydrogen evolution. For this to be the cause of the decrease in signal in Figure 5.6, hydrogen would have to have higher overpotential on Tl surfaces than that on Au surfaces, which has been reported by other researchers.[194] Since the accumulated metal ion is removed during the cleaning step, the shift in the baseline is only observed in the presence of the analyte.

For cathodic detection, the reduction potential required for peak detection varied with the nature of the metal ion. For some metal ions, Zn^{2+} in particular, peaks were observed at potentials well below that expected from voltammetric studies. This may be a result of underpotential deposition and the deposition during each pulse was less than a monolayer. Such processes may also affect the reaction potentials of other metal ions. Most of the metal ions gave good cathodic response at the reduction potential less than -700 mV, but potentials more negative than -1000 mV were required to detect Co^{2+} and Ni^{2+}.

In cathodic detection, the length of time required for the cleaning and detection parts of a pulse are interrelated, and several different combinations were examined.

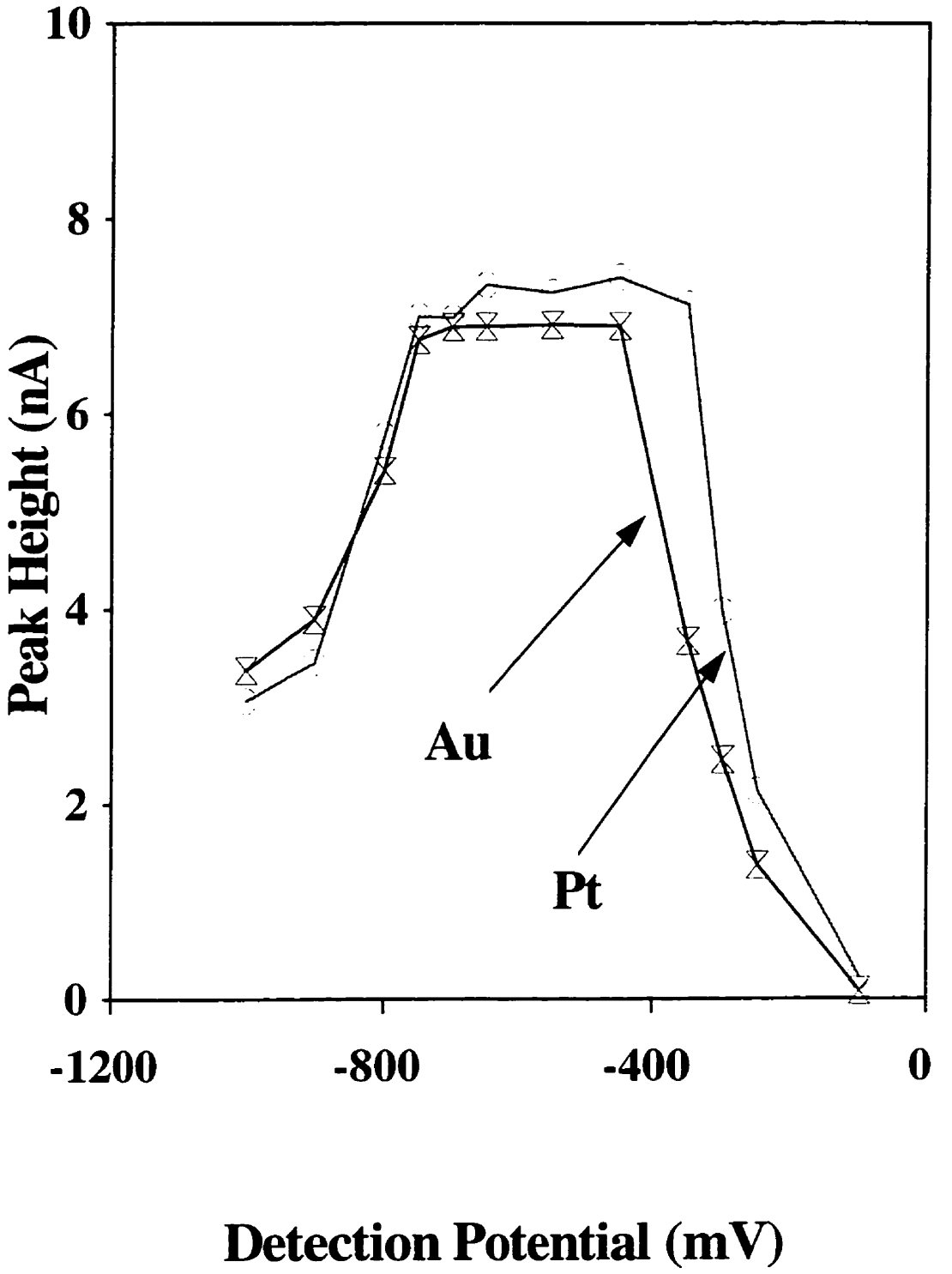

Figure 5.6 Influence of reduction potential on analyte current for cathodic PAD detection at a 25 μm Au electrode. Experimental conditions: detection interval, 72 ms with cleaning potential of 100 mV for 96 ms; 5 kV electromigration injection for 10 s; separation voltage, 20 kV over 25 μm i. d. × 60 cm capillary; electrolyte as for Figure 5.2; analyte concentration (Tl^+), 100 μmol/L.

It is of primary importance that the time for the cleaning pulse be sufficiently long to ensure there is no appreciable accumulation of analyte at the electrode; carryover of analyte from one pulse to the next may affect reproducibility and peak shape. A study of the reproducibility of the analytical signal for Tl^+ (100 μmol/L) at a Au electrode as a function of cleaning and reduction times is shown in Figure 5.7. In general, the cleaning times had to be longer than reduction times to keep precision at ~ 2%. At a fixed reduction potential, the relative standard deviation of the electrode response decreased with an increase in cleaning time. Curves A to D show that as the reduction time increased, shorter cleaning times were required to maintain good precision. Because individual noise is random, the longer ensemble averaging present for longer reduction times may been producing the improved stability from curves A to D. Results obtained with 25 μm Pt electrodes were similar to those for Au electrodes. The pulse conditions reported here used cleaning times of 96 to 120 ms and reduction times of 48 to 96 ms, which would permit the collection of 10 data points for a peak width of 2 s.

5.3.2. Anodic Detection

To study the effect of the value of the applied voltage on the anodic response obtained during PAD detection, analytical and background signals were examined at a series of different reduction and oxidation voltages. Figure 5.8 shows that the anodic

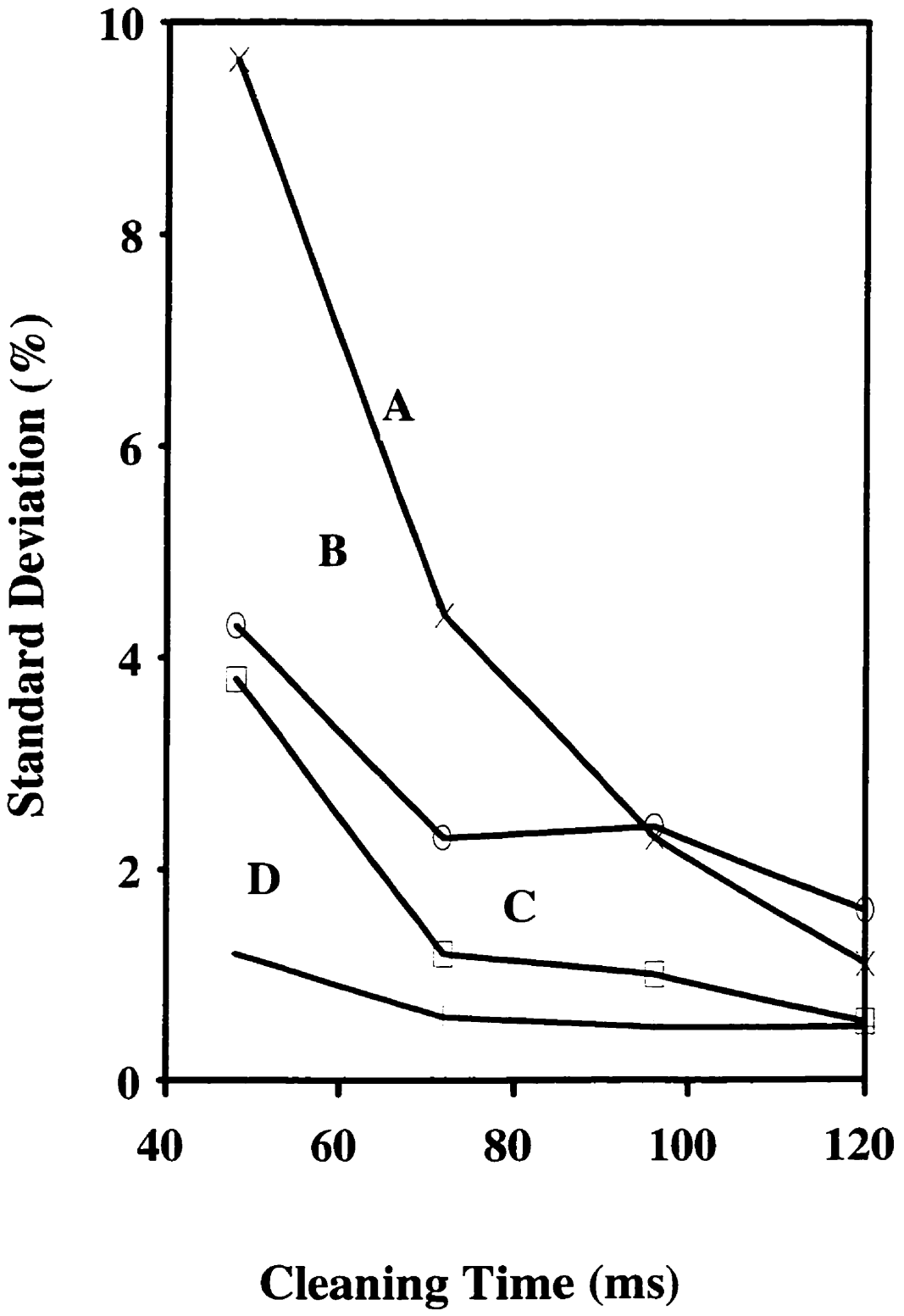

Figure 5.7 Influence of cleaning time on the peak height of analytical signal. Electrode, 25 μm Au; separation voltage, 20 kV over 25 μm i.d. × 60 cm capillary, electrode potential: -850 mV for detection, and 100 mV for cleaning; reduction time (A), 48 ms; (B), 72 ms; (C) 96 ms; (D) 120 ms; data collected during last 24 ms of reduction period; other conditions as for Figure 5.6.

analyte signal for Tl^+ increased to a plateau (± 5%) as the reductive voltage was adjusted to a value more negative than that required for diffusion limited current (-400 to -1200 mV). The reduction potentials required to obtain constant peak heights for other metal ions depend on the nature of the metal ion. When reduction potentials were more negative than -700 mV, analytical signal did not decrease (Figure 5.8) because in anodic detection there is no interference from oxygen reduction and/or hydrogen evolution. It was observed that background signal and reproducibility of the anodic signal were relatively constant over the reduction potential range of -400 to -1200 mV. For anodic analysis, optimal reduction potentials for Cd^{2+}, Pb^{2+}, Cu^{2+}, Hg^{2+}, Ag^+ were similar to that for Tl^+; for Zn^{2+}, Ni^{2+} and Co^{2+} more negative voltages were required for the reduction of these metal ions.

The magnitude of the anodic detection voltage also affected the analytical and background signals. Typical response for Tl^+ is shown in Figure 5.9 where maximum response was obtained around -100 to -300 mV. At potentials below -300 mV RSD increased above 5%, possibly because of incomplete removal of analyte during the anodic portion of the pulse; at sufficiently negative voltages, a cathodic peak was observed (positive peak height). The loss of analyte signal at more positive detection voltages may be related to the changes in background current. Oxidation of the electrode surface and/or increased charging current and/or O_2 reduction current due to removal of organic adsorption layer should be responsible for changes observed above 200 mV, where both average background current and peak-to-peak noise increased significantly.

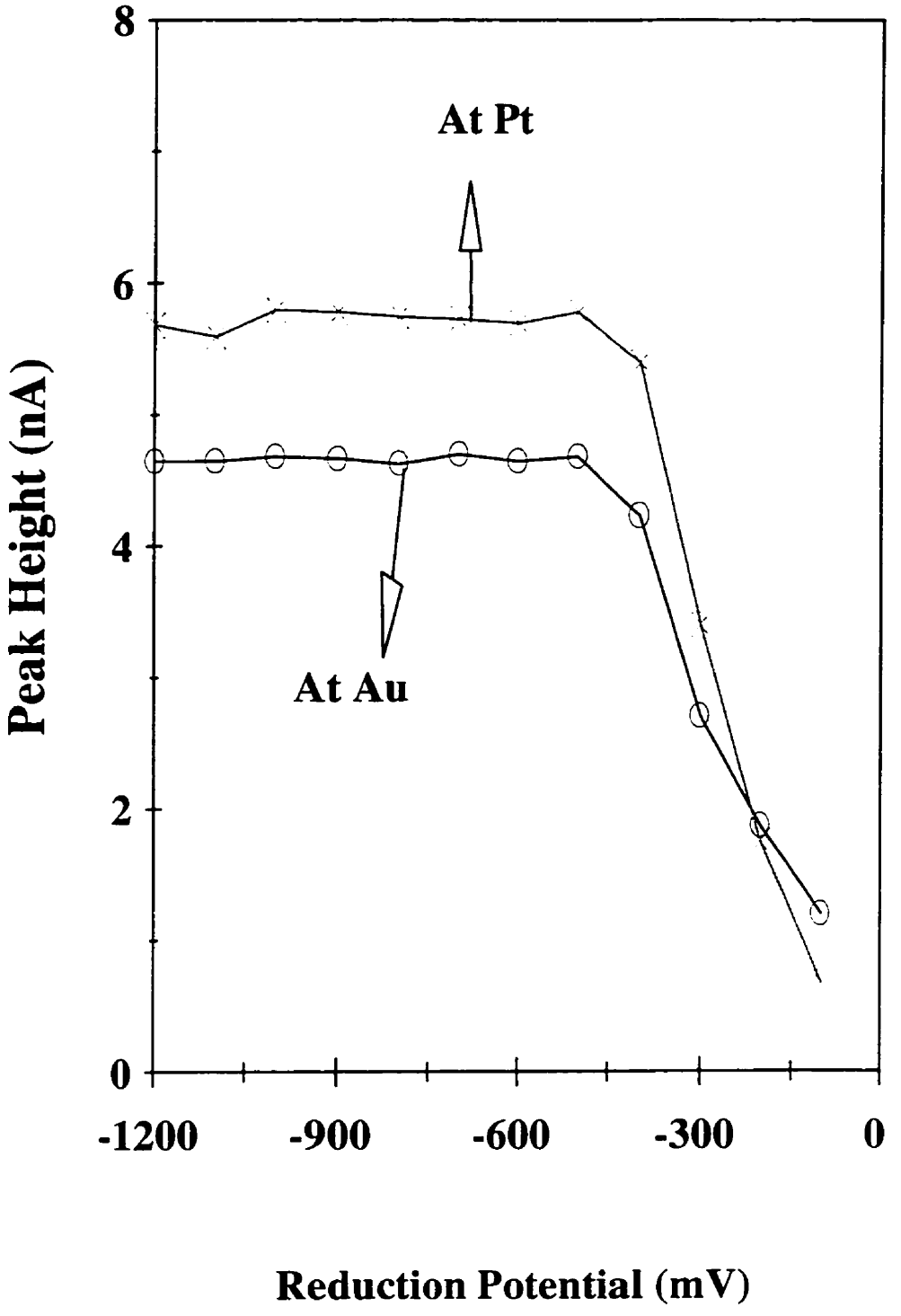

Figure 5.8 Influence of reduction voltage on analytical signal at 25 μm Au and Pt electrode. Detection potential, 100 mV for 96 ms(data collected over the first ~48 ms); reduction potential, -100 to -1200 mV vs SCE for 96 ms; analyte concentration, 200 μmol/L; other conditions as for Figure 5.7.

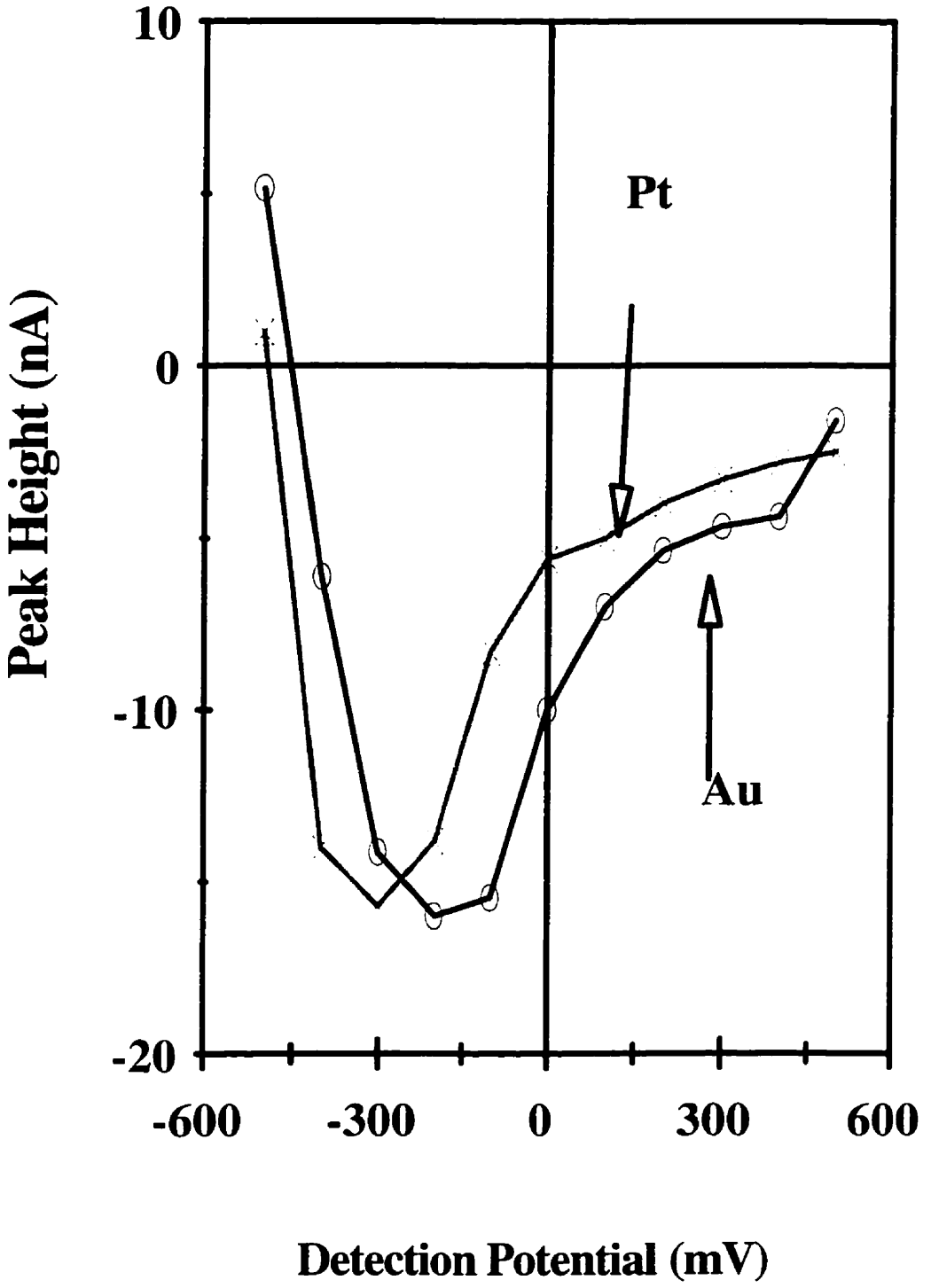

Figure 5.9 Influence of detection voltage on analytical signal at Au and Pt electrodes. Detection potential applied for 96 ms(data collected over the first ~48 ms); reduction potential, -800 mV vs SCE for 96 ms; other conditions as for Figure 5.8.

For anodic detection results reported here, a detection voltage of 200 to -100 mV was used. This value represented a compromise between maximum signal and minimum noise when one voltage was used to detect a wide range of metal ions. A potential more than 200 mV was required for Pb^{2+} to minimize peak broadening; for Cu^{2+}, Cr^{3+}, Hg^{2+}, Au^{3+}, Ag^{+} and Pd^{2+}, very positive oxidation potential (> 400 mV) were required for anodic signals.

5.4. Analytical Performance Features

5.4.1. Background Noise

When a series of voltage pulses are applied to an electrode background noise will vary across the pulse. This effect of the time period used to average the current was evaluated. A constant voltage of 200 mV was selected to ensure there was no reaction at the electrode. The results are shown in Figure 5.10. A major noise component is expected from 60 Hz power-line frequency,[195] and a minimum in noise is expected when signal averaging is over a period of multiples of 16.66 ms. Minima at these intervals can be seen in Figure 5.15, but the lowest minima were observed at multiples of 24 ms intervals. The source of the instrumental noise with a period of 24 ms is not known certainly, but frequency analysis tests indicated that it may be related to a capacitance coupling between the high input resistance and the small currents in the Faraday cage. To minimize the effect of this noise all data collection was taken over multiples of 24 ms. This time interval should not be a limiting factor for most CE applications where peak widths are not normally less than 2 to 4 s. The frequency of pulse waveforms used for

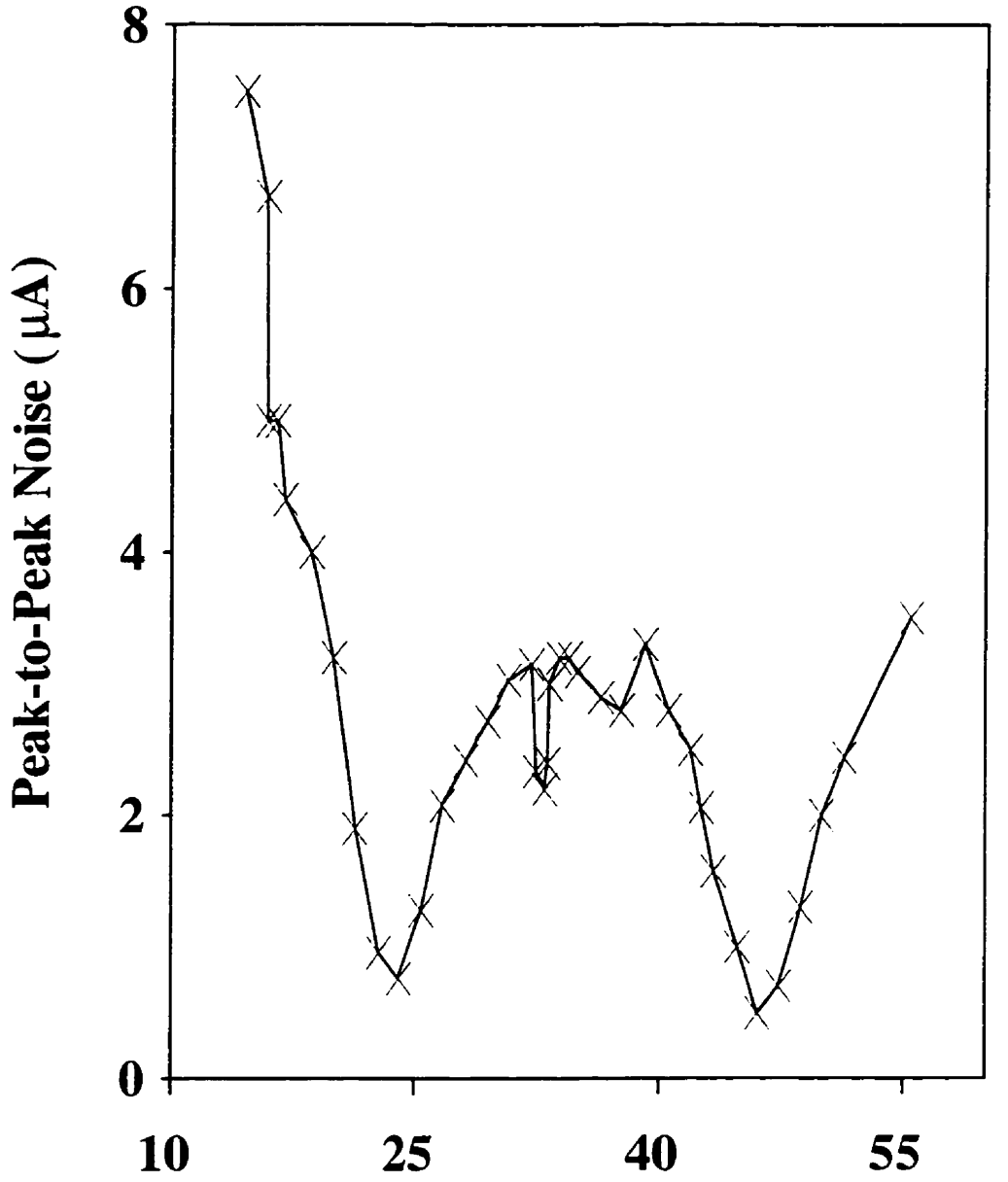

Figure 5.10 Background noise (peak-to-peak) as a function of integration time used to sample the current at 25 μm Au electrode. Electrode potential, 200 mV; electrolyte, as for Figure 5.6.

initial CE studies was 4 to 8 Hz to give at least 10 data points over one peak. For most cathodic analysis, the analytical signal used was the average current measured over the last 24, 48 and 72 ms of the reductive portion of the applied pulse, and for anodic analysis, the analytical signal was the average current over the first 48 or 72 ms of the oxidative step.

5.4.2. Electrode Response

Normally stable readings were obtained after a few minutes of placing freshly polished electrodes in the working electrolyte. Consistent electrode response as a function of time (<1%) and over repeated CE injections (5%) for most of the test metal ions with the concentration up to 1000 μmol/L indicated an excellent stability of the electrode, likely attributed to the constant application of a pulse train that conditions and maintains the consistency of the electrode surface. Background current (15 nA) under cathodic pulsed detection at the potential of -800 to 200 mV was mainly caused by the capacitance current, adsorption, and reduction currents from hydrogen, oxygen, and impurity reactions in the electrolyte; for anodic pulsed detection, data were selected on an oxidation step where the interference from some reduction reactions can be avoided, therefore, baseline was more stable compared to cathodic detection and background currents were ~ - 4.0 nA.

Calibration curves for Tl^+ in the range of 10 to 300 μmol/L for cathodic detection at a Au electrode are shown in Figure 5.11. Both peak height (nA) and peak area (nA × S) were used but peak area provided better quantitative information as shown in Figure 5.11.

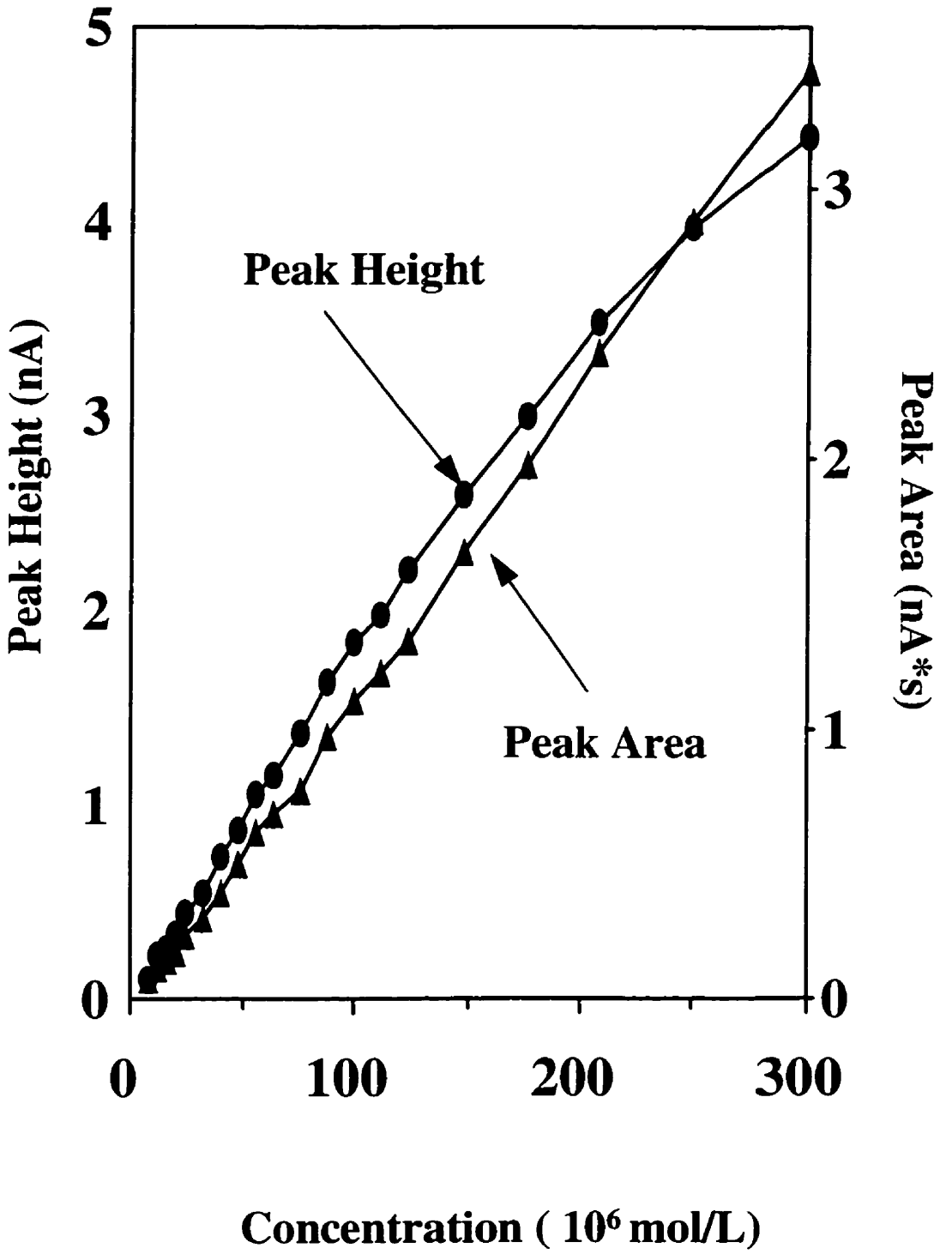

Figure 5.11 Calibration curves for cathodic detection of Tl(I). separation voltage, 20 kV ; electrode potential, -850 mV for 72 ms with data collected over last 24 ms and 200 mV for 120 ms; analyte concentration (mol/L); other conditions as for Figure 5.6.

The poor linearity for peak height response is probably attributable to sample overload that results in peak broadening.[196] The data for the peak area in Figure 5.11 appear to be a linear over the whole concentration range, and correlation coefficient was close to 1. However correlation coefficients of linear regression have some limitations. Firstly, correlation coefficients do not give information on specific data points. Secondly, correlation coefficients can be insensitive to deviations of the data over a short section of the calibration curve. Therefore, other method should be used to examine linearity of calibration curves.

A linearity plot is a simple method to evaluate the linear working range of calibration curves and can overcome the above limitations of correlation coefficients. In linearity plots, sensitivity of electrode response is plotted as a function of analyte concentration. The linearity plot of the data in Figure 5.11 is shown in Figure 5.12. The results in Figure 5.12 show that the data at low concentration deviated from linearity, a behavior that is always overlooked if one uses conventional least-squares calibration to evaluate linearity. This deviation may be due to the adsorption of the analyte on the capillary. Sensitivity varied $< \pm 5\%$ over the concentration range of 20 to 300 μmol/L; the two straight lines in Figure 5.12 represent deviation of +5% and -5%. Thus pulsed amperometric detection of Tl^+ at a Au electrode gave a stable electrode response over the concentration range. Sensitivities from calibration curves for a mixture containing Tl^+, Cd^{2+}, Pb^{2+}, and Zn^{2+}, with the concentrations from 5 μmol/L to 1000 μmol/L are shown in Figure 5.13, and clearly show the nonlinearity at the lower concentrations. However,

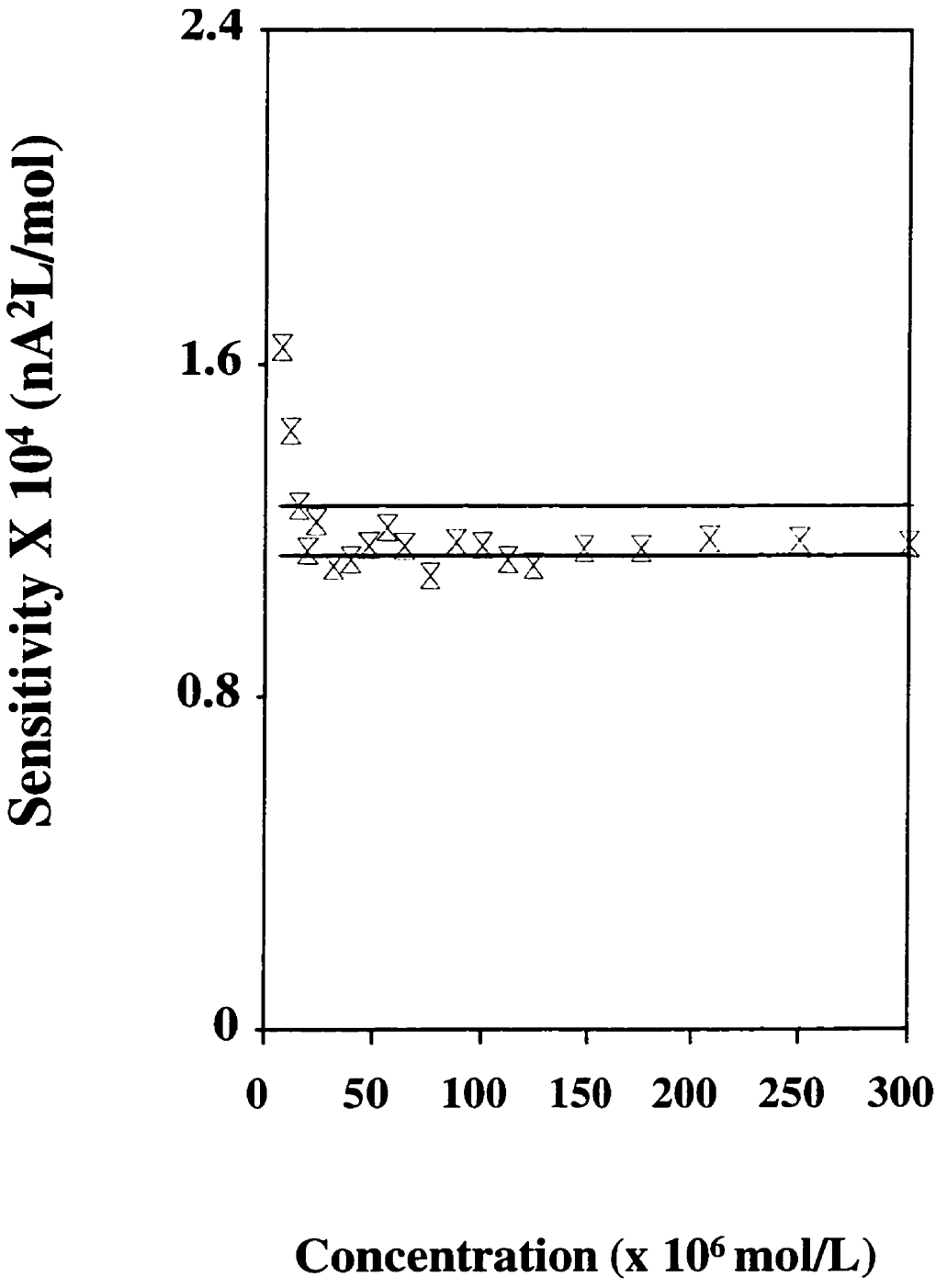

Figure 5.12 Linearity plot for Tl(I). Two straight lines represent deviations of +5% and -5%; separation voltage, 20 kV ; electrode potential, -850 mV for 72 ms with data collected over last 24 ms and 200 mV for 120 ms; sensitivity is given in units of peak areas (nA^2)/ analyte concentration (mol/L); other conditions as for Figure 5.11.

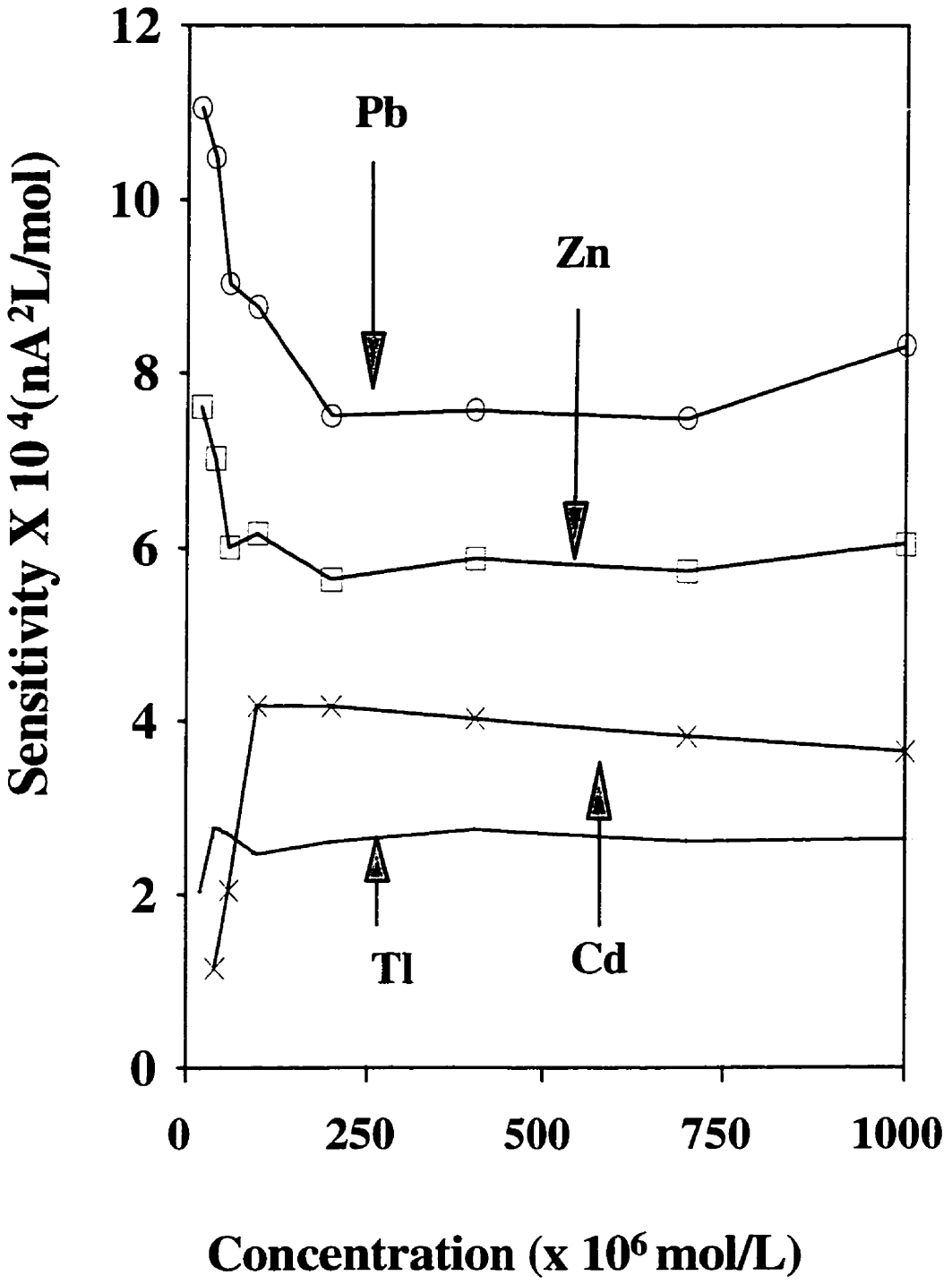

Figure 5.13 Linearity plots for anodic detection of Tl(I), Cd(II), Pb(II), and Zn(II). Separation voltage, 20 kV; electrode potential, -850 mV for Pb, Tl, Cd and -1100 mV for Zn for 72 ms with data collected over last 24 ms, and 200 mV for 120 ms; other conditions as for Figure 5.6.

for the metal ions evaluated, the response factors varied by only ± 10% from 50 μmol/L up to 1000 μmol/L. These results confirm that PAD detection is a effective method for the detection of metal ions separated by CE, and that constant electrode behavior can be maintained over a normal working day.

For both cathodic and anodic detection, sensitive signals can be obtained for Tl^{+}, Co^{2+}, Ni^{2+}, Zn^{2+}, Cd^{2+}, and Pb^{2+}. However, small and broadening peaks were often observed for the analysis of Cu^{2+}, Ag^{+}, Cr^{3+}, and Fe^{3+}. These degraded electrode responses were caused by the change in background currents as discussed in section 4.3.

Representative electropherograms for metal ion separation are shown in Figure 5.14 for cathodic detection and in Figure 5.15 for anodic detection. In cathodic detection, the pH needed to be controlled in the range of 4.7 to 5.0. Lower pH produced higher background current, and higher pH values compromised separation resolution due to larger electroosmotic flow. In anodic detection, detection occurs in the oxidative mode, and there is no interference from oxygen and H^{+}. This may be a factor in the observation that in general the baseline stability and peak shape for anodic detection were better than those for cathodic detection (compare Figure 5.14 with Figure 5.15). Wider pH ranges can be used in anodic detection. This feature can be important for optimizing the separation of some metal ions, such as Ni^{2+}, Co^{2+}, Zn^{2+}, which can not be fully separated at pH > 4.7; these metal ions can be resolved completely when the electrolyte pH is 4.5.

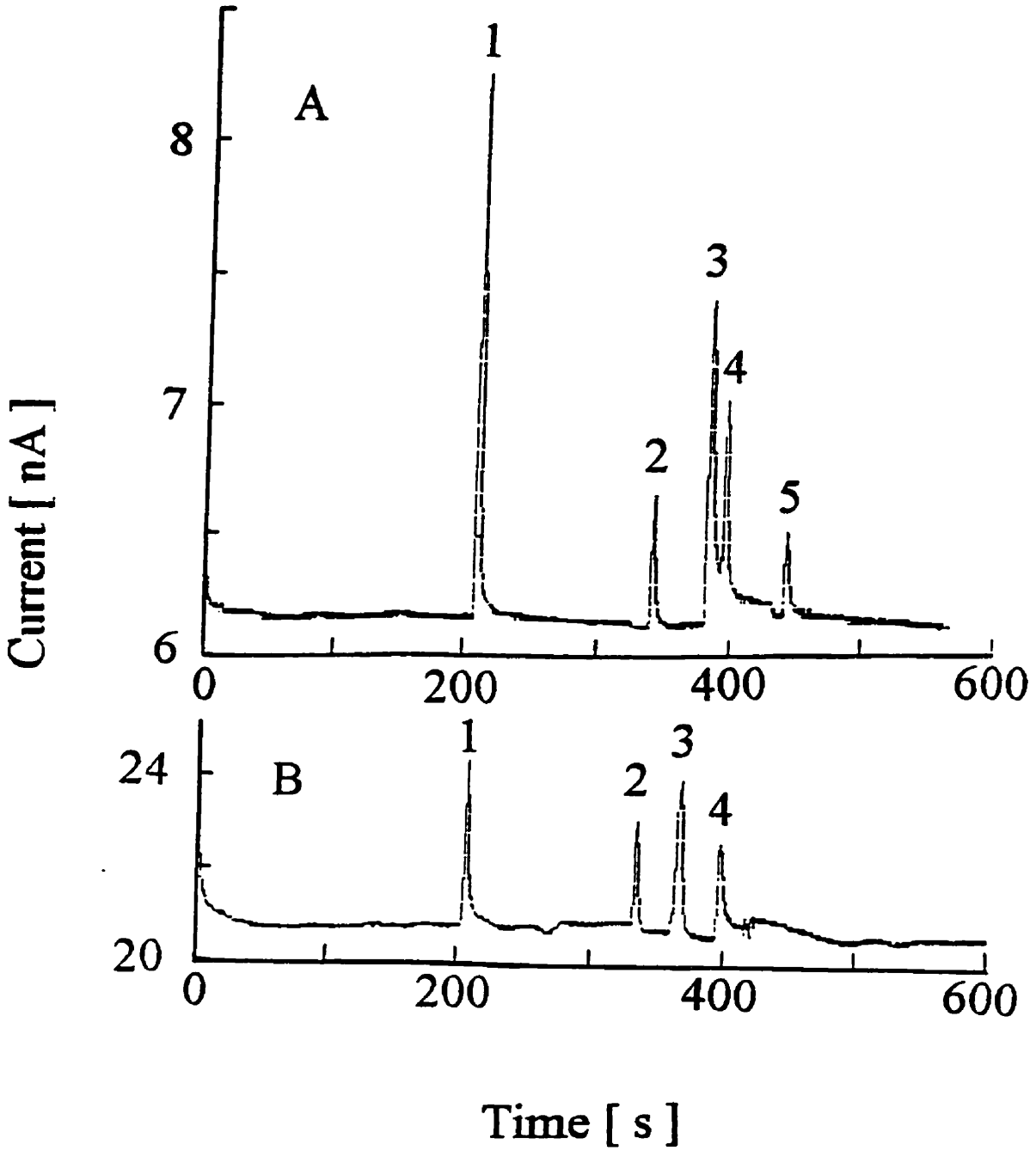

Figure 5.14 Electropherogram of metal ions with cathodic detection at a 25 μm Au electrode. Curve (a) pulse conditions; -700 mV for 96 ms with data collected over last 48 ms and 0 mV for 96 ms; analyte concentration, 200 μmol/L. Peak identification: (1), Tl(I); (2), Cd(II); (3), Pb(II); (4), Hg(II; (5), Ag(I). Curve (b) pulse conditions; -1100 mV for 96 ms and 0 mV for 96 ms. Peak identification: (1), Tl(I); (2), Co(II); (3), Ni(II): Zn(II); other conditions as for Figure 5.6.

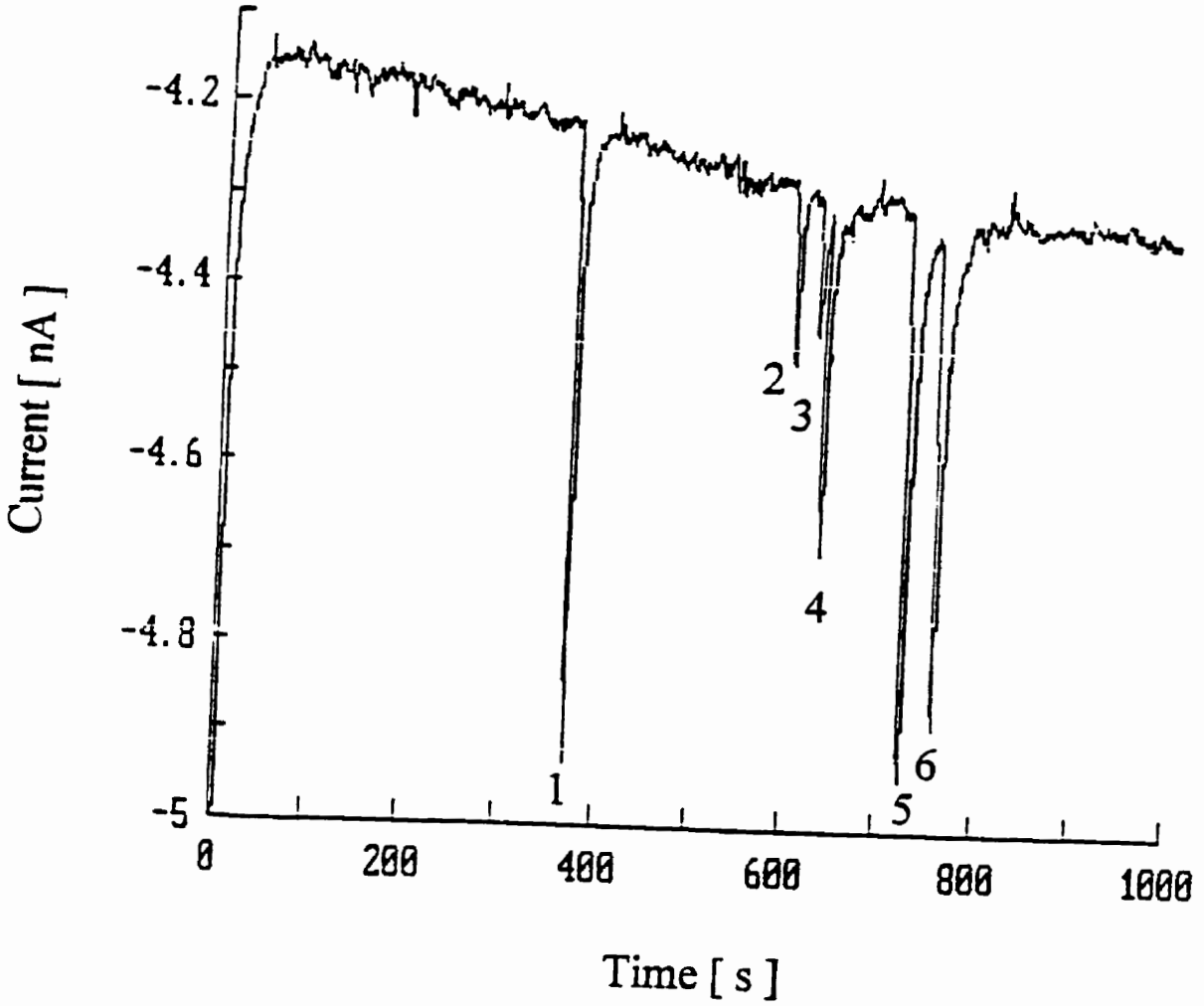

Figure 5.15 Electropherogram of metal ions with anodic detection at a 25 μm Au electrode. pulse conditions; -1100 mV for 96 ms and 100 mV for 96 ms with data collected over the first 48 ms; electrolyte, 0.035 mol/L creatinine, 0.008 mol/L HIBA with pH 4.5; analyte concentration, 2.5 μmol/L. Peak identification: (1), Tl(I); (2), Co(II); (3), Ni(II); (4), Cd(II); (5), Zn(II); (6), Pb(II); other conditions as for Figure 5.6.

5.4.3. Detection Limits

Detection limits were obtained by injection of analytes over the concentration range of 0.5 μmol/L to 50 μmol/L. Cathodic detection limits (twice peak-to-peak noise) were as follows: for Tl^{+}, Pb^{2+}, Zn^{2+}, Ni^{2+} and Co^{2+}, 2 to 3 μmol/L; for Cd^{2+} and Hg^{2+}, 5 to 7 μmol/L; for Ag^{+}, 11 μmol/L; and for Cu^{2+} and Cr^{3+}, 20 μmol/L (the copper peak was quite wide). These detection limits were obtained without purging the electrolytes to remove dissolved oxygen. Compared to cathodic detection, anodic stripping has lower detection limits, which were as follows: Tl^{+}, Cd^{2+}, Pb^{2+}, Zn^{2+}, 0.2-0.5 μmol/L; and for Co^{2+}, Ni^{2+}, 0.6-1.0 μmol/L.

For most samples in the above study, sample injection time was 10 s, and longer injection time may be used to improve detection limits. Thus, the electrode response for Tl^{+}, Co^{2+}, Ni^{2+}, Zn^{2+}, Cd^{2+} and Pb^{2+} as a function of injection time was evaluated over a range of 1.0×10^{-5} to 5.0×10^{-4} mol/L. Change of peak height with injection time for Tl^{+}, Cd^{2+} and Pb^{2+} is shown in Figure 5.16. This shows that the peak heights increased with injection time from 0 to 30 s. Consequently, use of longer injection time should lower detection limits by a factor of ~ 2 without loss in peak resolution.

5.4.4. Sample Analysis

To evaluate the performance of the detection system, pulsed amperometric detection was used for the determination of spiked and real samples. Spiked samples were prepared by adding standard analyte to the electrolyte used as separation electrolyte.

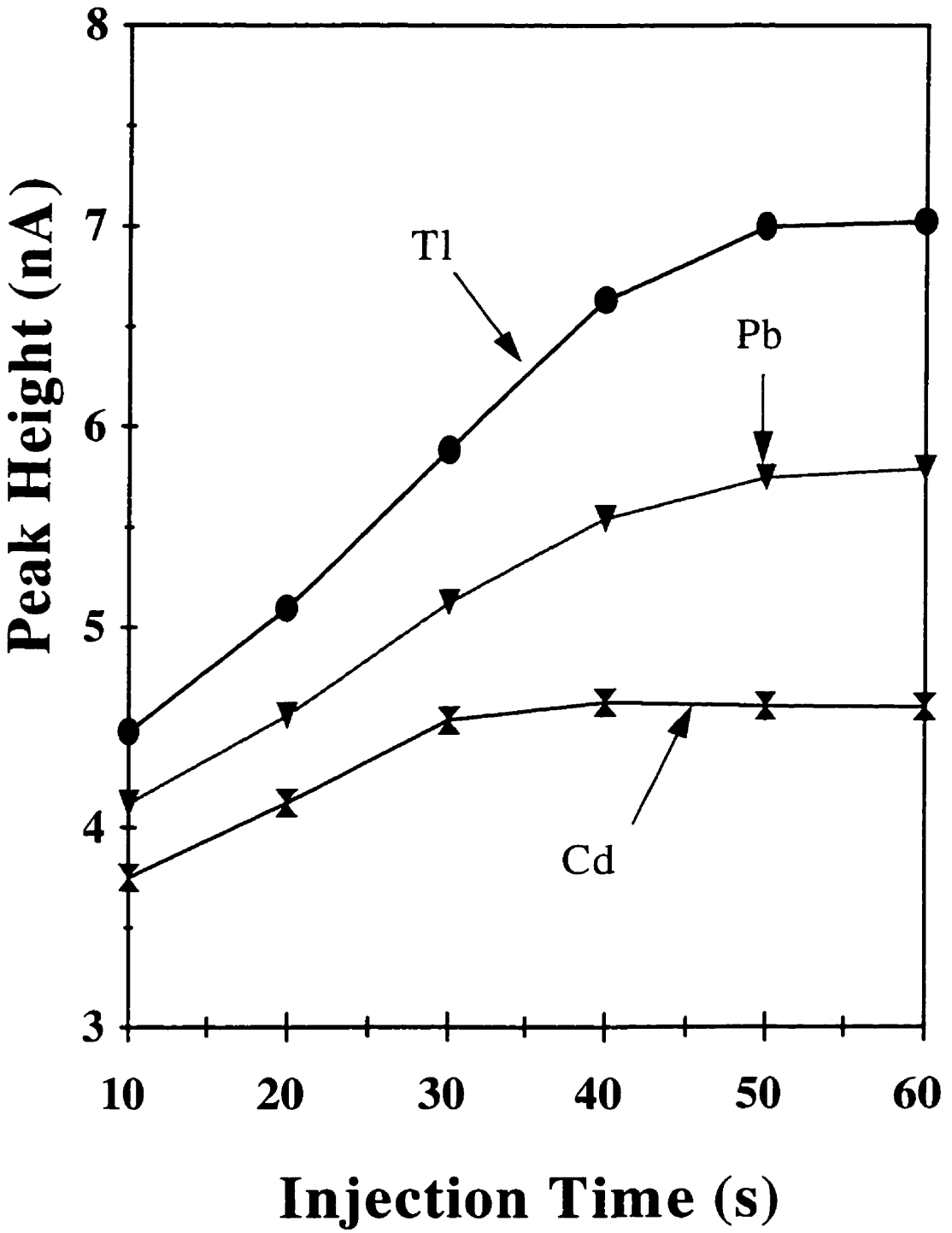

Figure 5.16 Effect of injection time on the electrode response at a 25 μm Au electrode. Experimental conditions: PAD detection, -700 mV for 96 ms with data collected over last 48 ms and 0 mV for 96 ms; electromigration injection at 5 kV; analytes, 5×10^{-5} mol/L; other conditions as for Figure 5.15.

Two spiked samples were analyzed by cathodic and anodic pulsed amperometric detection, the results were compared with flame atomic absorption spectrometry. Table 2, which lists all the results of three detection approaches, shows that there was good agreement (relative difference < 5%) among the three procedures. Cathodic and anodic detection and flame atomic absorption were also compared for the analysis of three snow samples collected beside busy city streets or in parking lots, these samples were selected as a test system since they should be contaminated from air pollution and with other foreign matter. When melted, each sample was light-brown in color, and after filtration appreciable black particulate was observed on each filter. An electropherogram for one of these samples is shown in Figure 5.17. The CE results indicated the presence of only Zn (Pb was not observed because Pb gasoline is not used in Saskatoon), and this was confirmed by atomic absorption tests with Zn, Pb, Cu, and Cd lamps; the identification of the other components in Figure 5.17 is not known. Direct calibration analysis gave poor agreement among these three analytical techniques due to appreciable matrix effects in these dirty samples. Thus the samples were determined by standard addition calibration, and the results are shown in Table 3. The three detection techniques provide good agreements. The standard deviations among the three procedures were: sample 1 0.04 μ M; sample 2, 0.02 μM; and sample 3, 0.08 μM.

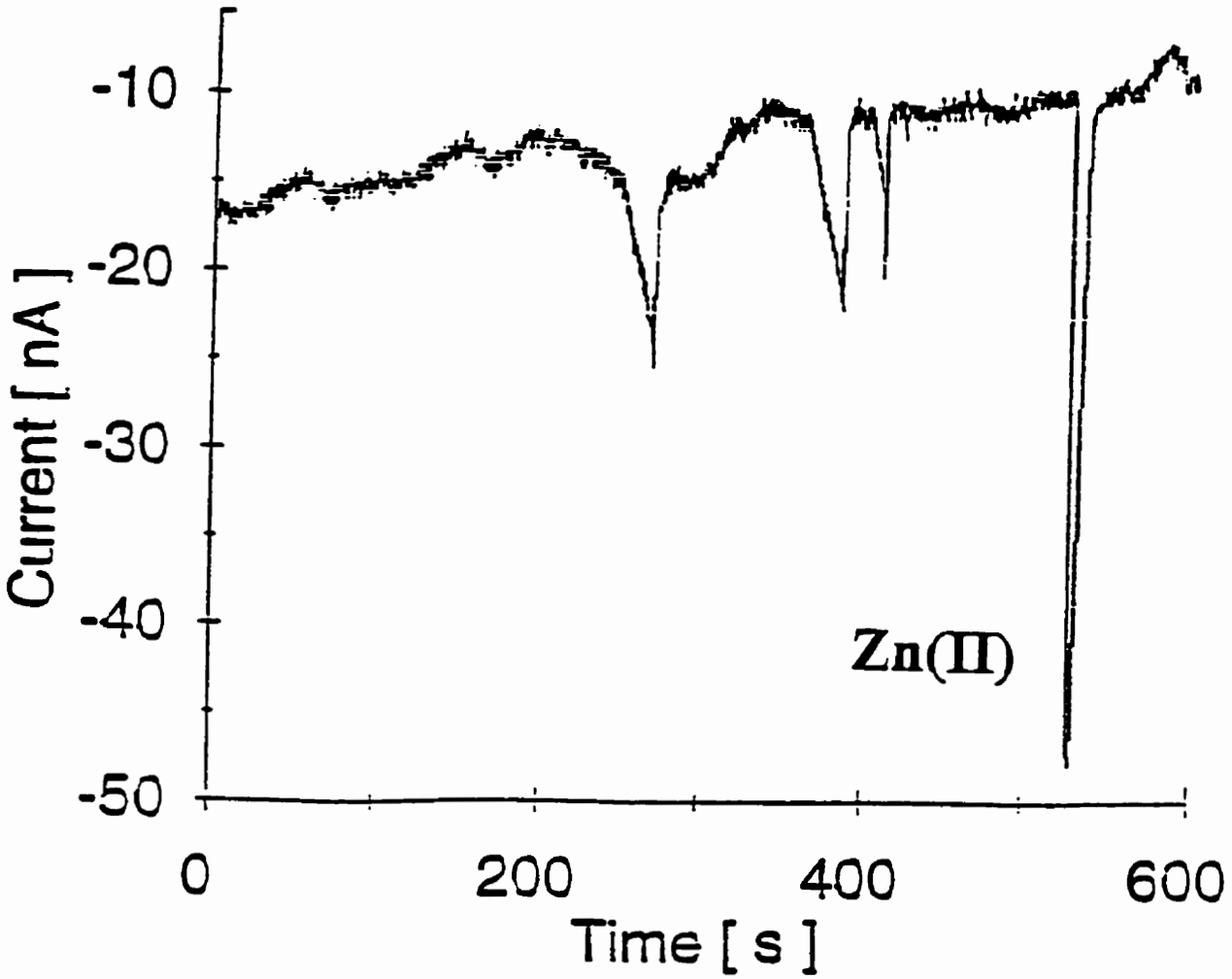

Figure 5.17 Electropherogram for the separation of a snow sample. Electrode potential -800 mV for 72 ms, and 100 mV for 144 ms with data collected over the first ~72 ms of the 100 mV pulse; other conditions as for Figure 5.8.

5.5. Conclusion

This study shows that PAD provides higher sensitivity and improved reproducibility relative to CVD for detection of metal ions. Anodic PAD provides better detection than cathodic PAD due to its ability to discriminate against interference from hydrogen and other reduction reactions in solution. Detection limits at the optimal conditions were in the range of 2×10^{-5} to 2×10^{-7} mol/L for most of the test metal ions.

Table 2. Determination of Cd(II) and Pb(II) in spiked samples. Experimental conditions: separation voltage, 20 kV over 25 μm X 60 cm capillary; 25 μm Au disk electrode; electrode potential, -600 mV for 72 ms and 100 mV for 96 ms.

	cathodic μM	anodic μM	FAAS μM
sample 1			
Cd(II)	8.1	8.3	8.3
Pb(II)	10.0	9.8	10.0
sample 2			
Cd(II)	16.4	16.5	16.6
Pb(II)	14.4	14.3	14.9

Table 3. Concentration of Zn in snow by standard addition calibration. Experimental condition: separation voltage, 20 kV over 25 μm × 60 cm capillary; 25 μm Au disk electrode; electrode potential, -800 mV for 72 ms and 100 mV for 144 ms.

	CE		FAAS
	cathodic (μM)	anodic (μM)	(μM)
sample1	1.68	1.60	1.61
sample2	0.84	0.84	0.80
sample3	0.86	0.74	0.71

6. APPROACHES TO IMPROVE S/N FOR PAD DETECTION

6.1. Overview

Results in section 5 showed that PAD detection of metal ions was reproducible ($\leq$ 5% over 14 h) with the detection limits in the range of 10^{-7} to 10^{-5} mol/L; these detection limits are similar to those reported for the PAD detection of other electroactive compounds in LC and CE.[77,82,84] Although these detection limits are sufficient for many samples, there are instances where lower detection limits are required. Thus, it would be desirable if other more sensitive electrochemical detection approaches could be developed. Two different approaches can be used to reach the goal: the signal can be increased, or the noise can be decreased.

Increasing the sample volume is the easiest way to increase signal, however, the injection volume may be limited by the availability of sample. On-column preconcentration is another way to enhance signal for microcolumn analysis. Several techniques used for LC and CE column preconcentration include: solid-phase extraction,[197] isotachophoretic pre-concentration,[198] and field amplified pre-concentration (sample stacking).[199] Of these approaches, sample stacking is one of the most common approaches used for CE, and this technique has been reported to enhance the detectability up to 1000 fold for some compounds.[200]

Most PAD in LC & CE used a simple 2 or 3 step potential waveforms,[76,78,201] and frequencies of 1 to 8 Hz.[97,201,202] Higher frequencies may offer larger currents and different detection selectivity. In addition, if the applied waveform contains sections where the potential is cycled very rapidly, it may be possible to momentarily trap analytes at the electrode to permit analyte detection over several adsorption/desorption steps.

In electrochemical analysis, there are several resources of contribution to baseline noise. Two common approaches that are used to reduce noise are analog filtering, and the use of grounding and shielding. Low-pass analog filters can be used to filter high-frequency noise, however, these can distort the frequency characteristics of the analytical signal,[203] leading to a decrease in analytical signal. Grounding and shielding minimize environmental noise, and in these studies the detection system was placed in a faradaic cage to minimize this source of noise. Another approach that may improve S/N is to make use of current-voltage characteristics that exist on the application of pulsed voltages to an electrode. The analysis of current vectors based on amplitude and phase-angle relationships can help differentiate between faradaic and capacitance currents;[100] this approach may reduce the capacitance current component which is an important part of background noise. Use of the different distributions of signal and noise in fundamental and higher harmonic components may also reduce noise. This approach can be achieved via both digital Fourier analysis and lock-in amplifiers. Recently studies with a flow injection system have shown that 2nd harmonics obtained from application of sinusoidal waveform provided some advantages for detection of carbohydrates at a Cu electrode.[25] All of the above approaches offer possible advantages, and it would be useful for the

development of electrochemical detection to have a systematic study and comparison of them.

6.2. Sample Stacking

Sample stacking is the process that occurs when a voltage is applied along a capillary containing a sample plug with a lower specific conductivity than that of the surrounding electrolyte. The resistance in the sample plug will be higher than that in the rest of the column, and consequently, a higher electric field is set up in this sample region. Under this high electric field ions will migrate rapidly toward the steady-state boundary between the sample plug and the electrolyte. Once the ions pass the concentration boundary, these ions immediately experience a lower electric field and slow down, producing a narrow zone of analyte.[204] There are several possible experimental procedures for performing sample stacking.[154,200,204,205] In our work, a lower concentration electrolyte containing a sample is introduced into a capillary by electromigration. In general, the larger the difference in the ionic strength between separation electrolyte and sample electrolyte, the more stacking will occur: this means the sample zone being narrower and the analyte being more concentrated. Although the highest sensitivities are obtained with sample solutions diluted with pure water,[154] there are considerable problems under these conditions.

In stacking conditions, laminar flow originates[206] by the difference in conductivity between sample region and the electrolyte region. The larger the difference in the concentration between electrolyte in sample and running buffer, the larger the laminar flow that causes the sample zone in the capillary to broaden. Vinther and Soeberg[207] have developed a mathematical model describing the dispersion under stacking condition. In initial studies with samples dissolved in pure water, a dramatic decrease in separation efficiency was observed, the peak broadened obviously, some metal ions were not completely resolved, especially when a sample with relative high concentration (> 1.0×10^{-5} mol/L) was injected, and appreciable decreases (up to 30 s) in migration times were noticed. Under this stacking condition, the response factors for Tl^{+}, Co^{2+}, Ni^{2+}, Zn^{2+}, Cd^{2+}, Pb^{2+}, varied by $\pm 9\%$ in the range of 2.4×10^{-8} to 4.0×10^{-6} mol/L, and more than $\pm 15\%$ over the range of 5.0×10^{-7} to 1.0×10^{-5} mol/L. A typical result for Cd^{2+} is shown in Figure 6.1, where the response factor continuously decreased by 44% over the range of 5.0×10^{-7} to 1.0×10^{-5} mol/L. RSD value from repeated CE injection of Tl^{+}, Co^{2+}, Ni^{2+}, Cd^{2+}, Zn^{2+} and Pb^{2+} in the range of 1.0×10^{-6} to 1.0×10^{-4} mol/L varied by more than 10%. The peak broadening, decrease in migration times, non-linear calibration curves, and irreproducible electrode response observed above were likely due to the laminar flow and high Joule heat caused by a low specific conductivity ratio of sample solution to surrounding running buffer and high applied potential within the sample zone.[208,209]

The above results showed that lack of background electrolyte caused serious problems for quantitative analysis, consequently a series of tests with samples having electrolyte concentrations from 0 to 20% of that in the separation electrolyte were taken to find a condition at which the sensitivity of an analyte can be enhanced without loss of separation efficiency and linearity. The results showed that when standards and sample were prepared in the electrolyte that was about 7 to 8 times less than that used for the electrophoretic separation, the migration time and electrode response of metal ions was constant ($\leq \pm$ 5%), and sensitivities were enhanced by 10 fold with consistent response factors (varied within < 5%). A typical result for Cd^{2+} shown in Figure 6.1 B clearly exhibits a more consistent response factor compared to that for sample prepared in pure water. For both cathodic and anodic amperometric detections, the response factor for Pb^{2+} varied by $< \pm$ 5%; for Tl^{+} by $< \pm$ 4%; and for Co^{2+}, Ni^{2+}, and Cd^{2+} by $< \pm$ 3% in the range of 1.0×10^{-6} mol/L to 1.0×10^{-4} mol/L. A comparison of results for two spiked samples containing 2 to 4 µmol/L of Cd^{2+}, Pb^{2+}, Zn^{2+} with atomic absorption spectrometry showed < ±5% difference between the two detection methods. Therefore, a sample prepared in electrolyte concentration ~12% of that for the electrophoretic separation should be the optimal condition for sample stacking of metal ions under the applied experimental conditions. At these sample stacking conditions detection limits obtained by injection of the analyte at a concentration of 2×10^{-7} mol/L were: for Tl^{+}, 0.07 µmol/L (cathodic) and 0.05 µmol/L (anodic); for Cd^{2+}, Co^{2+}, and Ni^{2+}, 0.03 to 0.05 µmol/L (cathodic) and 0.01 to 0.02 µmol/L (anodic); for Pb^{2+}, 0.1 µmol/L (cathodic) and 0.04 µmol/L (anodic).

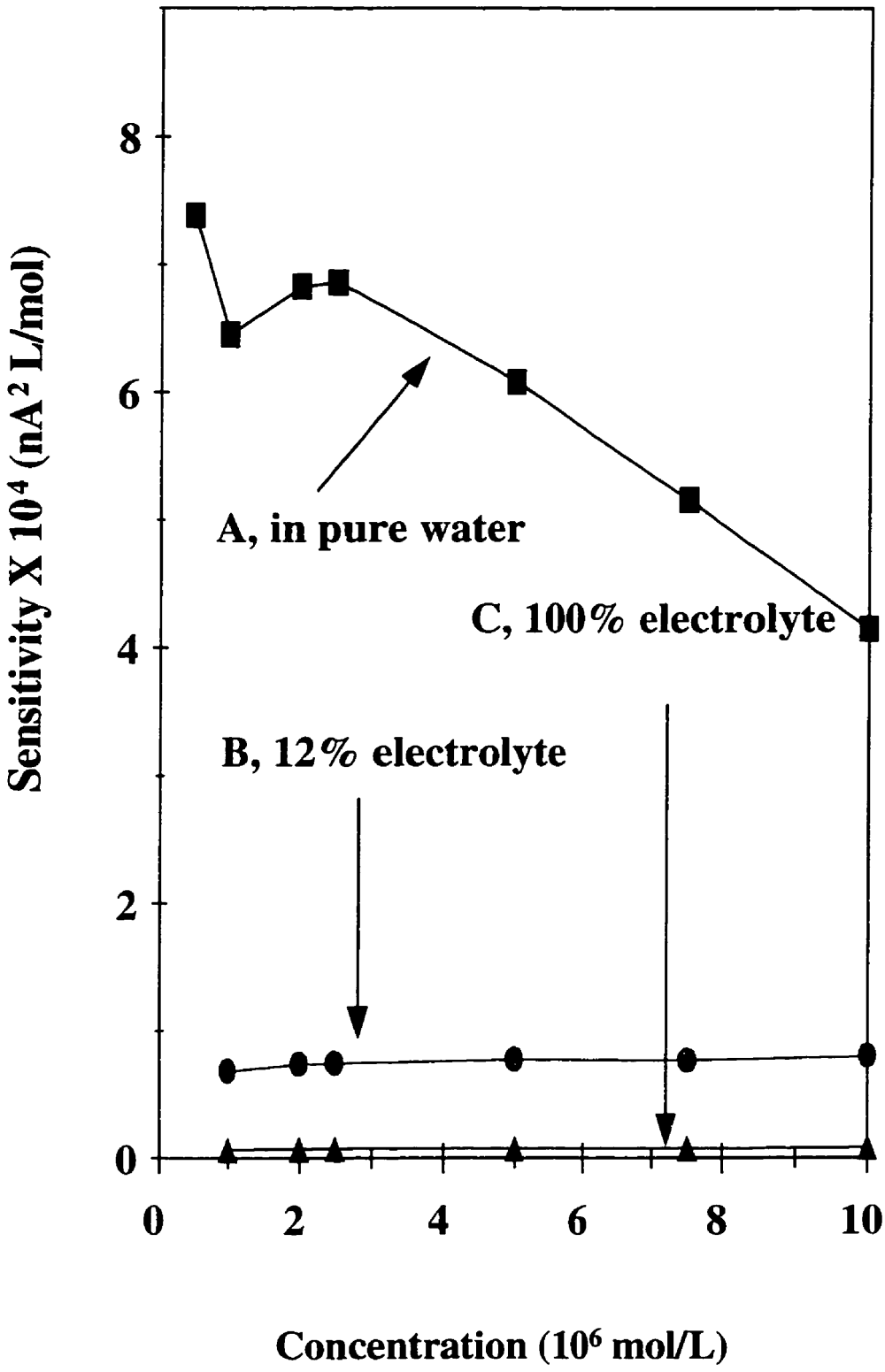

Figure 6.1 Linearity plots for pulsed detection of Cd^{2+}. Curve A, sample dissolved in pure water; curve B, sample dissolved in 12% electrolyte; curve C, sample dissolved in the electrophoretic electrolyte; the applied potential, -800 mV for 72 ms, and 200 mV for 96 ms with data collected in the first 24 ms; other conditions as for Figure 5.15.

6.3. Signal Enhancement

Compared to PAD with a simple bipolar waveform, the use of a multistep waveforms should offer improved S/N for two main reasons. First, multistep waveforms will permit isolation of the measurement voltage from large voltages that may be required for electrode cleaning and/or for rapid sample deposition. Secondly, the use of fast (relative to rates of diffusion) multiple-steps during signal measurement may enhance S/N due to multiple adsorption/desorptions of the analyte. In an effort to improve and widen the application of pulsed amperometric detection, different parameters of the pulse waveform were examined; these parameters included waveform shape, waveform frequency, and data collection within the pulse waveform.

6.3.1. Multistep Pulse Waveforms

A typical multiple-step waveform used is shown in Figure 6.2. A wide variety of conditions were examined. The preconcentration period (t_p) was at -800 to -1200 mV for 100 to 200 ms, and signal measurement was made during the fast bipolar pulses applied with frequencies of 20 to 200 Hz over a period 100 to 200 ms; the cleaning period was at 400 to 500 mV for ~ 100 ms. The analytical signal used for the evaluation of different waveform shapes was the total current measured over the high frequency pulses. The results showed that signals for all analytes increased quickly when t_p increased from 0 to 100 ms; only a gradual increase was seen at t_p >100 ms. When t_p was >200 ms,

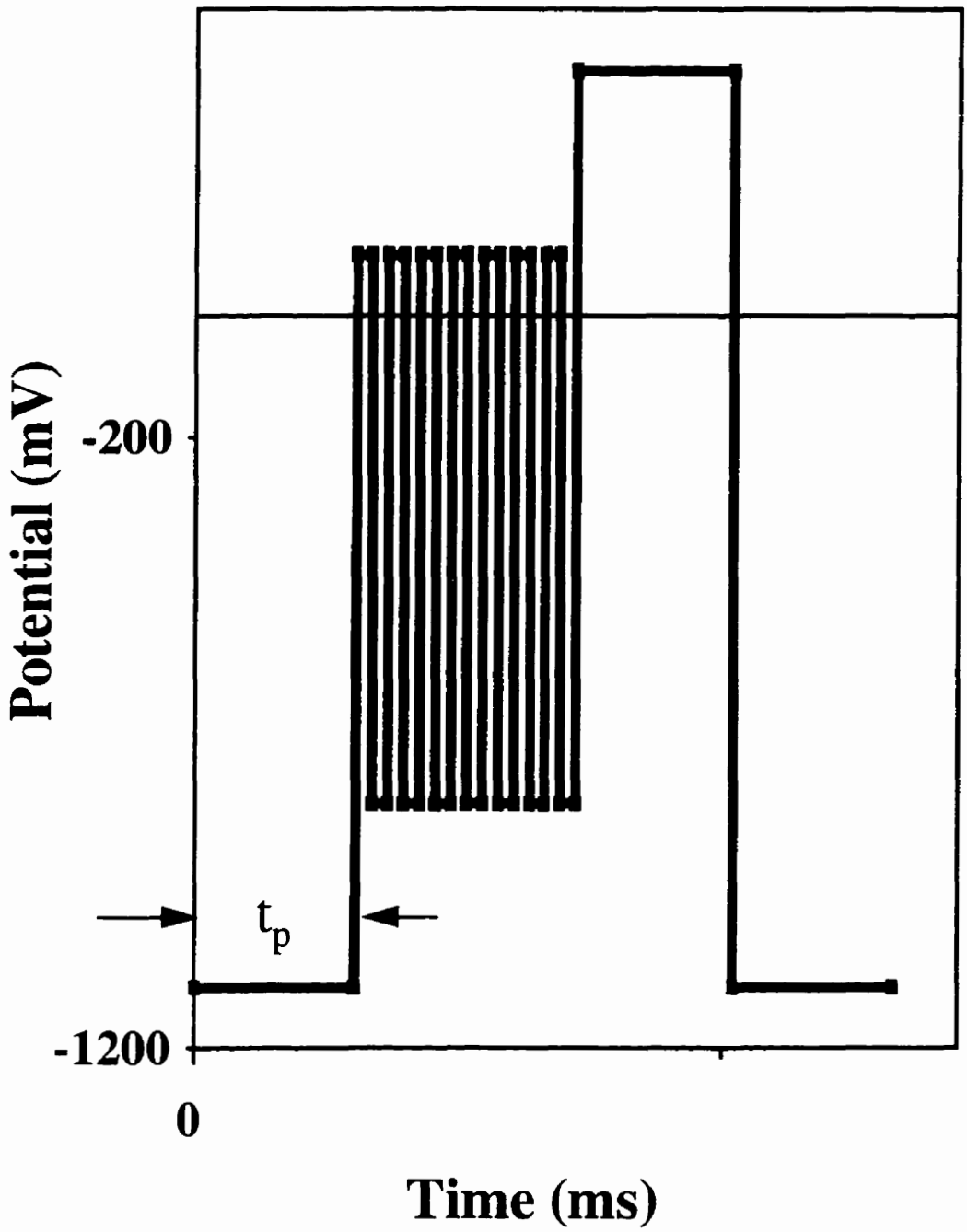

Figure 6.2 Multiple-step waveform applied to electrodes. Experimental conditions: initial preconcentration periods were at -800 to -1200 mV (depending on analytes) for 100 to 200 ms; signal measurement was made during application of the fast bipolar pulses with frequencies of 20 to 200 Hz over a period 100 to 200 ms; the cleaning period was at 400 to 500 mV for ~ 100 ms.

reproducibility of electrode response decreased (repetitive injection R.S.D.>5%). For Pb^{2+}, which adsorbed strongly on the electrode, a high cleaning potential improved peak shape and S/N; peak width was reduced more than 50% and S/N improved up to 2 to 3 fold when a cleaning potential of 400 mV was applied for 100 ms. The application of voltage oscillations during data collection (center portion of Figure 6.2) improved S/N by effectively trapping the analyte via repeated oxidation/reduction. Over the frequency range studied (20-200 Hz) the S/N increased slowly to give a ~3 fold improvement over the range of 50 - 150 Hz. Above 200 Hz, background noise increased faster than analyte signals. Relative to previous results obtained with a simple bipolar pulse, detection limits were improved by up to 10 fold for Tl^{+} and Pb^{2+}, and by 4 - 6 fold for the other test metal ions. Cleaning periods of ~ 100 ms were sufficient to prevent longer-term accumulation of the analytes, which would cause peak broadening. The maximum pulse length was limited to 400 ms to permit the collection of 10 data points for a 4 s peak.

6.3.2. Pulse Frequency

In an PAD, analytical signal (S), background signal (N_b) and instrumental noise (N_e) have the following relation with the pulse frequency (f),

$$S = a\sqrt{f}; \qquad (6.1)$$

$$N_b = k\,(a\sqrt{f} + b\,f\,); \quad N_e = c \qquad (6.2)$$

$$S/N \propto \sqrt{f}\,/(\,a\sqrt{f} + b\,f + c) \qquad (6.3)$$

where a, b, c are constant. Thus certain frequencies may give larger S/N. In previous

studies with a simple bipolar pulse, frequencies from 4 to 8 Hz were used. To determine the effect of the higher frequency used in the waveforms shown in Figure 6.2 changes in signals were evaluated over the frequency range of 7.5 Hz to 600 Hz for Tl^{+}, Co^{2+}, Ni^{2+}, Zn^{2+}, Cd^{2+} and Pb^{2+}. Square-wave pulses were applied to the electrode, the analytes were separated in CE, and the total cathodic and anodic current was measured as signal. A typical result for Tl^{+} is shown in Figure 6.3, which shows that the analytical signal increased with pulse frequency, that peak-peak noise was at a minimum at 200 Hz, and that maximum S/N occurred at 180 - 280 Hz. The general trends observed for the other metal ions were similar to those for Tl^{+}. The conditions for maximum S/N (180 ~ 280 Hz) gave a 3 fold enhancement in detection limits compared to those obtained previously for anodic pulse detection.

6.3.3. Data Collection

The electrode response curve (see Figure 5.5) showed that current changes with time upon the application of a step pulse voltage. Since the relative importance of noise, background currents, and faradaic currents depends on data sampling within a pulse, optimizing the data collection period may provide larger S/N. To obtain optimal sampling location for S/N, one pulse was divided into sixty-four equal sampling periods, and the analytical signal over each period was evaluated. In this work, a 180 Hz frequency bipolar pulse was selected for Tl^{+}, Zn^{2+}, Cd^{2+} and Pb^{2+}, and thus each period was ~ 0.087 ms.

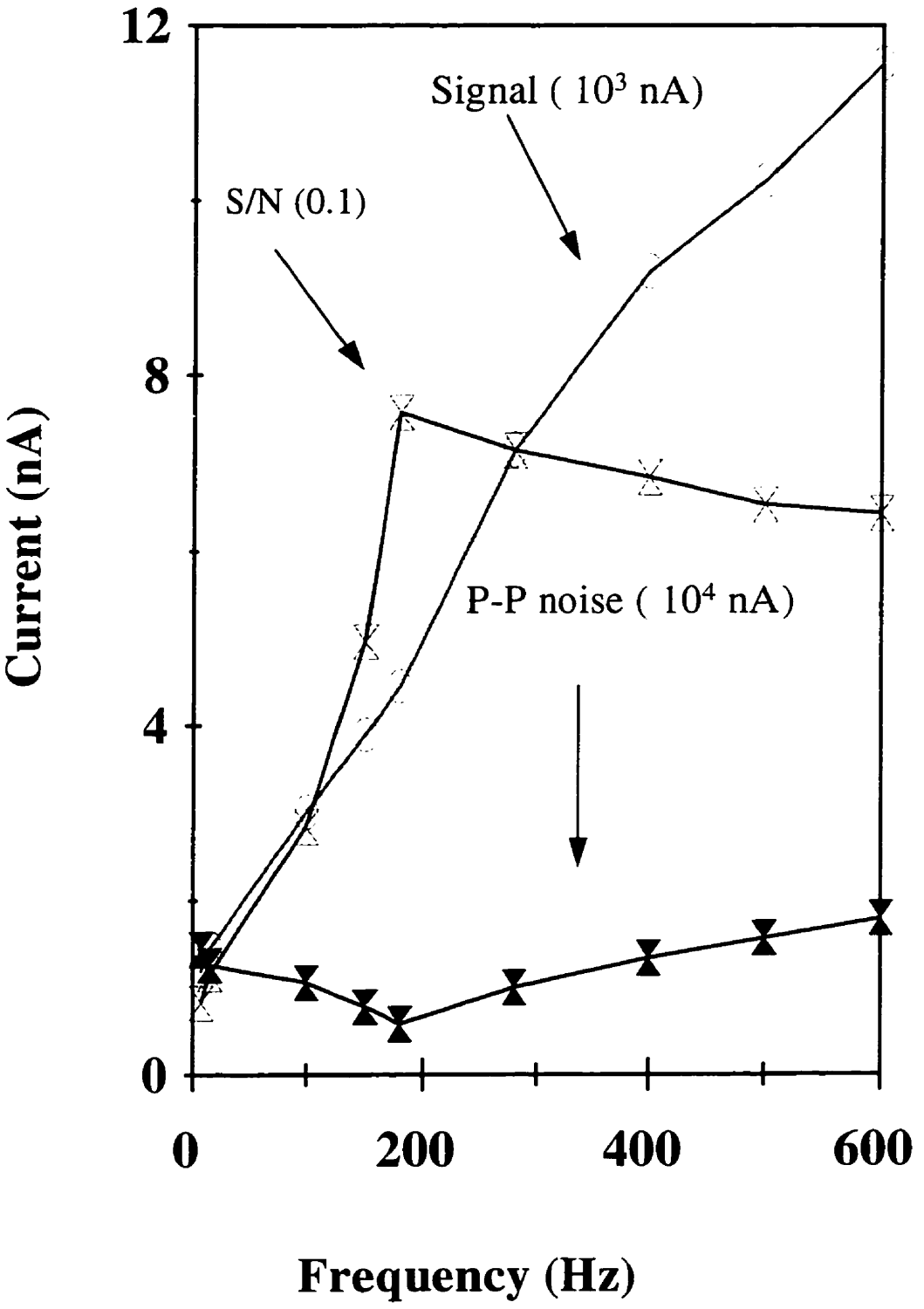

Figure 6.3 Effect of bipolar pulse frequency on analytical and background signals: Experimental conditions: cathodic current is considered as positive current; applied potentials, -800 mV for reduction and 200 mV for oxidation; analytical signal was an average current measured over the cathodic and anodic current; errors, ± 7 %; analyte (Tl^+) concentration, 2.0 µmol/L; 5 kV electrokinetic injection for 10 s; other conditions as for Figure 6.2.

The responses for Tl^{+} and Cd^{2+} within one square-wave pulse at the maximum of the CE peaks are shown in Figure 6.4, and other metal ions exhibit similar trends. For both anodic and cathodic signals, maximum response was obtained at ~ 0.2 ms after the change of potential polarity. Theoretically, maximum electrode response should immediately follow the change of potential polarity, and the small delay observed in Figure 6.4 is a result of finite bandwidth of the current transducer in the potentiostat (0.2 ms delay corresponds roughly to a 5000 Hz bandwidth); such shifts have been reported elsewhere.[31] Although the background noise was a maximum at the same point, overall S/N was still a maximum at 0.2 ms. When the optimal sampling period (~0.2) ms was used for the CE separation of the test metal ions over the concentration range of 5.0×10^{-6} to 1.0×10^{-4} mol/L it was found that the anodic signal gave slightly better detection limits (by ~ 2:1). However, these detection limits were poorer than those observed previously for integration of the whole anodic signal, and thus this approach was not investigated further.

6.4. Signal Analysis Techniques

6.4.1. Fourier Analysis

As discussed in the introduction section, Fourier analysis of PAD currents might offer a technique to differentiate between the symmetrical double-layer capacitance currents and the less symmetrical faradaic currents. To determine if this approach might

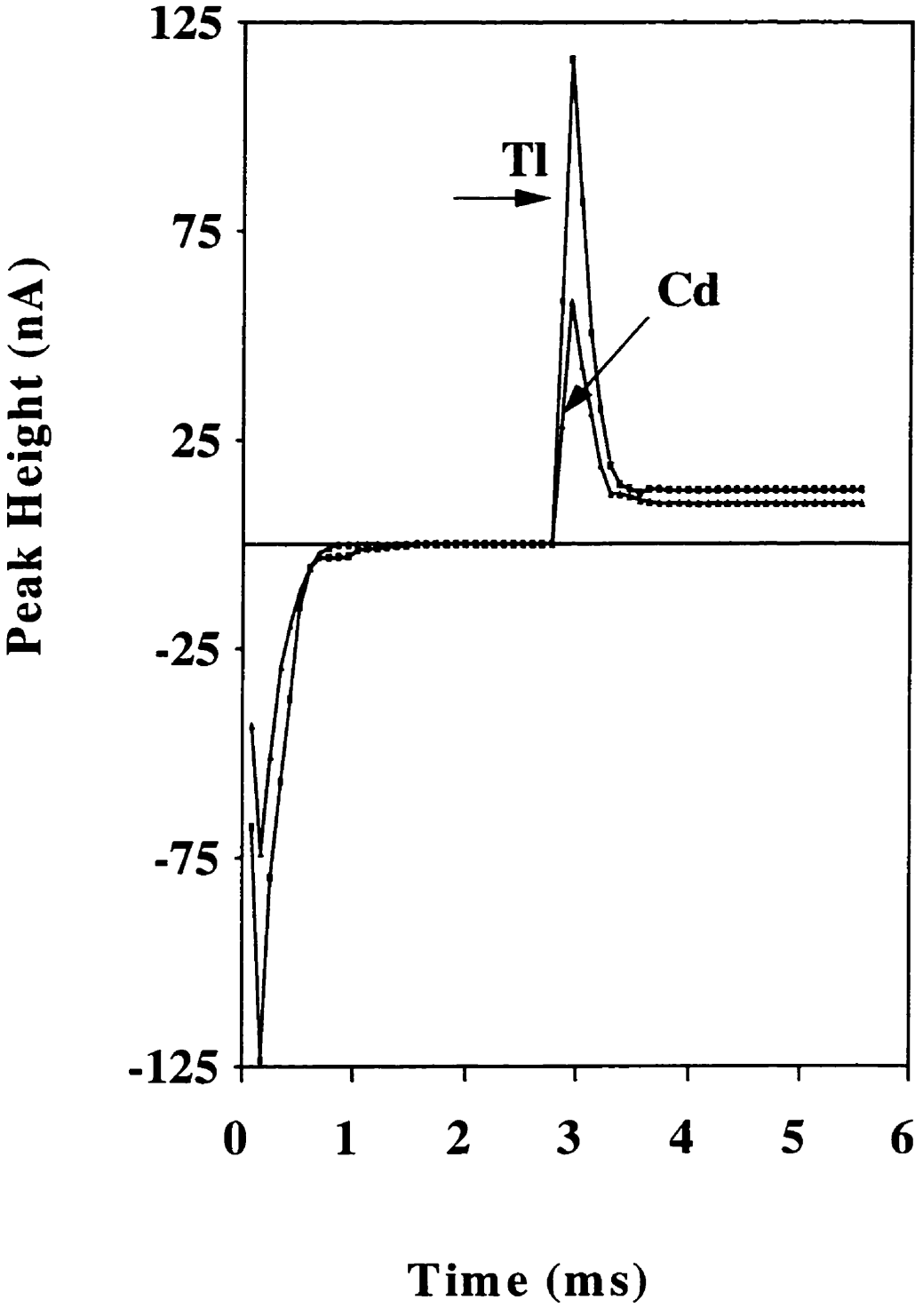

Figure 6.4. Response for Tl^{+} and Cd^{2+} at different points of applied bipolar pulse. Experimental conditions: applied bipolar pulse potentials, -1000 mV for reduction and 300 mV for oxidation with a frequency of 180 Hz; analytical data were collected over each short period (0.087 ms); errors, ± 6%; analyte concentration, 20 μmol/L; other conditions as for Figure 6.3.

improve S/N the magnitudes of the different harmonics of the current response from PAD detection were examined for the CE separation of Tl^{+}, Co^{2+}, Ni^{2+}, Zn^{2+}, Cd^{2+} and Pb^{2+} over the concentration range of 5.0×10^{-6} - 1.0×10^{-4} mol/L with a square-wave frequency of 7.5 to 120 Hz. A typical response observed by application of a 75 Hz square-wave pulse is shown in Figure 6.5 (see discussion below). The CE data in this figure has been displayed as both the average current (curve A) and as the total current (curve B, anodic-cathodic). Both curves in Figure 6.5 exhibit a shifted baseline, a feature often observed for these analytes when cathodic currents contribute to the signal used for analysis (see CV discussion in section 4). The average-current response is expected to be smaller for symmetrical signals (fast, reversible reactions), and this is one of the reasons for the difference in relative peak heights between curve A and B in Figure 6.5. The S/Ns for the peaks in curve B were similar to previous results for anodic detection, but baseline stability was much poorer because cathodic currents were part of the analytical response. The S/N values in curve B were used as a standard for comparison of the different signal-analysis techniques discussed below. When the observed current is treated as an AC current and subjected to Fourier analysis, the magnitude of the different harmonics can be isolated. Curve A in Figure 6.6 shows the electropherogram obtained at the fundamental frequency. Since this frequency is expected to contain the major portion of all symmetrical signals, it is not surprising to find that peaks for the more irreversible analytes, Co^{2+} and Ni^{2+} (peak 2 and 3) are reduced (relative to other peaks) compared to normal PAD (total current, curve B, Figure 6.5). It can also be seen that Zn^{2+} and Cd^{2+},

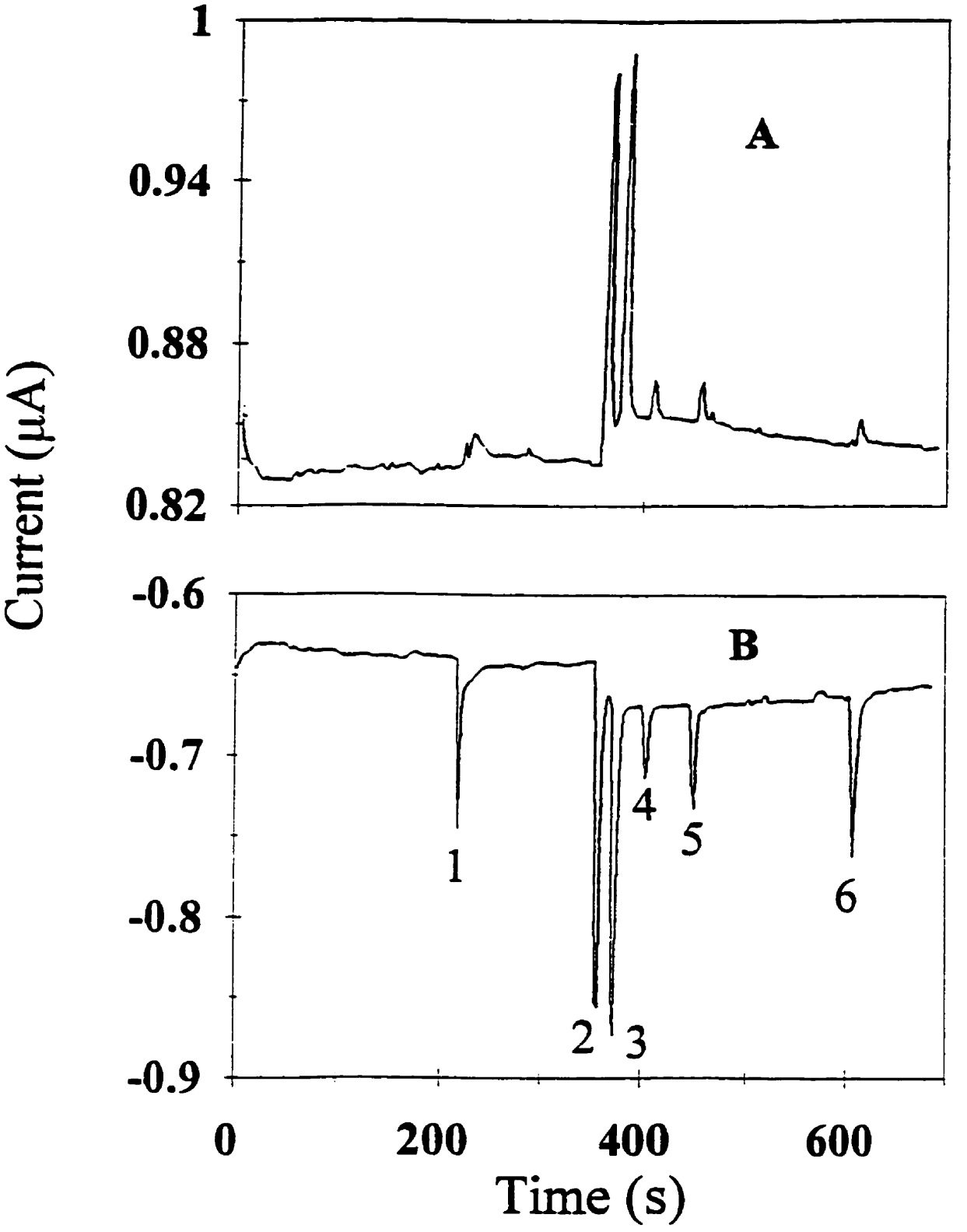

Figure 6.5 Electropherogram of metal ions with bipolar pulsed amperometric detection. Experimental conditions: cathodic current is considered as positive current; applied potentials, -1100 mV for reduction and 300 mV for oxidation with a frequency of 75 Hz; analyte concentration, 50 μmol/L; curves A and B represent average and total currents respectively; peak identification, (1), Tl(I); (2), Co(II); (3), Ni(II); (4), Zn(II); (5), Cd(II); (6), Pb(II); other conditions as for Figure 6.3.

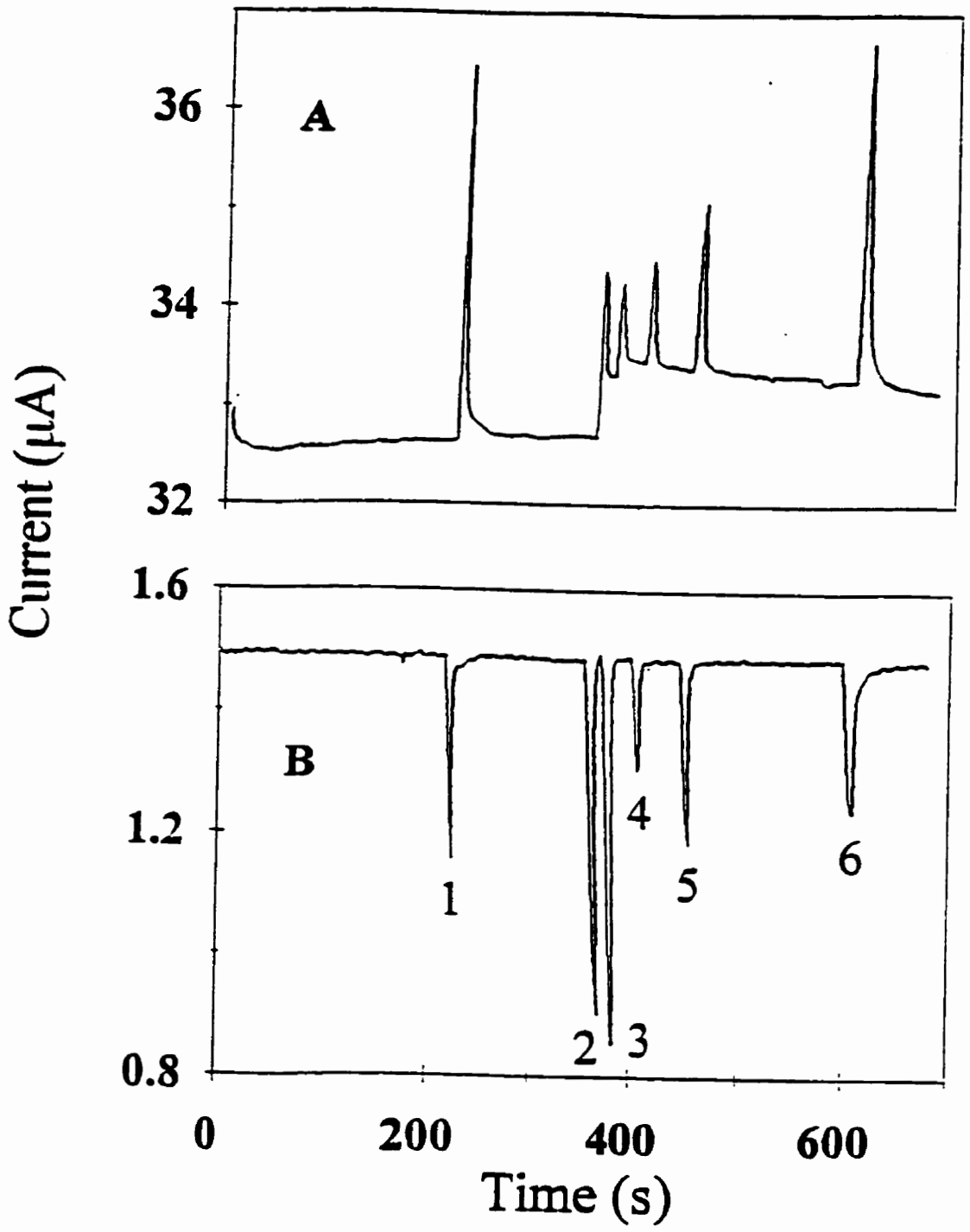

Figure 6.6 Electropherograms obtained using first (curve A) and second (curve B) harmonics. Experimental conditions: fundamental frequency is 75 Hz; data used for the analysis is that collected in Figure 6.5; peak identification and other conditions as for Figure 6.5.

which have an intermediate reversibility, follow slightly different patterns relative to the other metal ions. When the second harmonic is used for the electropherogram (curve B, Figure 6.6) unsymmetrical signals are detected. Thus relative peak heights for Co^{2+} and Ni^{2+} are increased, and are similar to that observed for the total current in curve B of Figure 6.5. Two other important features to note for the response for the second harmonic are the lower overall signal strength and the more stable baseline; both of these features are likely a result of the removal of symmetrical components. In spite of the lower signal in curve B of Figure 6.6, there is still an enhancement of S/N by 2 to 4 times relative to curve B of Figure 6.5. An evaluation of this approach over a wide range of conditions gave improvements in S/N that were essentially the same. Compared to results reported previously for pulsed anodic detection (see above), the detection limits for Ni^{2+} and Co^{2+} were ~ 3 fold improved, and for other metal ions, detection limits were similar.

An alternative approach for minimizing contributions from capacitance currents is to treat the currents as vectors and to use a phase angle shift to minimize contributions from charging currents (see experimental). The results for this approach with the first and second harmonics are shown in Figure 6.7. Again, the best improvements in S/N were seen for Co^{2+} and Ni^{2+} , and in general the trends are similar to those shown in Figure 6.6. Thus the second harmonic response, curve B in Figure 6.7, showed improved baseline stability and better S/N. The improvements in S/N were 3 to 6 fold relative to total current (curve B, Figure 6.5), and thus this approach is slightly better than that for the harmonic analysis conditions used in Figure 6.6.

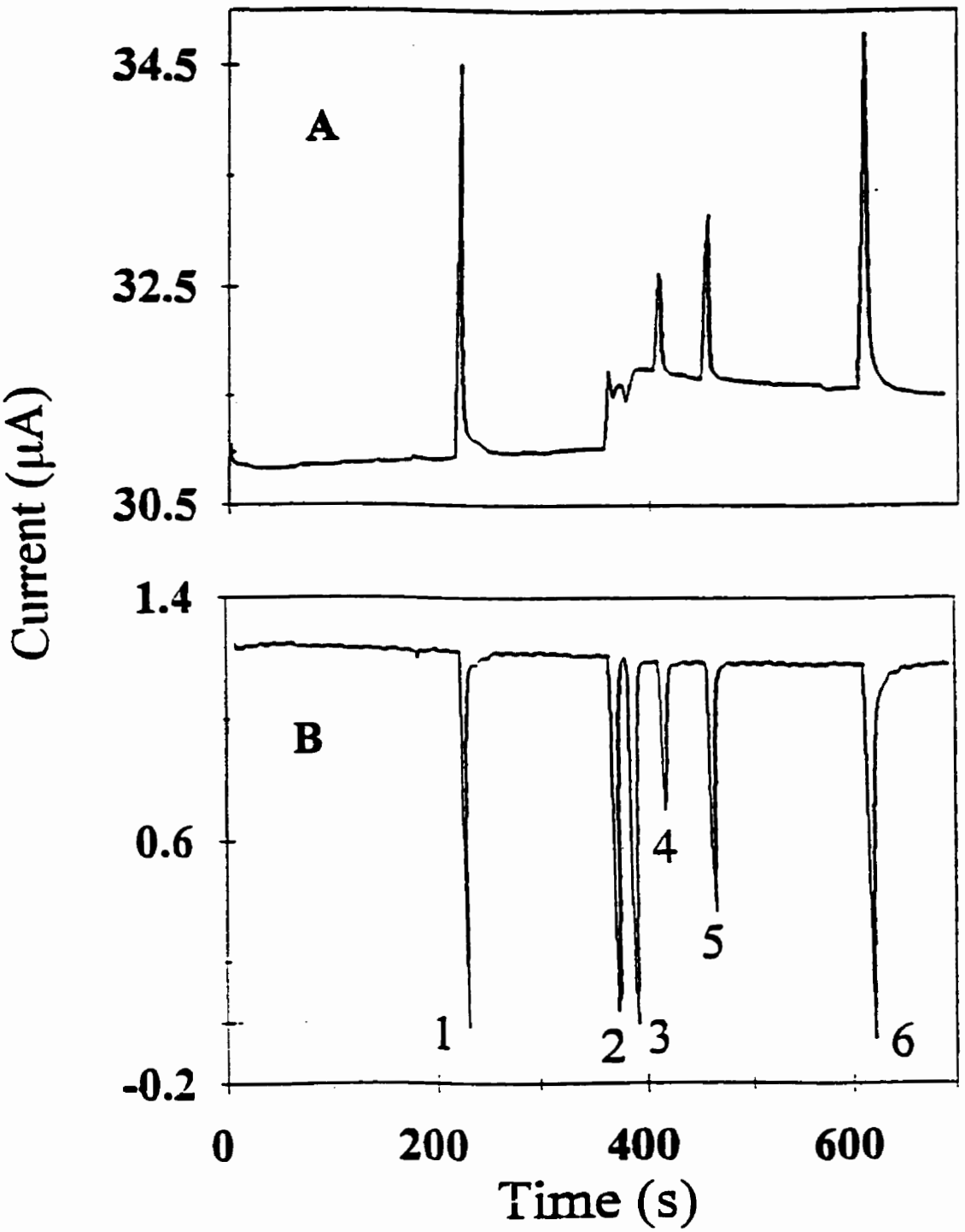

Figure 6.7 Electropherograms obtained using first (curve A) and second (curve B) harmonics from vector analysis. Experimental conditions as for Figure 6.6.

6.4.2. Lock-in Amplifier

Lock-in amplifiers can be set to detect signals at specific frequencies. In some cases the use of a lock-in amplifier can offer improved S/N via the isolation of the 1st and 2nd harmonic contributions to the analytical signal; as explained above this permits differentiation between symmetric and unsymmetric signals. Thus this approach was examined over the frequency range of 7.5 to 1000 Hz for square-wave pulses, and the applied frequency was used as the reference frequency of the lock-in-amplifier. The lock-in amplifier was equipped with several filter functions and could isolate first & second harmonics. The results showed little (maximum 3 fold) or no improvement in S/N relative to previous anodic detection[12] for either the first or second harmonic. Such a small improvement may be because the optimal frequency for a lock-in amplifier is from a few hundred Hz to 10 kHz. However, at low frequencies, 1/f noise, including both that developed in the Model 5301 lock-in amplifier and that originating in the experiment itself. may have limited the S/N of the lock-in amplifier for low-frequency signals; at high frequencies, the lock-in amplifier could not differentiate the analytical signal from the background noise.

6.5. Digital Signal Processing

6.5.1. Average Smoothing

The simplest method to reduce noise in digital signals is average smoothing, such as ensemble averaging. Two commonly used smoothing functions, moving average and polynomial average, were examined for Tl^{+}, Cd^{2+} and Pb^{2+} over range of 1.0×10^{-6} to

1.0×10^{-4} mol/L in terms of noise reduction, signal distortion and signal-to-noise ratio. In average smoothing, window size which is the number of original data averaged for one smoothing point, was important for analytical and background signals. When the window size was increased from 0 to 40 points, the peak-peak noise reduced, but this had a detrimental effect on peak height, especially for narrow analyte peaks such as Tl^+. The effect of the window size on the peak height for Tl^+ is shown in Figure 6.8. The results show that the signal for moving average smoothing decreased faster than that for polynomial average smoothing. When the window size for moving and polynomial average smoothing was 15 and 25 points, respectively, S/N improved 2-5 times. Over whole average smoothing process, peak area did not change. Therefore, for average smoothing, the peak area should be used as an analytical signal for calibration curve.

6.5.2. Digital Filtering

Digital filtering is based on the reduction of unwanted noise via selection and removal of certain signal frequencies. Since the frequencies from noise usually are much higher than signal frequencies in analytical measurements, low-pass filters may be useful to preserve signal and to remove noise. An important parameter in digital filter is the cutoff frequency, and low-pass filters set a frequency above which no signal passes. Here, two commonly used digital filters, rectangular and exponential low-pass filters, were examined for the electrode response of Tl^+, Cd^{2+} and Pb^{2+}. With a low-pass rectangular filter, the peak-peak noise reduced when the cutoff frequency decreased from 5 to 0.6 Hz, and lower cutoff frequencies led to an increase of the background noise, likely due to the introduction of lobes to the original signal.[142,210] This occurs due to abrupt truncation of

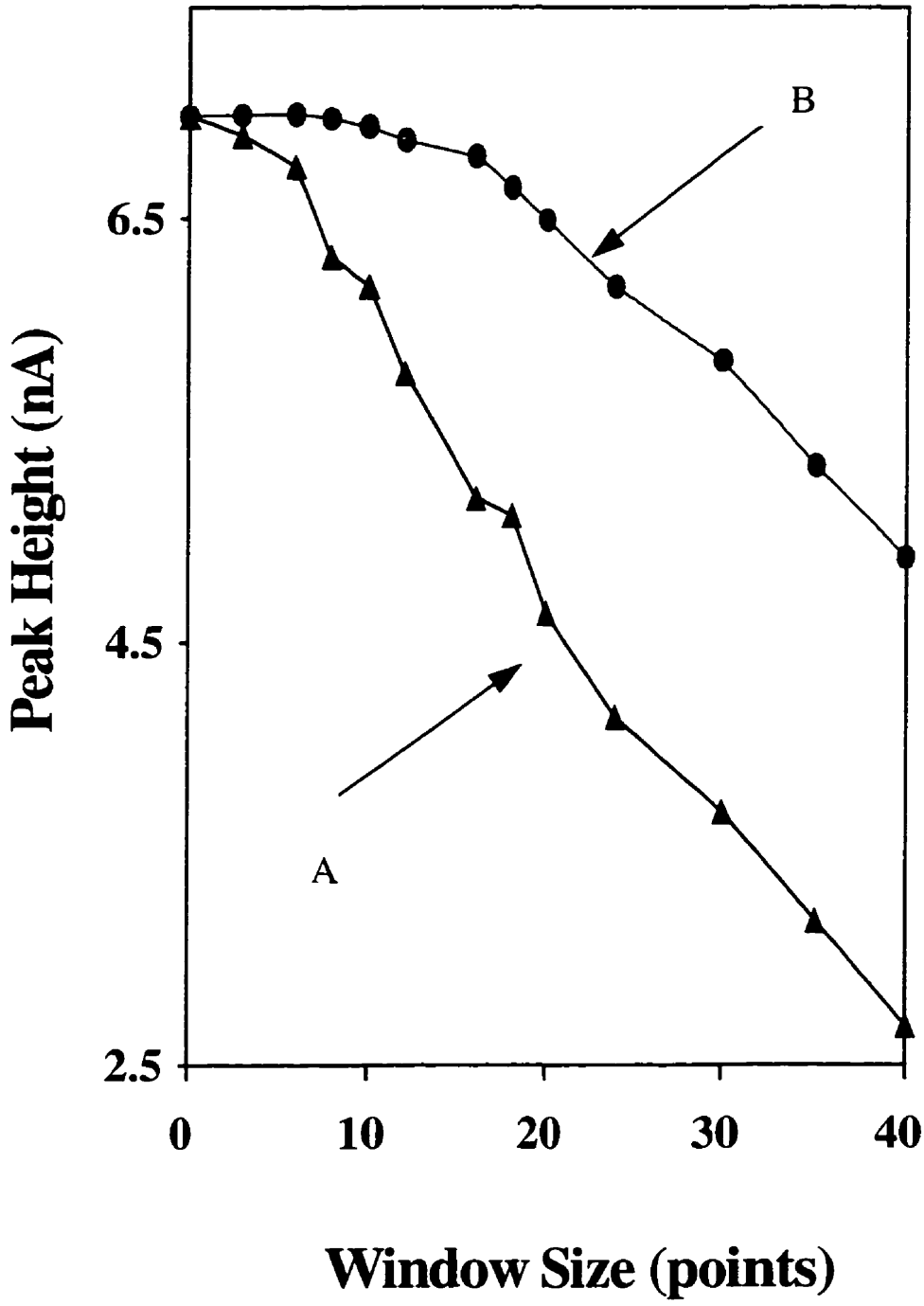

Figure 6.8 Effect of the window size on the peak height for Tl^+ with moving (A) and polynomial average smoothing (B). Experimental conditions: applied potential, -800 mV for reduction and 200 mV for oxidation with a frequency of 75 Hz; analyte, 5×10^{-6} mol/L; other conditions as for Figure 6.3.

Fourier spectrum after back transformation when the cutoff frequency is too small. An exponential low pass filter can minimize the limitation, and with this filter, the background noise gradually reduced with a decrease in cutoff frequency. The analytical signal with both rectangular and exponential filters was unchanged until the cut off frequency was less than 0.5 Hz. S/N as a function of the cutoff frequency via the exponential filter for Tl^{+}, Cd^{2+} and Pb^{2+} is shown in Figure 6.9. This result shows that the optimal cut off frequency is 0.4~0.7 Hz, at which the S/N was improved 2~5 times.

6.6. Conclusion

Of the various approaches examined for the enhancement of analytical S/N, the best results were obtained with the addition of a multiple-step potential waveform to a bipolar pulse. Up to a 10 fold improvements (detection limits in 2×10^{-8} to 2×10^{-7} mol/L range) have been observed for species that can be concentrated at the electrode, but such approaches may also prove useful for analytes that physically adsorb at electrode surfaces (this is discussed further in section 7). Although the harmonic analysis techniques offered improved baseline stability, the smaller improvements in S/N (3 to 6 fold for vector approach) make this approach a bit less attractive. However, this procedure may prove useful for correction of the baseline shifts and for application to analytes that can not be preconcentrated at the electrode surface. Digital filtering and data smoothing techniques can be combined with most data analysis technique, and a brief examination of these techniques showed improvements of 2-5 fold. Another detection approach, which has not been examined in these studies, is the use of rapid-scanning cyclic voltammetry.

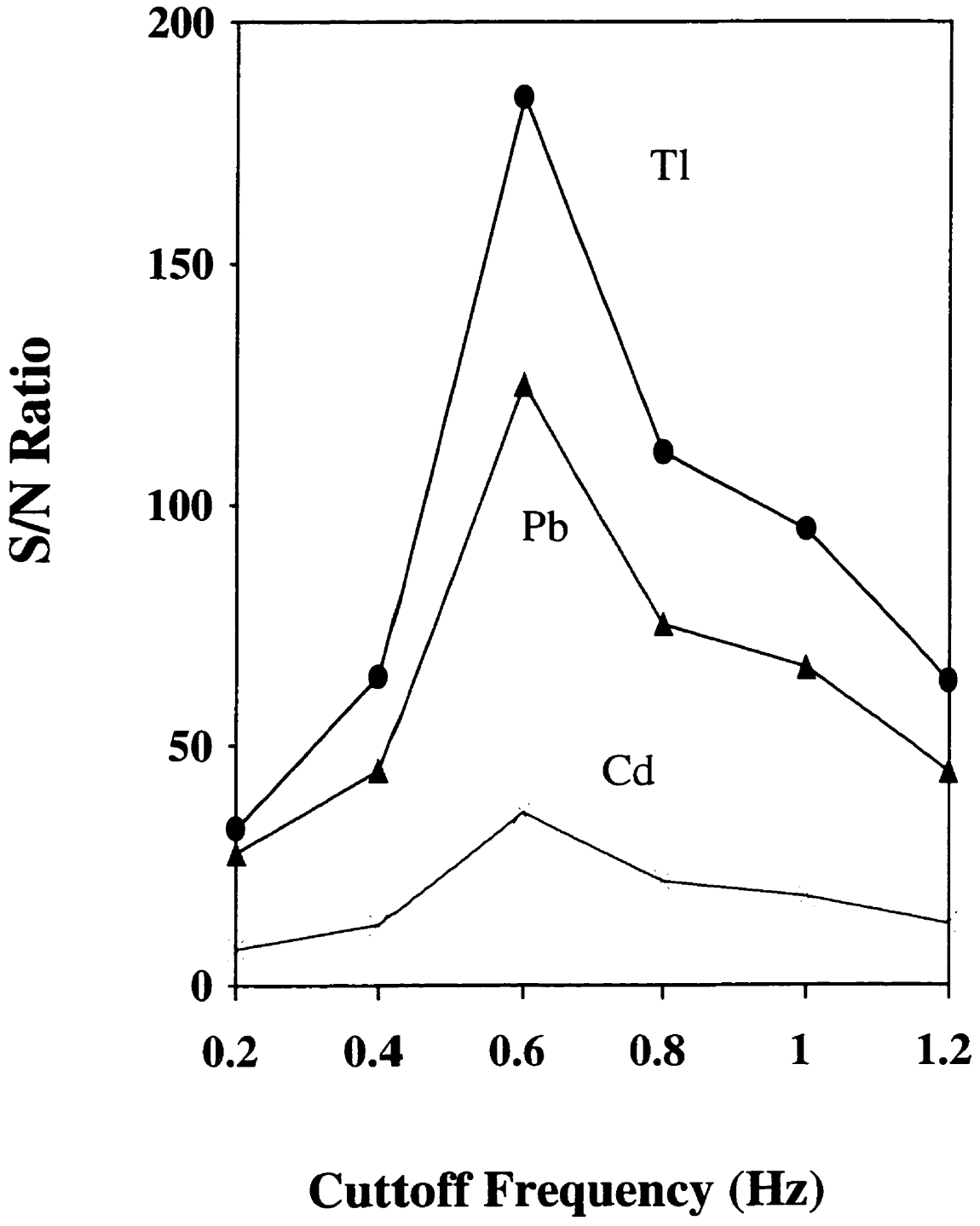

Figure 6.9 Dependence of S/N ratio on the cuttoff frequency via an exponential filter. Experimental conditions: analytes, 2.0 x 10^{-5} mol/L; other conditions as for Figure 6.8

7. FAST CYCLIC VOLTAMMETRY DETECTION

7.1. Introduction

Of all the electrochemical techniques presently available, stripping voltammetry is one of the most sensitive techniques for trace-metal analysis, but the slow scan rates (≤ 10 V/s) used in the conventional voltammetric techniques are not suitable for CE detection. However, with μm-electrodes, fast-scan voltammetric techniques can provide good S/N, and when combined with preconcentration may provide sensitive detection in CE. Another potentially important feature for this approach is the ability to resolve co-migrating species because it provides time- and potential- domain signals simultaneously. Fast single-scan voltammetry has been reported for the detection of histamine and 5-hydroxytryptamine in HPLC,[110] and it has been suggested that fast voltammetry should be able to resolve co-migrating species in CE if their electrochemical potentials are sufficiently different.[143] Repetitive voltammetric scanning has also been recently reported for CE,[211,212] but scan rates were relatively low and resistance problems associated with fibres being inserted into capillaries were apparent.[213] In the on-line CV studies reported in section 4, a rapid-scanning CV was used to characterize the electrochemical behavior of analytes, and the sensitivity of this on-line CV technique suggested that it might be useful for EC detection in CE. Thus, its potential for CE analysis of metal ions was examined, and the experimental parameters that affect the analytical and background signals, such as

sweep rate, electrochemical potential, size of working electrode, and preconcentration time, were also evaluated.

7.2. Potential Waveform and Electrode Response

The potential waveform used in these studies is shown in Figure 7.1. It consisted of two parts: an initial constant potential (preconcentration period) followed by a triangular potential over a time period determined by the scan rate. For CE detection, this CV waveform was applied repeatedly to the electrode over the potential range in which the analytes were oxidized/reduced as the sample band moved past the working electrode. As a result, both time domain (electropherogram) and potential domain (voltammogram) signals could be obtained, and a representative sample is shown in Figure 7.2 for Pb^{2+}. The analyte response used for the electropherograms can be either CV current or CV charge. CV current is the value of the maximum current in each CV, and CV charge is the integrated CV current over applied time window.

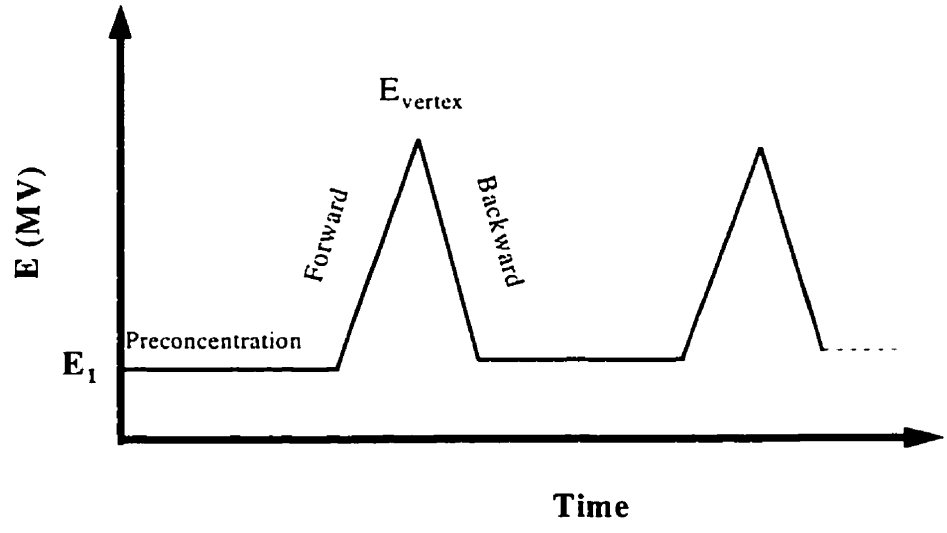

Figure 7.1 Fast-scan potential waveform.

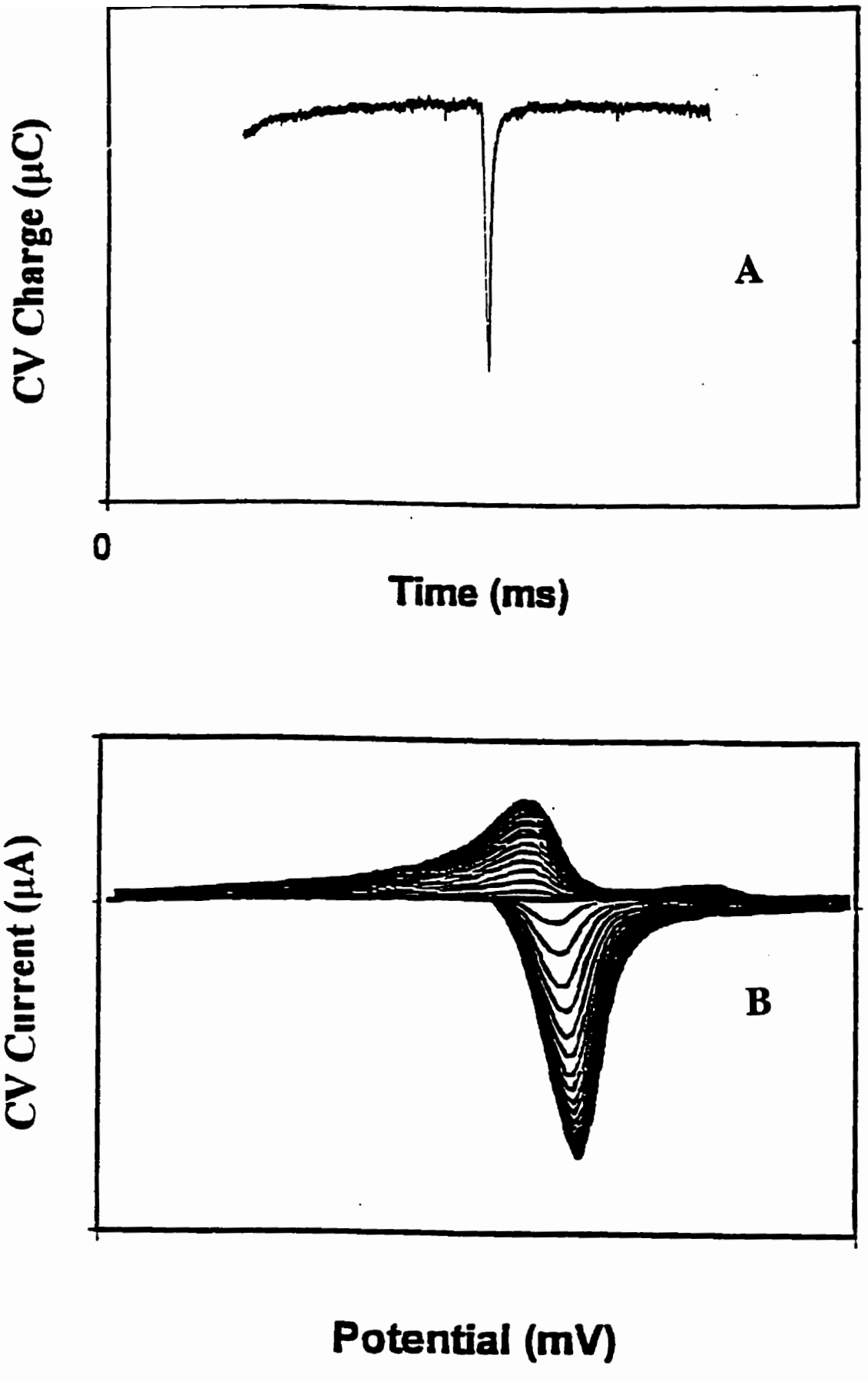

Figure 7.2 Signals for fast CV detection for Pb. A, CV charge in electropherogram is from integration of the CV current versus time; B, CV current in cyclic voltammograms obtained across the above peak.

7.3. Optimization of Experimental Parameters

7.3.1. Preconcentration Time

High sensitivity for conventional stripping voltammetric techniques in bulk solution is mainly attributed to analyte preconcentration. Preconcentration may also enhance S/N for fast-scan voltammetric detection in CE. Therefore, the effect of preconcentration time on the electrode response and peak shape was evaluated for Tl^{+}, Co^{2+}, Ni^{2+}, Zn^{2+}, Cd^{2+}, Pb^{2+} over the range of 2.0×10^{-7} to 1.0×10^{-4} mol/L at 25 μm and 10 μm Au electrodes. Results were studied over a preconcentration range of 55 to 330 ms at sweep rates of 25 V/s to 1000 V/s. The results in Figure 7.3 for Tl^{+}, Cd^{2+}, Pb^{2+} obtained at a sweep rate of 350 V/s with a 25 μm Au electrode show that the electrode response increased with preconcentration time. Results for Zn^{2+}, Ni^{2+} and Co^{2+} were similar to that for Cd^{2+}. The rate of increase, $Tl^{+} > Pb^{2+} >> Cd^{2+}$ was in the same relative order as the charge-transfer kinetics determined previously with on-line CV studies (section 4.3). Although the typical preconcentration time in conventional anodic stripping voltammetry is usually in the range of 5 to 10 min, maximum preconcentration time in CE is limited by the narrow analyte peaks. Peak broadening was noted when the preconcentration time was ≥ 250 ms. For example, the peak width at half-peak height for Tl^{+} with 275 ms preconcentration time was 25% larger than that with 55 ms preconcentration time. Such an increase likely because of carryover due to the incomplete removal of the analyte adsorbed onto the

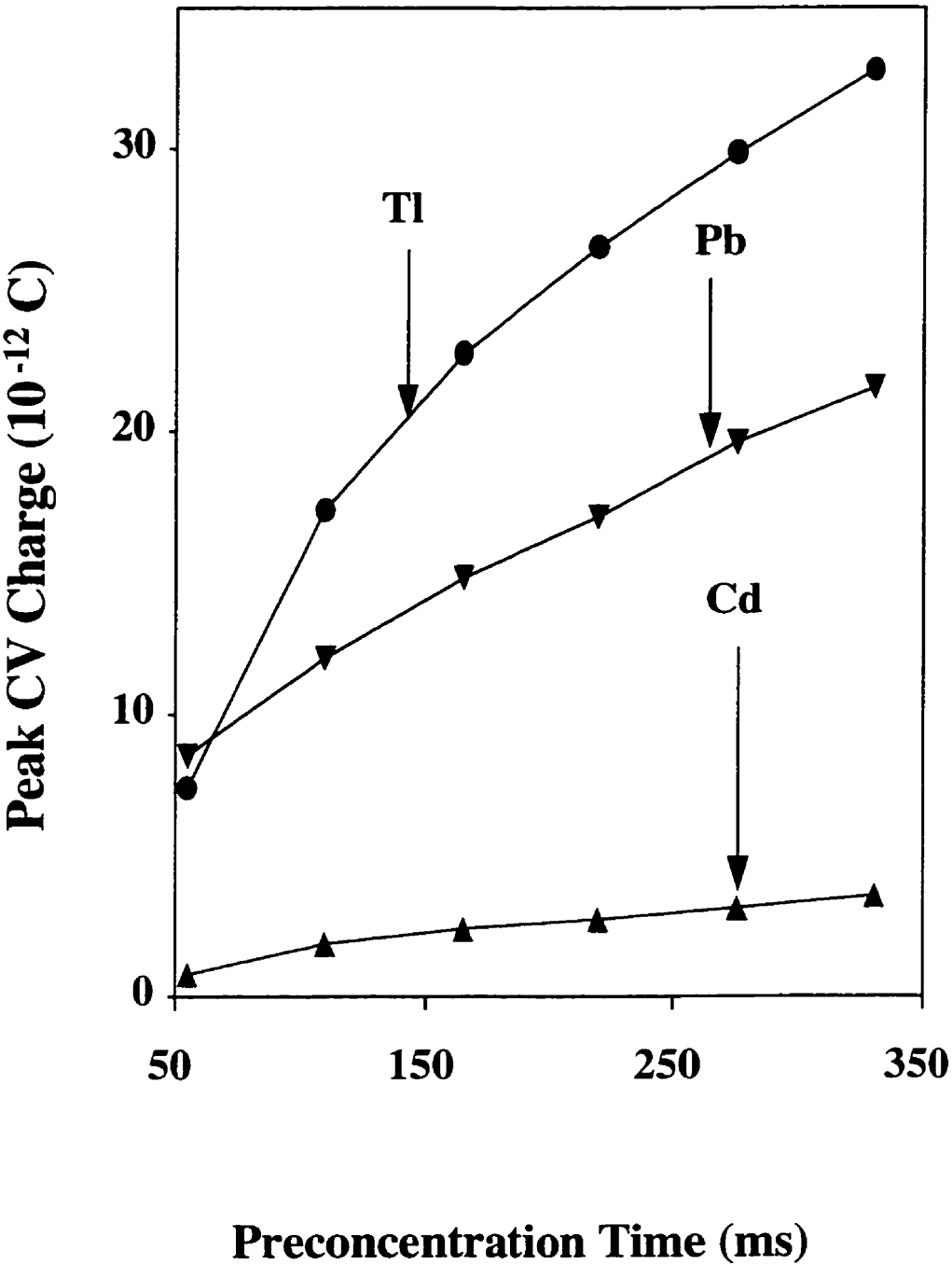

Figure 7.3 Influence of preconcentration time on the CV charge at CE peak maximum at a 25 μm Au electrode. Experimental conditions: CV potential, -700 to 100 mV; sweep rate, 350 V/s; analyte concentration, 1.0 μmol/L; 5 kV electromigration injection for 10s; electrolyte, 0.030 mol/L creatinine and 0.008 mol/L HIBA at pH 4.8; separation voltage, 20 kV over a 25 μm × 60 cm capillary.

electrode. In addition, long preconcentration times reduced the number of data points for plotting the electropherogram, which caused apparent peak broadening and decreased peak height. Therefore, preconcentration times in these studies were 110 to 220 ms, as a compromise between maximum S/N and minimum peak broadening. The use of a 110 ms preconcentration period gave a ~ 2 fold improvement in S/N relative to the use of no preconcentration. Thus, if these CV approaches described here were applied to analytes that could not be preconcentrated, the maximum loss in S/N might only be in the range of 2-4 fold. This is a significant point because it means that the general applicability of the CV approach described below is also valid for a wide range of other electroactive species.

7.3.2. Electrode Response

In fast voltammetric analysis, the sweep rate is an important factor because it affects the analyte signal, background noise and peak shape. Depending on experimental conditions, the peak CV current can be proportional to $\sqrt{v}$ (v is a sweep rate) in bulk solution;[214] or directly proportional to v at thin layer cells,[100] or at Hg film electrodes.[102] Little information has been reported on the dependence of CV current on sweep rate at Au μm-electrodes in CE. If the CV current is integrated over time to give a response termed CV charge, then this analytical signal should provide better S/N because the integration process can minimize noise, compress the information, and overcome problems associated with slow kinetics which can reduce peak current. Theoretically, the

CV charge should be independent of sweep rate and this has been observed in slow-scan voltammetric techniques.[101,102] However, the relationship between the CV charge and sweep rate for fast-scan techniques is quite complicated due to the effect of several factors such as, electrochemical kinetics, mass transport of the analyte to and from the electrode/solution interface, the ohmic drop, and the time-dependence of the double layer capacitance caused by surface reconstruction processes. Since metals are oxidized and removed from the electrode only during the forward sweep, in some instances carry-over of the analyte from a previous CV to the next CV can occur at high sweep rates. Thus increased CV charge can be observed especially if the reaction rates of analytes are fast relative to the mass transport rates; slow reaction rates will result in more efficient removal of analytes from the electrode diffusion area by diffusion.

To find the optimal sweep rate for maximum S/N, the dependence of electrode response on sweep rate was examined under CE conditions for Tl^{+}, Co^{2+}, Ni^{2+}, Zn^{2+}, Cd^{2+} and Pb^{2+} over 2.0×10^{-7} to 5.0×10^{-5} mol/L at 25 and 10 μm Au electrodes over a sweep rate of 25 to 1000 V/s. Typical results for CV current at a 25 μm Au electrode for Tl^{+}, Cd^{2+} and Pb^{2+} over 25 to 400 V/s are shown in Figure 7.4. The CV current increased linearly with sweep rate, with correlation coefficients in the range of 0.998 to 0.999; Plots of the logarithm of peak CV current versus the logarithm of the sweep rate gave the slopes of 1.14 ± 0.02 for Tl; 1.08 ± 0.05 for Pb; 1.01 ± 0.02 for Cd. Co^{2+}, Ni^{2+} and Zn^{2+} and results at a 10 μm Au electrode were similar. The order of the increase in slope was the same as that for the reversibility of the electrochemical reaction (see section 4).

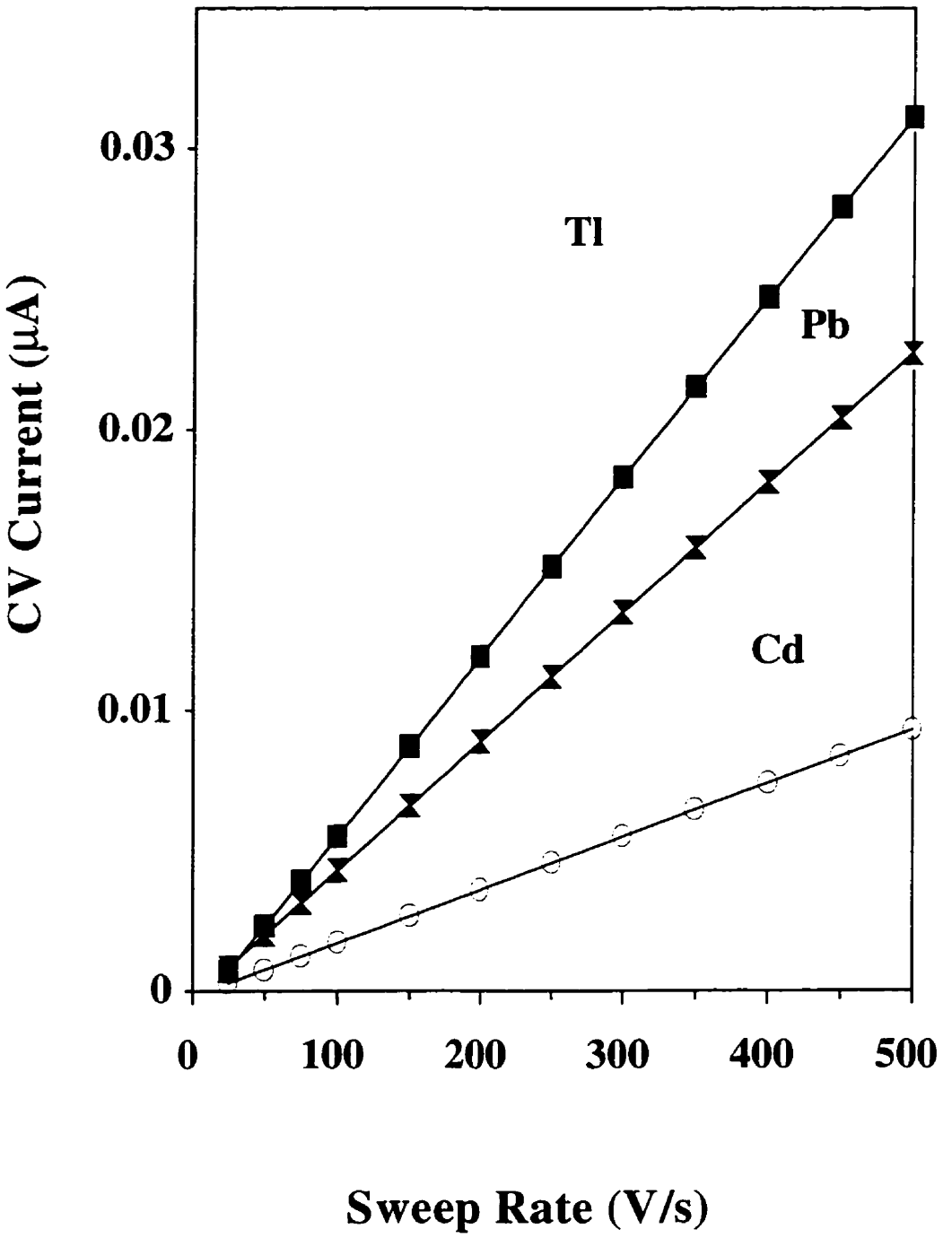

Figure 7.4 Dependence of CV current at the CE peak maximum on sweep rate at a 25 μm Au electrode. Experimental conditions: on-line CV detection; CV potential, -900 to 100 mV; analyte concentration, 1.0 μmol/L; preconcentration time, 220 ms; other conditions as for Figure 7.3.

These linear relationships observed for the Au μm-electrode are similar to those reported for a thin layer cell[100] and a thin Hg-film electrode.[102] Typical results for similar study of the change in CV charge with sweep rate are shown in Figure 7.5 for Tl^+, Cd^{2+}, Zn^{2+} and Pb^{2+}. In contrast to the linear dependency observed between CV current and sweep rate, the relationship observed between CV charge and sweep rate depended on the analyte. A variety of different trends were observed, and Ni^{2+} and Co^{2+} gave results similar to Zn^{2+} and Cd^{2+}. The different patterns observed in Figure 7.5 appear to be associated with a relationship between rates of reaction and mass transport rates with changes in sweep rate. For Tl^+ and Pb^{2+}, which have faster charge-transfer kinetics (small shifts in voltammograms), analyte carry-over began to occur from one waveform to the next as the sweep rate increased; a complicating factor in the interpretation of these results is the fact that they were obtained for a CE peak rather than in a constant bulk concentration. As a result of analyte carry-over, the CV charge of Tl^+ and Pb^{2+} increased with sweep rates (Figure 7.5) up to 200 V/s, and then became more or less constant with the sweep rate. This linearity off ma be sue to the fact that at these higher sweep rate positive shifts of the oxidation potentials were observed in the cyclic voltammograms; this can be attributed to reaction rates now becoming slow relative to scans, and the electrochemical reaction now starts to show irreversible behavior. For the other metal ions, the charge-transfer kinetics were not fast enough to match mass transport rates even at lower sweep rates, and thus analyte carry-over was not significant.

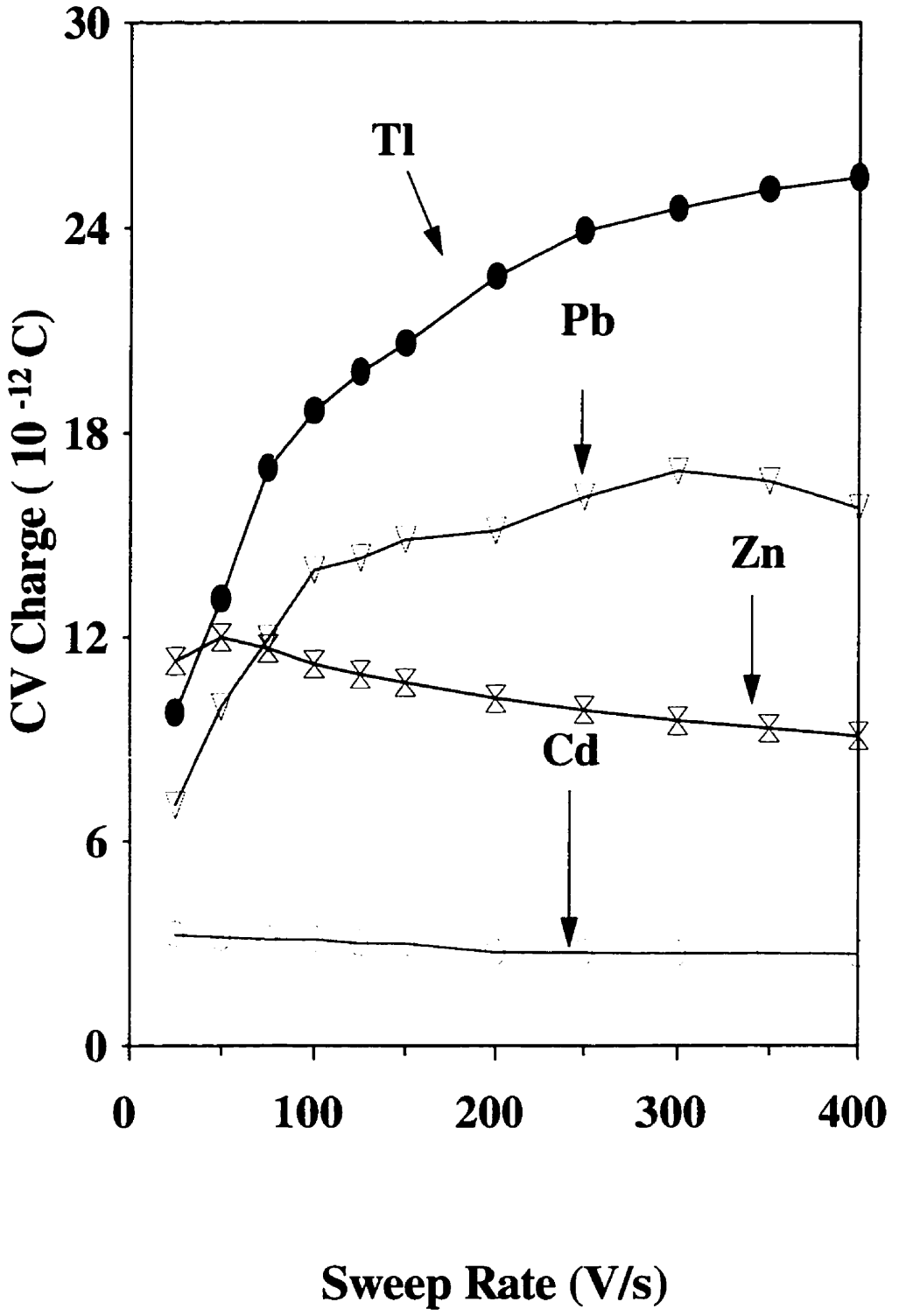

Figure 7.5 Dependence of CV charge on sweep rate at a 25 µm Au electrode. Experimental conditions: on-line CV detection; CV potential, -900 to 100 mV; analyte concentration, 1.0 µmol/L; preconcentration time, 220 ms; other conditions as for Figure 7.3.

The positive shifts observed in the oxidation potential are expected from theory,[215] and have been shown in other experimental studies.[216] With a change in the sweep rate from 20 to 400 V/s, the anodic peak potential shifted in a positive direction: 50 - 60 mV for Tl^{+}, 40 - 50 mV for Pb^{2+}, and 25-35 mV for Cd^{2+}, Zn^{2+}, Ni^{2+} and Co^{2+}. Cathodic peak potentials shifted to slightly more negative values. According to the Nernst equation, $E = E_o + nEF/RT \ln[O/R]$, the shift of peak potential was due to an increase in the local concentration of metal ions (O oxidized form) caused by fast stripping of analytes from the electrode. Other factors which contribute to the observed shift are ohmic drops and in some cases slow electrode kinetics. Thus an increase in sweep rate can cause a decrease in CV charge due to the incomplete electrochemical reaction. Maximum S/N was achieved at sweep rates of 150 to 350 V/s for analytes with fast charge-transfer kinetics. Thus for Tl^{+} and Pb^{2+} there was a 2-3 times enhancement in S/N relative to low sweep rate. For analytes with slower charge-transfer kinetics, sweep rate affected S/N only slightly. Similar results were also observed at Pt μm-electrodes.

Most of above studies used 25 μm Au or Pt electrodes. Since the ohmic drop and mass transport rates are influenced by electrode size, the relationship between electrode response and sweep rate may be different at a smaller electrode, and it is of interest examine this relationship. Therefore, the fast voltammetric detection at a 10 μm Au

electrode was evaluated with Tl^{+}, Co^{2+}, Ni^{2+}, Zn^{2+}, Cd^{2+} and Pb^{2+} over a sweep rates of 25 to 900 V/s. The value of CV charge obtained at the 10 μm Au electrode was smaller relative to 25 μm electrode by a factor of 4 ~ 5 (electrode-area decrease by a factor of ~ 6). The dependence of CV currents on sweep rate observed for this 10 μm electrode were linear and similar to those obtained at a 25 μm electrode (Figure 7.2). However, the behavior of CV charge was different. Typical results for Tl^{+}, Zn^{2+}, Cd^{2+} and Pb^{2+} are shown in Figure 7.6. These results show that the CV charge signal for Tl^{+} and Pb^{2+} rose up and dropped down more quickly than that obtained at a 25 μm Au electrode. These differences in behavior for 10 μm electrodes appear to be primarily related to their faster mass transport rates. Thus as sweep rates increase carryover will begin to occur, but when the rates of electrochemical reaction begin to slow down at high sweep rates, the rate of mass transport away from the electrode is faster relative to larger electrode, and signal begins to decrease. Consequently, detection at a 10 μm electrode did not provide better performance, and was not examined further in these studies.

The above results showed that some metals were not completely oxidized at high sweep rates. Since the application of higher positive potentials should accelerate oxidation reaction, the performance of CV detection was evaluated at the CV vertex potential of 400 mV, and a typical result for Tl^{+}, Cd^{2+} and Pb^{2+} is shown in Figure 7.7.

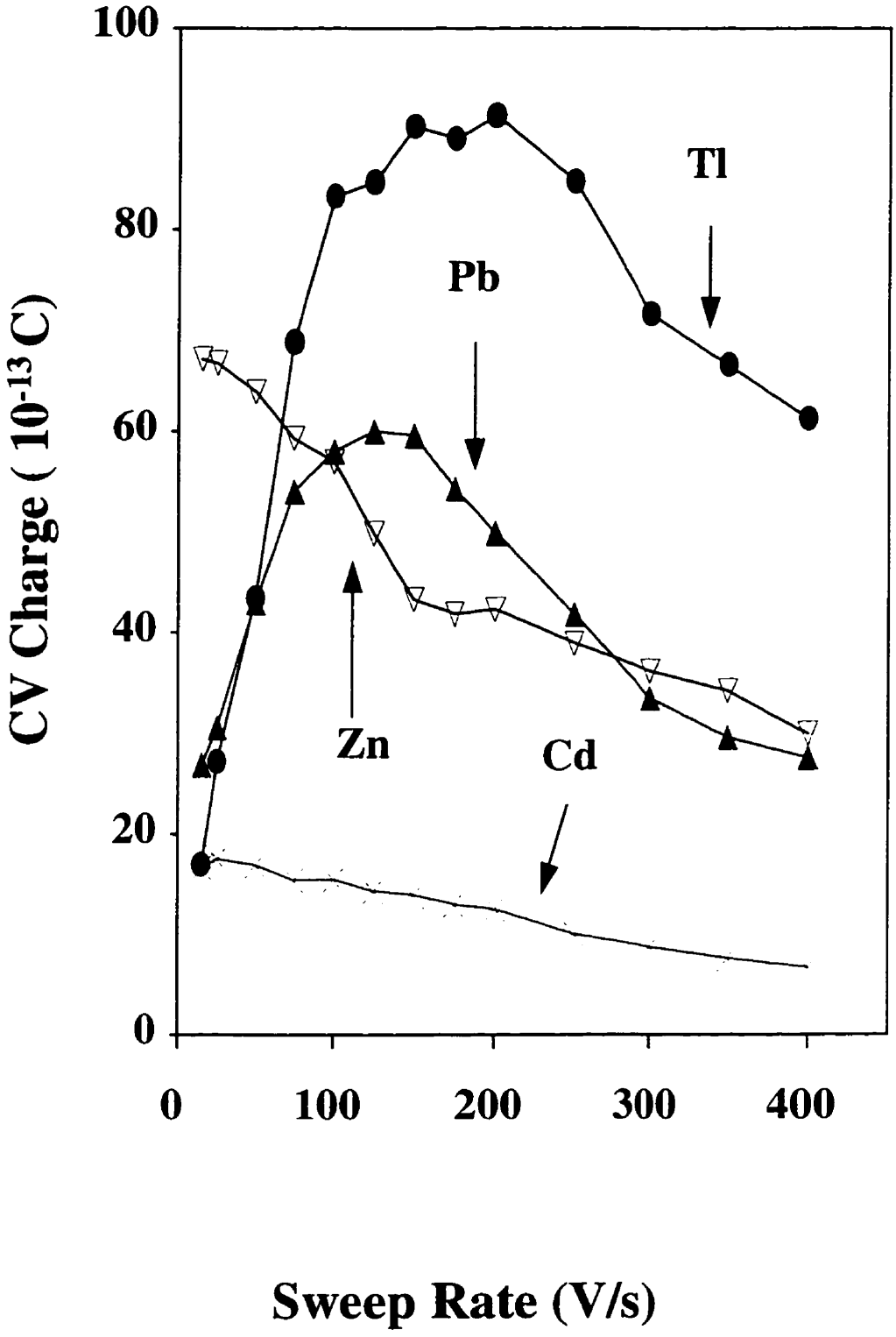

Figure 7.6 Dependence of CV charge on sweep rate at a 10 μm Au electrode. Experimental conditions: on-line CV detection; CV potential, -800 to 200 mV; analyte concentration, 1.0 μmol/L; preconcentration time, 220 ms; other conditions as for Figure 7.3.

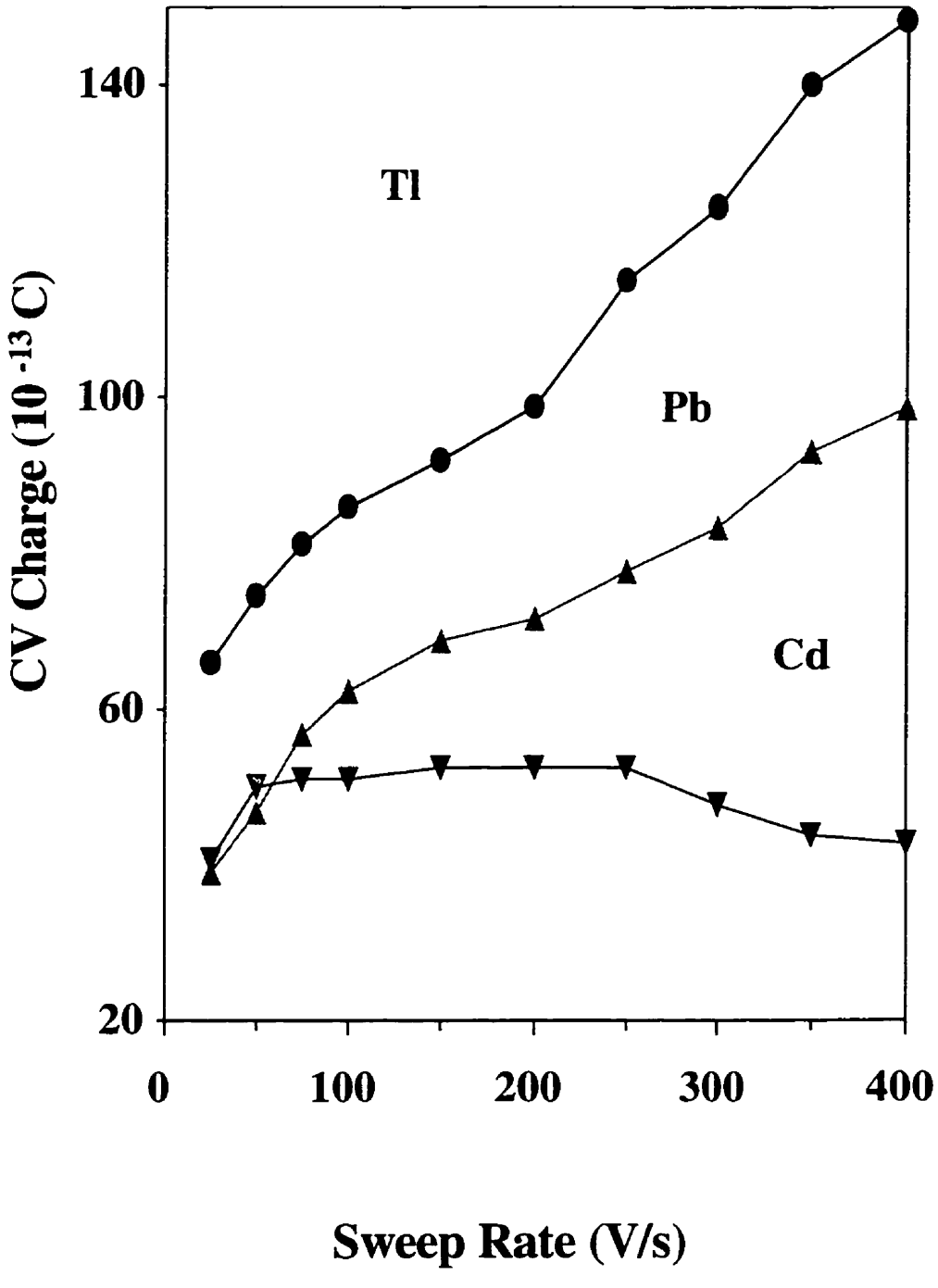

Figure 7.7 Dependence of CV charge on sweep rate at a 10 μm Au electrode. Experimental conditions: on-line CV detection; CV potential, -800 to 400 mV; analyte concentration, 1.0 μmol/L; preconcentration time, 220 ms; other conditions as for Figure 7.3.

Figure 7.7 shows that the CV charges of Tl^{+} and Pb^{2+} increased with sweep rate over the range of 20 to 450 V/s, and for Cd^{2+} peak CV charge increased to a plateau as sweep rate was adjusted to 50 V/s and then reduced gradually at the sweep rate of > 250 V/s; Zn^{2+}, Ni^{2+} and Co^{2+} gave results similar to that for Cd^{2+}. The CVs of the metal ions showed that with the high positive potential Tl^{+} and Pb^{2+} were oxidized completely over CV sweep rates of 25 to 450 V/s. However, Cd^{2+}, Zn^{2+}, Ni^{2+}, Co^{2+} still could not be completely oxidized at 400 mV due to their slow and irreversible reaction kinetics. Since the oxidation reactions of the analytes at 400 mV were more complete, the CV charge of the analyte should increase up to higher scan rates, and this can be observed to be the case if one compares the results in Fig 7.7 with Fig 7.6. Unfortunately the application of higher positive potentials (> 400 m V) led to higher background currents and larger peak-to-peak noise; these effects are related to the increase of capacitance current and the appearance of hydrogen and oxygen reduction reactions because of stripping of the organic electrolyte film off the Au electrode at the higher potentials (see section 4.1). Consequently, in spite of higher signals, detection limits obtained at 400 mV were almost the same as those obtained at 200 mV, and more positive CV potentials gave lower S/N. Although the background noise at the 10 μm electrode was 3 ~ 4 fold smaller than that at the 25 μm electrode, S/N was not improved due to the decrease of the electrode response.

7.3.3. Peak Shape

The above studies show that maximum S/N was obtained at high sweep rates. Unfortunately, these conditions led to incomplete oxidation and carry-over of analyte from one waveform to the next, and thus tailing of the peaks in the electropherogram also increased with sweep rate. To evaluate the optimum conditions for both S/N and peak resolution, peak shapes of Tl^{+}, Co^{2+}, Ni^{2+}, Zn^{2+}, Cd^{2+} and Pb^{2+} were examined in the range of 5.0×10^{-7} to 1.0×10^{-5} mol/L over the sweep rate of 25 to 1000 V/s. For most analytes, peak width at half-peak height depended on both sweep rate and the applied CV vertex potential. When the CV vertex potential was ≤ 200 mV, the increase in peak width over the sweep rate of 25 to 400 V/s was for Tl^{+}, < 5%; Cd^{2+}, ~ 30%; Co^{2+}, Ni^{2+} and Zn^{2+}, 20-25%, and for Pb^{2+}, > 100%. In addition, it was noted that the peak width for Pb^{2+} was much larger compared to those for other metal ions likely due to the interaction of Pb with the electrode surface as discussed in the on-line CV studies.

Since peak broadening, caused by the fast voltammetric process, was in the form of tailing and this tailing depended on the sweep rate, the dependence was examined for Tl^{+}, Cd^{2+}, Zn^{2+} and Pb^{2+} by a tailing percentage, which is ratio of peak area in tailing part to total peak area in an electropherogram. A typical result for Tl^{+} over a concentration range of 1.0×10^{-7} to 5.0×10^{-6} mol/L is shown in Figure 7.8. It is observed in Figure 7.8 that the tailing percentage was less than 10% when the sweep rate was less than 400 V/s

for all test concentrations, but this percentage rapidly increased up to 23% when the sweep rate was > 400 V/s. These results suggest that the reaction kinetic rate of Tl^+ was also limited by the factor existing at sweep rate above 400 V/s at the Au electrode when the applied CV potential was -800 to 200 mV. To achieve optimal peak shape for Tl^+, a sweep rate of ≤ 400 V/s should be chosen. The choice of sweep rate depended on the analyte concentration and other experimental conditions. In general, above 400 V/s peak tailing increased rapidly for all analytes.

When the CV vertex potential was adjusted to 400 mV, the peak width of metal ions, Co^{2+}, Ni^{2+}, Zn^{2+}, Cd^{2+} and Pb^{2+} still increased with sweep rate, however, such increases were much smaller relative to those obtained with the CV vertex potential of 200 mV: Tl^+, < 5%; Co^{2+}, Ni^{2+}, Zn^{2+} and Cd^{2+}, < 10%; Pb^{2+}, < 20% over a sweep rate of 25 to 450 V/s. A typical result for Tl^+, Zn^{2+}, Cd^{2+}, Pb^{2+} is shown in Figure 7.9. High CV vertex potentials help reduce peak broadening due to acceleration of the reaction kinetics, but high positive potentials (>400 mV) also caused higher background noise. Consequently, sweep rate of 200 to 400 V/s and a vertex CV potential 200 to 400 mV should be chosen for the fast CV analysis of the test analytes, as a compromise between maximum S/N and minimum peak tailing.

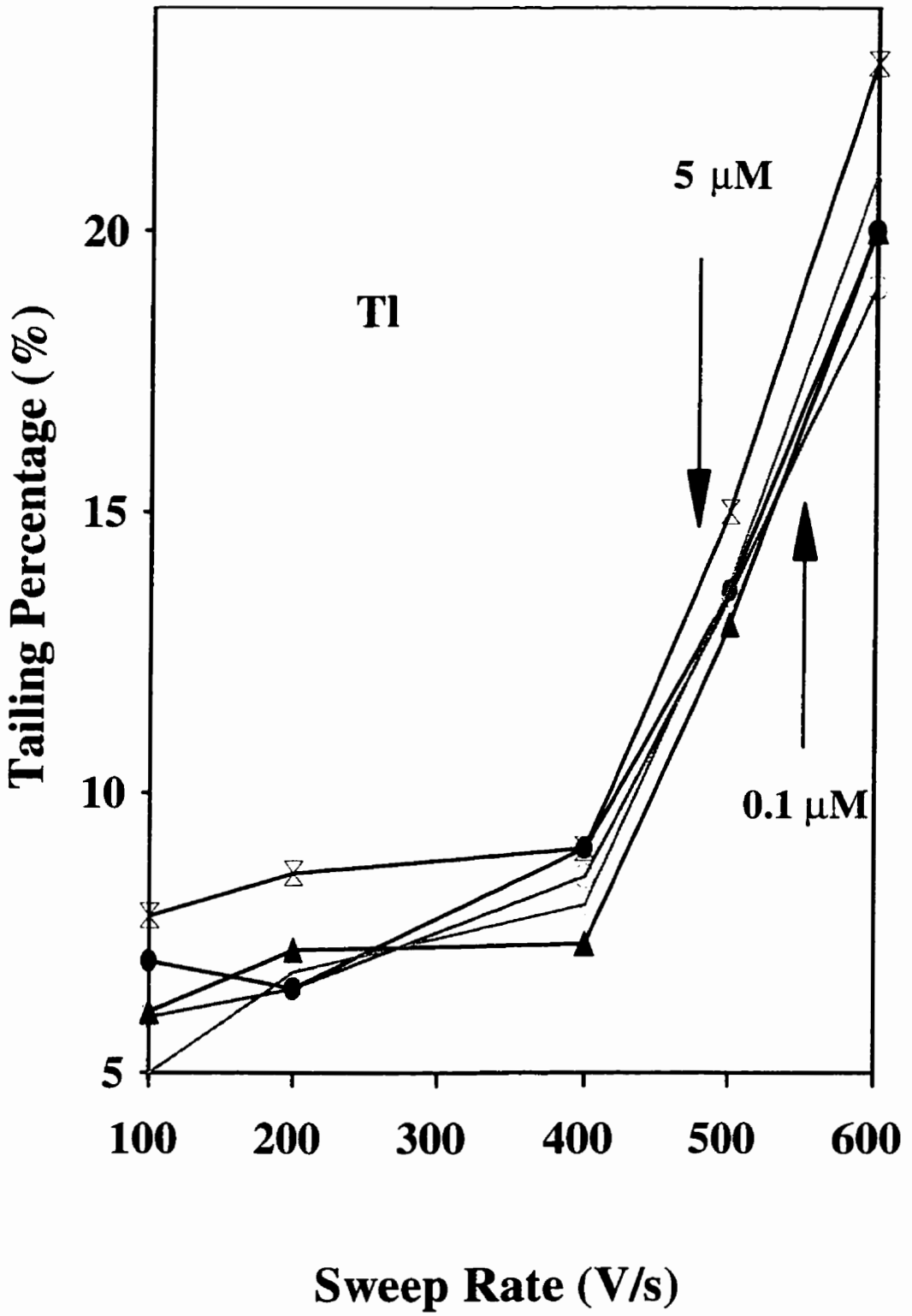

Figure 7.8 Effect of sweep rate on the peak tailing of Tl. Experimental conditions: analyte concentration, 0.1 to 5 μmol/L; sweep rate, 25 to 600 V/s; preconcentration, 220 ms; CV potential, -800 to 200 mV; other conditions as for Figure 7.3.

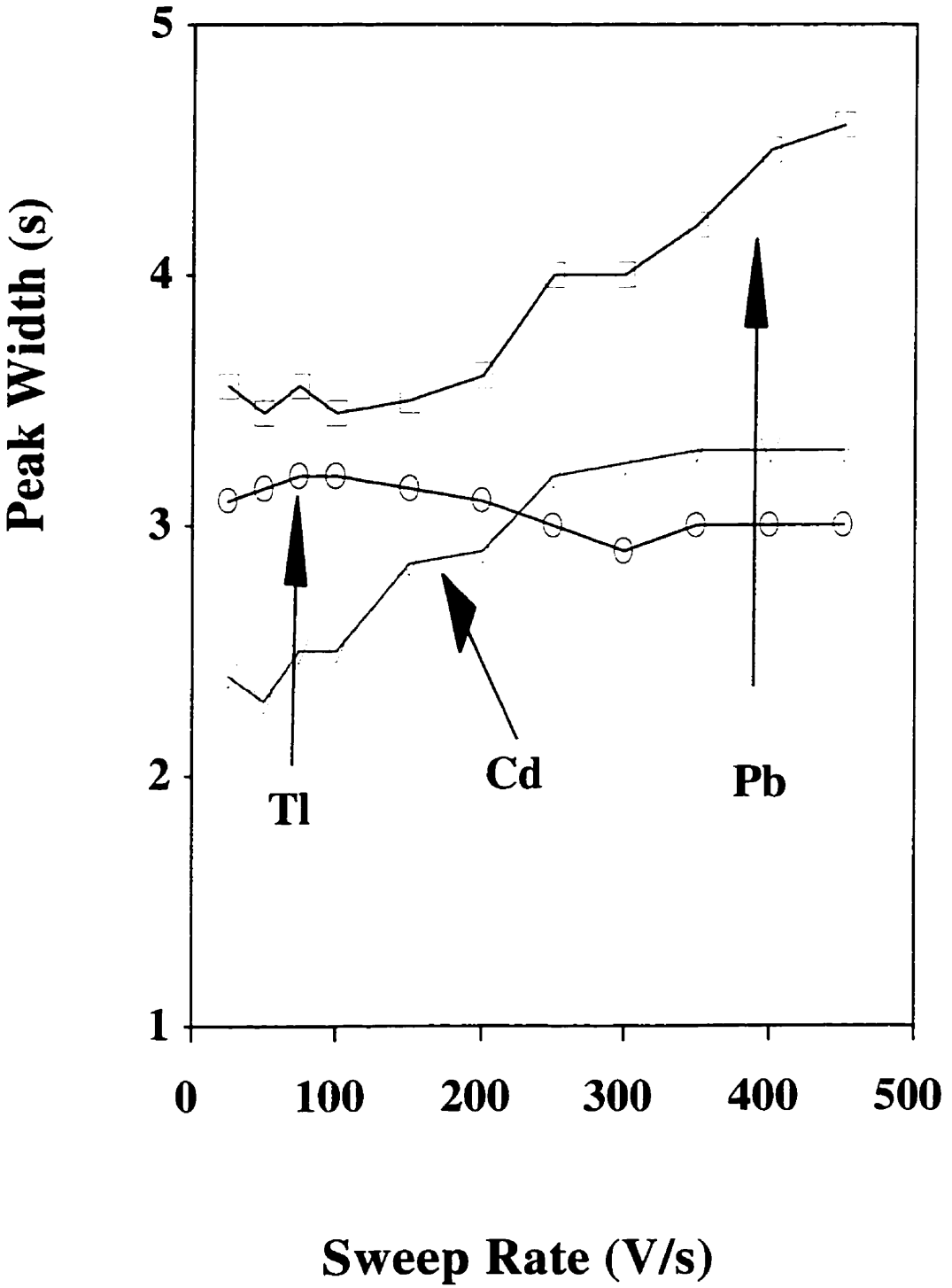

Figure 7.9 Effect of sweep rate on the peak broadening at the CV vertex potential of 400 mV. Experimental conditions: analyte concentration, 1.0 µmol/L; sweep rate, 25 to 450 V/s; preconcentration, 220 ms; CV potential, -800 to 400 mV; other conditions as for Figure 7.3.

7.4. Analysis of Co-migrating Analytes

Any method of detection in CE gives meaningful analytical information only if the analytes are sufficiently separated. Fast voltammetric technique may enhance resolving power in CE based on both electropherogram and voltammogram information. When two metal ions are co-migrated in CE, fast voltammetric techniques may provide qualitative and quantitative analysis if the analytes posses different electrochemical behavior. To examine the potential of this approach, it was applied under experimental conditions where Pb^{2+} and Zn^{2+} co-migrated (Figure 7.10 A). The series of cyclic voltammograms collected as this co-migrating peak moved past the electrode (Figure 7.10 B) shows that there were two sets of peaks. The peaks near -900 mV in Figure 7.10 B are the oxidation and reduction peaks of Zn; and the peaks near -300 mV are the Pb electrochemical peaks. Thus, identification of the two components was straightforward. It can be seen in Figure 7.10 B that the anodic signal from Zn overlapped the current from Pb. Therefore, it was necessary to examine if quantitative analysis was reliable for each co-migrating analyte. For this purposes calibration curves were examined for Zn^{2+} and Pb^{2+} using both anodic and cathodic peaks, and with both CV current and CV charge as the analytical signal; CV currents were obtained from the maximum peak heights in the voltammograms, and the CV charges for Zn^{2+} were obtained from integration of the current from -1200 mV to -500 mV, and for Pb^{2+}, from -500 mV to 200 mV. Since the anodic current of Zn and

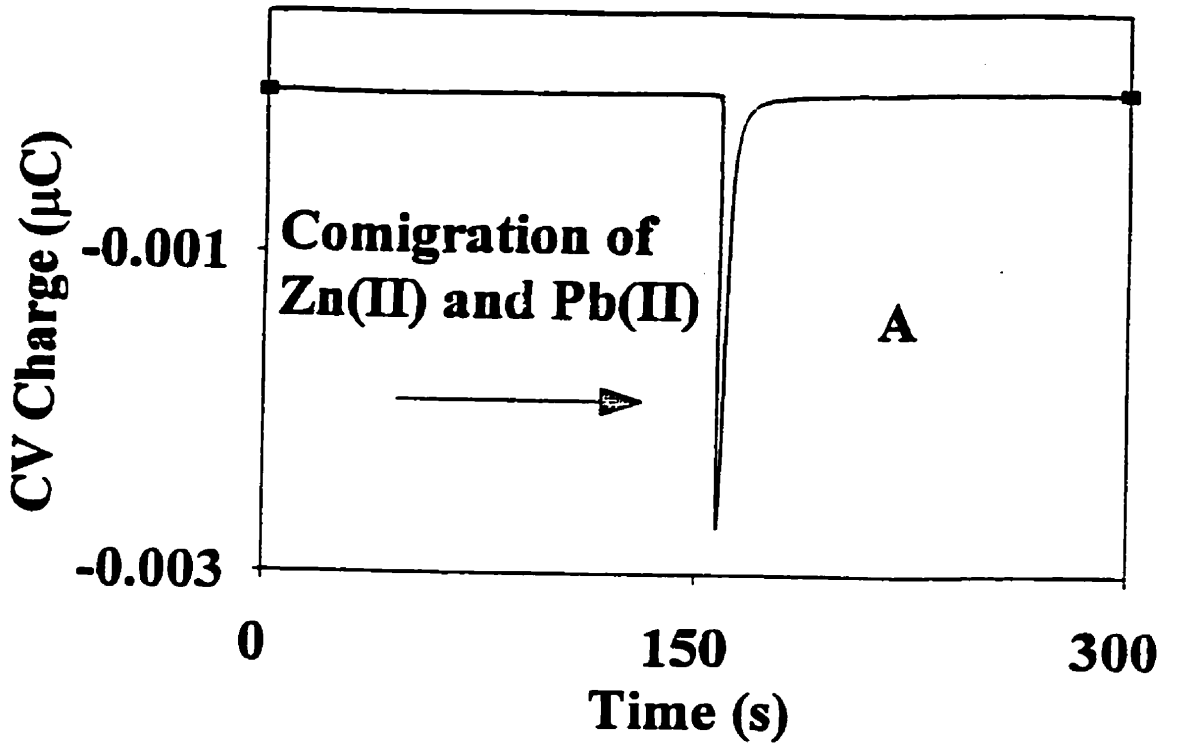

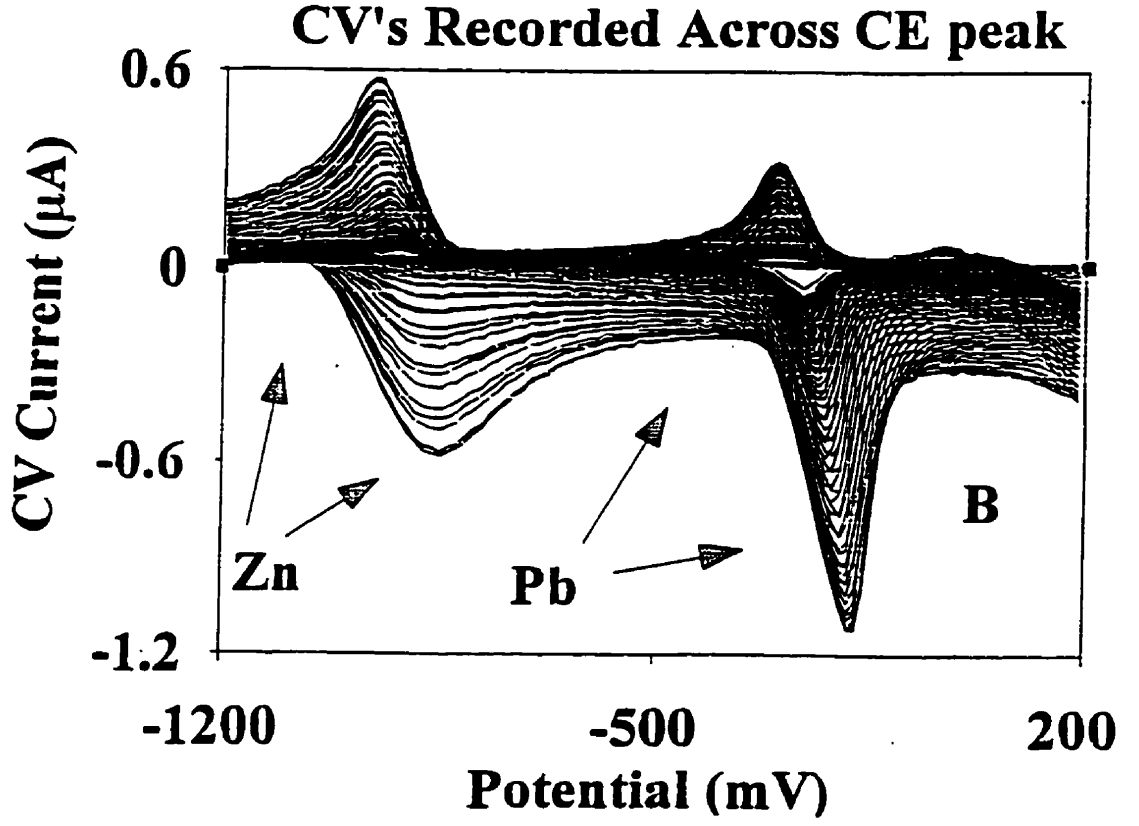

Figure 7.10 Electropherogram (curve A) of co-migrated metal ions Zn^{2+} and Pb^{2+} with fast voltammetric detection at 25 µmol/L Au electrode. Experimental conditions: CV potential, -1200 to 100 mV; analyte concentration, 10 µmol/L for Pb and 40 µmol/L for Zn; sweep rate, 100 V/s; preconcentration, 220 ms; electrolytes, 0.030 mol/L creatinine, 0.008 mol/L HIBA at pH 5.0. other conditions as for Figure 7.3. Curve B, Voltammograms of the co-migrated Zn^{2+} and Pb^{2+} peaks.

Pb overlapped, the cathodic signal was expected to provide more consistent response. This result was observed for Zn^{2+}. The calibration curves for Zn^{2+} show that the cathodic CV current and CV charge response factors varied by $< \pm 5\%$ over the concentration range of 1.5×10^{-5} to 3.6×10^{-4} mol/L, and the anodic response factors varied by $< \pm 13\%$ due to the interference from the current of Pb^{2+}. But the results for Pb^{2+} were surprising: with anodic response (both current and charge) as the signal, response factors varied by $< \pm 5\%$ over the range of 2.0×10^{-6} to 3.6×10^{-5} mol/L; for cathodic analysis, response factors varied by $\pm 7\%$ for CV current and $< \pm 20\%$ for CV charge. The poor behavior for Pb^{2+} cathodic signals is not understood with certainty, but the change in Pb cathodic peak with concentration suggests that it is probably associated with Pb reduction and migration processes. The comigrating peaks gave constant ($\leq 5\%$) response factors for Pb^{2+} (anodic) and Zn^{2+} (cathodic) with correlation coefficients in the range of 0.998 to 0.999, shown in Figure 7.11. Therefore, with proper selection of the analytical signal CV detection has the ability to identify and quantify co-migrating species in CE if their electrochemical behavior is sufficiently different.

7.5. Analytical Performance

Repeated sampling and calibration were carried out to examine the feasibility of the analytical application of fast CV detection in CE. The reproducibility for repeated injection (~ 5 times) showed that the relative standard deviations of the electrode

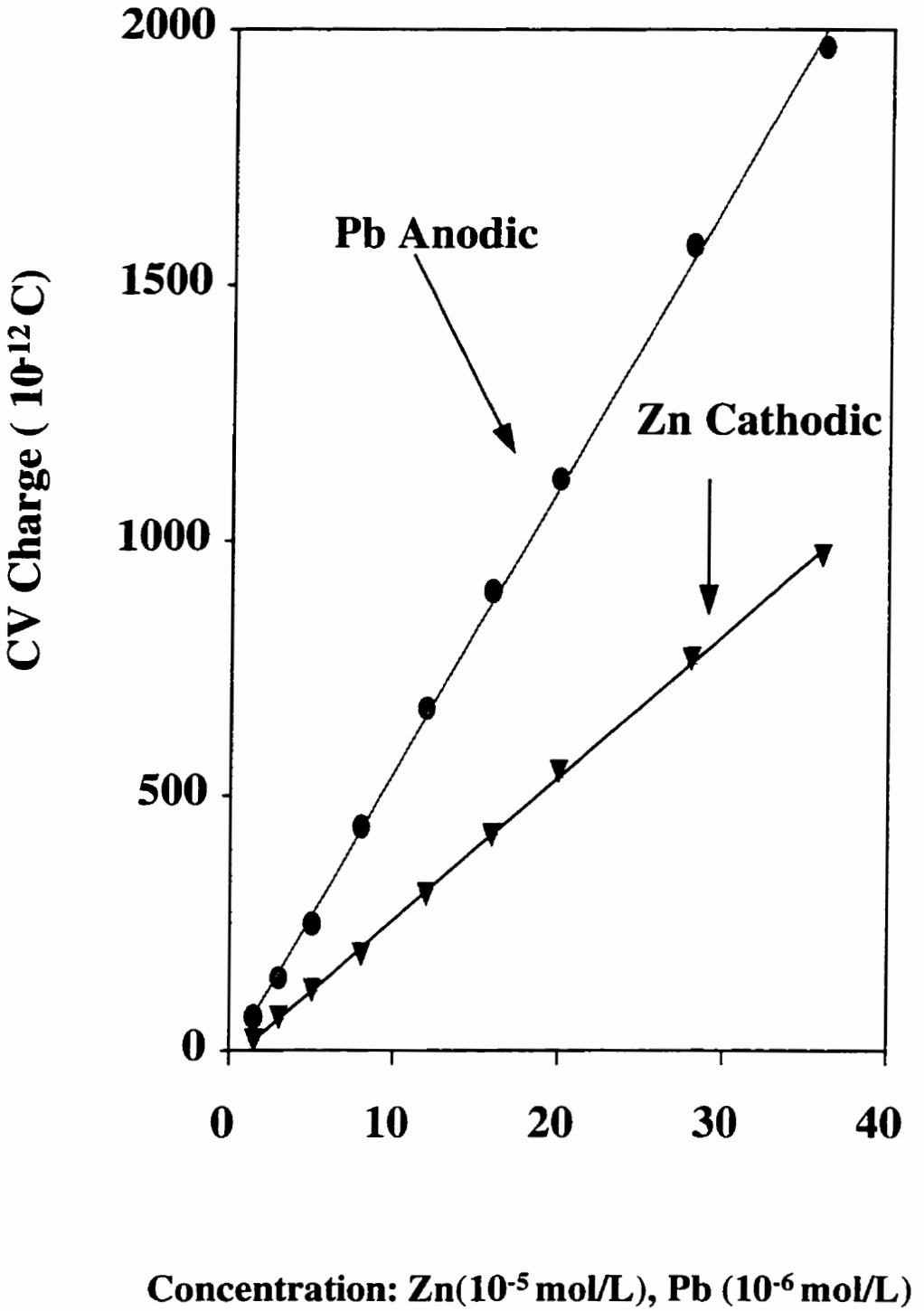

Figure 7.11 Calibration curves for co-migrating analytes. Experimental conditions: sweep rate, 275 V/s; preconcentration, 220 ms; CV potential, -900 to 300 mV; analyte concentration, Pb, 2.0 to 3.6 µmol/L; Zn, 15 to 360 µmol/L; other conditions as for Figure 7.3.

response were < 5% for Tl^+, Pb^{2+}, Cd^{2+}, Zn^{2+} Ni^{2+} and Co^{2+} over the concentration range of 5.0×10^{-8} to 5.0×10^{-5} mol/L. Calibration curves for Tl^+ with CV charge as the analytical signal (1.0×10^{-7} to 5×10^{-6} mol/L) with sweep rates from 25 V/s to 600 V/s are shown in Figure 7.12; correlation coefficients were in the range of 0.994 to 0.999 and electrode response factors were constant to $< \pm 6\%$. Plots of CV currents gave similar results. Calibrations for Tl^+, Zn^{2+}, Cd^{2+}, Ni^{2+}, Co^{2+} and Pb^{2+}, over concentrations from 5.0×10^{-8} to 5.0×10^{-5} mol/L gave correlation coefficients in the range of 0.996 to 0.999 and the response factors were constant to $< \pm 5$ %. A typical calibration result for Tl^+, Zn^{2+}, Cd^{2+} and Pb^{2+}, with concentration from 5.0×10^{-7} to 1.0×10^{-5} mol is shown in Figure 7.13; these calibration curves gave response factor constant to within $\pm 2\%$. The performance of the CV detection was also examined by analysis of two spiked samples, containing Tl^+, Zn^{2+}, Cd^{2+}, and Pb^{2+} with concentrations in the range of 1.0×10^{-7} to 1.0×10^{-6} mol/L. The results were identical (within< 5%) to those obtained with anodic pulsed amperometric detection.

A representative electropherogram for the separation of Tl^+, Pb^{2+}, Cd^{2+}, Zn^{2+} Ni^{2+} and Co^{2+} at 1.0×10^{-7} mol/L, is shown in Figure 7.14. Detection limits of metal ions under fast scan voltammetric analysis depend on predeposition time, sweep rate, size of working electrode and other experimental conditions. Under optimal experimental conditions (sweep rate of 400 V/s at 25 μm Au electrode, and 250 V/s at 10 μm Au electrode and with CV charge as the response signal) detection limits were: Tl^+, 5×10^{-9} mol/L; Pb^{2+}, 8×10^{-9} mol/L; Ni^{2+} and Co^{2+}, 1×10^{-8} mol/L; and Cd^{2+} and Zn^{2+},

$2 - 4 \times 10^{-8}$ mol/L. These results were obtained by injecting analyte at a concentration of 1.0×10^{-7} to 10^{-8} mol/L. The use of CV current for the analytical response gave poorer detection limits by a factor of ~ 10.

7.6. Conclusion:

The above study shows that fast CV provides a useful detection method for metal ions separated by CE. Analytes in a mixture can be identified by their migration times in the electropherogram as well as by their characteristic potentials in their CVs. Co-migrating analytes can be identified and quantified if the analytes have sufficiently different electrochemical behavior. Very sensitive analytical signals are obtained at a relatively high sweep rate with the detection limits 1 or 2 orders of magnitude lower than detection limits obtained under optimum PAD conditions.

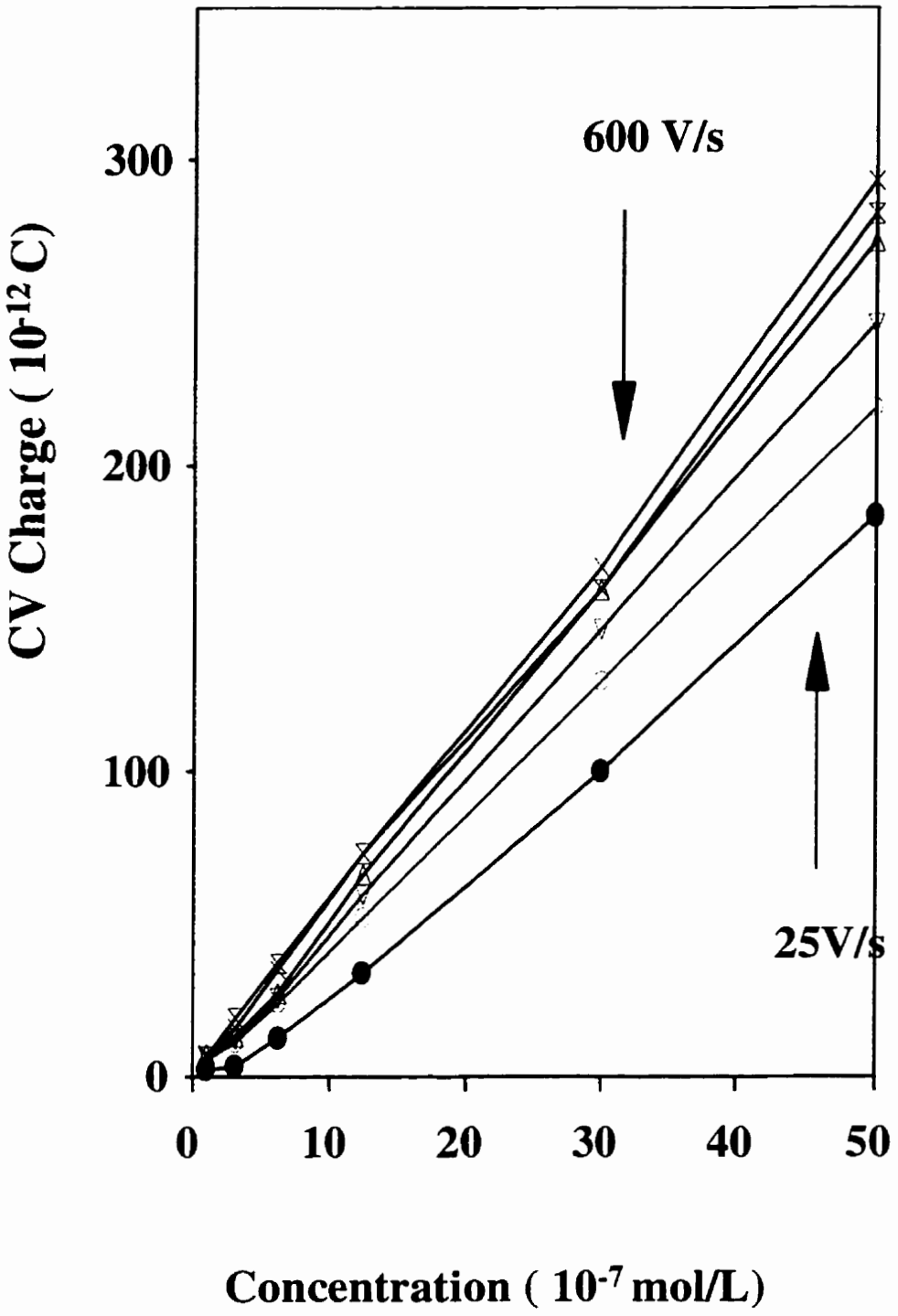

Figure 7.12 Calibration curves for different sweep rates at a 25 μm Au electrode. Experimental conditions: analyte concentration, 0.1 to 5 μmol/L; sweep rate, 25 to 600 V/s; preconcentration, 220 ms; CV potential, -800 to 200 mV; other conditions as for Figure 7.3.

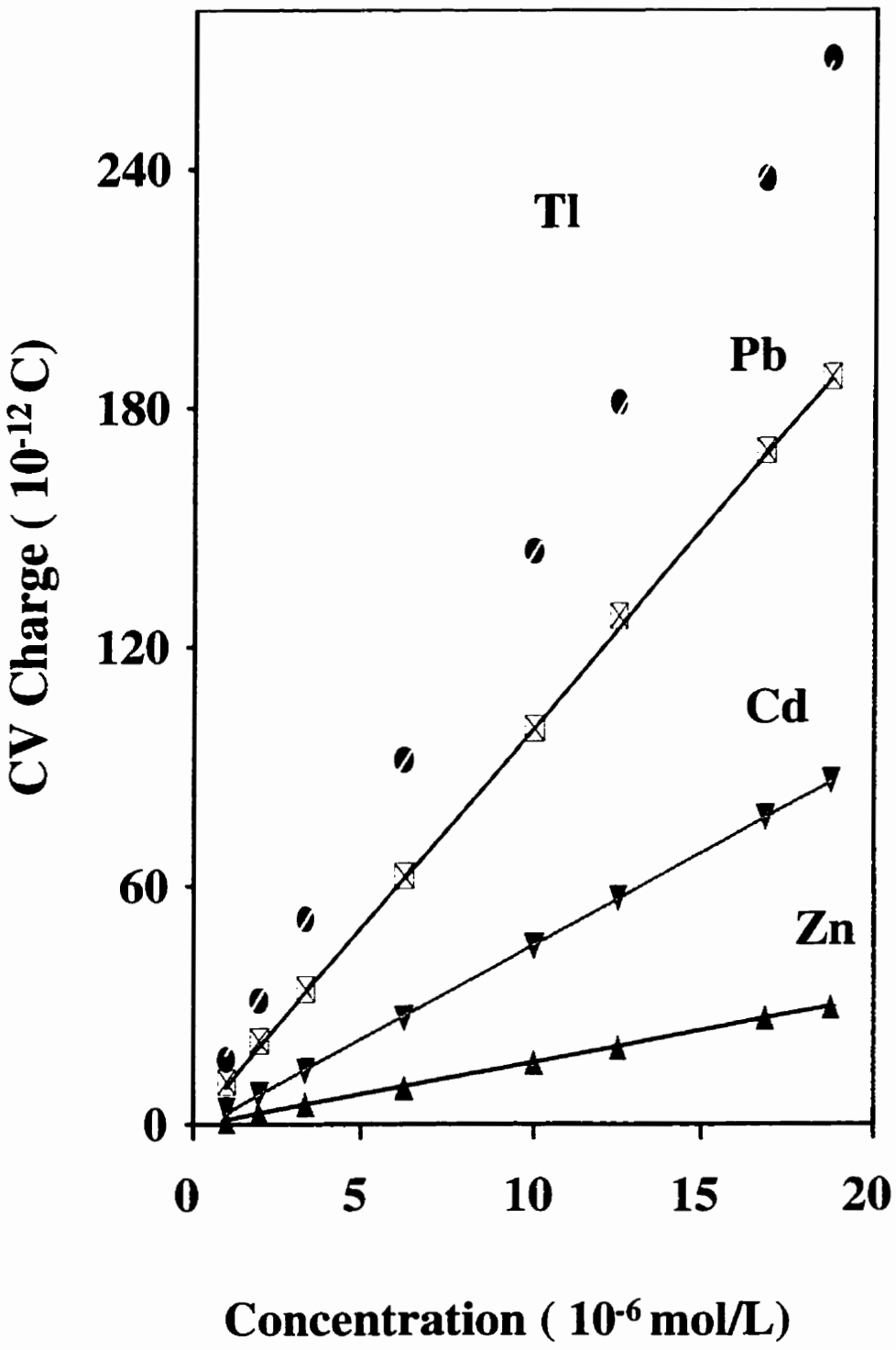

Figure 7.123 Calibration curves for Tl, Cd, Zn, Pb at a 25 μm Au electrode. Experimental conditions: analyte concentration, 0.5 to 10 μmol/L; sweep rate, 275 V/s; preconcentration, 220 ms; CV potential, -900 to 300 mV; other conditions as for Figure 7.3.

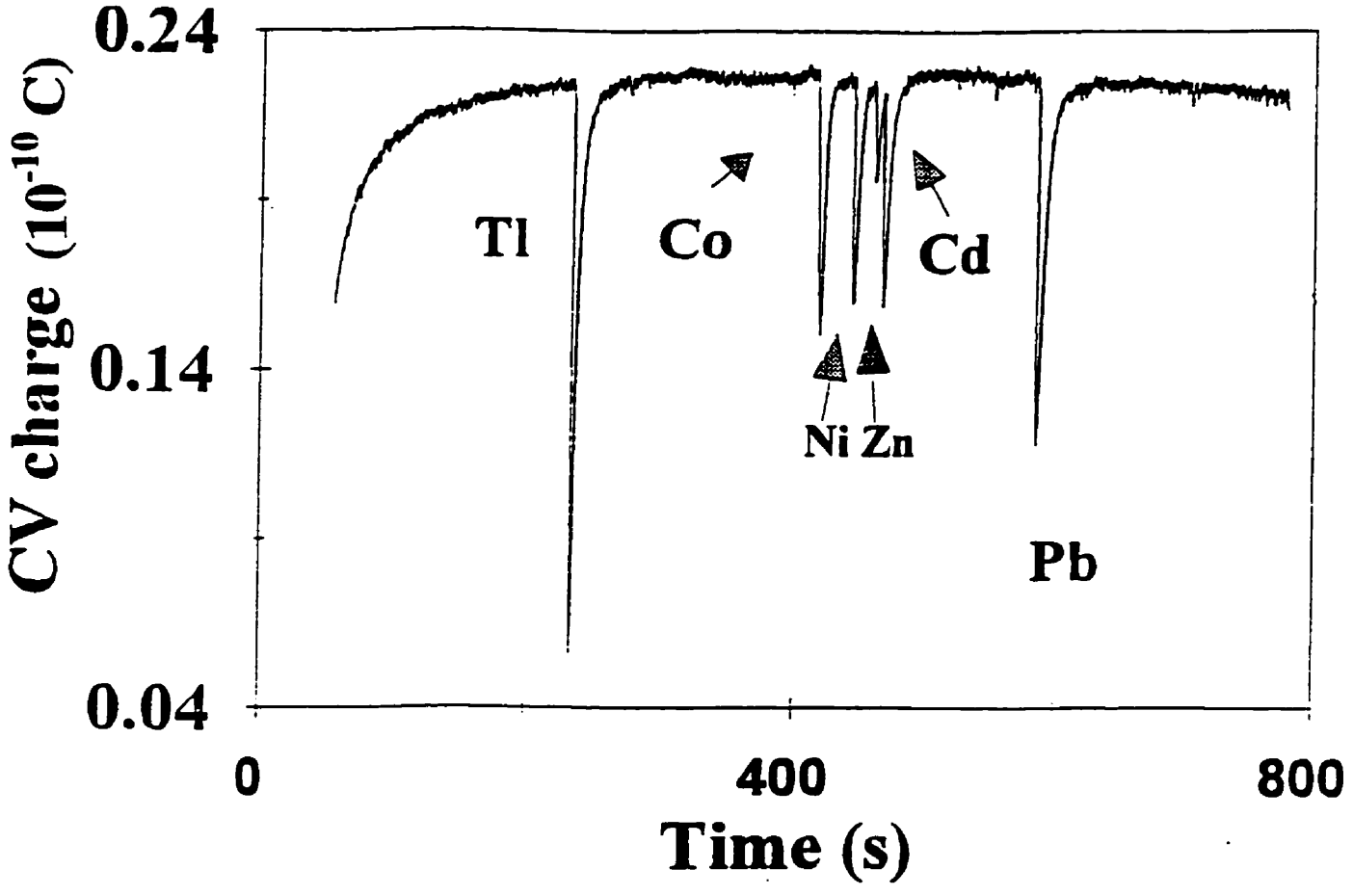

Figure 7.14 Electropherogram of metal ions with fast CV detection at 25 μm Au electrode. Experimental conditions: sweep rate, 275 V/s; preconcentration, 220 ms; CV potential, -900 to 300 mV; analyte concentration, 0.1 μmol/L; other conditions as for Figure 7.3.

8. FUTURE WORK

Future developments of electrochemical detection for CE will provide improvements in detection limits and new applications. Fast-scan voltammetric techniques can offer higher sensitivity than other EC approaches in CE. More biological techniques, such as coupling CZE to microdialysis to monitor vivo release of biological molecules should have practical importance. The development of solid, chemically and biologically modified electrodes should extend the range of analytes.

8.1. Application

Capillary zone electrophoresis has been introduced as a highly efficient separation technique for ionized solutes. This separation technique has offered promising separations for both small- and macro- molecules. For example, separations for relative small molecules have yielded efficiencies on the order of several hundred thousand theoretical plates,[217-219] and for proteins having small diffusion coefficients, efficiencies approaching 1 million theoretical plates have been reported.[220] Extremely small amount of samples are required for CE analysis, and this feature is very useful for biological and environmental samples due to limited amount of sample.

EC detection at Au or Pt μm-electrodes in CE offers a highly sensitive and reproducible detection for small amounts of samples. Although metal ions in this work were selected as the test analytes, the detection methods that have been developed should be applicable for other type of analytes. EC detection at Au electrodes has been applied to detect mercury in high-purity gallium arsenide[221] or waters and fertilizers,[222] and selenium (IV) in blood serum.[223] The potential of EC detection for biological and

environmental samples in CE should be evaluated due to the importance of life and environmental sciences.

Direct amperometric is useful for readily oxidizable species such as phenols, catecholamines, aromatic amines, cyanides, sulfite, and ascorbic acid. But for analytes that required the working electrode surface to be continuously cleaned, PAD should be considered; these analytes would include metal ions, carbohydrates, oligosaccharides, alcohols, aldehydes, and aliphatic amines. For samples requiring higher sensitive detection, the approaches that improve S/N should be useful.

Compared with pulsed amperometric detection, fast-scan voltammetry offer a higher sensitive EC detection for metal ions in CE. Potentially, this technique should be also a promising detection method for other electroactive molecules separated in CE. Fast voltammetric analysis has the added advantage of analyte identification which is attractive for unknown, as different compounds yield different characteristic voltammograms. In addition, co-migrating analytes can be identified and quantified if their electrochemical behavior is sufficient different. Therefore, the application of the fast-voltammetric detection in CE should be further extended, particularly for biological and environmental molecules.

8.2. Other Electrodes

μm-electrodes arrays have been developed recently, and their applications in CE may improve S/N because the analytical and background signals are measured simultaneously. For example, this electrode has been used to detect carbamate and

urea pesticides, with detection limits of 1-8 ng.[224] The optimization of the design of μm-electrode arrays (shape, size, and spacing) should be further required for improved EC performance.

Although EC detection at Au and Pt possess high sensitivity, the selectivity of the technique limits the range of observable analytes. Other electrodes can expand the range of EC detection in CE. For example, copper/copper oxide electrode has been used in the determination of such nonelectroactive species as amino acids and peptides[225-227] and carbohydrates.[51,228] The electrode response is produced by a change in the copper oxide film solubility, resulting from complexation of an analyte with Cu^{2+} ions on the electrode surface which alters the electrode' steady-state current. Thus, the use of copper/copper oxides electrode should expand the application of EC detection, particularly for biological molecules.

Development of biosensors is the subject of considerable current interest because of their role in biological application. Although the first glucose enzyme electrode was described in 1960s by Clark[229], no fully satisfactory in vivo sensor has yet been produced. Immobilized-enzyme membrane electrodes for oxygen-sensitive continuous-flow analysis of β-D-glucose and L-lactate, and the enzyme membranes are stable for periods of weeks to months.[230] A packed-bed enzyme reactor has been used for the detection of flow-through glutamin.[231] Further development of enzyme electrodes still is required, and these electrodes should offer high stability, sensitivity and selectivity in CE for biological compounds.

9. CONCLUSION

For end-capillary electrochemical detection in CE, capillaries of ≤ 25 μm ID should be selected to minimize the influence of high separation voltage on electrochemical detection. Placement of the electrode is also important for the analytical and background signal, and should be adjusted to maximize S/N. Since the residual electric field from high separation voltage shifts the electrode potential, the applied potential should be chosen according to the electrode potential obtained by a on-line cyclic voltammetry. Adsorption of the organic electrolytes can improve the performance of EC detection by reducing the capacitance current and/or inhibiting some reactions that contribute to background noise, such as, H^+ and O_2 reduction. Although metal ions were chosen for these studies, the EC approaches that have been developed can potentially be used for other analytes.

PAD studies indicate that PAD detection at solid Au and Pt electrodes can provide reproducible and sensitive detection for metal ions in CE because the positive potentials renew the electrode surface and prevent the accumulation of analytes. Both cathodic and anodic currents can be used as analytical signal. Anodic current detection should offer higher S/N due to no interference from O_2 and H^+ reductions. For both cathodic and anodic detection, the choice of reduction and oxidation potentials, and pulse duration are important because the analytical and background signals depend on these parameters. The results from calibration curves and from the analysis of spiked and real samples suggest that PAD can provide reliable determination.

Some approaches can be used to improve the sensitivity of PAD detection up to 10 fold. These approaches included sample stacking, multiple-step potential waveforms,

high-frequency waveforms, and signal treatments, such as digital Fourier analysis and use of a lock-in amplifier. Sample stacking is useful to enhance sensitivity under certain conditions, but the practical application of this approach is limited by the conductivity of sample. Multiple-step and fast frequency potential waveform should improved S/N, especially for analytes that physically adsorb at the electrode. Monitoring the second harmonic response by Fourier transformation can isolate analytical signal from capacitance signal to improve baseline stability, and enhance S/N for analytes that can or can not be preconcentrated at the electrode surface; this enhancement is limited to < 10 fold. Digital filtering and data smoothing is also useful to improve S/N.

Fast-scan CV detection can offer much higher S/N than PAD detection for most of the analytes studied. Since this approach can offer both current-time and current-potential information, it can be used to identify analytes by their characteristic voltammetric information, and this is useful for identification of unknown. In addition, fast voltammetric detection can identify co-migrating analytes, and under appropriate conditions it is possible to quantify them. Thus, this approach can offer an extra resolving power for the analytes separated by CE. The performance of the CV detection for specific analytes depends on sweep rate, applied potentials, and the electrochemical behavior of the analytes; thus for practical applications these parameters need to be optimized. The results for calibration curves and replicate injections indicate that the fast CV detection offers linear and reproducible response. Consequently, this detection technique should have great potential for CE analysis.

References:

1. Picton and Linder, *J. Chem. Socity*, **1897**, 72: 568.

2. Kohlrausch, F. *Ann. Phys.* **1897**, 62, 209.

3. Hardy, W. B. *Proc. Roy. Soc.* London, **1900,** 66, 110.

4. Hardy, W. B. *J. Physiol.* (London), **1905**, 33, 251.

5. Tiselius, A. *Trans. Faraday Soc.* **1937**, 33, 524.

6. Smoluchowski, M. Z. *Phys. Chem.* **1918**, 93, 129.

7. Schwerin, B. **1914**. *Reviewed in Electrophoresis, electroromose, elektordialyse in flussigkeiten*, by P. H. Pratusnitz and J. Rietstitter. Dresden U. Leipzig **1931,** From reference 5.

8. Kendall, J.; Crittendan, E. D.; *Proc. Nat. Acad. Sci.* **1923**, 9, 75.

9. Hjerten, S.; Jerstedt, S.; Tiselius, A. *Anal. Chem.* **1965,** 11, 211.

10. Virtanen, R.; *Acta Polytech. Scand*, **1974,** 123, 1.

11. Mikkers, F.; Everaerts, F.; Verheggen, T. *J. Chromatogr.* **1979,** 169, 11.

12. Jorgenson, J. W.; Lukacs, K. D. *Anal. Chem.* **1981**, 53, 1.

13. Jorgenson, J. W.; Lukacs, K. D. *Science*, **1983**, 222, 266.

14. Jorgenson, J. W.; Lukacs, K. D. *J. Chromatogr.* **1981**, 218.

15. Monning, C. A.; Kennedy, R. T. *Anal. Chem.* **1994**, 66, 280R.

16. Jandik, P.; Jones, W. R.; Weston, A.; Brown, P. R. *LC-GC* **1991**, 9, 634.

17. Landers, J. P.; Oda, R. P.; Spelsberg, T. C.; Nolan, J. A.; Ulfelder, K. *J. BioTechniques* **1993**, 14, 98.

18. Kuhn, R.; Erni, F.; Bereuter, T.; Haeusler, *J. Anal. Chem.* **1992**, 64, 2815.

19. Weston, A.; Brown, P. R.; Jandik, P.; Heckerberg, A. L.; Jones, W. R. *J. Chromatogr.* **1992,** 608, 395.

20. Jandik, P.; Bonn, G. *Capillary Electrophoresis of Small Molecules and Ions,* Chapter 3, **1993,** VCH Publishers, Inc.

21. Smoluchowski, M. V. *Physik. Z.* **1905**, 6, 530.

22. Adamson, A. W.; A *Textbook of Physical Chemistry*, Academic Press, New York, NY, **1973.**

23. Burton, D. E.; Sepaniak, M. J. Maskarinee, M. P. *J. Chromatogr. Sci.* **1986**, 24, 347.

24. Gassman, E.; Kuo, J. E.; Zare, R. N. *Science,* **1985,** 230, 813.

25. Ewing, A. G.; Wallingford, R. A.; Olefirowicz, T. M. *Anal. Chem.* **1989,** 61, 292A.

26. Stulik, K.; Pacakova, V. *Electroanalytical Measurements in Flowing Liquids*, John Wiley & Sons, New York, USA. **1984.**

27. Cruikshank, W. *Ann. Physik*, **1801**, 7, 105.

28. Butler, J. A. V. *Trans. Faraday Soc.* **1932**, 28, 379.

29. Volmer, M.; Erdey-Gruz, T. *J. Phys. Chem. Abt.* A, **1930,** 150, 203.

30. Erdey-Gruz, T.; Volmer, M. *J. Phys. Chem. Abt.* A, **1931**, 157, 165

31. Heyrovsky, J. *Discuss. Faraday Soc.* **1847,** 1, 212.

32. Heyrovsky, J. *Chem. Listy*, **1922**, 16, 256.

33. Manz, A.; Simon, W. *J. Chromatogr. Sci.* **1983,** 21, 326.

34. Knecht, L. A.; Guthrie, E. J.; Jorgenson, J. W. *Anal. Chem.* **1984**, 56, 479.

35. White, J. G.; St. Claire, R. L.; Jorgenson, J. W. *Anal. Chem.* **1986**, 58, 293.

36. Kennedy, R. T.; Jorgenson, J. W. *Anal. Chem.* **1989**, 61, 436.

37. Doherty, A. P.; Forster, R. J.; Smyth, M. R.; Vos, J. G. *Anal. Chem.* **1992**, 64, 572.

38. Martens, D. A.; Frankenberger, W. T.; Jr. *J. Liq. Chromatogr.* **1992,** 15, 423.

39. O'Shea, T. J.; Lunte, S. M. *Anal. Chem.* **1993,** 65, 247.

40. Vandeberg, P. J.; Johnson, D. C. *Anal. Chem.* **1993,** 65, 2713.

41. Lacourse, W. R.; Johnson, D. C. *Anal. Chem.* **1993,** 65, 50.

42. Wagner, H. P.; MsGarrity, M. J. *J. Am. Soc. Brew. Chem.* **1992**, 50, 1.

43. Wallingford, R. A.; Ewing, A. G. *Anal. Chem.* **1987**, 59, 1762.

44. Yik, Y. F.; Lee, H. K.; Li, S. F. Y.; Khoo, S. B. *J. Chromatogr.* **1991**, 585, 139.

45. O'Shea, T. J.; Greehagen, R. D.; Lunte, S. M.; Lunte, C. E.; Smyth, M. R.; Radzik, D. M.; Watanabe, N. *J. Chromatogr.* **1992**, 593, 305.

46. Kok, W. T.; Sahin, Y. *Anal. Chem.* **1993,** 65, 2497.

47. Wallingford, R. A.; Ewing, A. G. *Anal. Chem.* **1988**, 60, 1972.

48. Wallingford, R. A.; Ewing, A. G. *Anal. Chem.* **1989**, 61, 98.

49. Huang, X.; Luckey, J. A.; Gordon, M. J.; Zare, R. N. *Anal. Chem.* **1989**, 61, 766.

50. Huang, X.; Zare, R. N.; Sloss, S.; Ewing, A. G. *Anal. Chem.* **1991**, 63, 189.

51. Ye, J.; Baldwin, R. P. *Anal. Chem.* **1993**, 65, 3525.

52. Lu, W.; Cassidy, R. M. *Anal. Chem.* **1994**, 66, 200.

53. Krasinski, P.; Galus, Z. *J. Electroanal. Chem.* **1993**, 346, 135-146.

54. Kissinger, P. T., in Harvey, J. and Ewing, G. *Pesticide Analytical Methodology,* ACS Symp. Ser. No. 136, American Chemical Society, Washington, DC. **1980,** 57.

55. Johnson, D. C.; LaCourse, W. R. *Anal. Chem.* **1990,** 62, 589A.

56. Gaitonde, C. D.; Pathak, P. V. *J. Chromatogr.* **1990**, 514, 389.

57. Gilman, S.; *In Electroanalytical Chemistry*: Bard, A. J. Ed. Marcel Dekker: New York, **1967,** 2, 111.

58. Ossendorfava. N.; Pradac, J.; Pradacova, J.; Koryta, J. *J. Electroanal. Chem.* **1975,** 58, 255.

59. Mattson, J. S.; Jones, T. T. *Anal. Chem.* **1976,** 48, 2164.

60. Alexander, P. W., Akapongkul, U., *Anal. Chim. Acta*, **1983,** 148, 103.

Anal. Chim. Acta, **1984,** 166, 119.

61. Wang, J.; Brennsteiner, A.; Angnes, L. *Anal. Chem.* **1992**, 64, 151.

62. Lu, W.; Cassidy, R. M. *Anal. Chem.* **1993,** 65, 1649.

63. Tenygl, J. Electrochemical Sensors and Detectors with Renewable Electrode Surface in Electrochemical Detectors, Fundamental Aspects and Analytical Applications, T. H. Ryan, Plenum Press, New York, **1984.**

64. Tenygel, J. Vana, J. Czech, Pat. *Appl.* **1977**, PV 7588.

65. Vana, J.; Tenygel, J. Czech. Pat. *Appl.* **1979**, PV2022.

66. Ewing, A. G.; Mesaros, J. M.; Gavin, P. F. *Anal. Chem.* **1994,** 66, 527A.

67. O'Shea. T. M. Lunta, S. M. *Anal. Chem.* **1994**, 66, 307.

68. Anastasions Economou and Peter R. Fielden, *Anal Chim. Acta,* **1993,** 273, 27.

69. Cataldi, T. R. I.; Casella, I. G.; Desimom, E. *Anal. Chim. Acta*, **1992,** 270, 161.

70. Zen, J. M.; Chi, N. Y.; Hsu, F. S.; Chung, M. J. *Analyst,* **1995**, 120, 511.

71. Wang, J.; Tuzhi, P.; Golden, T. *Anal. Chimi. Acta*, **1987,** 194, 129.

72. Wang, J.; Freiha, B. *Anal. Chem.* **1984**, 56, 2266.

73. Korfhage, K. M.; Ravichandran, K.; Baldwin, R. P. *Anal. Chem.* **1984,** 56, 1514.

74. Hsuch, C. C.; Brajter-Toth, A. *Anal. Chem.* 66, **1994,** 2458.

75. Adams, R. N. Electrochemistry at Solid Electrodes, Dekker, New York, **1969.**

76. Polta, J. A.; Johnson, D. C. *J. Liq. Chromatogr.* **1983,** 6, 1726

77. Welch, L. E.; LaCourse, W. R.; Mead, D. A. Jr.; Hu, T.; Johnson, D. C. *Anal. Chem.* **1989**, 61, 555.

78. Polta, J. A.; Johnson, D. C. *J. Chromatogr.* **1985,** 324, 407.

79. Thomas, M. B.; Sturrock, P. E. *J. Chromatogr.* **1986**, 357, 318.

80. Lacourse, W. R.; Jackson, W. A.; Johnson, D. C. *Anal. Chem.* **1989**, 61, 2466.

81. Larew, L. A.; Mead, D. A. Jr.; Johnson, D. C. *Anal. Chim. Acta*, **1988,** 204, 43.

82. Johnson, D. C.; Polta, T. Z. *J. Chromatogr.* **1986**, 1, 37.

83. Ngoviwatchai, A.; Johnson, D. C. *Anal. Chim. Acta*, **1988,** 215, 1.

84. Hughes, S.; Johnson, D. C. *Anal. Chim. Acta*, **1983,** 149, 1.

85. Hughes, S.; Meschi, P. L.; Johnson, D. C. *Anal. Chim. Acta,* **1981**, 132, 1.

86. Hughes, S.; Johnson, D. C. *Anal. Chim. Acta*, **1982**, 3, 11.

87. Johnson, D. C. *Nature,* **1986**, 321, 451.

88. Swartzfager, D. G. *Anal. Chem.* **1976,** 48, 2189.

89. MacDonald, A.; Duke, P. D. *J. Chromatogr.* **1973,** 83, 331.

90. Stulik, K.; Hora, V. *J. Electroanal. Chem.* **1976,** 70, 253.

91. Meschi, P. L.; Johnson, D. C. *Anal. Chim. Acta*, **1981,** 124, 303.

92. Snider B. G.; Johnson, D. C. *Anal. Chim. Acta,* **1979,** 105, 25.

93. Kissinger, P. T. *Anal. Chem.* **1977,** 49, 447 A.

94. Andrew, R. W.; Johnson, D. C. *Anal. Chem.* **1976**, 48, 1056.

95. Armentrout, D. N.; McLean, J. D.; Long, M. W. *Anal. Chem*, **1979**, 51, 1039.

96. MacDonald, A.; Duke, P. D.; *J. Chromatogr.* 83, **1973**, 83, 331.

97. O'Shea, T. M.; Lunte, S. M. *Anal. Chem.*, **1993**, 65, 948.

98. Malone, M. A.; Weber, P. L.; Smyth, M. R.; Lunte, S. M. *Anal. Chem.* **1994**, 66, 3782.

99. Olefirowicz, T. M.; Ewing, A. G. *Anal. Chem.* **1990**, 62, 1872.

100. Bard, A. J.; Faulkner, L. R. *Electrochemical Methods*, Wiley, New York, **1980.**

101. Baranski, A. S.; *Anal. Chem.* **1987,** 59, 662.

102. Wu, H. P. *Anal Chem.* **1996**, 68, 1639.

103. Bret, C. M. A.; Brett, A. M. O.; Tugulea L. *Anal. Chim. Acta,* **1996,** 322, 151.

104. Deuries, W. T. *J. Electroanal. Chem.* **1965,** 9, 448.

105. Wong, D. K. Y.; Ewing, A. G. *Anal. Chem.* **1990,** 62, 2697.

106. Vehmeyer, K. R.; Wightman, R. M. *Anal. Chem.* **1985**, 57, 1989.

107. Nomura, S.; Nozaki, K.; Okazaki, S. *Electroanalysis,* **1991**, 3, 617.

108. Barbeira, P. J. S.; Mazo, L. H.; Stradiotto, N. R. *Analyst,* **1995**, 120, 1647.

109. Lukaszewski, Z.; Zembrzuski, W.; Piela, A. *Anal. Chim. Acta*, **1996**, 318, 159.

110. Pihel, K.; Hsieh, S.; Jorgenson, J. W.; Wightman, R. M. *Anal. Chem.* **1995**, 67, 4514.

111. Gunasingham, H.; Tay, B. T.; AngK. P. *Anal. Chem.* **1987**, 59, 262.

112. Bond, A. M. *Analyst*, **1994**, 119, R1.

113. Gouy, G. Ann. *Chim. Phys.* **1908**, 8, 8.

114. Delahay, P. *Double Layer And Electrode Kinetics*, Interscience, New York, 2nd, **1966.**

115. Avouris, P.; Demoth, J. E. *J. Chem. Phys.* **1981,** 75, 4783.

116. Parsons, R. *Surf. Sci.* **1980**, 101, 316.

117. Conway, B. E. *Theory and Principles of Electrode Processes*, Ronald Press, New York, **1964.**

118. Fawcett, W. R.; Fedurco, M.; Kovacova, Z.; Borkowska, *Z. Lanmuir* **1994,** 10, 912.

119. Roelfs, B.; Baumgartel, H. Ber. Bunsen-Ges. *Phys. Chem.* **1995,** 99, 677.

120. Rodes, A.; Pastor, E.; Iwasita, T. *J. Electroanal. Chem.* **1994,** 369, 183.

121. Orts, J. M.; Gomez, R.; Feliu, J. M.; Aldaz, A.; Clavilier, *J. Electrochim. Acta,* **1994,** 39, 1519.

122. Gao, X. P.; Edens, G. J.; Weaver, M. J. *J. Electroanal. Chem.* **1994**, 376, 21.

123. Mo, Y. B.; Hwang, E.; Sherson, D. A. *Anal. Chem.* **1995**, 67, 2415.

124. Bron, M. Holze, R. *J. Electroanal. Chem.* **1995,** 385, 105.

125. Savich, W.; Sun, S. G.; Lipkowski, J.; Wieckowski, A. *J. Electroanal. Chem.* **1995,** 388, 233.

126. Zelenay, P.; Waszczuk, P.; Dobrowolska, K.; Sobkowski, *J. Electrochim. Acta,* **1994,** 39, 655.

127. Strbac, S.; Hamelin, A.; Adzic, R. R. *J. Electroanal. Chem.* **1993,** 362, 14.

128. Fawcett, W. R.; Fedurco, M.; Kovacova, Z. *J. Electrochem. Soc.* **1994,** 141, L30.

129. Horanyi, G.; Vertes, G. *J. Electroanal. Chem.* 45, **1973,** 63.

J. Electroanal. Chem. 55, **1974**, 45.

130. Kolb, D. M. in Gerischer, H. and Tobias, *Advances in Electrochemistry and Electrochemical Engineering,* Vol.11, Wiley, New York, **1978.**

131. Conway, B. E.; Mozota, J. *J. Chem. Soc. Faraday Trans.* **1982,** 1, 78, 1717.

132. Mairanovski, S. G. *Catalytic and Kinetic Waves in Polarography*, Nauka, Moscow, **1966.**

133. Koryta, J.; Dvorak, J.; Bohackova, V. *Electrochemistry*, chapter 4, METHUEN & CO LTD. **1966.**

134. El-shafei, A. A. *J. Electroanal. Chem.* **1995**, 380, 269.

135. Clavilier, J.; Granon, J. P.; Petit, M. *J. Electroanal. Chem. 265*, **1989**, 231.

136. Adzic,R. R.; Markovic, N. M.; Vesvic,V. B. *J. Electroanal. Chem.* **1984,**165, 105

137. Mlvarez-Rizatti, M.; Jutter, K.; *J. Electroanal. Chem.* 144, **1985,** 351.

138. Kinidis, G. K.; Jannakaodakis, D. *J. Electroanal. Chem.* **1984,**162, 163.

139. Abe, T.; Swain, G. M.; Sashikaka, K.; Itaya, K. *J. Electroanal. Chem.* 382, **1995,** 73.

140. Bewick, A.; Thomas, B. *J. Electroanal. Chem.* **1977**, 84, 127.

141. Jovic, V.; Jovic, B.; Despic, A. *J. Electroanal. Chem.* **1990**, 288, 229.

142. Lu, W.; Cassidy, R. M. *Anal. Chem.* **1993,** 65, 2878.

143. Bialkowski, S. E. *Anal. Chem.* **1988,** 60, 403A

Ferris, S. S.; Lou, G.; Ewing, A. G. J. Microcolumn Sep. 1994, 6, 263.

144. Savitzy, A.; Golay, M. J. E. *Anal. Chem.* **1964,** 36, 1627.

145. Fukushi, K.; Hiiro, K. *J. Chromatogr.* **1990,** 523, 281.

146. Shi, Y.-C.; Fritz, J. S. *J. Chromatogr. A*, **1993,** 640, 473.

147. Simunicova, Kaniansky, D.; Loksikova, K. *J. Chromatogr.* **1994,** 665, 203.

148. Swalle, D. F.; Sepaniak, M. J. *Anal. Chem.* **1991**, 63, 179.

149. Lee, Y.-H.; Lin, T.-I. *J. Chromatogr. A*, **1994,** 675, 227.

150. Lin, T. I.; Lee, Y.-H.; Chen, Y. C. *J. Chromatogr. A*, **1993,** 654, 167.

151. Buchberger, W.; Semanova, O. P.; Timerbaev, A. R.; Resolut, J. H. *J. Chromatogr.* **1993,** 16, 153.

152. Lee, H. J.; Lee, S. H.; Chung K. S.; Lee, K. W. *Bulletion of the Korean Chemical Society*, **1994,** 15, 945.

153. Saitoh, T.; Hoshino, H.; Yotsuyanagi, T. *J. Chromatogr.* **1989**, 469, 175.

154. Regan, F. B.; Meaney, M. P.; Lunte, S. M. *J. Chromatogr. B,* **1994,** 657, 409.

155. Wang, T. L.; Li, S. *J. Chromatogr. A*, **1995,** 718, 421.

156. Kajiwara, H. *J. Chromatogr.* **1991**, 559, 345.

157. Timerbaev, A. R.; Semenova, O. P. *J. Chromatogr.* A, **1995**, 690, 141.

158. Weston, A.; Brown, P. R. *J. Chromatogr.* **1992**, 602, 249. and **1992**, 593, 289.

159. Krattiger, B.; Bruin, G. J. M.; Bruno, A. E. *Anal. Chem.* **1994,** 66, 1.

160. Haddad, P. R.; Jackson, D. E. *Ion Chromatogr.* **1990,** 46, 312.

161. Chen, M.; Cassidy, R. M. *J. Chromatogr.* **1992,** 602, 227.

162. Hirokawa, T.; Aoki, N.; Kiso, Y. *J. Chromatogr.* **1984**, 312, 11.

163. Foret, F.; Fanali, S.; Nardi, A.; Bocek, P. *Electrophoresis*, **1990,** 11, 780.

164. Lambert, W. J.; Middleton, D. L. *Anal. Chem.* **1990,** 62, 1585.

165. Altria, K.; Simpson, C. *Anal. Proc.* **1986**, 23, 453.

166. Altria, K.; Simpson, C. *Chromatographia* **1987,** 24, 527.

167. Timerbaev, A. R.; Semenova, O. P.; Jandik, P.; Bonn, G. K. *J. Chromatogr. A.* 1994, 671, 419.

168. Shi, Y.; Fritz, J. S. *J. Chromatogr. A.* **1994**, *671*, 429.

169. Ahuja, E. S.; Little, E. L.; Foley, J. P. *J. Liq. Chromatogr.* **1992,** 15, 1099.

170. Stathaki, C.; Cassidy, R. M. *J. Chromatogr.* **1995,** 699, 353.

171. Schewer, C.; Kenndler, E. *Anal. Chem.* **1991,** 63, 1801.

172. Huang, X.; Gordon, M. J.; Zare, R. N. *Anal. Chem.* **1988**, 60, 1837.

173. Wanders, B. J.; van de Goor, T. A. A. M.; Everaerts, F. M. *J. Chromatogr.* **1993,** 652, 291.

174. Van De Goor, A.; Wanders, B.; Everaerts, F. *J. Chromatogr.* **1989,** 470, 95.

175. Vindevogel, J.; Sandra, P. *J. Chromatogr.* **1991,** 541, 483.

176. Fujiwara, S.; Honda, S. *Anal. Chem.* **1986**, 58, 1811.

177. Fujiwara, S.; Honda, S. *Anal. Chem.* **1987**, 59, 487.

178. Vanorman, B. B.; Liversidge, G. G.; McIntire, G. L. *J. Microcol. Sep.* **1991,** 2, 176.

179. Yao, X. W.; Wu, D.; Regnier, F. E. *J. Chromatogr.* **1993**, 636, 21.

180. Chen, C. H.; Vesecky, S. M.; Gewirth, A. A. *J. Am. Chem. Soc.* **1992**, 114, 451.

181. Trevor, D. J.; Chidsey, C. E. D.; Loiacona, D. N., *Phys. Rev. Lett.* **1989**, 62, 929.

182. Latimer, W. M. *The Oxidation State of the Elements and Their Potentials in Aqueous Solutions*, Prentice-Hall, Englewood Cliffs, N. J. **1952.**

183. Turner, D. R.;Whitefield, M. *J. Electroanal. Chem.* **1979**, 103, 43.

184. Buffle, J. *J. Electroanal. Chem.* **1981,** 125, 273.

185. Nicholson, M. M. *Anal. Chem.* **1960,** 32, 1058.

186. Brainina, K. Z. *Stripping Voltammetry in Chemical Analysis*, Wiley, New York, **1974**, 32.

187. Green, M.; Hansen, R. *Surf. Sci,* **1991,** 259, L743.

188. Kokkinidis, G.; Sazou, D. *J. Electroanal. Chem.* **1986,** 199, 165.

189. Bewick, A.; Thomas, B. *J. Electroanal. Chem.* **1977,** 84,127.

190. Chen, C.H.; Gewirth, A. A. *Phys. Rev. Lett.* **1992**, 68, 1571.

191. Parson, R. *Trans. Faraday Soc.* 1958, 54, 1035; Gerischer, H. Bull. *Soc. Chim. Belg*, **1958,** 67, 506.

192. Gerischer, H. *Trans. Faraday Soc.* **1958,** 67, 506.

193. Paul, M. T.; Dennis, C. *J. Anal. Chim. Acta,* **1980,** 118, 233.

194. Yang, Q.; Smeyers-Verbeke, J.; Wu, W.; Khots, M. S.; Massart. D. L. *J. Chromatogr. A,* **1994**, 688, 339.

195. Neuburger, G. G.; Johnson, D. C. *Anal. Chim. Acta*, **1987**, 192, 205.

196. Stephen E. Moring, *Quantitative Aspects of Capillary Electrophoresis Analysis*, Chapter 3, Principle of Capillary Electrophoresis, **1992.**

197. Morita, I.; Sawada, J. *J. Chromatogr.* **1993**, 641, 375.

198. Everaerts, F. M.; Verheggen, T. P. E. M.; Mikkers, F. E. P. *J. Chromatogr.* **1992,** 169, 341.

199. Chie, R.-L.; Burgi, D. S. *Anal. Chem.* **1992,** 64, 489A

200. Wolf, S. M.; Vouros, P.

201. Ngoviwatchai, A.; Johnson, D. C. *Anal. Chim. Acta*, **1988**, 215, 1.

202. VanRiel, J. A. M.; Oliman, C. *Anal. Chem.* **1995,** 67, 3911.

203. Chien, R. L.; Helmer, J. C. *Anal. Chem.* **1991,** 63, 1354.

204. Chien, R. L.; Burgi, D. S. *Anal. Chem.* **1992,** 64, 1046.

205. Palmarsdottir, S.; Edholm, L. E. *J. Chromatog.* **1995**, 693, 131.

206. Burgi, D. S.; Chien, R. L. *Anal. Chem.* **1991,**63, 1354.

207. Vinther, A.; Soebery, H. *J. Chromatogr.* **1991**, 559, 3.

208. Vinther, A.; Soeberg, H. *J Chromatogr.* **1991,** 559, 27.

209. Vinther, A.; Soeberg, H.; Nielsen, L. *Anal. Chem.*, **1992**, 64, 187.

210. Bialkowski, S. E. *Anal. Chem.* **1988**, 60, 355A

211. Swanek, F. D.; Chen, G.; Ewing, A. G. *Anal. Chem.* **1996**, 68, 3912.

212. Park, S.; McGrath, M. J.; Smyth, M. R.; Diamond, D.; Lunte, C. E. *Anal. Chem.* **1997,** 69, 2994.

213. Baranski, A. S.; Norouzi, P.; Nelson, L. J. *Proc. Electrochem. Soc.* **1996**, 96-9, 41.

214. Gosser, D. K. *Cyclic Voltammetry*: simulation and analysis of reaction mechanisms, VCH; New York, **1993.**

215. Roe, D. K.; Toni, J. E. A. *Anal. Chem.* 37, **1965,** 1503.

216. Forster, R. J. *Chem. Soc. Rev.* **1994,** 289.

217. Jorgenson, J. W.; Lukacs, K. D. *Anal. Chem.* **1981**, 53, 1298.

218. Tsuda, A.; Kazuhiro, N.; Nakagawa, G. *J. Chromatogr.* **1983,** 264, 385.

219. Green, J. S.; Jorgenson, J. W. *Anal. Chem.* **1986**, 58, 479.

220. Lauer, H. H.; McManigill, D. *Anal. Chem.* **1986,** 58, 165.

221. Rievaj, M.; Bustin, D. *Analyst*, **1992,** 117, 1471.

222. Rievaj, M.; Mesaros, S.; Bustin, D. *An. Quim.* **1993,** 89, 347.

223. McLaughlin, K.; Boyd, D.; Hua, C.; Smyth, M. R. *Electroanalysis*, **1992,** 4, 689.

224. VonNehring, Q. G.; Hightower, J.; Anderson, J. L. *Anal. Chem.* **1986,** 58, 2777.

225. Gao, Y.; Colon, L. A.; Dadoo, R. Zare, R. N. *Electrophoresis,* **1995**, 16, 493.

226. Ye, J.; Baldwin, R. P. *Anal. Chem.* **1994**, 66, 2669.

227. Zhou, J.; Lunte, S. M. *Electrophoresis,* **1995,** 16, 498.

228. Huang, X.; Kok, W. T. *J. Chromatogr. A* **1995**, 707, 335.

229. Clark, L. C., Jr.; Lyons, C. *Ann. N. Y. Acad. Sci.* **1962,** 102, 29.

230. Scindler, J. G.; Schindler, M. M.; Herna, K.; Pohl, M. *J. Clin. Chem.* **1994**, 32, 599.

231. Huang, Y. L.; Khoo, S. B.; Yap, M. G. S. *Anal. Lett.* **1995**, 28, 593.

IMAGE EVALUATION
TEST TARGET (QA-3)

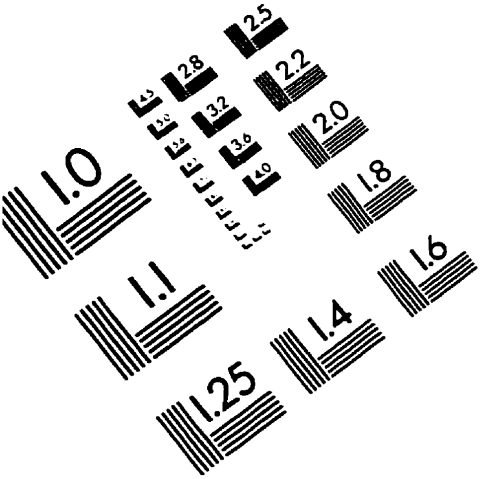

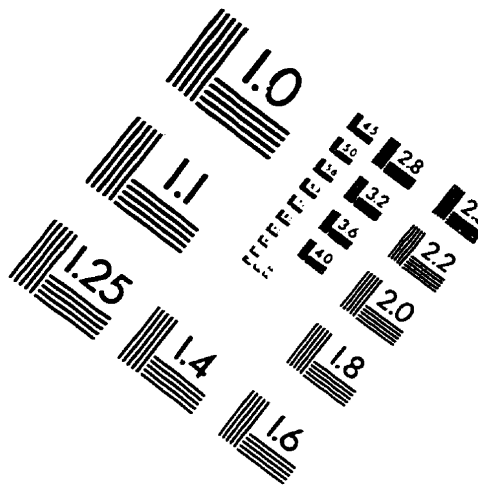

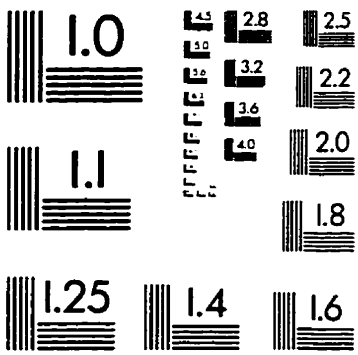

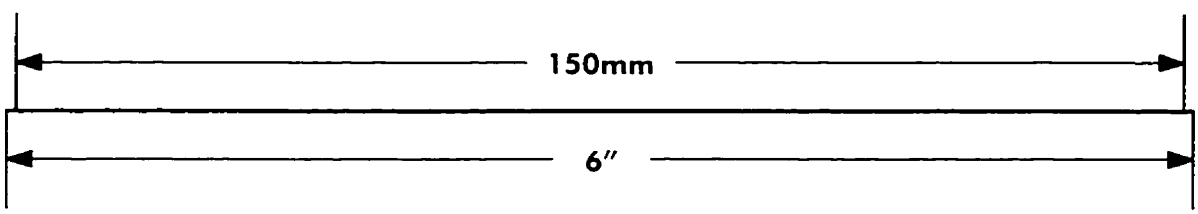

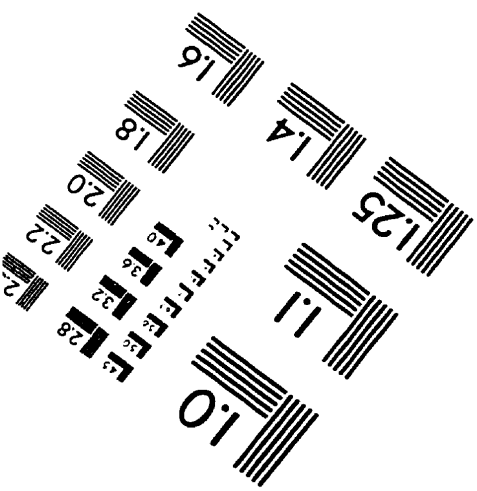

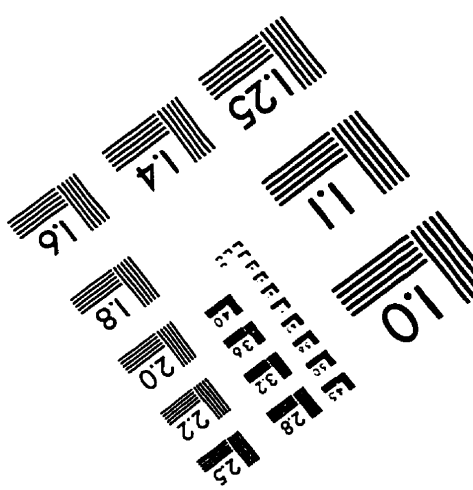

APPLIED IMAGE, Inc
1653 East Main Street
Rochester, NY 14609 USA
Phone: 716/482-0300
Fax: 716/288-5989